The Cellular Phenotype of the Neurodegenerative Disease Autosomal Recessive Spastic Ataxia of Charlevoix-Saguenay

Teisha Y Bradshaw

A thesis submitted to Queen Mary, University of London, for the degree of Doctor of Philosophy

September 2014

Centre for Endocrinology

William Harvey Research Institute

Barts and the London School of Medicine and Dentistry

Queen Mary University of London

Abstract

Autosomal recessive spastic ataxia of Charlevoix Saguenay (ARSACS) is an early onset neurodegenerative disorder resulting from mutations in the *SACS* gene that encodes the protein sacsin. Sacsin is a 520kDa multi-domain protein localised at the cytosolic face of the outer mitochondrial membrane with suggested roles in proteostasis and most recently in the regulation of mitochondrial morphology. An excessively interconnected mitochondrial network was observed as a consequence of reduced levels of sacsin protein following *SACS* knockdown in neuroblastoma cells as well as in an ARSACS patient carrying the common Quebec homozygous *SACS* mutation 8844delT. Moreover, it was suggested that sacsin has a role in mitochondrial fission as it was found to interact with mitochondrial fission protein Dynamin related protein 1 (Drp1). The aim of this thesis was to explore sacsin's role in the regulation of mitochondrial morphology and dynamics in non-Quebec ARSACS patients and sacsin knockdown fibroblasts.

This study shows that loss of sacsin function promotes a more interconnected mitochondrial network in non-Quebec ARSACS patients and in sacsin knockdown fibroblasts. Moreover, recruitment of the essential mitochondrial fission protein Drp1 to the mitochondria was significantly reduced in ARSACS patient cells and in sacsin knockdown fibroblasts. This reduced recruitment of Drp1 to mitochondria also occurred when cells were treated to induce mitochondrial fission. Furthermore, both the size and intensity of Drp1 foci localised to the mitochondria were significantly reduced in both sacsin knockdown and patient fibroblasts. Finally, reduced ATP production, decreased respiratory capacity of mitochondria and an increase in mitochondrial reactive oxygen species demonstrated impaired mitochondrial function in ARSACS patient and sacsin knockdown fibroblasts.

These results suggest a role for sacsin in the stabilisation or recruitment of cytoplasmic Drp1 to prospective sites of mitochondrial fission similar to that observed by other mitochondrial fission accessory proteins.

Acknowledgements

I would first like to take this opportunity to thank the Ataxia Charlevoix-Saguenay foundation and Queen Mary, University of London for funding this work.

I would like to express my appreciation and gratitude to my supervisors Professor Paul Chapple and Dr Greg Michael. Their guidance, support and their fervent attention to detail have truly been invaluable. I would also like to express my sincere thanks to members of the Chapple group past and present, Dr David Parfitt, Dr Esmeralda Vermeulen, Emma Duncan and Dr Suran Nethisinghe for their encouragement and friendship. It has been great to be a part of Team Sacsin!

I have been privileged to work amongst such world renowned academics in the Centre for Endocrinology at Barts and the London School of Medicine and Dentistry. Their passion for research and innovative methodologies has been truly inspirational. In particular I would like to thank Dr Eirini Meimaridou and Dr Harshini Katugampola for stimulating good discussions, for being there when I needed to troubleshoot, for their helpful advice and for cake and coffee.

Thank you to my family and friends for their tremendous support and love, getting through these years would not have been possible without you. I dedicate this thesis to my parents, Ishmael and Ruthlyn Bradshaw who have inspired me to follow my dreams. Last but not least, thanks to God, who makes all things possible.

Statement of Originality

I, Teisha Yo-Stella Bradshaw, confirm that the research included within this thesis is my own work or that where it has been carried out in collaboration with, or supported by others, that this is duly acknowledged below and my contribution indicated. Previously published material is also acknowledged below.

I attest that I have exercised reasonable care to ensure that the work is original, and does not to the best of my knowledge break any UK law, infringe any third party's copyright or other Intellectual Property Right, or contain any confidential material.

I accept that the College has the right to use plagiarism detection software to check the electronic version of the thesis.

I confirm that this thesis has not been previously submitted for the award of a degree by this or any other university.

The copyright of this thesis rests with the author and no quotation from it or information derived from it may be published without the prior written consent of the author.

Signature:

Date: 30th September 2014

Table of Contents

Table of Figures

Table of Figures

Table of Tables

Table of Tables

List of Abbreviations

Abbreviation	Full Name
2DG	2-Deoxy-D-Glucose
3D	Three Dimensional
ABL	Abetalipoproteinemia
ACA	Aniridam Cerebellar Ataxia And Mental Retardation
AD	Alzheimers Disease
ADCA	Autosomal Dominant Cerebellar Ataxia
ADLD	Autosomal Dominant Leukodystrophy
ADP	Adenosine Diphosphate
ANOVA	Analysis Of Variance
AOA1	Ataxia Oculomotor Apraxia 1
ARCA	Autosomal Recessive Cerebellar Ataxias
ARSACS	Autosomal Recessive Spastic Ataxia Of Charlevoix Saguenay
AT	Ataxia Telangiectasia
ATLD	Ataxia Telangiectasia-Like Disorder
ATP	Adenosine Triphosphate
AVED	Ataxia With Vitamin E Deficiency]
AU	Arbitrary Units
BTDD	Biotinidase Deficiency
C-terminus	Carboxyl Terminus
Ca2+	Calcium
CCCP	Carbonyl Cyanide M-Chlorophenyl Hydrazone
CDG1A	Congenital Disorder Glycosylation Type 1A
CLN4B	Ceroid Lipofuscinosis Neuronal 4b
CMT2A	Charcot Marie Tooth Disease Type 2A
CRATD	Carnitine Aycetyltransferase
CRISPR	Clustered Regularly Interspaced Short Palindromic Repeats
CTX	Cerebrotendinous Xanthomatosis
DAPI	4’,6-Diamidino-2-Phenylidole
DMEM	Dulbecco’s Minimum Eagle Medium
DNA	Deoxyribonucleic Acid
dNTP	Deoxynucleotide
DRD	Dopa Responsive Dystonia
Drp1	Dynamin Like Protein 1
E.Coli	Escherichia Coli
ECACC	European Collection Of Cell Culture
ECAR	Extracellular Acidfication Rate
EDTA	Ethylenediaminetetraacetic Acid
EOCARR	Earyl Onset Cerebellar Ataxia With Retained Tendon Reflexes
EA1/2	Episodic Ataxia Type ½

ER	Endoplasmic Reticulum
ETC	Electron Transport Chain
FAD	Familiar Alzheimer's Disease
FADH2	Flavin Adenine dinucleotide
FARR	Friedreich's Ataxia With Retained Reflexes
FBS	Fetal Bovine Serum
FCCP	Carbonyl Cyanide-P-Trifluoromethoxyphenyl Hydrazone
Fluc	Firefly Luciferase
FRAP	Fluorescence Recovery After photobleaching
FRDA	Friedreich's Ataxia
FXN	Frataxin
FXTAS	Fragile X Tremor Ataxia
g	Standard Acceleration Due To Gravity
GDAP1	Ganglioside Induced Differentiation Associated Protein 1
GDP	Guanine Diphosphate
GTP	Guanine Triphosphate
GED	Gtpase Effector Domain
GFP	Green Fluorescence Protein
GPX1	Glutathione Peroxidase
GSH	Glutathione
GTP	Guanine Triphosphate
H_2O_2	Hydrogen Peroxide
HEPN	Higher Eukaryotic And Prokaryotic Nucleotide
HPA	Health Protection Agency
HPD	Histidine Proline Aspartic Acid
HSP90	Heat Shock Protein 90
IMM	Inter Mitochondrial Membrane
IOSCA	Infantile Onset Spinocerebellar Ataxia
IP3R	Inositol 1,4,5,-Triphosphate Receptor
JNK	C-Jun NH2-Terminal Kinase
kDa	Kilodalton
MAM	Mitochondria Associated Membrane
MAPK	Mitogen-activated protein kinases
MEF	Mouse Embryonic Fibroblasts
Mff	Mitochondrial Fission Factor
Mfn	Mitofusin
MiD49/51	Mitochondrial Dynamics Proteins of 49 and 51 kDa
MIRAS	Mitochondrial Recessive Ataxic Syndrome
MLD	Metachromatic Leucodystrophy
MLS	Mitochondrial Localisation Sequence
MnSOD	Manganese Superoxide
MOPS	3-(N-Mopholino)Propanesulfonic Acid
mRNA	Messenger Ribonucleic Acid
MSUD	Maple Syrup Urine Disease
mtDNA	Mitochondrial Deoxynucleic Acid

MTP18	Mitochondrial Protein 18kDa
Nac	N-Acetyl-L-Cysteine
NADH	Nicotinamide Adenine Dinucleotide
NER	Nucleotide Excision Repair
Nfr1/2	Nuclear Respiratory Factor
NGS	Normal Goat Serum
O_2	Oxygen
OCR	Oxygen Consumption Rate
OH^-	Hydroxyl Ions
OMIM	Online Mendelian Inheritance In Man
OMM	Outer Mitochondrial Membrane
OPA 1	Optic Atrophy Protein 1
OXPHOS	Oxidative Phosphorylation
PACS2	Phosphofurin Acid Cluster Sorting Protein 2
PBS	Phosphate Buffered Saline
PCARP	Posterior Column Ataxia And Retinitis
PCR	Polymerase Chain Reaction
PD	Parkinson's Disease
PEMT	Phosphatidylethanolamine Methyltransferase
Pen/Strep	Penicillin/Streptomycin
PEOA1	Progressive External Opthalmopegia With Mitochondrial DNA Deletions, Autosomal Dominant Type1
PGC1α	Peroxisome Proliferator Activator Receptor Gamma Co-Activator 1 A
PINK1	Pten Inducing Kinase 1
PKA	Protein Kinase A
PMP70	Peroxisome Membrane Protein 70
PolyQ	Poly Glutamine
PP2A	Protein Phosphatase 2A
PS1	Presenilin 1
PtdCho	Phosphatidylcholrine
PTDSS2	Phosphatidylserine Synthase 2
PtEt	Phosphatidylethanolamine
PtSer	Phosphatidylserine
Qpcr	Quantitative Polymerase Chain Reaction
Rad23A	Radiation-Sensitive Mutant 23A
RD	Refsum Disease
RNA	Ribonucleic Acid
ROS	Reactive Oxygen Species
RT-PCR	Real Time PCR
SAC	Sacsin
SAD	Sporadic Alzheimer's Disease
SCA	Spinocerebellar Ataxia
SCAN1	Spinocerebellar Ataxia With Axonal Neuropathy SCAN 1
SCRM	Scrambled

SDS	Sodium Dodecyl Sulphate
SEC61b	Protein Transport Protein Sec 61 Subunit Beta
SEM	Standard Error Of The Mean
shRNA	Short Hair Pin RNA
SiRNA	Silencing RNA
SIRPT	Sacsin Internal Repeats
SLSJ	Saguenay Lac-St-Jean
SOCS6	Suppressor of Cytokine sigalling 6
SOD	Superoxide Dismutase
SPG3A	Spastic Paraplegia 3 Autosomal Dominant
SRR	Sacsin Repeated Region
SUMO	Small Ubiquitin Like Modifier
TALEN	Transcription Activator Like Effector Nucleases
TCA	Tricarboxylic Acid Cycle
TFAM	Mitochondrial Transcription Factor A
TGF	Transforming Growth Factor
TMRM	Tetramethylrhodamine Methyl Ester
TOM2o	Translocase Of Outer Membrane 20
UBL	Ubiquitin Like
VD	Variable Domain
VDAC	Voltage Dependant Anion Channel
VLCFA	Very Long Chain Fatty Acids
WND	Wilson's Disease
XPCB	Xeroderma Pigmentosum Complementation Group C-Binding

Chapter 1

Introduction

Autosomal recessive spastic ataxia of Charlevoix Saguenay (ARSACS) is a recessive cerebellar ataxia caused by mutations in the gene encoding the sacsin protein. The cellular role of sacsin and its involvement in the pathology of ARSACS has not been fully defined, although over the past few years sacsin has been linked to both proteostasis and the regulation of mitochondrial dynamics.

1.1 Cerebellum and Cerebellar Dysfunction

The cerebellum is a portion of the hind brain that plays an important role in regulation and co-ordination of motor control as well as the maintenance of posture and balance. The cerebellum has also been identified as important in cognitive affective syndrome. Depressive and anxiety symptoms and personality changes seem to be more frequent in patients with spinocerebellar ataxia (Wolf et al., 2009). The cerebellum is made up of a highly regular arrangement of several types of neurons including Purkinje cells and granular cells. While damage may not impair intellect or reflexive function, it disrupts co-ordination of voluntary muscular movement as well as balance and eye movements.

Cerebellar dysfunction usually results in a gait disorder with upper and lower limb dysmetria and hypotonia (Holmes, 1939, Draicchio et al., 2012). Cerebellar ataxia is an ataxia resulting from cerebellum dysfunction. Individuals with cerebellar ataxia may display a range of different symptoms. The most common deficits include nystagmus, dysarthria and dysdiadochokinesia (Harding, 1983). It is important to note, cerebellar ataxia is not in itself suggestive of a hereditary neurodegenerative disorder. Cerebellar ataxias can be acquired or sporadic (Manto and Marmolino, 2009, Klockgether, 2010). These symptoms can be induced by multiple system atrophy, immune and infectious disorders, toxic effects like alcohol abuse, metabolic disorders, stroke and paraneoplastic disorders (Iwanami et al., 2011, Sandyk and Brennan, 1984, Yabek, 1973, Papp and Dorsey, 2009)

Progressive unremitting cerebellar ataxias are diagnosed as neurodegenerative on the ruling out of acquired subacute chronic cerebellar ataxia and following the examination of cerebrospinal fluid in some circumstances and an MRI scan.

1.1.1 Inherited Cerebellar Ataxias

Inherited ataxias are a complex, heterogeneous group of neurodegenerative disorders characterised by progressive degeneration of the cerebellum and spinocerebellar tract. Clinnically hereditary ataxias are characterised by a cerebellar syndrome as described earlier. There are often additional neurological or systemic signs which are highly variable and depend on genetic subtype as well as on the individual phenotype (Manto and Marmolino, 2009). Inherited ataxias are classified into three groups based on mode of inheritance. These groups are Autosomal recessive, Autosomal dominant and X-linked Ataxia(Manto and Marmolino, 2009). Gene discovery technologies have meant identification of many of the causative genes associated with these disorders.

1.1.1 X-Linked Ataxia

X-Linked ataxias are very rare inherited ataxias with variable age of onset caused by mutations on chromosome X. Affected males display a slowly progressive ataxia with tremor, parkinsonism, autonomic dysfunction, polyneuropathy and cognitive deficits. The most recognised form of this ataxia is late onset, fragile X tremor ataxia syndrome (FXTAS). Patients with these forms of ataxia present with upper motor neuron signs, mild learning difficulty, Parkinsonism, dysdiadochokinesis and dysmetria (Berry-Kravis et al., 2007, Pagon et al., 1985).

1.1.2 Autosomal Dominant Ataxia

Autosomal dominant cerebellar ataxias (ADCA) are rare dominant disorders are often associated with neurological signs such as pyramidal and or extrapyramidal signs, cognitive dysfunction and ophthalmoplegia (Harding, 1981, Harding, 1982, Harding, 1983). These disorders are usually described as late onset diseases despite having a

large variation in age of onset as well as disease progression (Harding, 1981, Harding, 1982, Harding, 1983). Due to clinical heterogeneity, ADCAs were initially difficult to distinguish. However, Harding's introduction of an ADCA classification in 1982 (Table 1.1), which characterised these ataxias by clinical phenotype, has since improved diagnostic criteria. Although this classification was useful, making a reliable diagnosis on clinical grounds alone proved to be difficult due to the large overlap of clinical phenotype amongst ADCA individuals. Gene identification and new techniques in genetic sequencing have led to these disorders being better characterised and the replacement of Harding's classifications with the Spinocerebellar ataxia (SCA) classification. The SCA classification couples clinical phenotype with genetic subtype, based on the disease associated gene or chromosomal locus. There are over 30 reported SCAs, the disease locus has been identified in approximately 1/5 of them (Table 1.2) (Bird, 2014).

Classification of Autosomal Dominant Cerebellar Ataxia

Group	Autosomal Dominant Cerebellar Ataxia
I	Autosomal Dominant ataxia with ophthalmoplegia optic atrophy, dementia, extrapyramidal features and amyotrophy.
II	Autosomal Dominant ataxia with pigmenary retinal degeneration
III	Autosomal Dominant ataxia with 'Pure' cerebellar syndrome and late onset (60 years or older) without ocular or extrapyramidal features or dementia
IV	Autosomal Dominant ataxia with myoclonus and deafness

Table 1.1 Group classifications of autosomal dominant cerebellar ataxia. This grouping preceded SCA classification. Adapted from AE Harding Brain 1982

The majority of autosomal dominant cerebellar ataxias are associated with genes containing unstable expanded trinucleotide repeats. A polyglutamine (PolyQ) expansion within the coding regions of the respective genes, account for Spinocerebellar Ataxias; SCA1, SCA2, SCA3, SCA6, SCA7, SCA17 and Dentatorubral-pallidoluysian atrophy (DRPLA) (Durr, 2010), while trinucleotide or pentanucleotide repeat expansions in non-coding regions cause SCA8 SCA10, SCA11 and SCA12 (Moseley et al., 2006, Matsuura et al., 2000, Houlden et al., 2007, Holmes et al., 1999, Manto and Marmolino, 2009).

The PolyQ expansion in the resulting protein leads to a toxic gain of function (potentially coupled with loss of function), which in turn causes cell death and neurodegeneration (Todd and Paulson, 2010, Williams and Paulson, 2008, Liu et al., 2007, Ikeda et al., 1996, Burright et al., 1995). In the non-coding expansion SCA disorders, it is suggested that the CUG expanded RNA species is kept in the nucleus, hindering the processing of mRNA (Albin, 2003).

Interestingly, the severity of the ADCA is associated with length of polyglutamine tract. In the instance of SCA1 and SCA2 the length of the expanded allele inversely correlates to age of onset and disease phenotype (Geschwind et al., 1997), (Ranum et al., 1995, Durr, 2010). Polyglutamine expansions occur in other proteins associated with neurodegeneration, for example Huntingtin in Huntington's disease. The expansions tend to cause misfolding of the proteins and in turn disrupt protein homeostasis leading to aggregation of the mutant protein, like in SCA1. In addition, for SCA5, SCA 14, SCA13 and SCA27, point mutations in respective genes have been found to be pathogenic (Ikeda et al., 2006, Chen et al., 2003a, Herman-Bert et al., 2000, Brusse et al., 2006).

Autosomal Dominant Spinocerebellar Ataxias

OMIM	SCA	Gene	Locus	Protein
160120/ 108500	Episodic Ataxia Type1 EA1 / Episodic Ataxia Type 2 EA2	CACNA1A/ KCNA1	19p13.2	Calcium ion channel
169500	Leukodystrophy, demyelinating adult onset Autosomal dominant (ADLD)	LMNB1	5q23.2	Lamin B1
162350	Ceroid Lipofuscinosis, Neuronal, 4b Autosomal Dominant, CLN4B	DNAJC5	20q13.33	
128230	Dystonia, Dopa-responsive DRD	GCH1	14q22.2	Potassium channel
182600	Spastic paraplegia, Autosomal dominant, SPG3A	ATL1	14q22.1	
157640	Progressive external opthalmopegia with mitochondrial DNA deletions, PEOA1	POLG	15q26.1	DNA polymerase
137440	Gerstmann-Straussler	PRNP	20p13	
206700	Aniridia Cerebellar ataxia and mental retardation, ACA	PAX6	11p13	PAX6
164400	Spinocerebellar ataxia 1	ATXN1	6p22.3	Ataxin-1
601517	Spinocerebellar ataxia 2	ATXN2	12q24.12	Ataxin-2
109150	Machado-Joseph disease Spinocerebellar ataxia 3	ATXN3	14q13.12	Ataxin-3
600223	Spinocerebellar ataxia 4		16q22.1	
600224	Spinocerebellar ataxia 5	SPTBN2	11q13.2	beta-III spectrin
183086	Spinocerebellar ataxia 6	CACNA1A	19p13.2	
164500	Olivopontocerebellar atrophy III Spinocerebellar ataxia 7	ATXN7	3P14.1	Ataxin-7
608768	Spinocerebellar ataxia 8	ATXN8/AT XN8OS	13q21 /13q21.33	
603516	Spinocerebellar ataxia 10	ATXN10	22q13.31	Ataxin 10
604432	Spinocerebellar ataxia 11	TTBK2	15q15.2	tau tubulin kinase-2
604326	Spinocerebellar ataxia 12	PPP2R2B	5q32	
605259	Spinocerebellar ataxia 13	KCNC3	19q13.33	voltage-gated potassium channel, Shaw-

				related subfamily, member-3
176980	Spinocerebellar ataxia 14	PRKCG	19q13.42	
606658	Spinocerebellar ataxia 15	ITPR1	3p26.1	
607136	Spinocerebellar ataxia 17	TBP		TATA box binding protein
607458	Spinocerebellar ataxia 18		7q22-q32	
607346	Spinocerebellar ataxia 19		1p21-q21	
608687	Spinocerebellar ataxia 20	Duplica-tion	11q12	
607454	Spinocerebellar ataxia 21		7p21.3-p15.1	
610245	Spinocerebellar ataxia 23	PDYN	20p13	
608703	Spinocerebellar ataxia 25		2p21-p13	
609306	Spinocerebellar ataxia 26		19p13.3	EEEF2
69307	Spinocerebellar ataxia 27	FGF14	13q33.1	fibroblast growth factor-14
610246	Spinocerebellar ataxia 28	AFG3L2	18p11.21	
117360	Spinocerebellar ataxia 29		3p26	
613371	Spinocerebellar ataxia 30		4q34.3-q35.1	
117210	Spinocerebellar ataxia 31	BEAN	16q21	
613909	Spinocerebellar ataxia 32		7q32-q33	
133190	Spinocerebellar ataxia 34	ELOVL4	6p12.3-q16.2	
613908	Spinocerebellar ataxia 35	TGM6	20p13	
614153	Spinocerebellar ataxia 36	NOP56	20p13	

Table 1. 2 Autosomal Dominant Cerebellar Ataxias are a heterogeneous group of neurological disorders. Spinocerebellar ataxia (SCA) classifications has been assigned to the majority of these disorders. The disease causing gene or region has been identified in > 30

1.1.3 Autosomal Recessive Cerebellar Ataxia

Like the ADCA, autosomal recessive cerebellar ataxias (ARCA) are a group of clinically and genetically heterogeneous neurodegenerative disorders characterised by ataxia caused by progressive degeneration of cerebellum, spinocerebellar tracts of the spinal cord and associated structures. They are usually characterised by Purkinje cell degeneration and are loss of function disorders at the molecular level (Mariotti, 2001, Palau and Espinós, 2006). ARCA are usually early onset disorders with the age of onset usually under 20 years and are chiefly classified by their pathological mechanisms (Harding, 1983, Mariotti, 2001). Recessively inherited cerebellar ataxias are more difficult to classify than dominant ataxias in fact appropriate classification of ARCA has yet to be agreed. The heterogeneity amongst the ARCA makes their clinical diagnosis complicated. Previously, all early onset ataxias were deemed recessive, which led to misdiagnosed ataxias. In 1983 Harding based ARCA classification on age of onset and pathological mechanisms (Table 1. 3); (Harding, 1983). In recent years the development of molecular genetic studies has improved the diagnosis and classification of frequent recessive ataxias of unknown cause. The identification of novel loci and genes has led to an increase in the number of recognised ARCAs (Table 1. 4).

Classification of Autosomal Recessive Cerebellar Ataxia

Group	Ataxia
I	Cerebellum and brain stem development
II	Mitochondrial energy generation
III	Intermediate metabolism
IV	DNA repair
V	Cerebellar integrity mechanism

Table 1. 3 Autosomal Recessive Cerebellar Ataxias were placed into one of five classifications based on age of onset and the pathological mechanisms of the disease. Adapted from AE Harding 1983

Autosomal Recessive Cerebellar Ataxia

OMIM	ARCA	Gene	Locus	Protein
277460	Ataxia with vitamin E deficiency (AVED)	α-TTP	8q13	Alpha-tocopherol transfer potein
208900	Ataxia telangiectasia (AT)	ATM	11q22.3	Phosphatidylinositol 3 kinase
208920/606002	Ataxia Oculomotor apraxia 1 (AOA1)/ (AOA2)/SCAR1	APTX/SETX	9p13/9p34	Aprataxin/Sentaxin
607250	Spinocerebellar ataxia with axonal neuropathy (SCAN1)	TDP1	14q31	Tyrosyl-DNA phosphodiesterase 1
604391	Ataxia-telangiectasia-like disorder (ATLD)	MRE1 IA	11q22.3	
271245	Infantile onset spinocerebellar ataxia (IOSCA)	C10 orf2	10q22.3-q24.1	Twinkle
229300	Friedreich's Ataxia. (FRDA)	FXN	9q13	Frataxin
270550	Autosomal recessive spastic ataxia of Charlevoix Saguenay(ARSACS)	SACS	13q12	Sacsin
248800	Marinesco-Sjögren syndrome	SIL1	5q32	
606175	Carnitine acetyltransferase deficiency (CRATD)	CRAT	9q34	Carnitine acetyltransferase

Table 1. 4 Genetic classification of ARCA. Autosomal Recessive Cerebellar Ataxias are associated with loss of function of specific cellular proteins.

1.1.4 Prevalent Forms of Autosomal Recessive Cerebellar Ataxia

1.1.4.1 Friedreich's Ataxia

Friedreich's Ataxia (FRDA, OMIM: 229300) is the most common autosomal recessive ataxia. The estimated carrier frequency is between 1 in 50 and 1 in 100, with a prevalence of 1 in 50000 (Cossée et al., 1999). First described in 1861 as a locomotive ataxia, Friedreich's is a degenerative disease characterised by progressive gait limb ataxia, lack of tendon reflexes in legs and loss of posture (Cossée et al., 1999, Campuzano et al., 1996, Dürr et al., 1996). Like the majority of ARCA, FRDA usually has an early age of onset. It is primarily caused by a homozygous expansion of Guanine-Adenine-Adenine (GAA) trinucleotide repeat in intron 1 of the frataxin gene (*FXN*) on chromosome 9q13. Normal *FXN* alleles can have up to 40 GAA repeats whereas repeats in disease associated alleles range from 100 to 1000 repeats, most commonly 700 to 800 repeats (Campuzano et al., 1996, Dürr et al., 1996). This expansion leads to a transcriptional defect of frataxin and hence results in a loss of protein function. Interestingly, although this trinucleotide repeat is in a non-coding region of the gene, both severity of the disorder and age of onset can be correlated to the length of expansion as observed in other trinucleotide expansion related disorders such as Huntington's disease (Dürr et al., 1996, Durr, 2010).

1.1.4.2 Ataxia Telangiectasia

Ataxia telangiectasia (AT, OMIM: 208900) is recognised as the second most common ARCA and the most common ataxia in children under the age of five years with a prevalence of 1:100000 (Swift et al., 1986). AT is characterised by cerebellar ataxia, which presents in early childhood, oculocutaneous telangiectases which appears between 2-8 years of age and progressive neurodegeneration. This disorder is due to mutations in *ATM*. ATM is involved in DNA damage checkpoint monitoring and the cellular response to DNA damage (Zakian, 1995, Lavin and Shiloh, 1997). Notably patients with AT have increased susceptibility to cancer, with the risk for malignancy in patients reported to be as high as 38% (Swift et al., 1991, Chun and Gatti, 2004). As

well as this, immunodeficiency with reduced levels of immunoglobulins IgA, IgE, IgG and T-cells have been described (Hecht and Hecht, 1990). Additionally endocrine and skin abnormalities have been associated with AT (Mariotti, 2001 (Hecht and Hecht, 1990). Commonly distinct phenotypes such as an altered age of onset as well as varying severity of disease in both FRDA and AT, have been attributed to the type of mutations in *FXN* and *ATM* respectively (Anheim et al., 2010, Dürr et al., 1996, Schöls et al., 1997, Berciano et al., 2005, Verhagen et al., 2009).

1.2 Autosomal Recessive Spastic Ataxia of Charlevoix Saguenay and Sacsin

1.2.1 Autosomal Recessive Spastic Ataxia of Charlevoix Saguenay

Autosomal Recessive Spastic Ataxia of Charlevoix Saguenay (ARSACS) is an early onset neurodegenerative disorder first described in 1978. ARSACS is the most common inherited disorder in the Saguenay Lac- St- Jean (SLSJ) and Charlevoix regions of Quebec with an elevated carrier frequency of 1 in 22 and an estimated incidence of 1 in 1932, from 1941-1985 (Bouchard et al., 1978, De Braekeleer et al., 1993). ARSACS has an autosomal recessive mode of inheritance showing no sex bias. ARSACS originated from French early settlers in Charlevoix and later in the SLSJ region between 1608 and 1838 (Charbonneau and Robert, 1987). Although previously described as a rare founder disorder in Quebec (Engert et al., 2000) additional ARSACS cases have been documented from a further fifteen countries in the last decade. ARSACS therefore has a worldwide distribution with distinct mutations observed in different countries and an increasing incidence.

1.2.2 ARSACS Clinical Features

The early signs of ARSACS are an unsteady gait with the tendency to fall as well as progressive ataxia at around 12 to 18 months. Progressive signs also include spasticity, dysarthria and distal amyotrophy (Bouchard et al., 1998). Early non progressive signs include increased tendon reflexes, prominent myelinated retinal fibres and bilateral abnormal plantar response (Bouchard et al., 1979a, Ouyang et al., 2006, Bouchard et al., 1998). ARSACS has a rapid disease progression in young adults, with severe denervation in distal muscles in most patients by their 3rd decade and consequential necessity for a wheelchair by their 5th decade. Neurological features of this disorder include atrophy of the superior cerebellar vermis, atrophy of the cervical spinal cord, progressive atrophy of cerebellar hemisphere, loss of Purkinje cells, abolished sensory nerve conduction with reduced motor nerve velocity and reported hypermyelination of retinal fibres (Bouchard et al., 1979b, Bouchard et al., 1998, Gerwig et al., 2010, Martin et al., 2007).

Specific markers such as atrophy of the superior cerebellar vermis can be found in hereditary and acquired cerebellar ataxias however, this occurs more precociously in ARSACS and is therefore used as a core component of the diagnostic criterion. It is usually observed on Magnetic resonance images (MRI) and computerised tomography (CT) scans even in young patients (Martin et al., 2007, Gerwig et al., 2010).

Hypermyelinated retinal nerve fibres were once described as unique to ARSACS (Bouchard, 1991). However, it has subsequently been realised this is not an essential feature of the disease as it is not always observed in patients without the common Canadian mutations, described later on in this section (Ouyang et al., 2006, Hara et al., 2005a, Grieco et al., 2004). A recent publication challenged Bouchard's initial diagnosis of retinal hypermyelination, based on insufficient histological evidence (Desserre et al., 2011). Desserre et al instead, describe a thickening of the peripapillar retinal fibres, which can be measured and is easily observed via fundoscopy. They have suggested that this is a more accurate form of diagnosis implying that the previous characteristic may have led to undiagnosed ARSACS (Desserre et al., 2011, Vingolo et al., 2011, Stevens et al., 2013).

Of interest, the autopsy of two ARSACS patients revealed dense lipofuscin-like granules present within the lysosomes of swollen neurons. Further analysis of lysosomal enzymes showed that they were within normal limits (Richter A et al., 1996).

Originally impairment of intellectual function was not found to be a defining feature of ARSACS as most patients had a verbal IQ which was within normal limits. However recently, cognitive and behaviour dysfunction was identified in two adult male siblings (Verhoeven et al., 2012b). Unlike FRDA, there is no cardiac involvement (Bouchard, 1991). Note, fertility is unaffected (Bouchard et al., 1998).

Although ARSACS has distinct clinical features used to assist diagnosis, there is a moderate overlap between ARSACS and FRDA/FARR clinical features, which can often lead to confusion. Friedreich's ataxia with retained reflexes (FARR) is a subset of FRDA where patients have a very early onset of the ataxia with preserved tendon reflexes. They have a higher tendency of skeletal deformities as well as hypopallesthesia in the lower limbs (De Castro et al., 1999). Especially in these cases, a positive ARSACS diagnosis depends on confirmation by genetic testing.

Phenotypically, ataxias can be misdiagnosed due to the clinical overlap observed in recessive and dominant forms of the disorder. Clinical diagnosis of these disorders includes the molecular analysis of ataxia-associated genes. The number of ARSACS patients and prevalence of the disease has dramatically increased over the past eight years due to the genetic screening of the *SACS* gene. Increased identification of pateints has also highlighted the phenotypic variability of ARSACS in which clinical characteristics identified in non-Quebec individuals have veered from those originally described by Bouchard et al in 1978.

1.2.3 Molecular Genetics

ARSACS was mapped to chromosome 13 in 1998 (Bouchard et al., 1998). Subsequent extensive genotyping and segregation analysis further refined that region to 1.58cM on chromosome 13q11 (Richter et al., 1999).

In 2000, mutations in *SACS* were identified as the cause of ARSACS. *SACS* was found to be expressed in fibroblast, brain, skeletal muscle and at low levels in pancreas (Engert et al., 2000). The *SACS* protein product, sacsin, was initially thought to be encoded by one large exon, however additional upstream exons were identified in 2006 and experimentally confirmed in 2009 by Parfitt et al (Parfitt et al., 2009, Ouyang et al., 2006). As of June 2014, >100 mutations have been identified in *SACS* from patients in Tunisia, Italy, Japan, the Nertherlands, Serbia, Hungry, France, Belgium, Spain, Turkey and the UK (Table 1. 5) (Anheim et al., 2010, Baets et al., 2010, Bouhlal et al., 2011, Breckpot et al., 2008, Criscuolo et al., 2004b, Criscuolo et al., 2005, El Euch-Fayache et al., 2003, H'mida-Ben Brahim et al., 2011, Kamada et al., 2008b, Ogawa et al., 2004b, Okawa et al., 2006, Ouyang et al., 2008, Richter et al., 2004, Shimazaki et al., 2007b, Takiyama, 2006, Vermeer et al., 2008, Yamamoto et al., 2005, Yamamoto et al., 2006, Engert et al., 2000). The majority of these mutations occur in the large exon, exon 9. The most common mutation, R2502X, is found in 97% of ARSACS patients in Quebec (Engert et al., 2000). This is one of two mutations identified in patients from this area. This along with the extent of linkage disequilibrium (LD) implies that this mutation has arisen from the same ancestral allele (Engert et al., 2000, Richter et al., 1999).

A direct phenotype-genotype correlation has recently been reported. Using collated clinical and mutation data from previous studies, Romano et al were able to describe a correlation of disease severity to mutations within 4 conserved regions of sacsin (Romano et al., 2013). This correlation will be discussed further in section 1.2.4.1 of this chapter. Increased identification of *SACS* mutations worldwide may shed light on the phenotypic heterogeneity in non-Quebec patients. Most distinctly, ARSACS patients identified outside of Quebec tend to have a later onset.

Of interest, three unusual cases of ARSACS lacking spasticity were identified in Japan (Shimazaki et al., 2005a, Shimazaki et al., 2007a, Miyatake et al., 2012). It is important to note that these patients were observed in adulthood and had severe peripheral nerve degeneration. This questions whether the lack of the spasticity is a unique phenotype or the degeneration has masked spasticity.

Once considered a core factor, retinal hypermyelination is now described as a variable feature of ARSACS as it was not found in patients from Japan, Italy, Belgium and the UK (Ouyang et al., 2006, Hara et al., 2007, Grieco et al., 2004, Pyle et al., 2012, Miyatake et al., 2012, Yu-Wai-Man et al., 2014, Garcia-Martin et al., 2013a, Garcia-Martin et al., 2013b). Such patients have been described to have an abnormal thickening of retinal nerve fibre layer, which predominate in the upper and lower temporal regions or retinal hypertrophy (Garcia-Martin et al., 2013a, Yu-Wai-Man et al., 2014, Masciullo et al., 2012, Desserre et al., 2011). This raises the question as to whether this classification should be added to the diagnostic triad of early onset ataxia, spasticity and neuropathy (Engert et al., 2000).

Neuropsychological testing in the initial Bouchard study showed the verbal IQ of ARSACS patients in the SLSJ region was within the normal limits (Bouchard et al., 1978). Since, studies by Takiyama and others have described intellectual impairment with markedly lower than average verbal IQ scores in patients from Japan, Italy and Turkey (Takiyama, 2006, Grieco et al., 2004, Criscuolo et al., 2004b, Hara et al., 2005b, Pyle et al., 2012, Verhoeven et al., 2012a, Richter et al., 1993, Richter et al., 2004). In addition to this, psychiatric symptoms including depression and psychosis were observed in four patients with late onset ARSACS (Mignarri et al., 2014). This study documents the psychiatric state of these patients soon after diagnosis, however it did not present details of psychiatric events which may have preceded onset.

In a recent UK whole-exome study, unexplained severe sensorimotor neuropathy affecting two siblings was attributed to *SACS* mutations (Pyle et al., 2012). Although neuropathy had been described in earlier publications, Pyle et al describe an increased damage of neurons, which was not previously mentioned. With such a difference in phenotype it does raise the question of whether these two siblings are indeed ARSACS

patients. With the expansion of clinical features in ARSACS it is important not to ignore that other genetic factors, independent of *SACS* mutations may also contribute these atypical phenotypes. The revolutionary approach of whole-exome sequencing has assisted the identification of causative variants in rare disorders. It has also allowed for potential diagnosis of patients who do not ascribe to the classical phenotype. The caveat is whether the phenotypes observed are solely due to *SACS* variants or if these differences are due to mutations in other genes that have been missed. The very experimental design of whole-exome sequencing relies on the depth of sequencing coverage. It is possible therefore to miss variants in the non-coding region, such as frameshifts, which has been the factor in a few instances (Gilissen et al., 2012, Bloch-Zupan et al., 2011).

Mutations in SACS

Mutation	Origin	Amino Acid Change	Protein Domain	Reference
216delT	Belgium	C72fs*76	HSP90-1	(Baets et al., 2010)
237insAfs*	Canada	S80Ifs*98		(Thiffault et al., 2013)
482delA	Japan	N161-fs*175	HSP90-1	(Kamada et al., 2008a)
414 C >G	Japan	Y138*	HSP90-1	(Shimazaki et al., 2012)
502 G> T	The Netherlands	D168Y	HSP90-1	(Vermeer et al., 2008)
600_604+1delAACAGG	Italy	I200M-fs*214	HSP90-1	(Terracciano et al., 2009)
602 C >A	Belgium	T201K	HSP90-1	(Baets et al., 2010)
814 C > T	Canada	R272C	HSP90-1	(Guernsey et al., 2010)
826 C > T	Italy	R276C		(Prodi et al., 2012)
922 C > T	Japan	L308F	HSP90-1	(Takado et al., 2007)
961 C > T	The Netherlands	R321*	HSP90-1	(Vermeer et al., 2008)
1184_1193delGTAACAGTGT	Japan	C395W-fs*407	HSP90-1	(Ouyang et al., 2006)
1190insAfs*	Canada	S397Kfs*405	HSP90-1	(Thiffault et al., 2013)
1228_1229delTT	Italy	S409fs*	HSP90-1	(Prodi et al., 2012)
1373 C >T		T458I	HSP90-1	(Synofzik et al., 2013)
1475 G> A	The	W492*	HSP90-1	(Vermeer et al., 2008)

	Netherlands			
1597 C > T	France	P536L	HSP90-1	(Anheim et al., 2010)
1647_1658del	Germany	L549_552del	HSP90-1	(Synofzik et al., 2013)
1667 T > C	Morocco	L556P	HSP90-1	(Baets et al., 2010)
2063delT	Japan	V687-fs*713		(Ouyang et al., 2006)
2076delG	United Kingdom	T692T fs*713		(Pyle et al., 2012)
2182 C >T	The Netherlands	R728*		(Vermeer et al., 2008)
2185+7748_9836 del12kb	Italy	G729_W3278del		(Prodi et al., 2012)
2387del	Germany	L796Yfs*13		(Synofzik et al., 2013)
2405 T > C	Japan	L802P		(Kamada et al., 2008b)
2881 C > T c11634ins A	Italy	R961*K3878fs*13		(Prodi et al., 2012)
2971 T > C	Belgium	C991R		(Baets et al., 2010)
2983 G > T	Germany	V995F		(Synofzik et al., 2013)
3161 T > C	Japan	F1054S		(Shimazaki et al., 2005b)
3328insA	Tunisia	I1110-fs*1111		(El Euch-Fayache et al., 2003)
3421_3422insAC	Belgium	L1141-fs*1150		(Baets et al., 2010)
3491 T > A	Belgium	M1164K		(Ouyang et al., 2006)
3585 delT	Tunisia	I1195-fs*1206		(El Euch-Fayache et al.,

				2003)
3769 G > T	Japan	G1257*		(Shimazaki et al., 2012)
3965-3966delAC	United Kingdom	G1322Vfs*1343		(Pyle et al., 2012)
12020 C>T	Japan	S4007F		(Miyatake et al., 2012)
4033 T > C	Japan	Q1345*		(Okawa et al., 2006)
4033insC	Italy	Q1345-fs*1349		(Criscuolo et al., 2004a)
4060 C > T	Italy	Q1354*		(Prodi et al., 2012)
4108 C > T	Italy	Q1370*		(Grieco et al., 2004)
4145_4146insA	Italy	H1382Qfs*		(Prodi et al., 2012)
4195 T > C	Turkey	C1398R	HSP90-2	(Richter et al., 2004)
4205 A > T	Canada	D1402V	HSP90-2	(Thiffault et al., 2013)
4593dupA	Italy	S1531fs*9	HSP90-2	(Prodi et al., 2012)
4724 G > C	Serbia	R1575P	HSP90-2	(Baets et al., 2010)
4744 G > A	Canada	D1582N	HSP90-2	(Thiffault et al., 2013)
4760 T > G	Belgium	H1587R	HSP90-2	(Baets et al., 2010)
4775_4776insA	Italy	I1592fs1	HSP90-2	(Prodi et al., 2012)
4954 C > T	Germany	Q16652*	HSP90-2	(Synofzik et al., 2013)
4957 G> T	The Netherlands	E1653*	HSP90-2	(Vermeer et al., 2008)
4882_4886 delCAGTT/insAGAA	Algeria	Q1628*	HSP90-2	(H'mida-Ben Brahim et al., 2011)

GC				
5125 C >T	The Netherlands	E1709*	HSP90-2	(Vermeer et al., 2008)
5143 A>T	The Netherlands	K1715*	HSP90-2	(Vermeer et al., 2008)
5151dupA	England	S1718fs*1736	HSP90-2	(Stevens et al., 2013)
5201_5202delAG	Japan	E1734G-fs*1736	HSP90-2	(Yamamoto et al., 2005)
5263-4delAA	Japan	K1755Vfs*1775	HSP90-2	(Shimazaki et al., 2012)
5544dupA	Germany	V1849Sfs*48		(Synofzik et al., 2013)
5629 C > T	Italy	R1877*		(Anesi et al., 2011)
5719 C >T	Italy	R1907*		(Prodi et al., 2012)
5836 T > C	Tunisia	W1946R		(El Euch-Fayache et al., 2003)
5948 C > T	England	S1983F		(Stevens et al., 2013)
5988-9delT	Japan	fs*1999		(Shimazaki et al., 2007a)
6006delA	Netherlands	R2002fs*2013		(Vermeer et al., 2008)
6093_6095delTTC	Serbia	S2032del		(Baets et al., 2010)
6172delT	Japan	S2058Lfs*2076		(Yamamoto et al., 2005)
6355C > T	Japan	R2119*		(Hara et al., 2007)
6352delT	England	F2131fs*2144		(Stevens et al., 2013)

6409 C > T	Algeria	Q2137*		(H'mida-Ben Brahim et al., 2011)
6890 T>G	Norway	L2297W		(Tzoulis et al., 2013)
6835insA	Italy	E2280Rfs*2291		(Grieco et al., 2004)
7121 T > C	Italy	L2374S		(Terracciano et al., 2009)
7250_7254del	Italy	T2417-fs*2429		(Grieco et al., 2004)
7255_7259	Italy	E2418fs*10		(Prodi et al., 2012)
7277 G > C	Germany	R2426P		(Synofzik et al., 2013)
7279 C > T	Belgium	R2426*		(Baets et al., 2010)
7374delT	Belgium	L2458Lfs*2474		(Baets et al., 2010)
7372_7376delCTTAT	Algeria	L2458-fs*2463		(H'mida-Ben Brahim et al., 2011)
7504 C > T	Canada	R2502*		(Engert et al., 2000)
7613 C > T	France	A2558V	HSP90-3	(Anheim et al., 2010)
8107 C > T	Spain	R2703C	HSP90-3	(Criscuolo et al., 2005)
8393 C > A	Morocco	P2798Q	HSP90-3	(Baets et al., 2010)
8401-8403del	Netherlands	E2801del	HSP90-3	(Vermeer et al., 2008)
8584 A > T	Germany	K2862*		(Synofzik et al., 2013)
	Japan	K2931-fs*2952		(Ogawa et al., 2004a)
8844delT	Canada	K2948-fs*2952		(Engert et al., 2000)
8920_8923dup	Germany	Y2975Ffs*29		(Synofzik et al., 2013)
9305_9306 insT	Germany	L3102Ffs*		(Synofzik et al., 2013)

9497_9498delTT	Canada	F3166*		(Thiffault et al., 2013)
9508C>T	Canada	R3170*		(Thiffault et al., 2013)
9742 T > C	Japan	W3248R		(Ogawa et al., 2004a)
9911_9912del	The Netherlands	L3304fs		(Vermeer et al., 2008)
10034 T > C	Italy	V3345A		(Prodi et al., 2012)
10290 C > G	Algeria	Y3430*		(H'mida-Ben Brahim et al., 2011)
10298delC	Turkey	T3433-fs*3458		(Richter et al., 2004)
10442 T > C	The Netherlands	L3481P		(Vermeer et al., 2008)
10517 T > C	Belgium	F3506S		(Breckpot et al., 2008)
10906 C > T	Belgium	R3636Q		(Baets et al., 2010)
10906 C > T	The Netherlands	R3636*		(Vermeer et al., 2008)
10954 C > A	Belgium	R3652T		(Baets et al., 2010)
10958 T > C	Belgium	F3653S		(Baets et al., 2010)
11012_11013delAA	Italy	Q3671Rfs*23	XPCB	(Masciullo et al., 2012)
11234_11235delTT	Belgium	L3745-fs*3746	XPCB	(Baets et al., 2010)
11242del688	Canada	3748fs3756*	XPCB	(Thiffault et al., 2013)
11265_11266delAT	Hungary	I3755-fs*3762	XPCB	(Baets et al., 2010)
11361-2insT	Japan	R3788Sfs*3820		(Shimazaki et al., 2012)
11375 C > T	Tunisia	R3792*		(Bouhlal et al., 2011)

11542_11544del	Germany	I3848del		(Synofzik et al., 2013)
11598delC	Italy	G3866fs*3		(Masciullo et al., 2012)
11624 G > A	Germany	R3875H		(Synofzik et al., 2013)
11707 C > T	Canada	R3903*		(Guernsey et al., 2010)
11829-32AGTT	Turkey	L3943-fs*3958		(Richter et al., 2004)
11984_11986dupTGT	Germany	L3995dup		(Synofzik et al., 2013)
12160 C >T	Netherlands	Q4054*		(Vermeer et al., 2008)
12220 G > C	Tunisia	A4074P		(El Euch-Fayache et al., 2003)
12232 C > T	Italy	R4078		(Prodi et al., 2012)
12428_12429insA	Italy	Y4143*		(Prodi et al., 2012)
12603 C > A	Germany	Y4201*		(Synofzik et al., 2013)
12847_12850delAGAG	Tunisia	Q4284-fs*4305		(Bouhlal et al., 2009)
12851_12854delAGAG	Algeria	E4284-fs*4307		(H'mida-Ben Brahim et al., 2011)
12973 C > T	Japan	R4325*	J-domain	(Yamamoto et al., 2005)
12982 delA	Italy	K4327fs*7	J-domain	(Prodi et al., 2012)
12991 C > T	Italy	R4331W	J-domain	(Prodi et al., 2012)
12992 G > A	Netherlands	R4331Q	J-domain	(Vermeer et al., 2008)
13027 G > A	Belgium	E4343K	J-domain	(Baets et al., 2010)
13048 G >T		E4350	J-domain	(Pyle et al., 2013)

13056 delT	Germany	F4352Lfs*11	J-domain	(Synofzik et al., 2013)
13132 C > T	Italy	R4378*	J-domain	(Anesi et al., 2011)
13352 T > C	Norway	L4451P		(Tzoulis et al., 2013)
13237 T > C	UK	Q4413*		(Terracciano et al., 2010)
13389 G > T	Tunisia	D4464Y	HEPN	(Bouhlal et al., 2011)
13523 A > C	Belgium	K4508T	HEPN	(Bouhlal et al., 2008, Baets et al., 2010)
13538 G > A	Germany	S4513N	HEPN	(Synofzik et al., 2013)
13645 A > G	Turkey	N4549D	HEPN	(Richter et al., 2004)
Del 0.7Mb 13q12.12				(Pyle et al., 2013)

Table 1. 5 Over 80 mutations in SACS have been reported. The mutations include missense, deletions, insertions and nonsense mutations.

1.2.4 Sacsin

Sacsin is a 520kDa multi-domain protein consisting of 4579 amino acids (Parfitt et al., 2009). Bioinformatic analysis of sacsin revealed regions of protein homology to protein domains of known function. These regions are; an ubiquitin like domain, three Heat Shock Protein 90 (HSP90) like regions, a Xeroderma Pigmentosum C-Binding domain (XPCB), a J-domain, and a Higher Eukaryote and Prokaryote Nucleotide binding domain (HEPN) domain (Figure 1. 1). As a multidomain protein, sacsin is likely to play several roles within the cell. Sacsin was described as a co-chaperone in 2009 due to its functional J domain and was postulated to be involved in protein homeostasis. These domains will be discussed further in the following section.

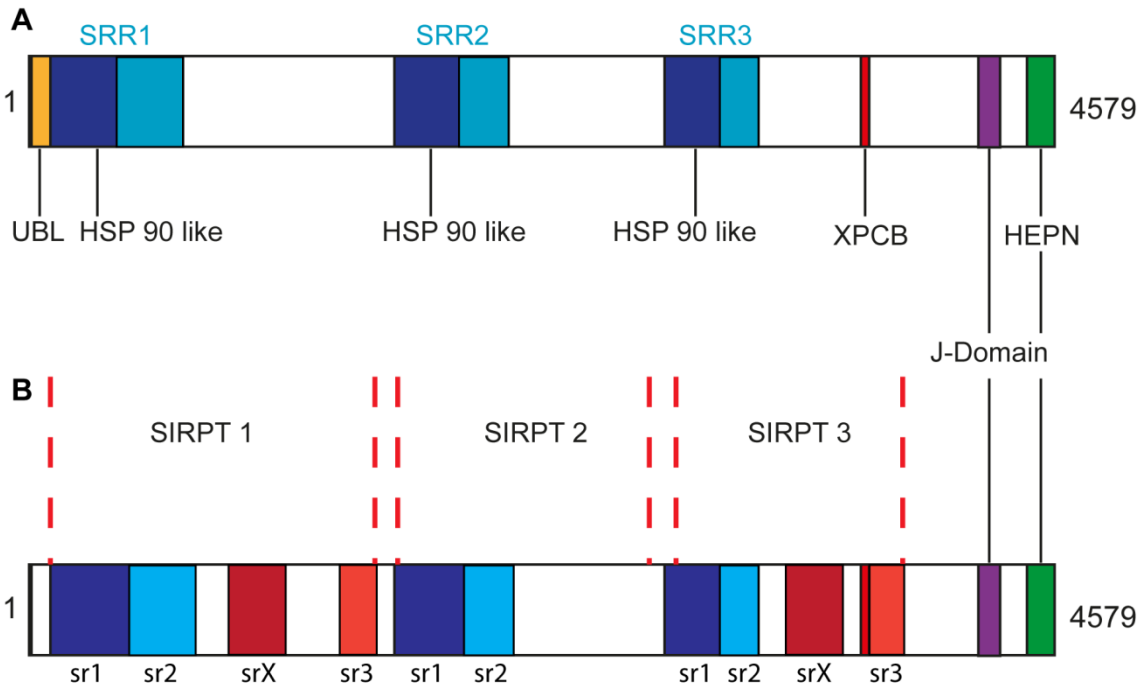

C

Domain	Region (amino acid)
UbL	1-69
HSP90	69-649
HSP90	1388-1785
HSP90	2509-2828
XPCB	3660-3755
J-Domain	492-4393
HEPN	4460-4567

Figure 1. 1 Sacsin is a multidomain protein

Schematic representation of sacsin domains. Sacsin is a large protein of 4579 amino acids with regions of similarity to known protein domains. Chaperone like activity has been reported in HSP90 like (blue) and J domain B) Schematic representation of SIRPTs and SIRPT subunits C) Domain and amino acid positions.

1.2.4.1 UbL Domain

The Ubiquitin like domain (UbL) domain is found at the extreme N-terminal end of sacsin. UbL domains are found in UbL proteins as well as in many proteins involved in signalling and in protein degradation (Madsen et al., 2007, Beasley et al., 2012). Moreover the UbL domain has been identified in proteins linked to cancer and neurodegeneration including SCA1 and Parkinson's (Madsen et al., 2007, Beasley et al., 2012). These domains are capable of interacting with components of the proteasome, such as the 26S subunit (Hartmann-Petersen and Gordon, 2004, Madsen et al., 2007, Beasley et al., 2012). The UbL domain has been shown to act as a catalyst during the formation of UbL conjugates and plays a role in targeting ubiquitinated proteins for degradation as well as in some instances, facilitating binding of molecular chaperones (Hartmann-Petersen and Gordon, 2004). The UbL domain of Rad23 and its human

homologs hHR23A/B was reported to interact with the S5a subunit of the 26S proteosome (Schauber et al., 1998, Kamionka and Feigon, 2004). Interestingly the UbL sequence of sacsin was shown to be 43% similar to the UbL domain found in yeast DNA repair protein, Rad23 and is predicted to be functional as it interacted with the proteosome (Parfitt et al., 2009). In the 2009 paper from the Chapple group, the 20S proteosomal alpha subunit C8 was shown to co-immunoprecipitate with flag tagged N-terminus of sacsin (residues 1-124). Mutation of conserved alanine residues in the UbL domain was demonstrated to reduce the co-immunoprecipitation of C8, hence confirming the interaction (Parfitt et al., 2009).

1.2.4.2 HSP90 Like Domains

Sacsin is described as having three large internal regions of sequence similarity which consist of a region homologous to the N-terminal domain of HSP90, but lack the C-terminus of HSP90 (Anderson et al., 2010, Engert et al., 2000, Parfitt et al., 2009). Recently, these repeats have been shown to have more extensive regions of self homology and have been newly termed as sacsin repeat regions (SRR) (Figure 1. 1A).SRR were found to be conserved in Eukaryotes, Bacteria and Archaea however these domains are not known to be conserved in common model organisms such as *Escherichia coli (E. Coli)* and *Caenorhabditis elegans (C. elegans*)(Anderson et al., 2010).

Biochemical analysis showed that the first, most N terminal SRR (SRR1) was able to hydrolyze ATP similar to yeast HSP90 (Anderson et al., 2010)**.** Interestingly, the ATPase activity of SRR1 was not inhibited by antibiotics geldanamycin or radiciol (Anderson et al., 2010). These antibiotics bind to the ATP site of HSP90 consequently inhibiting chaperone activity (Grenert et al., 1997, Panaretou et al., 1998). While the non-inhabitable nature of SRR1 is noteworthy, it is not uncommon. Insensitivity of HSP90 to geldanamycin and radiciol is also observed in *C.elegans* (Anderson et al., 2010, David et al., 2003). The authors attributed the insensitivity of SRR1 to it being too divergent from human HSP90. This is consistent with the observation that *C.elegans*, which shares 74% homology with human HSP90, also retained the ability to hydrolyze

ATP but like SRR1, lost sensitivity to these antibiotics (Anderson et al., 2010, Grenert et al., 1997).

Mutations within the SRR1/HSP90 domain may inhibit ATPase activity preventing the hydrolysis of ATP (Anderson et al., 2010). This was demonstrated by the introduction of ARSACS causing mutation D168Y, replacing conserved aspartic acid with tyrosine. This substituted an acidic negatively charged amino acid with one that is non-acidic with a neutral charge. While the mutation seems to abrogate ATP hydrolysis ability, it did not result in misfolding or aggregation of the protein domain (Anderson et al., 2010).

Surprisingly, this region was also demonstrated to have chaperone activity by a slight but significantly enhanced efficiency for refolding of firefly luciferase (Fluc) (Anderson et al., 2011). The refolding of denatured Fluc has been widely used to measure chaperone activity. Fluc is translated and conforms to its monomemeric multidomain structure during translation(Conti et al., 1996). Refolding of Fluc without assistance from chaperones can occur however this will be slow and inefficient due to minimal activity (Zako et al., 2000). Although it would seem unlikely that sacsin would have a general chaperone function it is important not to rule out a private chaperone role.

A moderate effect on yield of refolded Fluc, protection from the formation of aggregates and maintenance of protein conformation were shown to be functions of this N terminal region of sacsin. Moreover the assay used, showed that the sacsin region prevented Fluc aggregation and was capable of refolding Fluc independent of ATP (Anderson et al., 2011). The authors suggested that the moderate effects observed may be down to the fact that these assays can only interrogate the effect of a small fragment of sacsin. The author also suggests that any chaperone effects may be enhanced *in vivo* (Anderson et al., 2011).

Most recently, the structure of these SRR regions have been further classified by Romano et al. They described three large (>1100 amino acids) homologous repeated regions that they have called Sacsin Internal repeats (SIRPTs) (Romano et al., 2013). These SIRPTs are much larger than the SSR previously described and are conserved in

vertebrates (Figure 1. 1B). The putative domains incorporated three further subunits, sub repeat (sr) sr1, sr2 and sr3 (Figure 1. 1B). Sr1 and sr2 corresponded to the SRRs identified by Anderson et al while sr3 was not previously reported. A further region, sr-x was hypothesised in SIRPTs 1 and 3. This subunit was not previously identified in any other studies.

Romano et al considered the functional significance of the SIRPTs domains by mapping the pathogenic ARSACS missense mutations. These missense mutations were seemingly concentrated in conserved regions of the SIRPTs while non pathogenic single nucleotide polymorphisms (SNPs) were found in the non-conserved regions (Romano et al., 2013). In addition, to further show that these domains were significant, the study attempted to correlate previously reported ARSACS mutations within the SIRPTs with clinical phenotype and severity. Clinical severity of the disease in the patients was quantified by the SPAX score rating method (Romano et al., 2013). The SPAX score is based on the main clinical features of ARSACS (including spasticity, peripheral neuropathy and retinopathy) and combined the rating of Cerebellar Ataxia, Spastic Paraplegia and Charcot-Marie- Tooth Neuropathy score developed by Schmitz-Hütsch et al, Schüle et al and Murphy et al respectively (Murphy et al., 2011, Schüle et al., 2006, Schmitz-Hübsch et al., 2006). Compiling and scoring genotype and clinical data collected from patients in previous reports, Romano et al were able to show that patients with truncated sacsin had a higher Spastic Ataxia (SPAX) score than patients with missense mutations (Romano et al., 2013). The SPAX scores from patients with missense mutations in the SIRPTs varied, however it was noted that the scores on average decreased from sr1 to sr3 and sr-x (Romano et al., 2013). This implied that the lower scoring subunits sr3 and sr-x had a “minor” role in sacsin function and hence correlated to a less severe clinical phenotype (Romano et al., 2013). This study suggested that a phenotype/genotype correlation was evident in the patients presented and that the findings described support functionality of the novel domains. While informative, it is important to note that the patient subset used was quite small and that no biochemical analysis was performed. The patients within the subset however, were from different countries and included only one of the patients from the

SLSJ region (Engert et al., 2000). It is important to highlight that the majority were European patients without the common mutation.

1.2.4.3 XPCB

Xeroderma Pigmentosum C-Binding domain (XPCB) is a 75 residue protein-protein interaction domain. This domain consists of five amphipathic helices creating a mostly hydrophilic surface with a large hydrophobic patch (Kamionka and Feigon, 2004). The hydrophobic patch is the suggested region of protein interaction with the XPC protein (Kamionka and Feigon, 2004). This region is reportedly involved in nucleotide excision repair (NER) through the formation of XPC-hHR23A protein complex (Kamionka and Feigon, 2004, Sugasawa et al., 1998). The binding of XPC to the XPCB domain of hHR23A allows for the detection and subsequent repair of damaged DNA (Kamionka and Feigon, 2004, Sugasawa et al., 1998). It was suggested hHR23A/B function relies on the recruitment and interaction of S5a via its UbL, which in turn assist in the folding of XPC protein bound at the XPCB domain (Kamionka and Feigon, 2004). Interestingly, the XPCB of sacsin shares 35% sequence similarity with the XPCB domain of hHR23A/B, the human homologs of yeast protein Rad23 (Kamionka and Feigon, 2004). Markedly, other than sacsin, this domain has limited sequence homology with other proteins outside of the Rad23 family (Kamionka and Feigon, 2004).

Sacsin shares a potential interacting partner with Rad23, the protein UBE3A (Greer et al., 2010). UBE3A is an E3 ubiquitin ligase which is mutated in the neurodevelopmental disorder Angelman syndrome. Sacsin was found to be ubiquitinated in normal mice however levels of ubiquitinated sacsin were reduced in UBE3A knock-out mice, suggesting that sacsin is ubiquitinated by UBE3A via XPCB binding (Greer et al., 2010).

1.2.4.4 J-domain

Sacsin was initially suggested to be involved in chaperone mediated protein folding due to the presence of HSP90 like domains and a J-domain at the C terminus end (Engert et al., 2000). Sacsin's J-domain shares 60% homology to the HSP40/Hdj1 including the conserved histidine-proline-aspartic acid (HPD) motif(Parfitt et al., 2009). The presence of this domain suggested that sacsin may function with a HSP70 partner (Kelley, 1999). In 2009 Parfitt et al used a bacterial complementation assay to demonstrate that the J-domain of sacsin is functional. In this assay, the E.Coli strain OD259 containing disrupted genes for DNAJ and CbpA was used. This disruption prevents the growth of the bacteria at temperatures of 37°C and above. These strains have however been shown to grow at 37°C the once the lack of a functional DNAJ is compensated by the DNAJ of Agrobacterium tumefaciens (*Agt*) or other Agt-chimeric proteins. In this instance the J-domain of Agt was substituted with the J-domain of sacsin (DNAJ-sacsin). The complementation assay demonstrated that the DNAJ-sacsin allowed for growth of the E.Coli OD259 strain at 37°C. Mutating the highly conserved HPD motif in the sacsin J-domain portion of this chimera abolished function, preventing the needed interaction with DNAK, an E.Coli HSP70 protein (Parfitt et al., 2009). These analyses demonstrating J-domain function, as well as the structure of the DNAJ domain, supported the earlier suggestion of sacsin being a type III HSP40 protein and strengthened its alternative classification as DNAJC29(Parfitt et al., 2009, Kampinga et al., 2009, Cheetham and Caplan, 1998).

1.2.4.5 HEPN

A Higher Eukaryote and Prokaryote Nucleotide binding domain (HEPN) at the C-terminal end of human sacsin has also been identified in zebrafish, pufferfish, mouse and rat sacsin orthologues. HEPN is widely distributed in eubacteria and archaea though restricted to animals in Eukaryotes. HEPN is postulated to have an important role in nucleotide binding, which is facilitated through the dimerisation of the domain and the formation of a complex with adjacent nucleotidyltransferase (Grynberg et al.,

2003). Crystal structures and computed models from bacterial proteins TT1696 and the kanamycin nucleotidyltransferase indicate that HEPN domain proteins exist as dimers and the dimer formation of the HEPN domain contribute to the binding of substrate (Kozlov et al., 2011, Pedersen et al., 1995).

Crystallization of sacsin's HEPN domain (residues 4441-4579) demonstrated it also forms a dimer (Kozlov et al., 2011). The folding and stability of the sacsin HEPN dimer was examined by introduction of a mutation to the dimer interface. Bacterial expression of the HEPN dimer with ARSACS mutation N4549D, was shown to yield insoluble protein which was unable to undergo correct protein folding and form a dimer (Kozlov et al., 2011). The destabilisation was suggested to be caused by the loss of two polar contacts. This loss was a result of the introduction of a charge at the dimer interface on the replacement of asparagines with aspartic acid (Kozlov et al., 2011).

In addition, electrostatic potential measurements demonstrated that the dimer forms a large positively charged cavity found to bind GTP with a micromolar affinity of one GTP per HEPN dimer (Kozlov et al., 2011). Of interest, no GTPase activity was detected. It is important to note that while this dimer can bind to ATP, the affinity was ten-fold lower than that of GTP (Kozlov et al., 2011).

These findings support the hypothesis that the HEPN domain may act as an energy store by "trapping" ATP required for ATP hydrolysis during chaperone function (Grynberg et al., 2003). Although this has not been functionally demonstrated, it is postulated that an increase in the concentration of the nucleotides ATP or GTP trapped by the HEPN binding site will stimulate an exchange of nucleotides onto HSP70 (Kozlov et al., 2011). Further development of this role of the HEPN domain has been hypothesised to be important for sacsin function (Kozlov et al., 2011).

1.2.5 Sacsin Function

1.2.5.1 Proteostasis

Sacsin's role in proteostasis was investigated by examining its recruitment to inclusions of mutant ataxin 1. Mutant ataxin 1 inclusions are a characteristic of autosomal dominant spinocerebellar ataxia, SCA1. They result from expanded polyglutamine tracts in the ataxin 1 protein leading to its misfolding and the formation of intranuclear inclusions (Klement et al., 1998, Irwin et al., 2005, Lieberman et al., 1999). It has been reported that these inclusions contain ataxin 1 interacting proteins, including molecular chaperones such as HSP70 and its co-chaperones as well as components of the UPS (Latonen, 2011, Parfitt et al., 2009, Jorgensen et al., 2007). It was also previously shown that inhibition of the proteosome led to fusion of ataxin 1 nuclear inclusions and an increase in size of the inclusion (Irwin et al., 2005). Moreover, type 1 HSP40 protein DNAJ homolog subfamily A member 1 (HDJ-2/DNAJA1), was shown to localise to the nuclear inclusions and suppress ataxin 1 aggregation (Cummings et al., 1998). Sacsin, a reported member of the ataxia interactomes, localised to ataxia 1 intranuclear inclusions in cells expressing green fluorescent tagged ataxin 1 (Parfitt et al., 2009, Lim et al., 2006). Reducing levels of sacsin by siRNA, led to an increased incidence of cells with the PolyQ expanded ataxia 1 intranuclear inclusions and resulted in toxicity in neuroblastoma cell line SH-SY5Y, suggesting that loss of sacsin is detrimental to proteostasis (Parfitt et al., 2009).

1.2.5.2 Mitochondrial Dynamics

Sacsin is involved in the regulation of mitochondria dynamics. A loss of sacsin alters the balance between mitochondrial fission and fusion, resulting in a more interconnected mitochondrial network (Girard et al., 2012). This was demonstrated in SH-SY5Y cells where a reduction in the level of sacsin protein led to an increase in mitochondrial volume. Moreover, fluorescence recovery after photobleaching (FRAP) showed a quicker rate of fluorescence recovery in SH-SY5Y cells co-transfected with green

fluorescent protein (GFP) tagged mitochondrial marker Mito-GFP and SACS siRNA than with control cells transfected with scrambled siRNA and Mito-GFP (Girard et al., 2012). The increase in GFP recovery of a bleached section of the mitochondrial network in the knockdown cells indicating an increase in GFP "mobility" is indicative of a more interconnected mitochondrial network. The mitochondrial morphology displayed in the *SACS* knockdown cells was similar to that seen in other reports where fission has been disrupted due to loss of fission proteins like Drp1.

In addition, the defective mitochondrial morphology was also observed in dermal fibroblasts of ARSACS patients. A hyperfused mitochondrial phenotype was described in dermal fibroblasts from patients carrying the major founder mutation in Quebec, 8844delT (R2502X). This phenotype is again indicative of dysfunctional mitochondrial dynamics and has been observed in cells where Drp1 function has been disrupted (Girard et al., 2012, Lee et al., 2004).

Sacsin knockdown cells were also shown to have impaired mitochondrial function. Mitochondrial membrane potential sensitive dye tetramethylrhodamine methyl ester (TMRM) was used to analyse mitochondrial function. A moderate decrease in fluorescence was observed in sacsin knockdown cells indicating a decrease in mitochondrial membrane potential. In addition to this, sacsin knockdown cells labelled with membrane potential sensitive MitoTracker and treated with mitochondrial uncoupler cyanide m-chlorophenyl hydrazone (CCCP), were observed to have a slower recovery of fluorescence than the scrambled controls. This difference is suggestive of a problem with either proton pumping by the respiratory chain or increased proton leakage (Girard et al., 2012).

As well as mitochondrial dynamics, a loss of sacsin affects the cellular distribution of mitochondria in neurons. Sacsin hippocampal neurons were treated with *SACS* shRNA lentivirus (Girard et al., 2012). An altered distribution of mitochondria was observed in sacsin knockdown neurons with mitochondria clustered in the soma and proximal dendrites. It was hypothesised that this may result in the loss of normal ATP levels along the length of dendrites and may contribute toward defects in dendritic development (Girard et al., 2012).

1.2.5.3 ARSACS Mouse Model

A mouse model for ARSACS has been generated to further investigate disease pathology. The null mice (SACS $^{-/-}$) were generated by replacing the majority of exon 9 of *SACS* with IRES-βGal cassette and a loss of sacsin message was confirmed by RT-PCR in the offspring of the founders (Girard et al., 2012). In investigating the neurodegenerative and neurodevelopment characteristics of ARSACS they found that at birth the SACS$^{-/-}$ mice had no observable difference in gross brain morphology when compared to their wild-type littermates however there was a significant decrease in the number of Purkinje cells in the cerebellum at 120 and 200 days. This age dependant loss of Purkinje cells similarly reflected the pathology of ARSACS patients. This study also described the thick and highly disordered dendritic fields observed in 120day *SACS*$^{-/-}$ mice. This added to the hypothesis that the disruption of dendrite morphology is due to the impaired delivery of mitochondria to the dendrites due to a loss of sacsin function (Girard et al., 2012).

1.3 Mitochondria Biogenesis, Dynamics and Disease

Mitochondria function as suppliers of cellular energy, producing the majority of ATP needed for cellular processes via oxidative respiration/oxidative phosphorylation (OXPHOS). As well as this role, they are important in the regulation of apoptosis and the cell cycle along with providing a counteractive response to harmful by-products of OXPHOS. Oxidative respiration produces water and CO_2 as by-products, plus potentially damaging reactive oxygen species (ROS). The rapid clearance of the ROS by antioxidant enzymes regulated by the mitochondria is required to prevent damage to the mitochondria and ultimately cellular damage and death (Alfadda and Sallam, 2012, Brieger et al., 2012, Broadley and Hartl, 2008). Furthermore, mitochondria are closely maintained and regulated to ensure optimal function. This maintenance of mitochondrial homeostasis and abundance involves mitochondrial dynamics and mitochondrial biogenesis (Attardi and Schatz, 1988).

Notably, mitochondrial defects are a feature of the pathogenesis of a range of diseases including age related degenerative diseases, Parkinson's and Alzheimer's disease. Mechanisms include mutations in mitochondrial DNA, mitochondrial dysfunction via oxidative stress, iron overload or deregulation of mitochondrial dynamics. The brain and central nervous system have high demands for energy and appear to be particularly vulnerable to changes in mitochondrial function.

1.3.1 Mitochondrial Dynamics

Mitochondria are highly dynamic structures that continuously undergo fission and fusion events. Mitochondrial dynamics controls essential processes involved in biogenesis, cell division, distribution of mitochondria within cells and clearance of damaged mitochondria by the process of autophagy (mitophagy). Fusion can protect mitochondrial function and the cell against high levels of mtDNA mutations (Chen et al., 2010). While fission is important in mitochondrial disposal and ensuring energy requirements are met at sites away from the cell body – this is crucial in neurons where dendritic projections and synapses can be remote from the cell body (Cho et al., 2013). The process and regulation of mitochondrial dynamics is not fully understood however, recent advances have been made in the identification of proteins involved in this process.

1.3.1.1 Mitochondrial Fusion

In mammalian cells, fusion is mediated by Mitofusin 1 (Mfn1), Mitofusin 2 and Optic atrophy 1 (OPA1). Mfn1, Mfn2 and OPA1 are large dynamin-family GTPases which coordinate mitochondrial fusion and are reliant on GTPase activity (Cerveny et al., 2007).

1.3.1.1.1 Mitofusin 1 and 2

Mfn1 and Mfn2 are localised to the outer mitochondrial membrane (OMM) of the mitochondria and directly promote fusion via trans-interaction (Figure 1. 3) (Koshiba et al., 2004). Specifically, these proteins were found to form homotypic and heterotypic oligomers in mouse embryonic fibroblasts (MEF) and initiate fusion via the oligomerisation of Mfn resulting in tethering of two adjacent mitochondria (Chen et al., 2003b, Koshiba et al., 2004).

Mfn1 and 2 are essential for embryogenesis. Reports show that Mfn1 and Mfn2 knockout and double knockout mice were not viable (Chen et al., 2003b). In the single knockout model, murine embryos died midgestation. This was postulated, in part, to be the result of underdeveloped placenta, leading to placental insufficiency (Chen et al., 2003b). The double knockout embryos died earlier and showed severe developmental delay (Chen et al., 2003b).

Reduced levels of Mfn1/2 were shown to dramatically increase mitochondrial fragmentation, due to imbalance of fusion and fission (Chen et al., 2003b). It was however reported that this increase in fission had no effect on total level of mtDNA (Chen et al., 2003b).

1.3.1.1.2 OPA1

OPA1 (optic atrophy 1) is found on the inner membrane (IMM) of the mitochondria and mediates fusion and cristae remodelling of the inner membrane (Delettre et al., 2000). Importation of OPA1 to the IMM is reliant on its mitochondria localisation sequence (MLS), found at the N terminus of the protein (Cho et al., 2010).

Like Mfns, OPA1 forms higher order structures during mitochondrial fusion which comes about through the tetramerization of OPA1 (Figure 1. 3) (Olichon et al., 2003). Its function was demonstrated to be dependent on Mfn1 but not Mfn2 (Cho et al., 2010, Cipolat et al., 2004). Mitochondria in Mfn2 knockdown MEFs were able to undergo mitochondrial fusion upon the overexpression of OPA1 (Cipolat et al., 2004).

Contrastingly, mitochondria in Mfn1 knockdown MEF cells did not respond to OPA1 overexpression and remained globular and fragmented in appearance (Cipolat et al., 2004).

Similarly to Mfn1/2, reduced levels of OPA1 resulted in an increase of small fragmented mitochondria (Olichon et al., 2003). In addition to this, the silencing of OPA1 in HeLa cells was shown to induce the apoptotic cascade and cause malformation of mitochondrial cristae (Olichon et al., 2003).

Mutations in these fusion proteins are associated with a number of diseases such as Charcot- Marie- Tooth disease type 2A (CMT2A) caused by mutations in Mfn2 and autosomal dominant optic atrophy (ADOA), caused by mutations in OPA1 (Eiberg et al., 1994).

1.3.1.2 Mitochondrial Fission

1.3.1.2.1 Dynamin Related Protein 1

Mitochondrial fission is regulated by dynamin related protein-1 (Drp1). Drp1 is a large GTPase protein that was suggested, like dynamin, to have a role in vesicle formation and or endocytosis due to its structural similarity to dynamin (Smirnova et al., 2001, Praefcke and McMahon, 2004).

Structurally, Dynamin and Drp1 are very similar. Both have a GTPase, Middle (MID) and GTPase effector domain (GED) (Figure 1. 2) (Faelber et al., 2011, Ford et al., 2011, Strack et al., 2012).

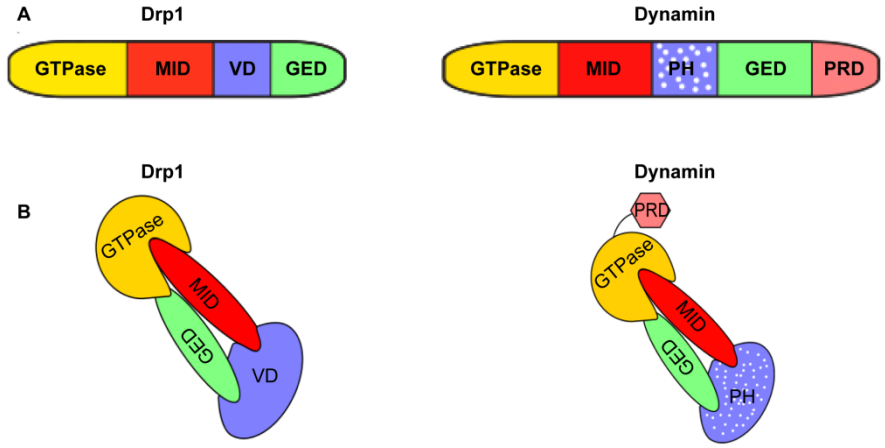

Figure 1. 2 Dynamin and Drp1 are structurally similar.

A-B) Schematic domain comparison of Drp1 and Dynamin domains. Drp1 and dynamin share GTPase (yellow), MID (red) and GED (green) domains. Drp1 however has a Variable Domain (VD) which is capable of modulating mitochondrial fission

The structures of the two proteins differ in the linker domain which separates the MID and GED domains. In Dynamin, this linker is a pleckstrin homology domain (PH) that mediates phosphoinositol lipid B binding (Strack et al., 2012, Figueroa-Romero et al., 2009, Ford et al., 2011). In Drp1 however this domain is replaced by a variable domain between amino acid residues 80-130 of the protein. The VD has eight SUMOylation sites that serve to regulate fission. Importantly, the VD is described as being an auto-inhibitory domain as it is capable of modulating fission. Strack et al demonstrated this to be the case as loss of the VD domain caused excessive fission brought about by increased localisation of the mutated form of Drp1 to the mitochondria (Figueroa-Romero et al., 2009, Strack et al., 2012, Chang and Blackstone, 2010b).

Drp-1 is an ~80kDa protein found as dimers/tetramers in the cytosol (Smirnova et al., 1998, Smirnova et al., 2001, Bhar et al., 2006). Drp1 shuttles between the cytosol and outer mitochondrial membrane (OMM) at potential sites of fission (Smirnova et al., 2001). Fission occurs through the oligermisation of Drp1 protein that forms spiral like structures at the OMM. GTP hydrolysis causes constriction of these oligomers and subsequent scission of the mitochondria (Ingerman et al., 2005, Mears et al., 2011, Smirnova et al., 2001) (Figure 1. 3).

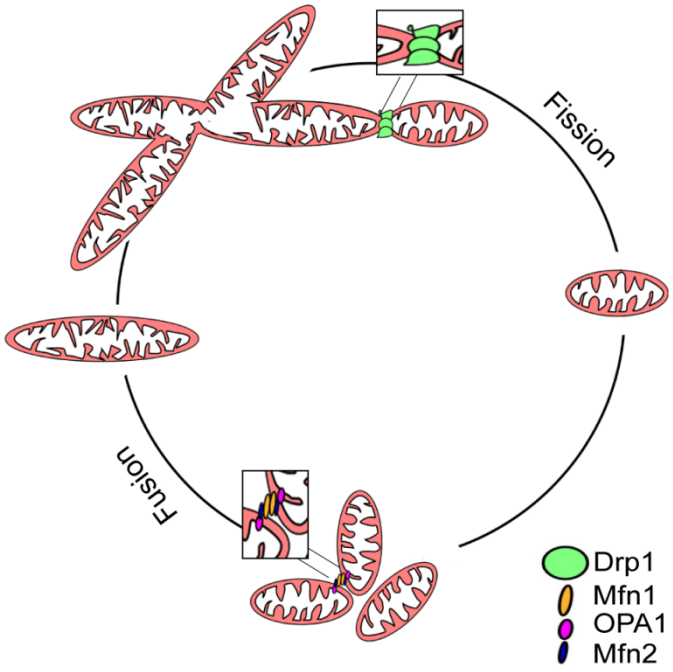

Figure 1. 3 Schematic representation of mitochondrial dynamics.

Mitochondria go through cycles of division and fusion in the cell. Mitochondrial dynamics are controlled by a group of GTPases which function in directing fission or fusion when required. Fusion is mediated by outer mitochondrial membrane proteins Mfn1 (yellow), Mfn2 (blue) and inner mitochondrial protein OPA1 (purple). For fission to occur, Drp1 (green) forms oligomeric spirals around the mitochondria. Fission is a result of scission caused by GTP hydrolysis.

Regulation of Drp1 recruitment to prospective sites of fission is not clearly understood. In yeast, Fis1p (hFis orthologue) recruits Dnm1p (Drp1 orthologue) to the mitochondrial outer membrane via Mdv1p or Caf4p adapter proteins (Mozdy et al., 2000, Tieu et al., 2002). This mechanism of recruitment is not thought to occur in higher organisms as there are no orthologues of Mdv1p or Caf4p in vertebrates. The role of hFis in Drp1 recruitment is controversial. Alternating levels of hFis has been reported to have no effect on Drp1 or on the levels of mitochondrial associated Drp1 (Lee et al., 2004, Suzuki et al., 2003). This along with the lack of adaptor proteins suggests that there are other factors involved in vertebrate mitochondrial fission regulation. To date five proteins, mitochondrial fission factor (MFF), MiD49, MiD51, MARCH-5 and endothelin, have been implicated in Drp1 recruitment in mammalian cells (Palmer et al., 2011b, Karbowski et al., 2004, Karbowski et al., 2007b).

Post-translational modification of Drp1 has a vital role in the regulation of Drp1 activity and function. Drp1 undergoes phosphorylation, SUMOylation and s-nitrosylation (Taguchi et al., 2007, Karbowski et al., 2002, Karbowski et al., 2007b, Wasiak et al., 2007). Phosphorylation of Drp1 can occur on either of two serine residues, each having separate effects.

Phosphorylation of Drp1 at serine 637 by calcium calmodulin dependant protein kinase 1 increases Drp1 translocation to the mitochondria (Han et al., 2008), whilst phosphorylation at the same residue by c-AMP dependant protein kinase inhibits Drp1 (Wilson et al., 2012). Notably Drp1 serine residue 637 is found on the border of the VD and GED. Phosphorylation of this residue is capable of disrupting fission by disrupting Drp1 assembly (Strack et al., 2012). Drp1 is known to be ubiquitinated by March V and Parkin E3 ligases. Moreover it has been postulated that regulation of fission can be initiated by ubiquitination mediated by March V (Karbowski et al., 2007a, Park et al., 2010).

Parkin ubiquitinates Drp1, targeting it for degradation by the proteosome (Gegg et al., 2010, Lutz et al., 2009, Van Laar et al., 2011).

Finally Drp1 is modified by small ubiquitin like modifier (SUMO). SUMOylation of Drp1 is thought to increase the recruitment of Drp1 to the mitochondria, but decrease the dissociation of Drp1 oligomers hence affecting Drp1 cycling and mitochondrial shape (Wasiak et al., 2007).

1.3.1.2.2 Mitochondrial Fission Accessory Proteins

MiD49 and MiD51 (MIEF1) have been recently described as mitochondrial fission proteins. At 49 and 51kDa respectively, these proteins are on the mitochondrial surface and were found to recruit Drp1. At low levels of expression, MiD49/51 form rings around the mitochondria in a similar pattern to the Drp1 spirals (Palmer et al., 2011a, Zhao et al., 2011).

Low level overexpression of MiD49/51 reportedly led to induced fission (Palmer et al., 2011b). While, Zhao et al and later Palmer et al demonstrate that greater levels of overexpression of MiD49/51 acts in a dominant negative manner by sequestering inactive Drp1 to the mitochondria, blocking fission and consequently promoting fusion by inducing Mfn1 and Mfn2 (Zhao et al., 2011, (Palmer et al., 2013).

Reduced levels of MiD49/51 brought about by siRNA, led to a decrease in Drp1 recruitment and an increase in mitochondrial fusion (Palmer et al., 2011a). Conversely, Zhao et al demonstrates that a knockdown of these proteins ultimately lead to a more fragmented mitochondria. It is also suggested that MiD49/51 can promote fusion of the mitochondria independent of mitofusins (Zhao et al., 2011).

MFF is localised to the outer mitochondrial membrane (OMM) and recruits Drp1 independent of Fis 1 (Otera et al., 2010, Gandre-Babbe and van der Bliek, 2008). Loss of MFF induced elongation of mitochondria while overexpression caused mitochondrial fission (Gandre-Babbe and van der Bliek, 2008, Otera et al., 2010). The interaction between MFF and Drp1 appeared to be transient, as it was only observable after chemical cross-linking (Gandre-Babbe and van der Bliek, 2008).

Briefly, Endothelin B1, assist the remodelling of the mitochondrial membrane during apoptosis (Karbowski et al., 2004). GDAP1 (ganglioside – induced differentiation associated protein) is located on the OMM. Loss of GDAP1 resulted in increased elongation of the mitochondria. Likewise loss of MTP18 (mitochondrial protein 18kDa) also led to increased elongation of the mitochondria upon treatment with RNAi, whilst overexpression of MTP caused Drp1 mediated fragmentation (Tondera et al., 2005).

The ER and cytoskeleton also contribute to the mitochondrial fission process. This is discussed in Chapter 5 of this thesis.

1.3.2 Mitochondrial Biogenesis

The formation of new mitochondria is regulated in response to cell cycle, energy requirements and cellular health as well as environmental stimuli by numerous transcription factors and signalling pathways (Attardi and Schatz, 1988, Moyes and Hood, 2003). Several molecular events ensure the succinct co-ordination of nuclear and mitochondrial genes that encode essential mitochondrial proteins and maintain the mitochondrial membrane (Figure 1. 4).

The key regulators controlling mitochondrial biogenesis are nuclear respiratory factor 1 (Nrf1) and nuclear respiratory factor 2 (Nrf2), mitochondrial transcription factor A (TFAM) and peroxisome proliferator activator receptor gamma co activator 1 α (PGC1α) (Wu et al., 1999, Evans and Scarpulla, 1990, Virbasius and Scarpulla, 1994). NRF1 and NRF2 regulate the expression of nuclear encoded mitochondrial protein whilst TFAM regulates and drives replication of mtDNA as well as transcription of mitochondrial proteins (Figure 1. 4). These three factors are regulated by PGC1α, which, once stimulated, coordinates the expression of genes involved in respiratory complexes by inducing the expression of Nrf1 and Nrf2 (Wu et al., 1999, Puigserver et al., 2001, Puigserver and Spiegelman, 2003) (Figure 1. 4).

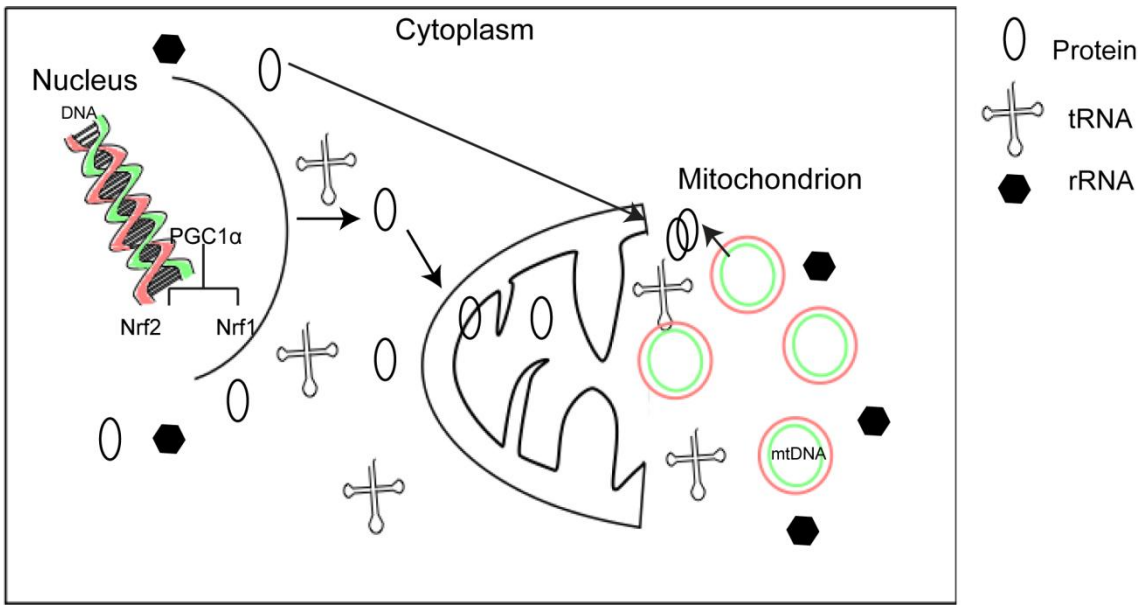

Figure 1. 4 Schematic representation of mitochondrial biogenesis.

The majority of mitochondrial proteins are encoded by nuclear genes while roughly 5% are encoded by mtDNA. Proteins synthesised in the cytosol as well as tRNA are then imported to the mitochondria where they can be utilised.

The biosynthesis of the majority of mitochondrial proteins also depends on the importation of proteins from the cytosol (Figure 1. 4). Proteins encoded by nuclear genes are synthesised in the cytoplasmic compartment prior to translocation to where they are needed in the membrane or matrix of the mitochondria. For instance, the function of mitochondrial redox carrier, complex 1, relies on importation of the NDUFS4 subunit from the cytoplasm (De Rasmo et al., 2008, Lee and Wei, 2005). mtDNA only encodes a small subset of proteins along with two rRNAs and twenty two tRNAs, therefore function of the enzyme complexes involved in respiration depend on correct assembly, coordinated by the interaction between products of mitochondrial genome and products of the nuclear genomes (Poyton and McEwen, 1996, Lee and Wei, 2005) (Figure 1. 4).

Mitochondrial disorders are caused by dysfunctional mitochondria. More specifically, they arise due to dysfunction of the respiratory chain, which can be a result of mutations in either nuclear DNA or mtDNA. Due to this, genetic classifications of these

diseases are known to be complex. Defects or rearrangements of mtDNA can either be heteroplasmic or homoplasmic and can involve tRNA, rRNA and mitochondrial proteins (Rahman and Leonard, 1997, DiMauro, 2004). Nuclear DNA encodes the majority of the respiratory complex and mitochondrial membrane proteins (Dimauro and Davidzon, 2005). Therefore, mutations in the protein's associated genes can give rise to mutated respiratory enzymes. In addition to this, mutations in the nuclear DNA can also lead to reduced transportation of mitochondrial proteins into the mitochondria and transcription of essential mitochondrial proteins (DiMauro, 2004, Lu and Claypool, 2015).

There is a diverse array of clinical features associated with mitochondrial disorders. Features can include; liver failure, hypoparathyrodism, hypogonadism, ataxia, peripheral neuropathy, dystonia, optic atrophy and cardiomyopathy, to name a few (Rahman and Leonard, 1997). Mitochondrial disorders may present at any age and is estimated to have a prevalence of 1:5000 (Thorburn, 2004, Kanabus et al., 2014). The heterogeneity of the disorder makes it complicated to treat, manage and diagnose affected individuals however advances in cell and animal models hold promise for future therapeutic strategies.

1.3.3 Mitophagy

The degradation of mitochondria is essential for the maintenance of healthy mitochondria as selective degradation of defective mitochondria can reduce the build up of potentially damaging toxins and maintain the efficiency of cellular respiration (Twig et al., 2008a, Kim et al., 2007).

The selective autophagy of mitochondria is via autophagic sequestration and subsequent hydrolytic degradation by lysosomes (Kim et al., 2007, Ding and Yin, 2012). Damage to the mitochondrion or induced mitochondrial permeability, leads to the depolarisation of the mitochondrion. This in turn results in the formation of autophagosomes followed by the fusing of autolysosomes and the degradation of the damaged mitochondrion (Kim et al., 2007)

Mitophagy is dependent on the mitochondrial fission. OPA1 overexpression, the reduction of Fis1 levels or overexpression of the dominant negative form of Drp1 have all been demonstrated to lead to reduced levels of mitophagy (Twig et al., 2008a). Interestingly, proteins such as Pten induced kinase 1 and parkin, which have been implicated in the neurodegenerative disease Parkinson's have been shown to be involved in the regulation of both mitochondrial dynamics and mitophagy (Vives-Bauza et al., 2010).

1.3.4 Mitochondrial Dysfunction in Neurodegenerative Disorders

The health of mitochondria is vital to the function and development of neurons, with dysfunction in many cases resulting in cell death. The role of mitochondrial dysfunction in neurodegenerative disorders and in particular cerebellar ataxias is becoming more apparent.

1.3.4.1 Mitochondrial Dysfunction in Ataxia

Mitochondrial dysfunction has been observed in several cerebellar ataxias. Fibroblasts from ataxia telangiectasia patients as well as thymocytes from ATM null mice have been demonstrated to have an imbalance of mitochondrial homeostasis resulting in dysregulation of mitochondria DNA (mtDNA) content (Eaton et al., 2007, Valentin-Vega et al., 2012). Inadequate removal of damaged mitochondria (mitophagy) causes an increase of defective mitochondria resulting in elevated levels of reactive oxygen species (ROS) in AT (Valentin-Vega et al., 2012).

Machado-Joseph disease models demonstrate reduced function of mitochondria due to decreased complex II activity (Laço et al., 2012). In addition, a decrease in the activity of antioxidant enzymes glutathione reductase, superoxide dismutase and catalase, was measured in SK-N-SH and COS-7 cells which expressed mutant ataxin-3. The authors suggested that these results contributed to the decrease in mtDNA copy number in SK-N-SH expressing mutant ataxin-3 and in the leukocytes of Machado-Joseph disease patients (Yu et al., 2009).

Cerebellar ataxias can be a result of mutations in mitochondrial proteins. Mitochondrial dysfunction in FRDA is predominantly due to mitochondrial iron overload caused by Fe-S disruption (Bulteau et al., 2004, Guillon et al., 2009, Rötig et al., 1997a, Campuzano et al., 1996, Babcock et al., 1997, Mühlenhoff et al., 2002). *FXN*, the causative FRDA gene, encodes 23kDa mitochondrial protein Frataxin. This protein is involved in the biogenesis of iron-sulphide (Fe-S) cluster (Rötig et al., 1997b, Lill et al., 2012), (Mühlenhoff et al., 2002). Fe-S clusters are inorganic co-factors, essential for many critical cellular processes. Iron metabolism, respiration and DNA repair are facilitated by the enabling of enzymatic complexes by Fe-S clusters. FXN deficiency therefore results in a disruption of many important pathways within the cell. Moreover Fe-S cluster deficiency leads to an impairment of mitochondrial respiratory chain, iron dysregulation and an increase in oxidative stress (Lodi et al., 1999, Schulz et al., 2000). As well as this, in 2000 Ristow et al demonstrated that FXN may also be important in oxidative phosphorylation and regulation of mitochondrial membrane potential (Ristow et al., 2000).

Mitochondrial dysfunction has also been observed in autosomal dominant ataxia SCA12. SCA12 is a late onset ataxia characterised by action tremor in the upper extremities in the fourth decade. It is associated with mutations in the gene *PPP2R2B*, encoding the protein phosphatase 2A (PP2A) Bβ regulatory subunit. Importantly this serine/threonine phosphatase has been shown to be involved in mitochondria mediated apoptosis (Dagda et al., 2003). CAG expansion within exon 7 of *PPP2R2B*, or its promoter region both account for SCA12 (Holmes et al., 1999, O'Hearn et al., 2012). The pathogenic expansions are usually 51 or more repeats. The pathogenic mechanism of the mutations has not been fully determined however dysregulation of the Bβ expression appears to contribute to the disorder.

Products of *PPP2R2B* are neuron specific regulators of PP2A and are essentially expressed during neurodevelopment (Dagda et al., 2003). Drosophila models of SCA12 developed by the overexpression of PPP2R2B drosophila homolog tws showed an increase in neurodegeneration, elevated levels of ROS, as well as increase in cytochrome c and caspase activity. Moreover, splice variants of Bβ regulate the translocation of PP2A to the mitochondria, where it has a role in regulating mitochondrial dynamics (Merrill et al., 2012, Dagda et al., 2003).

1.3.4.2 Mitochondrial Dysfunction in Alzheimer's Disease

Mitochondrial dysfunction also contributes toward age related neuronal disorders. In Alzheimer's disease (AD) elevated levels of ROS as well as signs of oxidative damage were identified in the brain. This was in the early stages of AD, preceding Aβ deposits (Rötig et al., 1997b). Aβ deposits induce mitochondrial dysfunction by inhibiting essential respiratory enzymes such as pyruvate dehydrogenase and cytochrome oxidase (Chen and Yan, 2007, Crouch et al., 2005, Casley et al., 2002). The oxidative stress caused by Aβ deposits induces fragmentation and abnormal distribution of mitochondria (Rui et al., 2006). Sustained elevated levels of ROS can also affect regulation of genes involved in maintaining mitochondrial biogenesis therefore leading

to irregular mtDNA replication, mitochondrial mass and expression of genes encoding respiratory complexes (Lee and Wei, 2005).

Over expression of mutant tau caused increased elongation of mitochondria and a decrease in mitochondrial localisation of Drp1 in Drosophila and Murine models of tauopathies (DuBoff et al., 2012). Moreover the altered mitochondrial dynamics led to enhanced neurotoxicity in these models. This was thought to contribute toward neurodegeneration observed in AD, although more evidence is needed to confirm that hypothesis. The study postulates that the blocking of the mitochondrial localisation of Drp1 is downstream of tau's ability to stabilise actin. Therefore excessive actin stabilisation alters mitochondrial fission through the dysregulation of Drp1 (DuBoff et al., 2012).

Tau models have been shown to have increased levels of ROS and accumulative oxidative stress which may plausibly lead to neurodegeneration following DNA damage and activation of apoptosis (David et al., 2005, Dias-Santagata et al., 2007). DuBoff et al demonstrated that increasing Drp1 and reducing MARF (fly homolog of Mfn) was capable of reducing superoxide and rescuing the elongated mitochondrial phenotype (DuBoff et al., 2012).

1.3.4.3 Mitochondrial Dysfunction in Parkinson's Disease

Damage caused by increased oxidative stress is also a feature of Parkinson's disease. Interestingly many genes implicated in Parkinson's disease have also been associated in the regulation of mitochondrial shape. Of interest both PINK1 (PTEN induced kinase 1) and Parkin are involved in the regulation of the balance between fusion and fission and mutations in these genes cause PD. Studies have demonstrated that loss of PINK1 and Parkin led to mitochondrial fragmentation and increased mitophagy (Exner et al., 2007, Lutz et al., 2009). Pink 1 and parkin are reportedly involved in mitochondrial homeostasis through a quality control pathway. Parkin has been demonstrated to translocate to depolarised mitochondria, where it ubiquitinylates proteins on the OMM causing a cascade which goes on to induce mitophagy. Pink 1 also accumulates

in damaged mitochondria and has been suggested to be an upstream regulator of parkin function, in which the recruitment of parkin is reliant on the kinase activity of PINK 1 (Vives-Bauza et al., 2010, Youle and Narendra, 2011, Narendra et al., 2010).

Mitochondrial protein complex 1 (NADH:ubiquinone oxidoreductase) is the first enzyme in the mitochondrial respiratory chain. It is involved in extracting energy from NADH through the translocation of protons across the inner mitochondrial membrane. Mutations in PINK1 and Parkin have been demonstrated to lead to an impairment of complex 1 activity resulting in decreased mitochondrial function (Morais et al., 2009, Mortiboys et al., 2008). Moreover, complex 1 inhibitors result in Parkinson's disease like phenotypes in cells and animal and has been shown to lead to neurodegeneration in mice (Perier et al., 2007, Duchen, 2004a).

1.3.4.4 Mitochondrial Dysfunction in Huntington's Disease

A decrease in ATP levels and increased cell death was observed in Huntington's disease. Increased levels of Huntington disease associated protein huntingtin (htt), induced mitochondrial fragmentation. Overexpression of *Mfn2* was shown to rescue these affects (Nakamura and Lipton, 2011). In addition, htt is thought to function in mitochondrial trafficking. Htt and the motor protein Dynactin, are bound through the mitochondria adapter protein Milton (Stowers et al., 2002, Trushina et al., 2004). Milton is required for the transportation of mitochondria along the axon to the synapse. In addition, Milton was also identified as a binding partner of PINK1 (Weihofen et al., 2009).

Further understanding on the link between morphology, dysfunction and disease is important for the advancement of research into neurodegeneration.

1.4 Aims and Objectives

This thesis aims to explore sacsin's role in the regulation of mitochondrial morphology and dynamics.

The mitochondrial morphology of neuroblastoma derived SH-SY5Y cells with reduced levels of sacsin, as well as the mitochondrial morphology of ARSACS patient fibroblasts carrying the Quebec homozygous *SACS* mutation 8844delT (R2502X), were respectively described by Girard et al as being more interconnected and having a hyperfused network (Girard et al., 2012).

In this thesis, chapter 3 aimed to further define the morphometric changes that occur to the mitochondrial networks of cells lacking sacsin. This chapter goes on to examine whether this morphology was also a phenotype in non-Quebec ARSACS patients harbouring different *SACS* mutations. To complete this objective, the mitochondrial morphology in fibroblasts from 4 Dutch ARSACS patients with compound heterozygous mutations and 4 controls were quantitatively and qualitatively compared using assays developed in the laboratory. These were based on confocal microscopy and image analyses. The morphometric analyses of the mitochondrial networks of cell lines from these patients are discussed.

The increased interconnectivity of the mitochondrial network observed in the fibroblasts of ARSACS patients, and previously in knockdown cells, were hypothesised to be the result of a dysregulation of mitochondrial dynamics (Girard et al., 2012). This phenotype along with the previously reported interaction of sacsin and Drp1 led to the postulation that sacsin was involved in mitochondrial fission. Studies have shown similar phenotypes in cells with reduced mitochondrial fission accessory proteins like Mff and MiD49/51 (Losón et al., 2013, Palmer et al., 2013, Gandre-Babbe and van der Bliek, 2008). Those studies demonstrated that the accessory proteins not only interacted with Drp1 but were also involved in Drp1 recruitment to the mitochondria (Losón et al., 2013, Palmer et al., 2013).

Leading on from the work described in Chapter 3, Chapter 4 is based on sacsin's potential role in fission and tests the hypothesis that it is involved in the recruitment of Drp1. To explore if Drp1 recruitment was impaired in cells lacking functional sacsin, the localisation of Drp1 in sacsin knockdown fibroblasts along with ARSACS patient fibroblasts was measured by two different means. These methods quantitatively assessed and allowed for the comparison of Drp1 localised to the mitochondria in sacsin knockdown, patient and control fibroblasts. In the first instance, the incidence of Drp1 foci associated with the mitochondria, per mitochondrial length in sacsin knockdown and patient fibroblasts was quantified by a technique developed for this thesis. The measurements were performed under basal conditions and again after mitochondrial fission had been induced by treatment with a mitochondrial uncoupler. Following on from this, the intensity and size of Drp1 foci was examined using confocal microscopy and image analysis software as a means of further assessing Drp1 dysfunction in ARSACS. In particular, we hypothesised that changes in the size of Drp1 foci may reflect problems with the formation of higher order Drp1 structures.

Chapter 5 further expounds on sacsin's role in Drp1 recruitment and consequent role in fission. The endoplasmic reticulum (ER) and the mitochondria share contact sites via mitochondria associated membrane (MAM), which allow for the uptake of ER released, Ca^{2+} into the mitochondria. Most interestingly, these contact sites have been shown to mark potential sites of mitochondrial fission and colocalise with mitochondria-associated Drp1 foci, implying that there is an involvement of the ER in mitochondrial fission (Friedman et al., 2011). Furthermore the ER is postulated to be important for the initiation of fission by constricting the mitochondria prior to the recruitment and oligomerisation of Drp1 (Schuldt, 2011). Changes in the size, tethering and number of contacts have been observed in neurodegenerative disease and in cells where essential mitochondrial dynamic regulatory proteins have been knocked down (de Brito and Scorrano, 2008, Area-Gomez et al., 2012). This chapter explores the hypothesis that sacsin's role in fission is through the mediation of Drp1 recruitment and not through an upstream event. This was examined by quantifying MAMs in sacsin

knockdown and patient fibroblasts using confocal microscopy and image analysis software.

Following on from this, mitochondrial fission accessory proteins such as MiD49/51, Mff and fission protein Drp1 have also been implicated in regulation of peroxisome fission (Palmer et al., 2013, Gandre-Babbe and van der Bliek, 2008, Waterham et al., 2007). Based on the hypothesis that mitochondrial fission proteins may also affect peroxisome morphology, sacsin's role in the regulation of peroxisome dynamics in our sacsin knockdown and ARSACS patient fibroblasts was investigated using confocal microscopy and image analysis software. A dysregulation of mitochondrial dynamics affects mitochondrial function in cells. This has been observed in cells where mitochondrial fission proteins have been reduced (Qian et al., 2012, Dagda et al., 2011, Hom et al., 2010). Moreover, a decrease in the mitochondrial membrane potential in sacsin knockdown cells has already been reported (Girard et al., 2012).

Chapter 6 addresses the mitochondrial function in ARSACS patient fibroblasts. Mitochondrial function was assessed by measuring cell metabolism and the production of mitochondrial superoxide in patient fibroblasts. Seahorse respirometer technology allowed for quantification of mitochondrial and glycolytic function in ARSACS patient fibroblasts and fluorogenic dyes allowed for the identification and quantification of mitochondrial superoxide production. In summary this chapter investigates the cellular bioenergetics and superoxide status of ARSACS fibroblasts.

Conclusions and details of potential future directions are detailed in chapter 7 of this thesis. Sacsin has a role in mitochondrial fission through regulating Drp1 recruitment from the cytosol to prospective sites of fission. Hence loss of sacsin leads to increased fusion due to impaired Drp1 recruitment. As a consequence, this results in increased superoxide production and reduced mitochondrial function in sacsin knockdown and patient cells. Reduced mitochondrial function can lead to cell degeneration therefore such reduction may contribute to loss of Purkinje cells, a feature of ARSACS. Future work on the regulation of Drp1 activity as well as refining the sacsin/Drp1 interaction domain is needed.

Chapter 2

Methods and Materials

2.1 Cell Culture

2.1.1 Culture of SH-SY5Y Cells

SH-SY5Y neuroblastoma derived cell line was purchased from the European Collection of Cell Cultures (ECACC) at the Health Protection Agency (HPA; Salisbury, UK). These cells were maintained in culture in 50% Dulbecco's Minimum Eagle Medium (DMEM)/50% F12 (Sigma, Poole, UK) supplemented with 10% heat inactivated Foetal Bovine serum (FBS; Biosera, East Sussex, UK) and 1% final concentration of penicillin and streptomycin (PenStrep) at 5U/ml and 50µg/ml respectively (Sigma, Poole, UK). Cells were kept at 37°C in a constant humidified atmosphere of 5% CO_2.

2.1.2 Culture of ARSACS Patient and Control Fibroblasts

Patient fibroblasts (Passage #4) and a control line were a kind gift from Dr Vermeer, Radbound University, Netherlands. Commercial human dermal fibroblasts were purchased from Promocell, Heidelberg, Germany. Additional cultured human dermal fibroblasts were supplied by Dr T McKay (Passage #5), Dr R Hannen (Passage #4) and Prof H A Navsaria (Passage #4) from Barts and the London, School of Medicine and Dentistry, Queen Mary University of London.

Fibroblasts were grown in Dulbecco's Modified Eagle Medium (DMEM) supplemented with 10% heat inactivated FBS (Invitrogen, Paisley, UK) and 1% final concentration of penicillin and streptomycin at 5U/ml and 50µg/ml respectively (Sigma, Poole, UK) (complete media) in a 37°C incubator in a constant humidified atmosphere 5%CO_2.

2.1.3 Maintenance of Cells in Culture

Cells were subcultured (passaged) into a new flask once they reached a confluence of 80-90%. Firstly, the growth medium was aspirated and the cells were washed twice in 5ml of Phosphate buffered saline without calcium and magnesium (PBS; Sigma, Poole, UK). After which the PBS was removed and cells were incubated in 1.5ml of

Trypsin/Ethylenediamine-tetraacetic acid (TE; Sigma, Poole, UK) at 37°C for 2 minutes or until cells had completely detached from the flask surface. Following this, 3.5ml of warm complete medium was added and the cell suspension was titurated to disperse cell clumps. Finally, 1ml of the cell suspension was placed in a new T75 flask, topped up with 9ml of complete media. Cells were then placed in 37°C, 5% CO_2 incubator. Unused cell suspension was disposed of in accordance with health and safety guidelines. Cells were split approximately every four days.

2.1.4 Freezing Cells

Cells were frozen for long term storage of low passage stocks. Growth medium (complete media) was aspirated and, cells were washed and trypsinized as described above. Once cells had become detached, 3.5ml of complete media was added and the entire cell suspension was transferred to 15ml Falcon tube. Cells were first centrifuged at 600g for 5 minutes after which, the supernatant was aspirated leaving a cell pellet. The pellet was fully resuspended in freezing solution consisting of 10% dimethyl sulfoxide (DMSO) and 90 %FBS. 1 ml aliquots of this new suspension were placed into cryogenic vials and stored in a Mr Frosty® (Thermo Scientific) freezing container at -80°C overnight. Mr Frosty® allows the cells to freeze at an optimal rate of -1°C/minute. The vials were transferred to liquid nitrogen the following day. When necessary, the cells were revived from frozen by quickly thawing in a 37°C water bath. The 1ml aliquot was transferred to a 15ml falcon tube and spun at 600g for 5 minutes. The supernatant was removed and the cells were resuspended in 10ml of complete medium and plated into a new flask. Flasks were incubated in a 5% CO_2, 37°C incubator and the growth media was changed the following day.

2.1.5 Cell Counting

The growth medium was removed and cells were washed twice in PBS and trypsinised as previously described. The cell suspension was transferred into 15ml tube and thoroughly resuspended using a pipette. 20µl of cell suspension was loaded into the injection area of the disposable C-Chip haemocytometer (Cronus technologies, Surrey, UK). Cells were counted in all of the large four corners (shaded in yellow) of one grid using 10x objective of a Leica DMIL light microscope (Figure 2. 1). The concentration of cells and volume needed to get required cell density were acquired using following formulae:

Cells per ml = average number of cells x dilution factor x 10^4 (volume factor).

$$C_1V_1=C_2V_2$$

C1 is the cell concentration of the stock solution

V1 Volume of stock solution required

C2 final concentration of diluted solution

V2 final volume of diluted solution

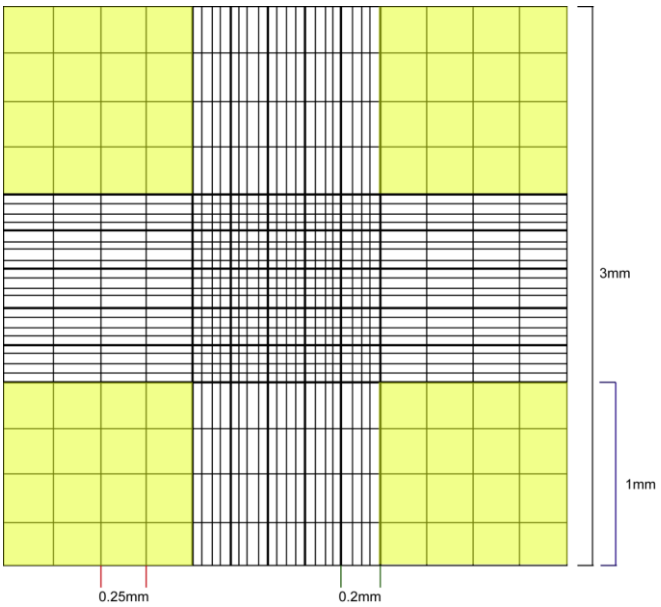

Figure 2. 1 Schematic of grid pattern of C-Chip disposable haemocytometer

Yellow shaded boxes represent areas where cells were counted.

2.1.6 Mycoplasma Testing

Cells were routinely sent for testing for mycoplasma contamination. Mycoplasma contamination has been shown to reduce respiration and cell metabolism in fibroblasts (Darin et al., 2003). Therefore this testing was essential as contamination of fibroblasts may have gone on to affect the sensitive assay used for assessing mitochondrial function through measuring cellular respiration. To carry out testing, fibroblasts were grown to 90% confluence in growth media lacking PenStrep. 100µl of growth medium was removed from cells and was boiled at 95°C for 5 minutes. The media was then briefly centrifuged to pellet any cell debris and the supernatant was removed and used in a polymerase chain reaction. The details of this are given in section 2.3.1. The presence of a band at approximately 300 base pairs on a 2% agarose gel signifies positive mycoplasma contamination (Figure 2.2).

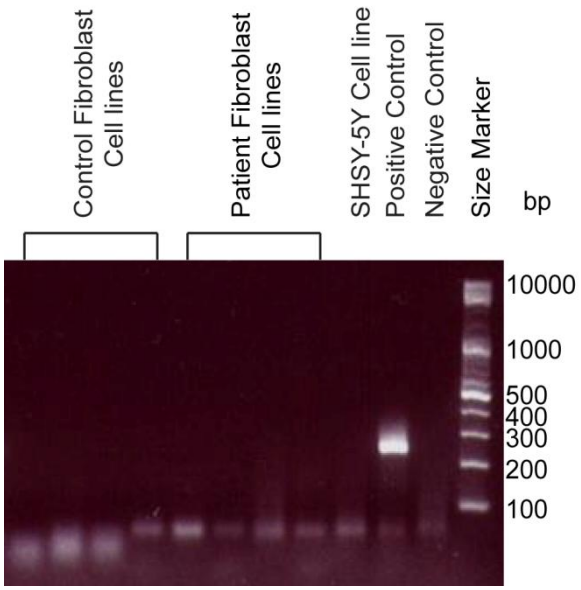

Figure 2. 2 Digital image of agarose gel electropherisis of Mycoplasma PCR.

All cell lines used were free of Mycoplasma contamination.

2.2 Genomic DNA extraction

For extraction of genomic DNA, cells were grown in 25cm^3 flask until 80-90% confluence in complete media. Media was aspirated and cells were washed twice in 3ml of PBS. Cells were then incubated with 2ml of TE until detached. TE was neutralised by the addition of 5ml of complete medium, cells were harvested and centrifuged at 400g for 5mins.

Genomic DNA (gDNA) was extracted using GenElute Mammalian Genomic Miniprep Kit (Sigma, Poole, UK). For harvesting, 200µl of resuspension solution was added to the cell pellet. As RNA free DNA was required, 20µl of Rnase A was added and the mixture was incubated at room temperature for 2 minutes. The cells were lysed by the addition of 20µl of Proteinase K (20mg/ml) followed by the addition of 200µl of Lysis Solution C. The mixture was vortexed for 15 seconds and then placed at 70°C for 10 minutes. Before using the GenElute columns, 500µl of column preparation solution was added and the column was centrifuged at 1200*g* for 1 minute to equilibrate the column. The homogenised lysated was mixed with 200µl of absolute Ethanol and vortexed for a further 10 seconds. The entire mixture was then added to the prepared GenElute column and spun at 6500*g* for 1 minute. The columns were washed twice with 500µl of wash solution PCR and centrifuged at 6500*g* for 1 minute in the first instance and then 12000g for 3minutes. DNA was eluted in 50µl of nuclease free water. The concentration of the DNA was measured using a nanodrop ND-spectrophotometer at λ=260nm. The ratio of absorbance at 260nm and 280nm was used to assess purity of the extracted DNA. DNA was deemed of good quality if 260/280nm = 1.8 – 2.

2.3 Polymerase Chain Reaction and Sequencing

2.3.1 PCR

The DNA extracted was incubated with DNA polymerase from *Thermus aquatius* (Taq), SACS primers to region of interest and dNTPs to allow amplification. PCR reaction mixtures were composed of the following:

2.5µl of 10x reaction buffer (Sigma, Poole, UK) (100mM Tris-HCL, pH8.3, 500mM KCL, 15mM $MgCl_2$,0.01% gelatin).

25-50ng of template

10µM forward primer

10µM reverse primer

0.2mM dNTPs

0.125µl of Taq DNA polymerase (Sigma, Poole, UK)

ddH_2O to a final volume 0f 25µl.

The thermocycling conditions were based on a standard PCR, where a primer specific annealing temperature of was used (Table 2. 1). The amplification proceeded over 35 cycles with the inclusion of a final extension step of 5 minutes. All PCR reactions were carried out on G-Storm GS1 thermocycler (G-Storm, Someset, UK). The PCR products were visualised on a 1% agarose gel using 1:20000 GelRed (Biotium, Hayward UK). 10µl of PCR reaction mixture was added to 3µl of sucrose loading dye and run, at 110 volts (V) in 1× Tris Acetate EDTA (TAE) buffer, with a suitable DNA sizing ladder.

Primer Name	Annealing Temperature (°C)
Mycoplasma	55
SACS (all)	59

Table 2. 1 Annealing Temperatures for Mycoplasma and SACS primers

2.3.2 Sequencing

Sequencing was carried out by the Genome centre, Barts and the London School of medicine and dentistry, Queen Mary University. 10µl of the PCR product was submitted along with primers of 10pmol/µl concentration. Prior to sequencing, 5µl of the PCR product was purified using ExoSAP-it. This purification was included in the service provided by the genome centre. Sequencing was carried out using BigDye 3.1 (Applied Biosystems) and visualised on ABI 3730. Sequencing results were analysed using sequence analysis software Finch TV (Geospiza, Washington, USA).

2.4 Transfection

Cells were seeded in either; 6 well plates, 12 well plates (VWR) or 8 well chamber slides (Nunc) until 70% confluence was reached. Cells were transfected using catatonic lipid mediated gene delivery using Lipofectamine and Plus reagent (Invitrogen, Paisley, UK) as per (Table 2. 2).

Vessel	Final volume (µl)	OptiMEM (µl)	Plus Reagent (µl)	DNA concentration	OptiMEM (µl)	Lipofectamine (µl)
8-well slide	100	12.5	1	100ng	84.5	1
12 well plate	400	50	2	500ng	341	2
6 well plate	700	100	4	1µg	591	4

Table 2. 2 Transfection mixtures used for different vessels for SH-SY5Y cells.

Briefly for a well of a 6 well plate, the mixture of 1µg of DNA, 100µl of serum free OptiMEM (Invitrogen, Paisely, UK) and 4µl of Plus reagent (Invitrogen, Paisely, UK) was incubated at room temperature for 20 minutes. 4µl of Lipofectamine (Invitrogen, Paisely, UK) and 591µl of OptiMEM was added to the mixture and incubated for 15 minutes at room temperature**.** Cells were washed twice in PBS before the addition of 700µl of the transfection mixture. DMEM containing 20% FBS and 2% PenStrep was added to the cells 3 hours post incubation at 37°C. Further cell processing occurred 24-48hour post transfection.

2.4.1 siRNA Transfection

Custom *SACS* siRNAs previously validated by our group were ordered from Ambion (Life Technologies LTD, UK). The siRNAs were designed to target exons 6, 7 and 9 of SACS. The lyophilised siRNAs were first resuspended in water to give a 100µM stock. The siRNAs were diluted to working concentration of 20µM for use in transfections where a final concentration of 20nM was required. Small volumes of the 20µM solution were aliquoted and stored at -20°C. For a well of a 6 well plate, the mixture of 0.7µl of siRNA (20µM), 100µl of serum free OptiMEM and 4µl of Plus reagent was incubated at room temperature for 20 minutes. 4µl of Lipofectamine and 591.3 µl of OptiMEM was added to the mixture and incubated for 15 minutes at room temperature. Cells were washed twice in PBS before the addition of 700µl of the transfection mixture. DMEM containing 20% FBS and 2% PenStrep was added to the cells 3 hours post incubation at 37°C. Further cell processing occurred 48 hours after transfection. In many instances EGFP (Clonetech Laboratories California ,USA) (green fluorescent protein) or pDsRed2-Mito (mtDsRed) (mitochondrial marker) (Figure 2. 7 SECTION 2.10) was co-transfected to indicate successful transfection. This was especially important in the fibroblasts cell lines where low transfection efficiency was obtained and therefore made verification of knockdown by immuoblotting difficult.

2.4.2 siRNA Sequences

Name of oligomers		Sequences
SACS exon 6	sense	GGAUGAUCCUCUGAAGGUC
	antisense	GACCUUCAGAGGAUCAUCC
SACS exon 7	sense	GCGGCCGAAUUCUAUAAAG
	antisense	CUUUAUAGAAUUCGGCCGC
SACS exon 9	sense	CGUAAGAUUUCUAGAUGAC
	antisense	GUCAUCUAGAAAUCUUACG

Table 2. 3 Sense and Antisense sequences of siRNA.

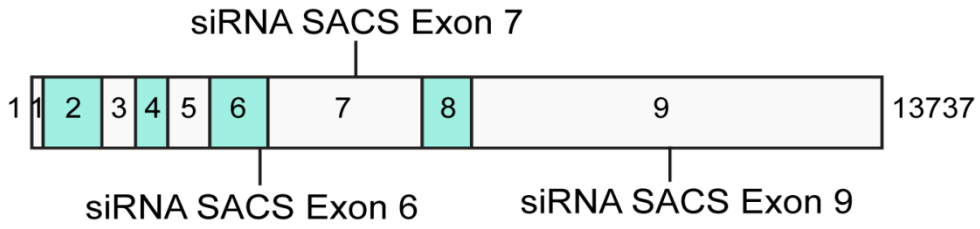

Figure 2. 3 Schematic of SACS mRNA.

The positions of SACS siRNAs used in relative to SACS mRNA is shown.

2.5 Western Blotting

2.5.1 Cell lysate preparation

Cells were harvested for separation by electrophoresis as follows. A T25 or single well of a six well plate at 80-90% confluence was used for each sample. Cells were washed in 1ml of cold PBS prior to the addition of 500µl of 2x Laemmli sample buffer consisting of 4%SDS, 20% glycerol, 10% Mercaptoethanol, 0.004% bromophenol blue and 0.125M Tris-HCL (Sigma, Poole, UK) to the cells surface. The cells were collected followed by homogenisation by passing the lysate through a 21G needle 10 times and boiling at 90°C for 10 minutes. The lysates were centrifuged at 18,500*g* for 1 minute before loading.

2.5.2 SDS-PAGE

The soluble fractions of cell lysates were run on precast 4-12% polyacrylamide NuPage BisTris gels (Invitrogen, Paisley, UK). The gels were electrophoresed in 1x 3-(N-morpholino)propanesulfonic acid (MOPS) running buffer (Invitrogen, Paisely, UK) consisting of 50mM Mops, 0.1% SDS, 50mM Tris and 1mM EDTA (pH7.7) along with high molecular weight marker HiMark or Novex (Invitrogen, Paisely, UK). SDS- PAGE gels ran for 2-3 hours at 150V.

2.5.3 Immunoblotting

Post electrophoretic separation, proteins were electrotransferred to a nitrocellulose membrane 0.45µm (GE Healthcare Life Sciences) by either semi-dry transfer using Trans-Blot cell (Bio-Rad, Hemel Hempsted, UK) or wet transfer using a mini Trans-Blot cell (Bio-Rad, Hemel Hempsted, UK). Wet transfer was used for sacsin blots. This method is usually recommended for transferring large, high molecular weight proteins greater than 100kDa as it yields a better transfer efficiency. Semi-dry transfer was used for proteins under 100kDa like Drp1. The nitrocellulose membrane and filter paper required were soaked in transfer buffer for 5 minutes prior to transfer. The transfer buffer consisted of 20mM Tris, 120mM glycine, and 20% methanol. Blots were transferred for duration of 45 minutes at 15V in instance of semi-dry transfer and 16 hours at 40V for wet transfers. After transfer, the membrane was stained with 0.1% Ponceau S (w/v) in 5% acetic acid to detect protein bands and to signify successful transfer. The membrane was destained by washing in PBST for 3 minutes on a shaking platform.

Following this, the membrane was blocked in a solution consisting of 5% semi skimmed milk powder in PBS with 0.1% Tween20 (PBST) for 1 hour. For the detection of sacsin, the affinity-purified antibody (r- sacsin$^{4489-4503}$) to the C-terminus of sacsin was used. This antibody was developed by our group and has been characterised in immunoblotting (Parfitt et al., 2009). R-sacsin$^{4489-4503}$ was used at 1:500 in 10ml of PBST (with 5% milk) for 3 hours. The membrane was then washed three times for 10 minutes. After incubation of the membrane for 1 hour with goat ant-rabbit IRDye800CW secondary antibody (Licor, Cambridge, UK) at a dilution of 1:10000 in 10ml of 5% milk PBST, the membrane was washed twice with PBST and once in PBS for ten minutes. The membrane was imaged using Licor Odessy infrared scanner and analysed using Licor Odessy, software (Licor, Cambridge. Densitometeric analysis was performed using Image Studio Lite (LiCor, Cambridge).

2.6 Measuring Mitochondrial Respiration and Glycolysis

The oxygen consumption rate (OCR) and extracellular acidification rate (ECAR) were assessed by the Seahorse XF^e96 Extracellular Flux Analyser (Seahorse Bioscience). The MitoStress (Seahorse Bioscience) and GlycoStress kit (Seahorse Bioscience) were also used in conjunction with Seahorse analyser to measure the response of the fibroblasts to mitochondrial and glycolytic stress.

Measurement of mitochondrial respiration and glycolysis was dependent on the creation of a transient microchamber in which the sensor cartridge and its sleeves was lowered to 200 µm above the cells (Figure 2. 4). This created a small volume of between 2-7µm. The sensor cartridge consisted of 2 fluorophores embedded in polymer. Each of the fluorophores distinctively measured either the quenching of oxygen (a measurement for mitochondrial respiration) or the change in acidity (measuring glycolysis). Further information on each test is given in chapter 6.3 and chapter 6.4.

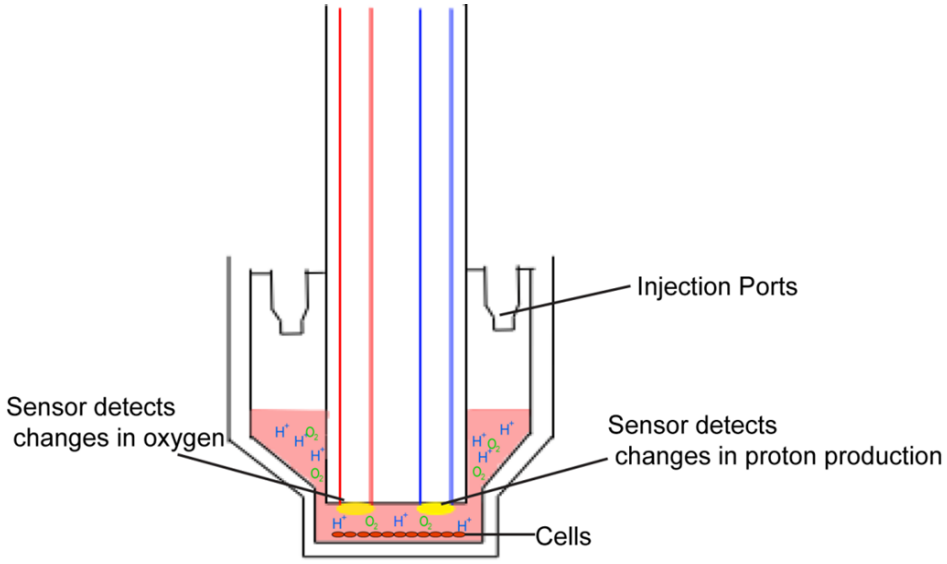

Figure 2. 4 Schematic of Seahorse mechanism depicting a single well of Seahorse Bioscience culture plate

The drugs were dispensed from one of the 4 drug ports incorporated in the sleeves into the wells of the plate at times specified by protocol. The probes also mixed the drugs into the medium after the addition of each drug at times and for durations specified by the protocol.

2.6.1 Optimisation of Cell Density and FCCP Concentration

The optimal cell density and carbonyl cyanide -4- (trifluoromethoxy)phenylhydrazone (FCCP) for dermal fibroblasts, were ascertained prior to oxygen consumption or extracellular rate stress test. Dermal fibroblasts were seeded at 4 different concentrations 40 $x10^3$ cells, 80 $x10^3$ cells, 450 $x10^3$ cells and 589 $x10^3$ cells. Seahorse Bioscience suggests that once optimal, cell density should yield basal OCR reading between 80-200pmoles/min(Invernizzi et al.). The basal oxygen consumption rate (OCR) measured in optimisation experiments, showed that the optimal density was 450 x 10^3 cells (Figure 2. 5).

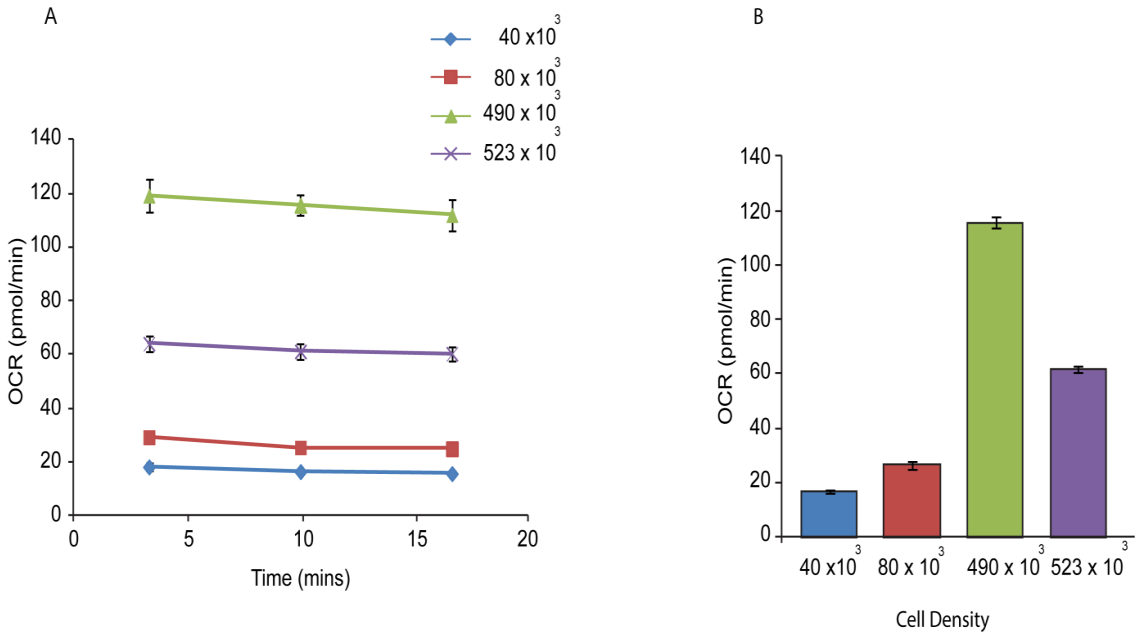

Figure 2. 5 Basal OCR level of human dermal fibroblast plated at four different concentrations

Three reading were taken at 1:38, 8:22 and 17:20 mins . B) Average OCR per cell density. Blue represents 40 x10^3 cells, Red represents 80 x10^3 cells, Green represents 450 x10^3 cells. And Purple represents 589 x10^3 cells. Error bars are ± SEM.

The maximal respiration was attained by optimising the FCCP concentration. The maximum respiration was achieved using 1µM, however the steep decline in OCR suggest that this concentration may be toxic, therefore the concentration of 0.5µM was chosen and used in the MitoStress experiments (Figure 2. 5). Oligomycin and Mito Inhibitor concentration was used at predetermined concentrations.

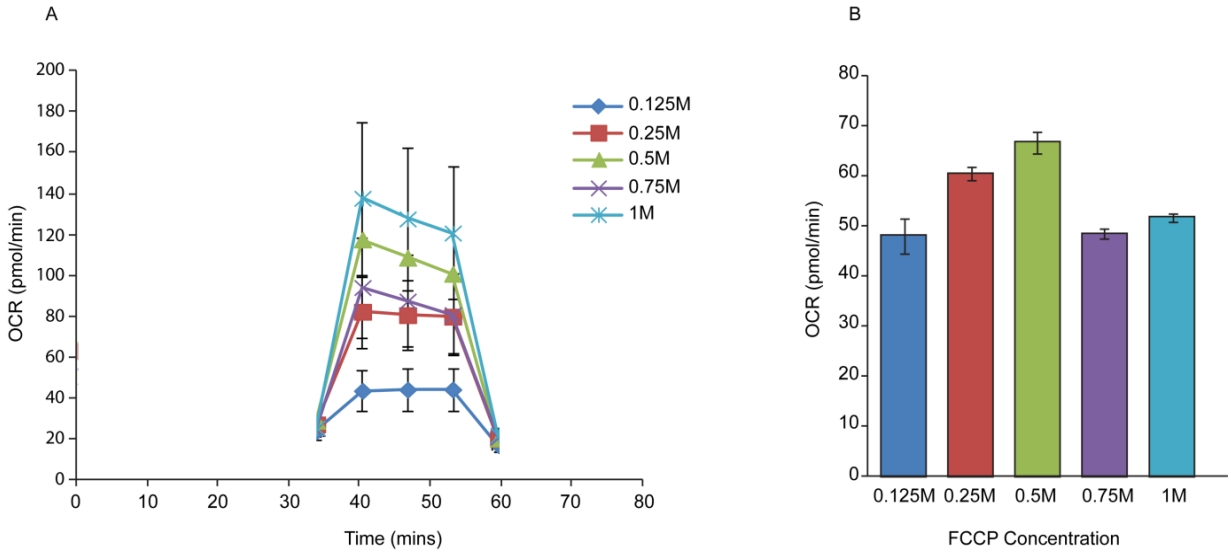

Figure 2. 6 Optimising FCCP concentration for control human dermal fibroblasts plated at 450x103 cells.

Blue represents FCCP concentration of 0.0125µM, Red represents FCCP concentration of 0.25µM, Green represents FCCP concentration 0.5µM Purple FCCP concentration 0.75µM and Cyan 1µM.

Lastly, cell age affects the cell oxygen consumption rate as increased passage number has been shown to reduce OCR (Jonckheere et al., 2010). Therefore all cells used in each experiment were of the same passage.

2.6.2 Preparation

Fibroblasts were seeded at $320x10^3$ cells/well in 80µl of complete media in XF^{e}96 cell culture plates (Seahorse Bioscience) and incubated for 24 hours at 37^{o}C in 5% CO_2 atmosphere. The XF^{e}96 sensor cartridge was hydrated overnight in 200µl XF Seahorse Calibrant and was incubated in a non CO_2 also for 24 hours.

Post 24 hours, fibroblasts were washed twice before adding 175µl of XF assay base medium (XF DMEM, 10mM glucose, 1mM sodium pyruvate and 2mM glutamine). This

XF medium was freshly prepared and pH adjusted to pH 7.4. Following this, the fibroblasts were incubated for an hour in a CO_2 free incubator at 37°C.

2.6.3 MitoStress Assay

The XF^{e}96 Sensor Cartridge was loaded with 25µl of 5µM Oligomycin, 25µl of 0.5µM FCCP, 25µl of 1µM, Mito inhibitor A (Rotenone) and 1µM Mito inhibitor B (Antimycin) at the end of the 24 hours hydration period. These will give a final concentration of 5µM Oligomycin, 0.5µM FCCP and 1µM, Mito inhibitor A (Rotenone) and Mito inhibitor B (Antimycin).

XF24 Analyzer and XF Assay cartridge were first calibrated. Following this, the XF^{e}96 cell culture plate was loaded and the experimental run initiated using the protocol below (Table 2. 4).

Start Protocol		
Command	***Time (mins)***	***Port***
Calibrate	5	
Equilibrate	12	
Mix	4	(Repeated 4 times)
Measure	5	
Inject		A (Oligomycin)
Mix	4	(Repeated 4 times)
Measure	5	
Inject		B (FCCP)
Mix	4	(Repeated 4 times)
Measure	5	
Inject		C (Mito inhibitors A&B)
Mix	4	(Repeated 4 times)
Measure	5	
End Protocol		

Table 2. 4 Instrument run protocol for MitoStress Test

2.6.4 Glycolysis Assay

The XF^{e}96 Sensor Cartridge was loaded with 25µl of 80mM Glucose, 25µl of 45µM Oligomycin and 25µl of 1M Deoxy-D-glucose (2DG) after 24 hours of hydration. The final concentrations per well was 10mM Glucose, 5µM Oligomycin and 100mM 2DG.

The assay program started following the calibration of the sensor cartridge and loading of the culture plate. The following protocol was used (Table 2. 5):

Start Protocol		
Command	***Time (mins)***	***Port***
Calibrate	5	
Equilibrate	12	
Measure	4	(Repeated 4 times)
Inject		A (Glucose)
Mix	4	(Repeated 4 times)
Measure	5	
Inject		B (Oligomycin)
Mix	4	(Repeated 4 times)
Measure	5	
Inject		C (2-DG)
Mix	4	(Repeated 4 times)
Measure	5	
End Protocol		

Table 2. 5 Instrument run protocol for Glycolysis Stress Test

Results for MitoStress and Glycolysis stress assays were analysed using the XF^{e}Wave software (Seahorse Bioscience). For both assays, 4 control dermal fibroblasts were compared to 4 patients. Data presented is an average of 10-12 replicate wells for each patient or control fibroblast cell line. Data was normalised to cell number.

2.7 Immunofluoresence

2.7.1. Chamber Slides

Cells were grown on glass 8 well chamber slides (Nunc,VWR, Leicester, UK) until 70% confluent. Cells were washed twice in PBS and fixed with 4% formaldehyde for 15 minutes followed by 5 minutes of membrane permeablisation with 0.2%Triton-X 100. Cells were washed quickly in PBS and blocked for 45 minutes in Buffer A (PBS with 0.02% Triton –X100, 1% bovine serum albumin (BSA), 10% normal goat serum (NGS). After blocking, the cells were incubated with 100µl primary antibody for 2 hours diluted in Buffer A. Cells were then washed 4 times for 2 mins in PBS followed by incubation with 100µl of secondary antibodies at a dilution of 1:1000 conjugated goat antibody in Buffer A (Invitrogen, Paisely, UK). Cells were then washed 2 times for 3 minutes in PBS, incubated for 1 minute with 2µg/ml 4'6-diamidino-2-phenylidnole dihydrochloride (DAPI, Sigma, Poole, UK) to counterstain nuclei and then washed for 5 minutes with PBS. The chamber was removed and mounted after the application of fluorescent mounting medium (Dako, Ely, UK).

2.7.2 Coverslips

Cells were grown on 5mm glass coverslips in 12 well plates (VWR, Leicester, UK) until 70% confluence was obtained. Immunostaining was performed as described above however notable changes were the made to the following; 300µl of primary antibody diluted in Buffer A was used after permeablisation and blocking stages, after the final wash step, the cover slips were removed from the plates and mounted on a glass slide

aided by the application of fluorescent mounting medium. The coverslips were sealed with a thin layer of nail polish to prevent the evaporation of the mountant hence preserving the sample.

Antibody	Species	Titre	Application	Catalogue Number	Company
Drp1	Mouse	1:100	IF	611113	BD Sioscience, New Jersey, USA
		1:500	WB		
Tom20	Rabbit	1:500	IF	SC11415	Santacruz, Texas, USA
Phalloidin		1:1000	IF	A22287	Alexaflor Invitrogen
GAPDH	Rabbit	1:5000	WB	G5262	Sigma, Poole
β-Actin	Mouse	1:10000	WB	A5441	Sigma, Poole
PMP70	Rabbit	1:500	WB, IF	AB3421	Abcam, Cambridge, UK
Tubulin	Mouse	1:200	IF	T9026	Sigma, Poole
Sacsin	Rabbit	1:500	WB	-	Eurogentec, Southampton UK

Table 2. 6 Antibodies used in immunofluoresence and western blotting experiments

Marker	Species	Titre	Wavelength		Emission colour	Company
			Excitation	Emission		
Alexa Fluor 488	Mouse/ Rabbit	1:1000	490	425	Green	Invitrogen, Paisley, UK
Alexa Fluor 568	Mouse/ Rabbit	1:1000	578	603	Red	Invitrogen, Paisley, UK
Alexa Fluor 680	Rabbit	1:1000	679	702	Far Red	Invitrogen, Paisley, UK
DAPI	-	1:5000		Blue	Blue	Sigma, Poole, UK
MitoTracker	-	250nM	579	599	Red	Invitrogen, Paisley, UK
MitoSOX	-	5µM	510	580	Red	Invitrogen, Paisley, UK
IRDye 680LT	Mouse/ Rabbit	1:10000		693	Far red	LiCor, Cambridge, UK
IRDye 800CW	Rabbit/ Mouse	1:10000		789	Far red	LiCor, Cambridge, UK

Table 2. 7 Markers/conjugated antibodies used in immunofluorescence and western blotting

2.8 Confocal analysis and data analysis

Cells stained for Drp1 and mitochondrial markers were visualised and imaged with the Zeiss LSM510 laser scanning microscope using the 63x oil immersion objective unless otherwise stated.

For the analysis of Drp1 foci localisation; the scan area of 1024 x1024 pixels – 16 bit depth, an 8-line average, a pixel dwell of 0.8µs, laser power and gain were set and remained uniform throughout the duration of the experiment (Table 2. 8).

The number of Drp1 foci was determined by the quantification of the number of peaks corresponding to the intensity of the fluorescently labelled Drp1 protein as detailed in Chapter 4. Both Drp1 and mitochondrial marker Tom20 were labelled by immunoflouresent staining.

Channel	Laser	Filter	Master Gain	Power (%)
DAPI	405	BP420-480	607	8
Cy2 (Green/ Drp1)	488	505-530	866	4
Cy3 (Red/ Mitochondria)	534	560-615	730	50

Table 2. 8 Confocal settings used for the analysis of Drp1 localisation. The pinhole for each detection was set to 1.0 Airy unit.

2.8.1 Live cell imaging

2.8.1.1 MitoTracker

MitoTracker (Invitrogen, Paisley, UK), is a cell permeant mitochondrial probe which stains the mitochondria of live cells. A stock solution was initially prepared by dissolving 50µg of lyophilized marker in DMSO to concentration of 1mM. This was then stored at -20°C. The excitation and emission maxima are given as 579nm and 599nm respectively by Invitrogen.

Cells for live cell imaging were seeded in 35mm dishes (Mat-Tek) until cells were 70-80% confluent. The stock MitoTracker solution was diluted to working concentration of 250nm complete medium (DMEM, 10%FBS, 1%PS). 1ml of MitoTracker was added to the cells and incubated for 30 minutes at 37ºC in 5% CO_2 atmosphere. After the incubation period had elapsed, cells were washed twice in warm complete media and replenished with 2ml of complete media before imaging.

Dishes were placed on a pre-warmed heated stage (37°C). Images were collected in Z-stacks 0.44µm thickness. The images were collected with 40x oil immersion objective. The scan area was 1024x1024 pixels of 12 bit depth and a line averaging of 16. The laser power was set at 50% and master gain at 435. The confocal settings remained the same throughout the experiment and between conditions. Further settings used are shown in the table below (Table 2. 9).

Channel	Laser	Filter	Master Gain	Power (%)	Pinhole (µm)	Airy Unit
Cy3	543	LP560	435	50	118	1

Table 2. 9 Confocal settings used for the mitochondrial morphometric analysis

2.8.1.2 MitoSOX

The fluorogenic dye, MitoSOX (Invitrogen) is an indicator of mitochondrial superoxide which has an excitation maximum of approximately 510nm and an emission maximum of 580nm.

Cells for live cell imaging were seeded in 35mm dishes (Mat-Tek) and MitoSOX performed when cells were 80% confluent. A stock solution of 5mM was prepared by dissolving 50µg of MitoSOX in 13µl of DMSO. The 5mM solution was diluted in PBS with calcium and magnesium (PBS/Ca/Mg) to give working concentration of 5µM. Cells were washed once in PBS/Ca/Mg prior to the application of 1ml of 5µm MitoSOX. Cells were subsequently incubated at 37ºC at 5% CO_2 for 10 minutes. Cells were washed 3 times with warm PBS/Ca/Mg before the addition of 2ml of warm PBS/Ca/Mg in preparation for imaging.

Dishes were placed on a 37°C heated stage and Z-stacks were collected using the 40x objective of a Zeiss LSM510 laser scanning microscope. Each stack in the Z-stacks was 0.5µm 1024 x 1024 pixel, 12bit depth images. Line average (8), pixel dwell (1.62µs), laser power (50%) and gain (702) remained constant. Further settings are shown in the Table 2. 10 below. Images were later analysed using Zeiss software. Further details on the method implemented are described in Chapter 5.

Channel	Laser	Filter	Master Gain	Power (%)	Pinhole (µm)	Airy Unit
Cy3	543	LP560	702	50	84	0.7

Table 2. 10 Confocal settings used for MitoSOX quantification

2.8.2 Imaris

Imaris (Bitplane) microscope image analysis software was used for 3D rendering, colocalisation and volumetric measurements. Multiple software algorithms equip the program to produce computer generated representations of mitochondria, peroxisomes and Drp1 allowing for the calculation of dimensions as well as colocalisation. More detail regarding thresholding used for experiments and processing can be found in chapters 3 and 4.

For mitochondrial morphometric analysis three dimensional Surface rendering was performed using the Surface module of Imaris (Bitplane). Background noise was reduced by eliminating any three-dimensional (3D) pixels which were below a value of 10 voxels. Here, voxels are used to describe the resolution of the volumetric structures which where surface rendered using image analysis software.

Co-localisation analysis was performed using the Coloc module of Imaris (Bitplane) and results were analysed using Manders coefficient as explained in chapter 4. Thresholding was obtained by using the Coloc automatic threshold wizard which removed researcher bias.

Drp1 foci intensity and diameter were measured using a combination of Surfaces and Measurement Pro modules. 3D rendering and thresholding allow for the accurate determination of mean intensity and diameter (see Chapter 4).

2.9 PCR and Sequencing Primers

Primers used for the PCR and sequencing of patient and control DNA were designed using the Primer 3 software. This software is publicly accessible on the internet (http://www_genome.wi.mit.edu/cgi-bin/primer/primer3_www.cgi/).

Primer		Sequence
SACS 1715	Forward	ACCCTTTTCCGACTGTCCTT
	Reverse	TGCTTTGGAAGAGCAGGATT
SACS intron	Forward	GTCGGCTTAACTGACTTGAAAA
	Reverse	CCTTTAAAGCAGCCACAAGG
SACS 4331	Forward	CTTCCAGAATCGGAACG AAA
	Reverse	GGGATGCTGAGGTTGAAAAT
SACS 4054	Forward	CTGGCCAATGAAGAAAAAGC
	Reverse	TGCATTACCAAATCGCTTCA
SACS 2002	Forward	GCTCATGGAAAAGGGAAAGA
	Reverse	TGGACCCAGTCTTCTTGAGG
SACS 2801	Forward	AAGGGCAAAATCACAGATGG
	Reverse	AATGCAGGCAGCTACTCCAC
Mycoplasma	GPO3	GGGAGCAAACAGGATTAGATACCCT
	MGSO	TGCACCATCTGTCACTCTGTTAACCTC

Table 2. 11 Primer sequences of all primers used for PCR and sequences

2.10 Statistics

Unless otherwise stated, error bars in this thesis represent ± SEM for dataset where the mean values are presented. Statistical significance was determined by a student's t-Test in the sacsin knockdown dataset or ANOVA in the ARSACS patient dataset. Statistical analyses were carried out using GraphPad Prism software. P values < 0.05 were considered to be statistically significant.

2.11 Plasmid Maps

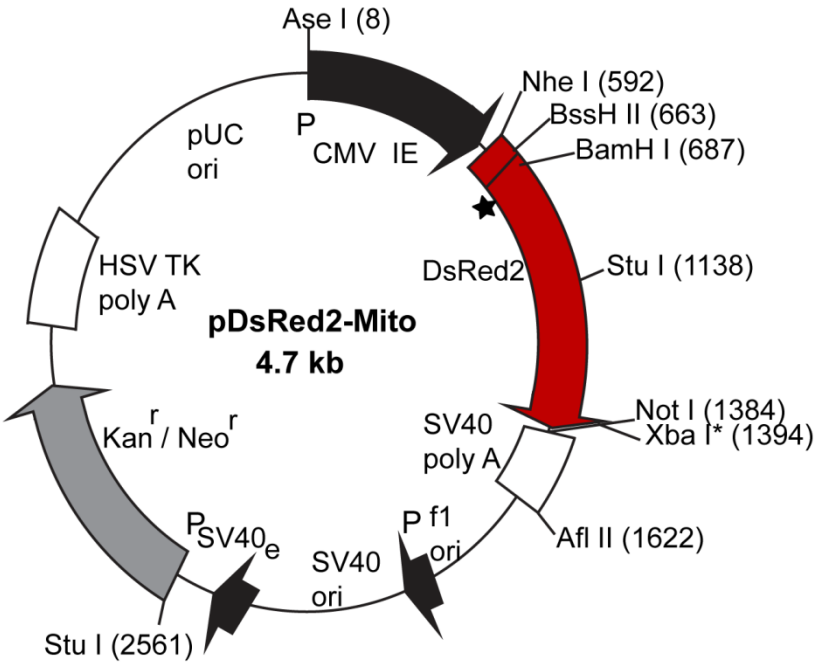

Features	Location
Human cytomegalovirus	1-589
Enhancer region	59–465;
Mitochondrial targeting sequence from subunit VIII of human cytochrome c oxidase	597(599)-683
Discosoma sp. Red fluorescent protein DsRed2 ★	705 – 1380
SV40 early mRNA polyadenylation signals	1534–1539 & 1563–1568; mRNA 3' ends: 1572 & 1584
single-strand DNA origin	1631–2086
Bacterial promoter for expression of Kan^r gene	35 region: 2148–2153; –10 region: 2171–2176 Transcription start point: 2183
SV40 origin of replication	2427–2562
SV40 early promoter	Enhancer (72-bp tandem repeats): 2260–2331 & 2332–2403 21-bp repeats: 2407–2427; 2428–2448 & 2450–2470 Early promoter element: 2483–2489 Major transcription start points: 2479, 2517, 2523 & 2528
Kanamycin/neomycin resistance gene Neomycin phosphotransferase coding sequences	codon (ATG): 2611–2613; stop codon: 3403–3405
Herpes simplex virus (HSV) thymidine kinase (TK) polyadenylation signal Polyadenylation signals: 3641–3646 & 3654–3659	pUC plasmid replication origin: 3990–4633

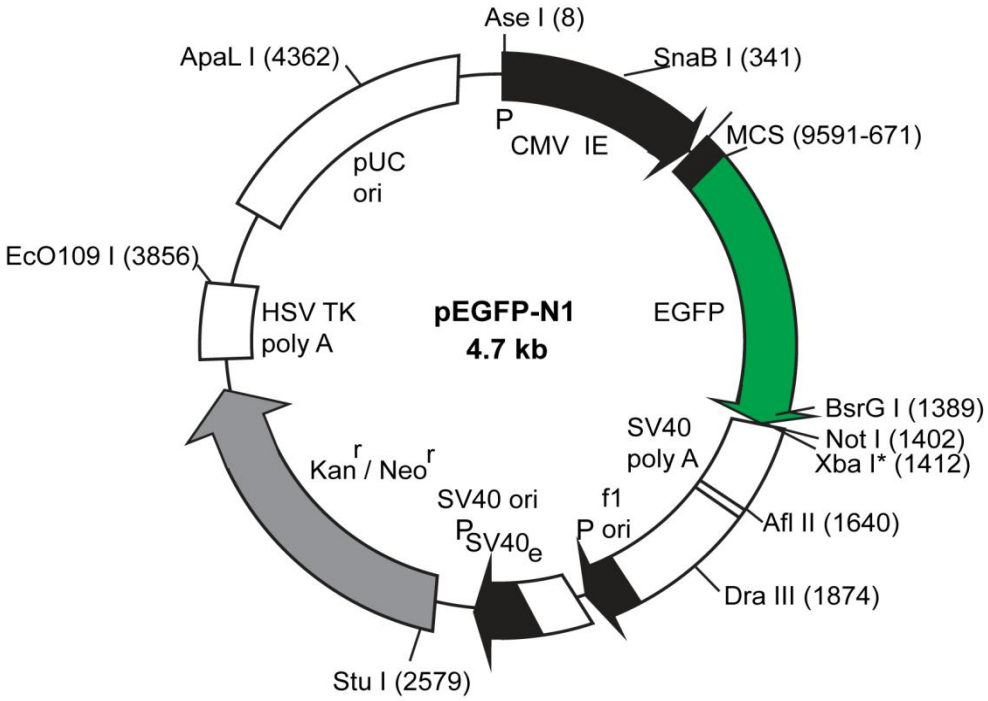

Feature	Location
Human cytomegalovirus (CMV) immediate early promoter	1–589 Enhancer region:59–465; TATA box: 554–560 Transcription start point: 583
MCS	591–671
Enhanced green fluorescent protein (EGFP) gene	Kozak consensus translation initiation site: 672–682 Start codon (ATG): 679–681; Stop codon: 1396–1398
SV40 early mRNA polyadenylation signalS	1552–1557 & 1581–1586; mRNA 3' ends: 1590 & 1602
f1 single-strand DNA origin	1649–2104
Bacterial promoterfor expression of Kan^r gene	35 region: 2166–2171; –10 region: 2189–2194 Transcription start point: 2201
SV40 origin of replication	2445–2580
SV40 early promoter	Enhancer (72-bp tandem repeats): 2278–2349 & 2350–2421 21-bp repeats: 2425–2445, 2446–2466 & 2468–2488 Early promoter element: 2501–2507 Major transcription start points: 2497, 2535, 2541 & 2546
Kanamycin/neomycin resistance gene	Neomycin phosphotransferase coding sequences: start codon (ATG): 2629–2631; stop codon: 3421–3423
Herpes simplex virus (HSV) thymidine kinase (TK) polyadenylation signal Polyadenylation signals	3659–3664 & 3672–3677
pUC plasmid replication origin	4008–4651

Figure 2. 7 Plasmid Maps of pDsRed2-Mito (mtDsRed) and EGFP. Maps adapted from Clontech Laboratories.

Chapter 3

Mitochondrial Network Morphology in ARSACS Patients and Sacsin Knockdown Fibroblasts

3.1 Introduction

The cellular morphology of mitochondria includes fragmented tubules and interconnected, elongated networks. Interchange between these phenotypes is dependent on the processes of fission and fusion (Figure 3. 1A-E). This continual change in mitochondrial network shape is important in determining mitochondrial distribution and function. The adaptive characteristic of mitochondria is also dependant on the energy requirements and health of the cell (Hermann and Shaw, 1998, Shaw and Nunnari, 2002, Benard et al., 2007b, Yaffe, 1999). These processes are regulated by a group of GTPases and their accessory proteins. For cellular health, it is important that there is a balance between fission and fusion events, as failure in the governance of the regulatory proteins and or accessory proteins that mediate these processes leads to mitochondrial dysfunction.

Cellular or mitochondrial damage caused by toxins, drugs, mutations in mtDNA or genomic DNA coding for mitochondrial proteins can push mitochondrial morphology toward a more extreme phenotype. Excess fragmentation or hyperfission (Figure 3. 1B), is common in cells entering apoptosis. During apoptosis, mitochondria enter a state of unopposed fragmentation due to an increase in Bak/Bax oligomerisation and Drp1 recruitment (Parone et al., 2006, Montessuit et al., 2010). Treatment of cells with mitochondrial uncouplers (such as CCCP which has been used in experiments described in this thesis) and other mitochondrial complex inhibitors can also drive toward a more extreme fission phenotype due to the dissipation of mitochondria membrane potential (Malka et al., 2005, Gottlieb et al., 2003). In contrast, the presence of bulbous like structures in mitochondrial networks is indicative of hyperfusion (Figure 3. 1E). The swelling of the mitochondria, seen in hyperfusion, is believed to be due to the formation of a ‘mesh’ of interconnected tubules (Nunnari and Suomalainen, 2012). Mitochondrial hyperfusion has been observed to occur in cells with reduced Drp1 protein, increased dominant negative forms of Drp1 and during the inhibition of apoptosis (Lee et al., 2004, Estaquier and Arnoult, 2007, Girard et al., 2012).

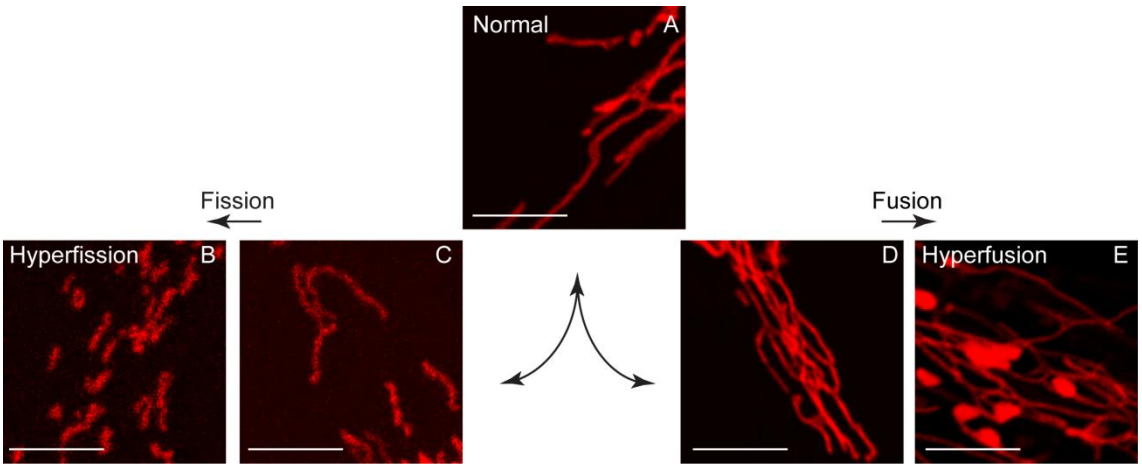

Figure 3. 1 Representative images depicting a range of mitochondrial phenotypes.

Fibroblasts were stained with Tom 20 (Red) A) Normal mixed tubular and branched mitochondria with few branches illustrating balance between fission/fusion. B) Hyperfission – small fragmented tubules depict increased fission. C) Fewer branches than in A representing onset of fission. D) Increased branching and elongation of mitochondrial tubules illustrates fusion. E) Hyperfusion- Swollen, bulbous like tubules with increased branches and few/no individual tubules seen. Scale bars represent 1µm.

Previously published work (from our group and collaborators) has shown that a loss of sacsin leads to increased mitochondrial network connectivity in SH-SY5Y cells (Girard et al., 2012). In the work described in this thesis, cultured human dermal fibroblasts were used to further analyse the effects of loss of sacsin on mitochondrial morphology. Fibroblasts were selected for this image analysis-based study as they have a mitochondrial network that is more evenly distributed throughout the cell than that seen in SH-SY5Y cells (Figure 3. 2A-B). The tightly packed mitochondrial network in SH-SY5Ys can result in problems detecting subtle changes in mitochondrial morphology. Fibroblasts have been used to explore mitochondrial morphology and distribution in a number of similar studies (Mortiboys et al., 2008, Chevrollier et al., 2012, Guillery et al., 2008). Moreover, fibroblasts have detectable levels of endogenous sacsin.

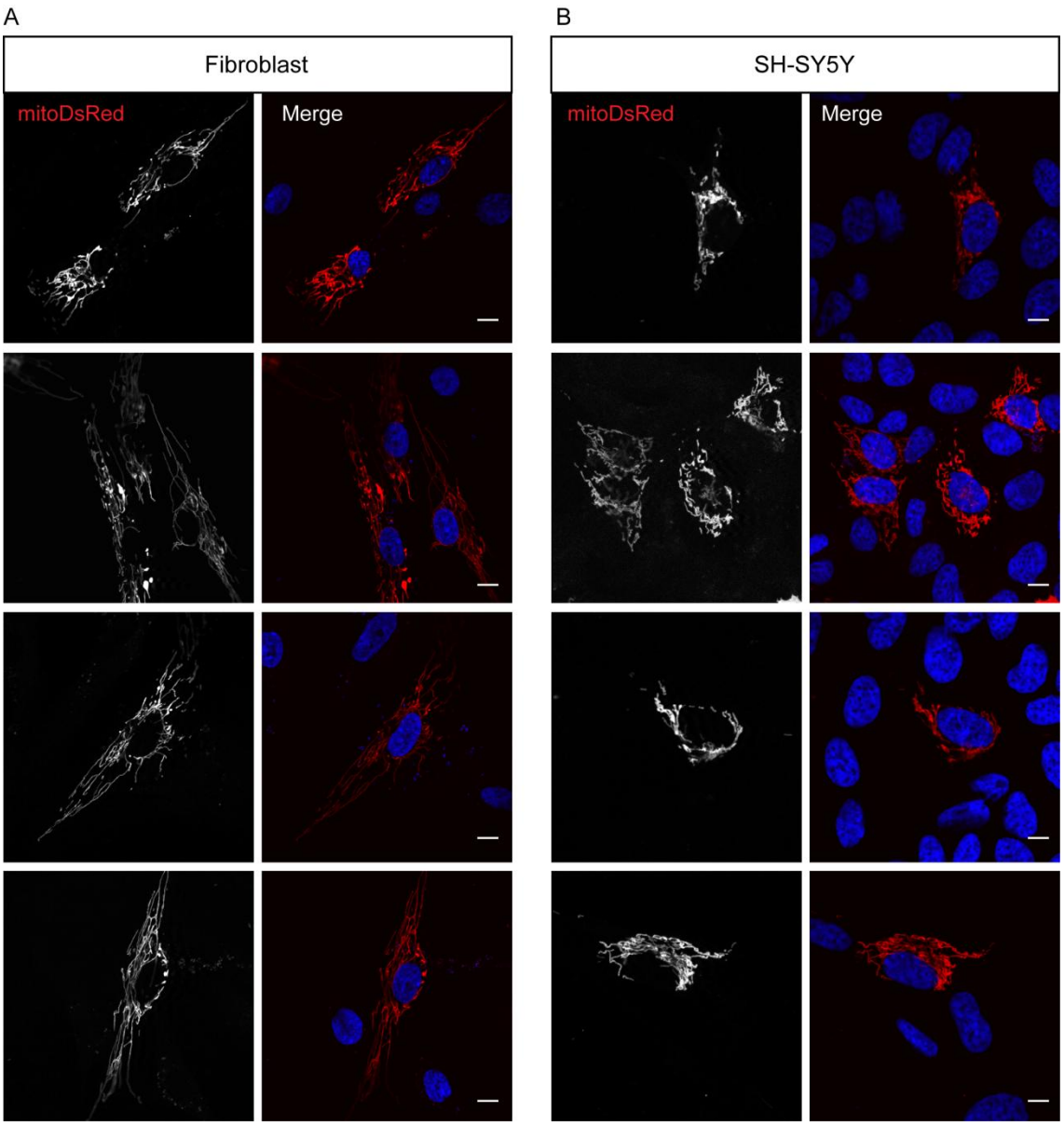

Figure 3. 2 The mitochondrial network is more evenly distributed throughout the cell in dermal fibroblasts compared to SH-SY5Y neuroblastoma cells.

Cells were transfected with mitoDsRed, and stained with DAPI to distinguish the nucleus. Cells were fixed, stained and imaged 48hrs post transfection. Representative images of four examples for each cell type are shown. A) Mitochondria were distributed relatively evenly throughout the cell in fibroblasts compared to SH-SY5Y cells where the mitochondrial network was more compact. Scale bars represent 10µm.

An added benefit of using fibroblasts, is the possibility of studying the mitochondrial morphology in ARSACS patients. Dermal fibroblasts are easily accessible by a minimal invasive procedure and can be readily cultured. ARSACS patient fibroblasts are useful cellular models as they contain pathological mutations in *SACS* as well as the whole genetic background of the affected individual. Hence they can provide more information on disease mechanism as the effect of the patient specific mutations and cellular phenotypes can be compared (Huang et al., 2005, Mortiboys et al., 2008, Chevrollier et al., 2012). Lastly, heterologous expression of sacsin is difficult due to its size. Therefore the effect of clinically occurring point mutations in ARSACS patients, are difficult to model in heterologous expression systems. Thus any morphological differences resulting from missense mutations would be difficult to ascertain without the patient fibroblasts.

The dynamic nature of the mitochondrial network contributes to the complex and varied morphology seen in human dermal fibroblast. Characterisation of the network can be complex and depends on multiple factors such as distribution, mitochondrial length, and network connectivity. Various methods have been employed to accurately describe morphology. These are largely based on imaging analysis and include measuring average mitochondrial length, mitochondrial volume and number of branches in the mitochondrial network (Rafelski et al., 2012, Palmer et al., 2011a, Niemann, 2005).

In mammalian fibroblasts, mitochondria can appear as small separate tubules (Figure 3. 3A), interconnected tubular network (Figure 3. 3C) or as a mixture of the two phenotypes with a spatial distribution of mitochondria throughout the cytosol (Figure 3. 3B, C-DF).

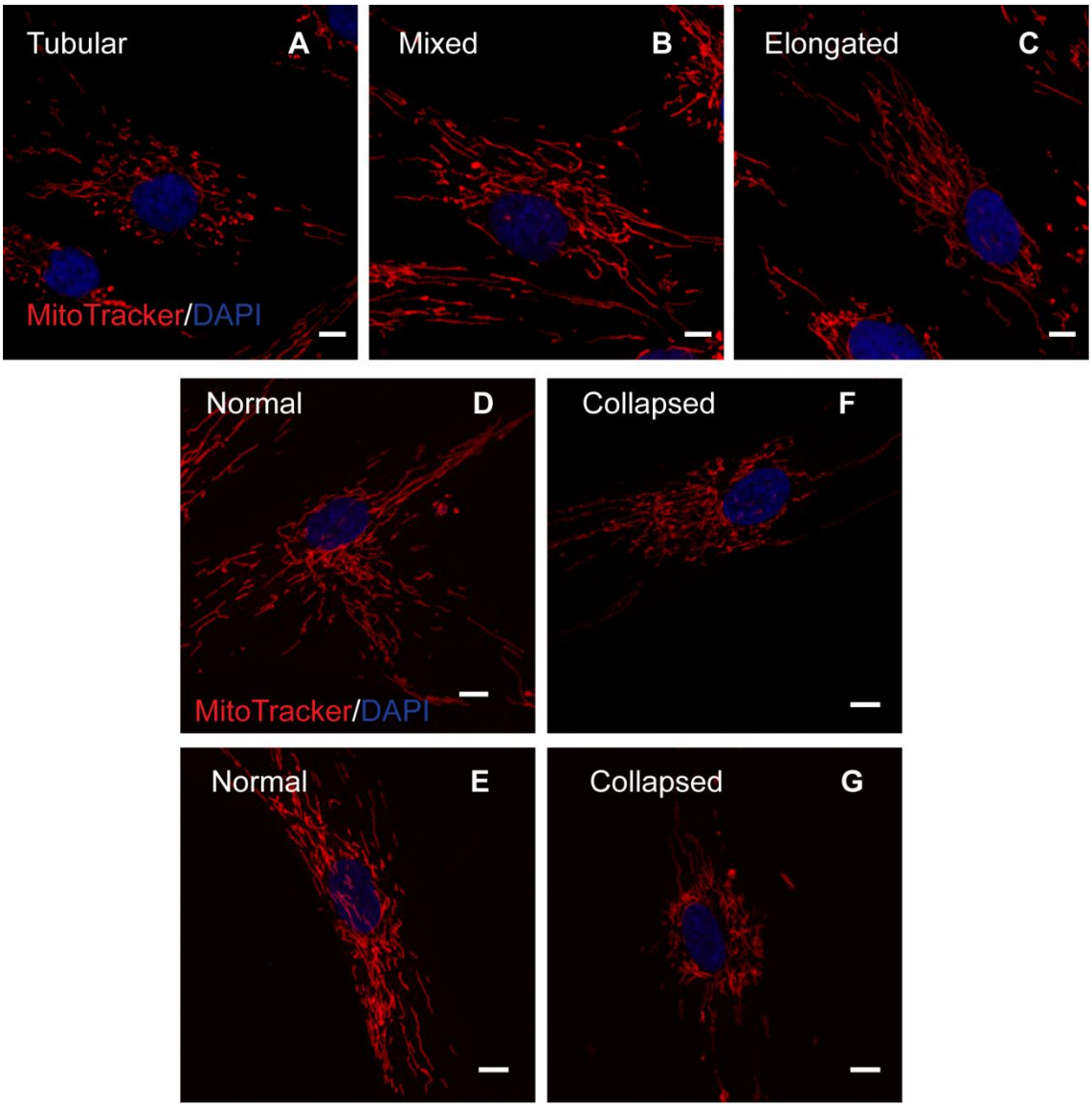

Figure 3. 3 Representative images of mitochondrial network phenotypes observed in Human dermal fibroblasts.

Commercially available control fibroblasts were incubated with 100nM of MitoTracker for 30minutes at 37°C. A) Fibroblast with a predominantly tubular network. B) Fibroblast with a mixture of tubular and elongated mitochondria. C) Fibroblast with an elongated mitochondrial network. D-E) Fibroblasts had a normal, even distribution of mitochondria. F-G) Fibroblasts had collapsed mitochondrial networks which were clustered around the nucleus. Scale bars represent 10µm

Elongated, hyperfused networks have the tendency, in some cases, of collapsing toward the nucleus (Figure 3. 3F-G) (Losón et al., 2013, Palmer et al., 2011a, Palmer et al., 2013, Wang et al., 2008, De Paepe et al., 2012, Okatsu et al., 2010, Smirnova et al., 2001). This phenotype has also been observed in cells with reduced levels of mitochondrial fission adapter proteins such as MiD51, MiD49 and Fis 1 (Palmer et al., 2011a, Palmer et al., 2013). Notably in 2012, work conducted in our laboratory in collaboration with Girard et al described an accumulation of the mitochondrial network in the cell body of cultured hippocampal neurons transduced with lentiviral encoded *SACS* shRNA (Girard et al., 2012). In these cases the majority of the network was perinuclear with very few mitochondria distributed towards the periphery of the cell. The increase in mitochondrial interconnectivity or length is hypothesized to impair mitochondrial trafficking either due to mitochondrion size or the failure of adequate attachment by Kinesin motor proteins (Chen and Chan, 2009, Baloh et al., 2007, Smirnova et al., 2001, Tanaka et al., 1998).

The analysis of mitochondrial morphology has been predominantly qualitative in many studies, where phenotypes were scored by observation blind to experimental status. In the area of age related disorders, Parkinson's and Alzheimer's, such qualitative methods have been used to imply disruption of mitochondrial dynamics as well as examine changes in mitochondrial morphology and distribution in patient fibroblasts and neurons (Regmi et al., 2014, Wang et al., 2009a, Wang et al., 2009b, Wang et al., 2008). Qualitative assessment of the mitochondrial network has relied on researcher defined descriptors to measure normal or aberrant shape. Questions arise however, as to whether conclusions on changes in the dynamic complex can be solely based on such qualitative characterizations. Mitochondria morphometric analyses have evolved from just purely observational to more quantitative methods. Quantitative description of mitochondrial biology uses microscope techniques and sophisticated image analyses software to give another method of measurement, which is less reliant on researcher defined categories. Microscopy techniques such as fluorescence recovery after photobleaching (FRAP) and the use of photoactivatable mitoGFP allows for the monitoring of interconnectivity and mitochondrial fusion (Karbowski et al., 2004,

Girard et al., 2012, Westrate et al., 2014, Mortiboys et al., 2008). These techniques are preferred in cells where the mitochondria are less motile and therefore are not always suitable, particularly in cells where networks are very dynamic (Berman et al., 2008).

Increased fusion increases the interconnectivity and branching of the mitochondrial network. Measuring mitochondrial branching and the slightly ambiguous "mass" (mitochondrial content including mtDNA and encoded proteins) have also been used to describe increased size of the mitochondrial network in neurodegeneration (Arthur et al., 2009, Mortiboys et al., 2008, Wang et al., 2009b). However an increase in mitochondrial fusion and branching may not cause an increase in the total mitochondrial mass of the cell as it may be counteracted by mitochondrial clearance or biogenesis. Therefore these analyses are rarely used in isolation. Assessing the mitochondrial volume may be a better indicator of mitochondrial phenotype as a geometric analysis of both shape and size.

In more dynamic cells such as neurons, it has been argued that the best measure of mitochondrial morphology should be the rate of fission to fusion events measured by time lapsed microscopy (Lovy et al., 2012). While these can be very precise means of analyses, problems can arise due to having to impose artificial fusion, prolonged imaging time and toxic consequences of some fusion assays causing cell death and skewed data (Lovy et al., 2012, Karbowski et al., 2004). Sole use of these methods can lead to varying descriptions of mitochondrial phenotype which can be quite restricted and limited, missing subtle variations and therefore leading to a reclassification of morphology not accounted for in previous studies.

This thesis builds on work published by the Chapple Group, combining qualitative assessment of the mitochondrial phenotype blind to experimental status and quantitative morphometric analyses to further define the mitochondrial network morphology associated with loss of sacsin function. Specifically, in this chapter, the mitochondrial morphology of siRNA-mediated sacsin knockdown fibroblasts and Dutch ARSACS patient fibroblasts are described.

3.2 Quantitative Mitochondria Network Analyses in Sacsin Knockdown Fibroblasts

Fibroblasts were transiently transfected with previously validated siRNAs for *SACS* mRNA along with mitochondria targeted red fluorescent protein, mitoDsRed, to reduce the levels of sacsin (*SACS*) and visualize mitochondria respectively. A scrambled non- targeting siRNA was also transiently transfected along with mitoDsRed as a control (*SCRM*). In these experiments, it was assumed that cells which expressed mitoDsRed had also been transfected with the siRNAs.

3.2.1 Volumetric and Numerical Analysis in Sacsin Knockdown Fibroblasts

Confocal image analyses revealed that the mitochondrial morphology in control fibroblasts was a mixture of tubular and elongated phenotypes with very few cells showing bulbous hyperfused structures (Figure 3. 4A). In contrast, the mitochondrial network in fibroblasts with reduced levels of sacsin appeared more compact and interconnected (Figure 3. 4A). More distinctly, significantly more sacsin knockdown fibroblasts displayed hyperfused mitochondria structures (Figure 3. 4A). Of interest, the morphology of the mitochondria in sacsin knockdown fibroblasts is similar to those of Canadian ARSACS patients carrying 8844delT sacsin mutation described by Girard et al (Girard et al., 2012). Hyperfused, highly interconnected mitochondrial networks are suggestive of a disruption of the dynamic equilibrium (Girard et al., 2012, Smirnova et al., 1998, Lee et al., 2004).

To further analyse the morphology of the mitochondrial network in a more quantitative manner, confocal Z-stacks through the whole cells were taken, on average, 30 images were acquired in the Z-dimension through approximately 13 µm. Subsequently three-dimensional (3D) reconstructions of the mitochondrial network were performed using the Surpass module of Imaris (Figure 3. 5). Imaris analysed the voxel (pixel depth) data collected in Z-stacks, using multiple volume rendering algorithms, to produce an artificial multidimensional object. This allowed for the

measurement of mitochondrion volume, mitochondria number and total (global) mitochondrial volume within a given cell.

For volumetric and quantitative analysis, an active threshold defined by the Imaris algorithm was used to ensure that only separate discernible structures were captured and calculated (Figure 3. 5). To further eliminate background, surfaces were classified as real surfaces as long as their pixel depth was above 10.00 voxels (Figure 3. 5). These analyses show that there were significantly ($p \leq 0.001$) less individual mitochondria per cell in *SACS* knockdown fibroblasts, compared to controls, with the mean number of 30.8 ±2 and 52.6 ±3.6 mitochondrial objects respectively (Figure 3. 6A-B). The total volume of the entire mitochondrial network within a cell (global volume) and the average volume of an individual mitochondrion were collected for both *SCRM* and *SACS* fibroblasts (Figure 3. 6C, D). While there was no significant difference in the global mitochondrial volume between the knockdowns and controls (Figure 3. 6D) there was a significant ($p \leq 0.01$) difference in the average volume for an individual mitochondrion (Figure 3. 6C). The average mitochondrion volume was larger in *SACS* knockdown 151.1μm^3 ± 15.5μm^3 compared to *SCRM* controls 104.9μm^3 ± 10.6μm^3. Furthermore, the distribution histogram indicates a subtle shift in the frequency of the volume data toward larger mitochondria, with an increase in the number of mitochondria having volumes larger than 701μm^3 in the *SACS* fibroblast (Figure 3. 6E). This is in keeping with hyperfused structures observed in the confocal images and supports volume analysis described in Girard et al 2012 (Girard et al., 2012).

A decrease in the number of mitochondria and an increase in mitochondrial size or volume is indicative of a problem in the regulation of dynamic equilibrium. Further investigation of mitochondrial morphology in patient fibroblast will increase understanding of the mitochondria phenotype of ARSACS.

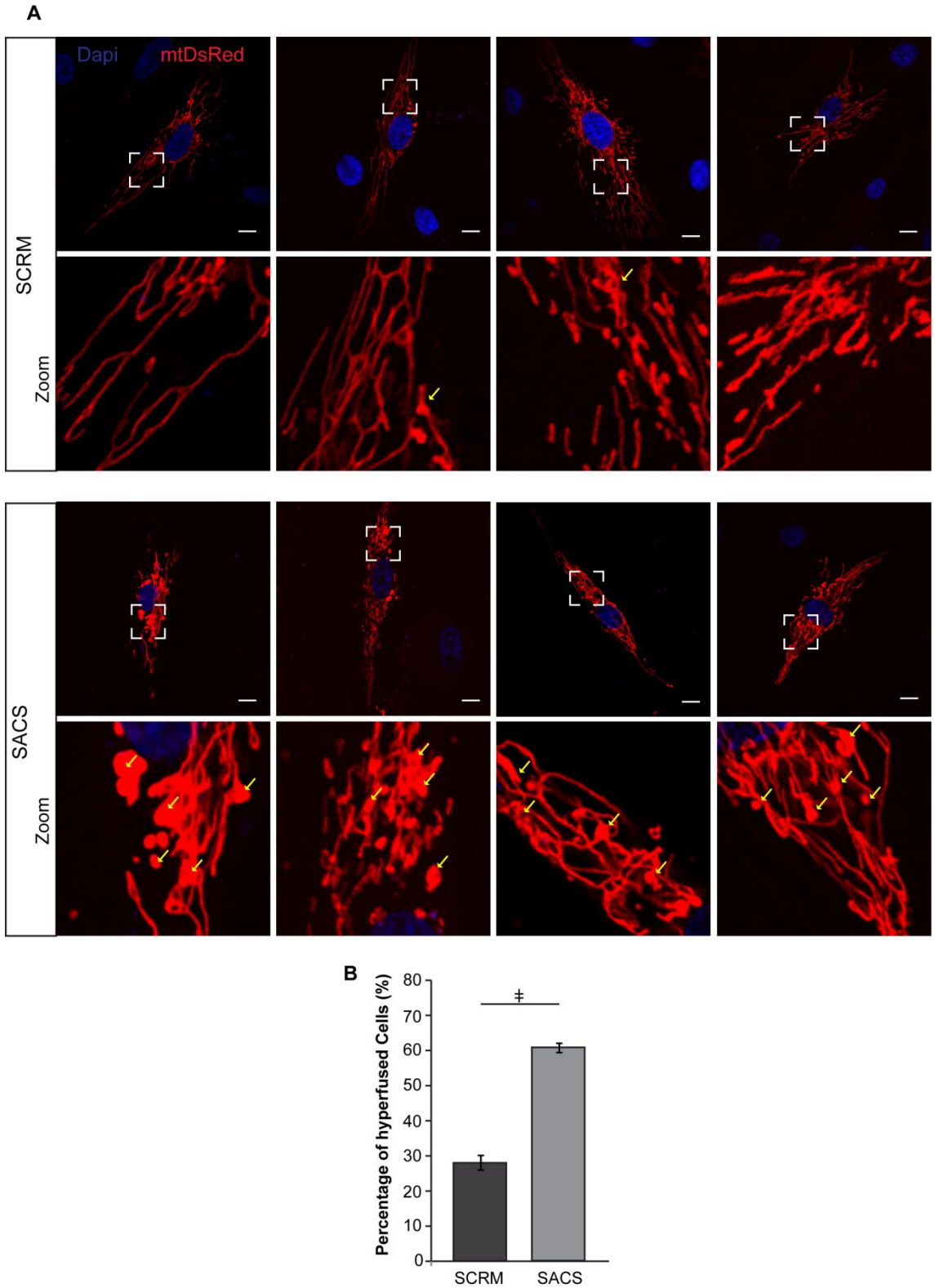
A
Dapi
mtDsRed
SCRM
Zoom
SACS
Zoom
B
Percentage of hyperfused Cells (%)
80
70
60
50
40
30
20
10
0
‡
SCRM
SACS

Figure 3. 4 Altered mitochondrial morphology in sacsin knockdown fibroblasts. Fibroblast were transfected with mitoDsRed and either *SCRM* or *SACS* siRNAs. Confocal Z-stacks were taken 48 hours post transfection. A) Confocal images showing knockdown and control fibroblast. Yellow arrows in zoomed panels show hyperfused mitochondrial structures B) Quantification of the percentage of fibroblasts with hyperfused structures scored for cellular phenotype with investigator blinded to experimental status. Scale bars represent 10µm. ‡≤ 0.05, 50 cells from 3 experiments n=150.

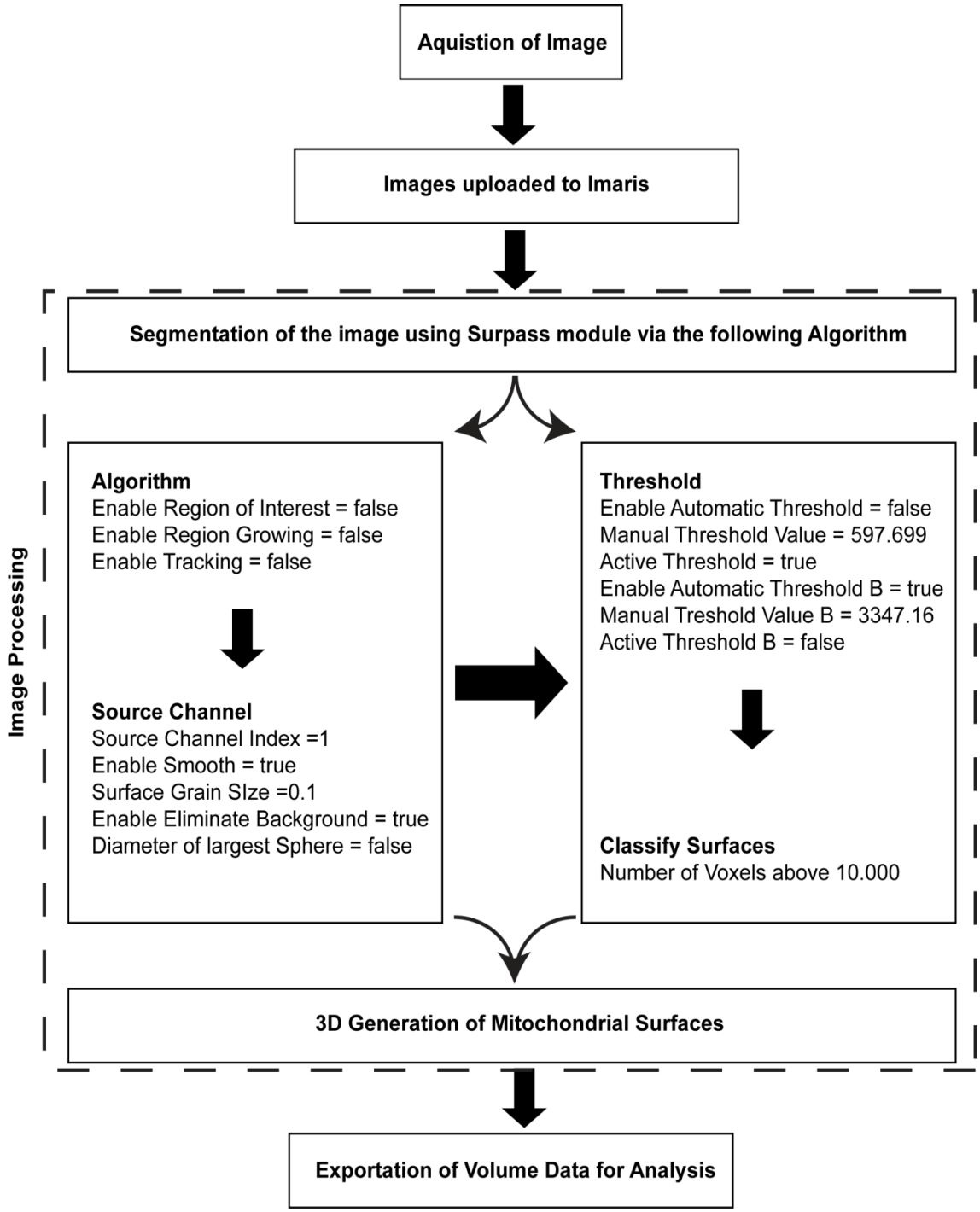

Figure 3. 5 Workflow of Imaris 3D image rendering.

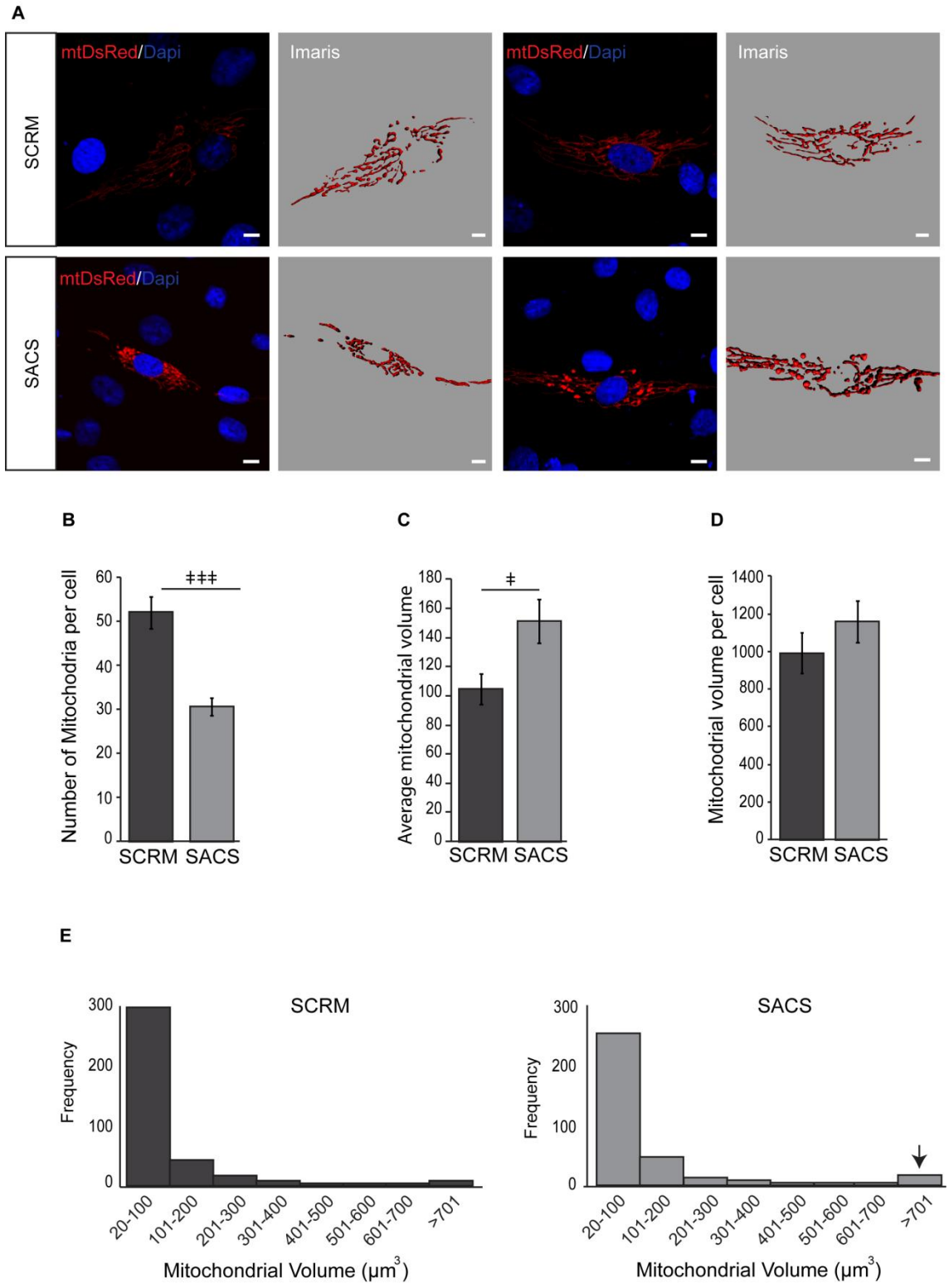
A
SCRM
SACS
mtDsRed/Dapi
Imaris
B
Number of Mitochodria per cell
‡‡‡
SCRM SACS
C
Average mitochondrial volume
‡
SCRM SACS
D
Mitochodrial volume per cell
SCRM SACS
E
SCRM
SACS
Frequency
20-100
101-200
201-300
301-400
401-500
501-600
601-700
>701
Mitochondrial Volume (μm3)

Figure 3. 6 SACS knockdown fibroblast had fewer mitochondria and a larger average mitochondrial volume.

Representative images of fibroblasts transfected with mitoDsRed and either *SCRM* or *SACS* siRNAs. Confocal Z-stacks were taken 48 hours post transfection. Imaris image analysis software was used to surface render the mitochondrial network for morphometric analysis. B) The mean number of mitochondria per cell. C) The average mitochondrial volume for a single mitochondrion. D) The mean global mitochondrial volume (volume of the entire mitochondrial network). E) Distribution histogram of mitochondrial volume. Arrow highlights the increase in larger mitochondria observed. Scale bars represent 10µm. ‡p≤ 0.05, ‡‡p ≤ 0.01, ‡‡‡p ≤ 0.001. Error bars are presented as ± standard error of the mean (SEM) unless otherwise stated.

3.3 Validation of Sacsin Mutations and Sacsin levels in ARSACS Patients

Four ARSACS patient fibroblast cell lines were a generous gift from Dr Vermeer, Netherlands. Skin biopsies of ARSACS patients were taken by clinicians in Nijmegen and primary fibroblasts were cultured and sub-cultured. Dr Vermeer holds ethical approval for the collection of fibroblasts from these patients. Cells were only sent to us after they had been expanded through to passage four and thus would not be considered relevant material by the UK Human Tissue Authority. The mutations of the ARSACS patients and consequent effect on sacsin expression were confirmed before any further examination. Genomic DNA was extracted from the fibroblasts using GenElute kit and used for direct sequencing. Sequencing of genomic DNA from the four ARSACS patients confirmed previously described mutations (Vermeer et al., 2008, Vermeer et al., 2009). Three of the ARSACS patients, patients 1, 2 and 3, carried compound heterozygous mutations in *SACS* whilst patient 4 carried a homozygous mutation (Figure 3. 7A-D). Patient 1 had a nonsense mutation Q4054* and splice site mutation c.2094-2 A>G (Figure 3. 7A), patient 2 had a missense mutation R4331Q and nonsense mutation K1715* (Figure 3. 7B). Patient 3 also had a nonsense mutation and a frame shift mutation caused by a 4 base pair deletion (Figure 3. 7C). Lastly, patient 4 had a homozygous in frame, 3 base pair deletion leading to loss of conserved glutamine at amino acid 2801, within the third HSP90 like domain of sacsin. The nonsense mutation in the second HSP90 like domain and missense mutation in patient 1 result in a truncation and loss of transcript by nonsense mediated decay respectively (Figure 3. 8A-B). Vermeer et al describe that the missense mutation in the acceptor site leads to skipping of exon 5 and the introduction of a premature termination codon (Vermeer et al., 2008). The missense mutation R4331Q in patient 2 is a mutation of a conserved amino acid in the highly conserved J-domain and was predicted to lead to a loss of function, however Parfitt et al has since disputed this hypothesis (Figure 3. 8B,D), using a bacterial complementation assay, they demonstrated that an introduction of the R4331Q mutation into the sacsin chimeric protein did not abolish or reduce J-domain function (Parfitt et al., 2009, Vermeer et al., 2008). It is important

to note that bacterial complementation assays do have their limitations as they are not a mammalian system looking at human protein-protein interactions. The frame shift mutation of arginine in patient 3 introduces a premature truncated protein (Figure 3. 8A-B). In this study, the patients will be identified by their specific mutations.

Immunoblot analysis of lysates from patients fibroblasts revealed no detectable sacsin in patients c.2094-2 A>G/Q4054* and patient R2002fs/Q4054* using carboxy-terminus sacsin antibody (r-sacsin$^{4489\text{-}4503}$). Sacsin was detected in patient 2801delQ and patient R4331Q & K1715* (Figure 3. 8C).

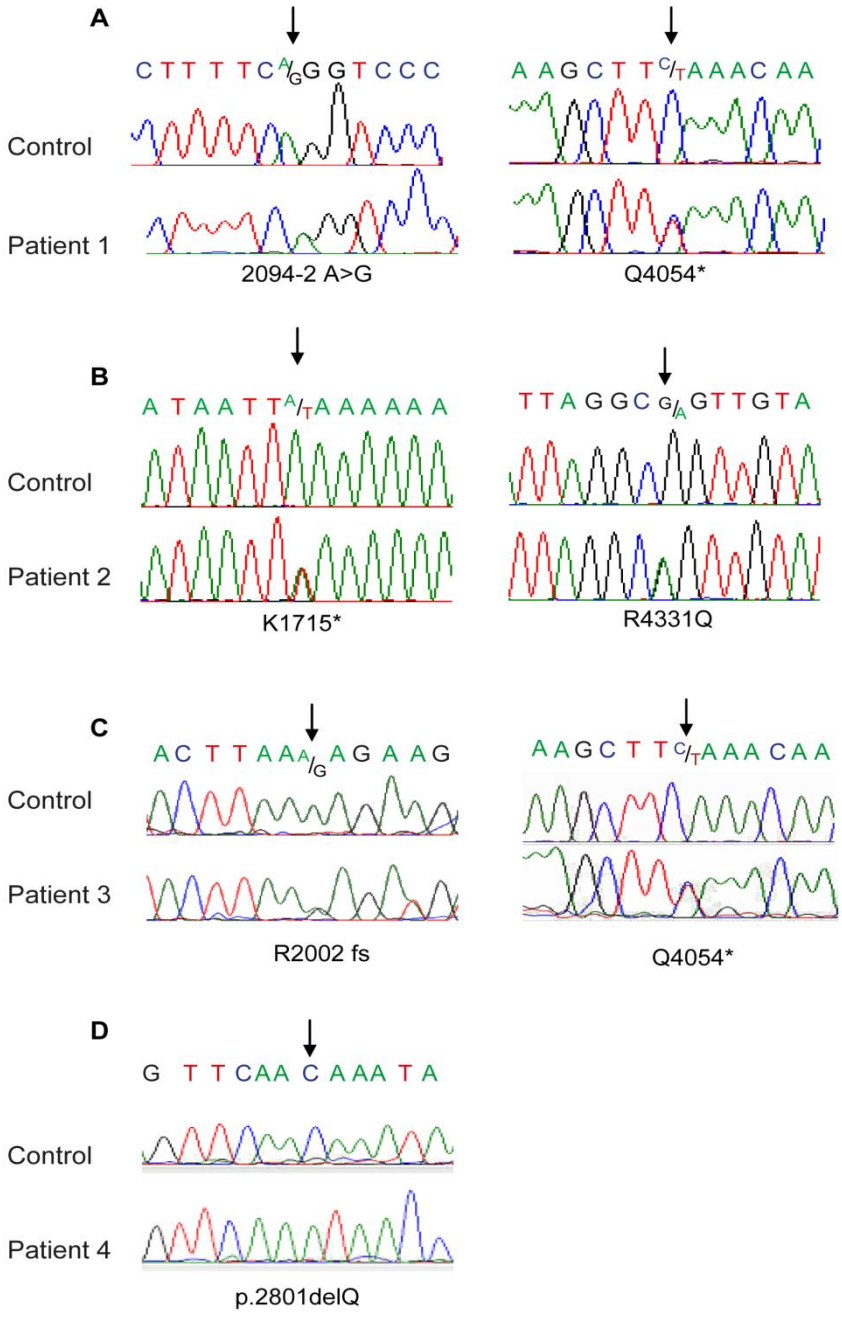

Figure 3. 7 Sequence chromatograms confirming compound heterozygous SACS mutations in Dutch ARSACS patient fibroblasts.

Patient 1 had splice site mutation c.2094-2 A>G and nonsense mutation Q4054* B) Patient 2 had nonsense mutation K1715* and missesnse mutation R4331Q C) Patient 3 had frame shift mutation R2002fs and Q4054* D) Patient 4 is the only patient in this study with a homozygous mutation p2801delQ.

A

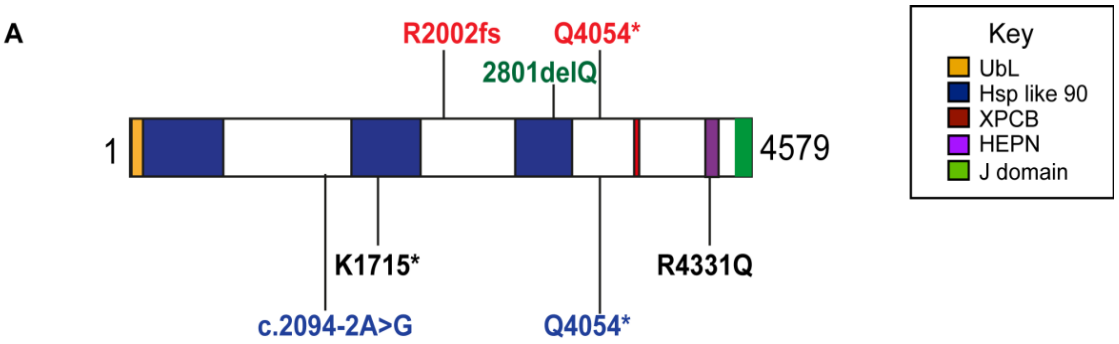

B

Mutation	Allele 1	Allele 2
c.2094-2A>G / Q4054*	Exon skipping of exon 5 leading to introduction of premature truncation codon and nonsense mediated decay.	Truncated Protein
K1715* / R4331Q	Truncated Protein	Missense mutation in the J-Domain
p.R2002fs / Q4054*	Truncated Protein	Truncated Protein
p.2801delQ	Deletion of Glutamine	Deletion of Glutamine

C

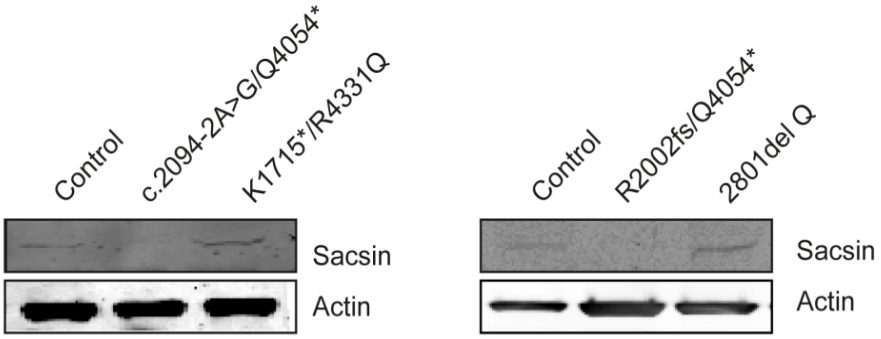

Figure 3. 8 Predicted consequences of patient SACS mutations.
Schematic representation of sacsin protein showing relative positions of ARSACS mutations. B) Predicted consequences of *SACS* mutation on each allele. C) Sacsin immunoblot of control and ARSACS patients fibroblasts. No detectable sacsin in patients c.2094-2A>G/Q4054* and R2002fs/Q4054* using C-term sacsin antibody. In contrast, sacsin was detected in patients K1715*/R4331Q and 2801delQ.

D

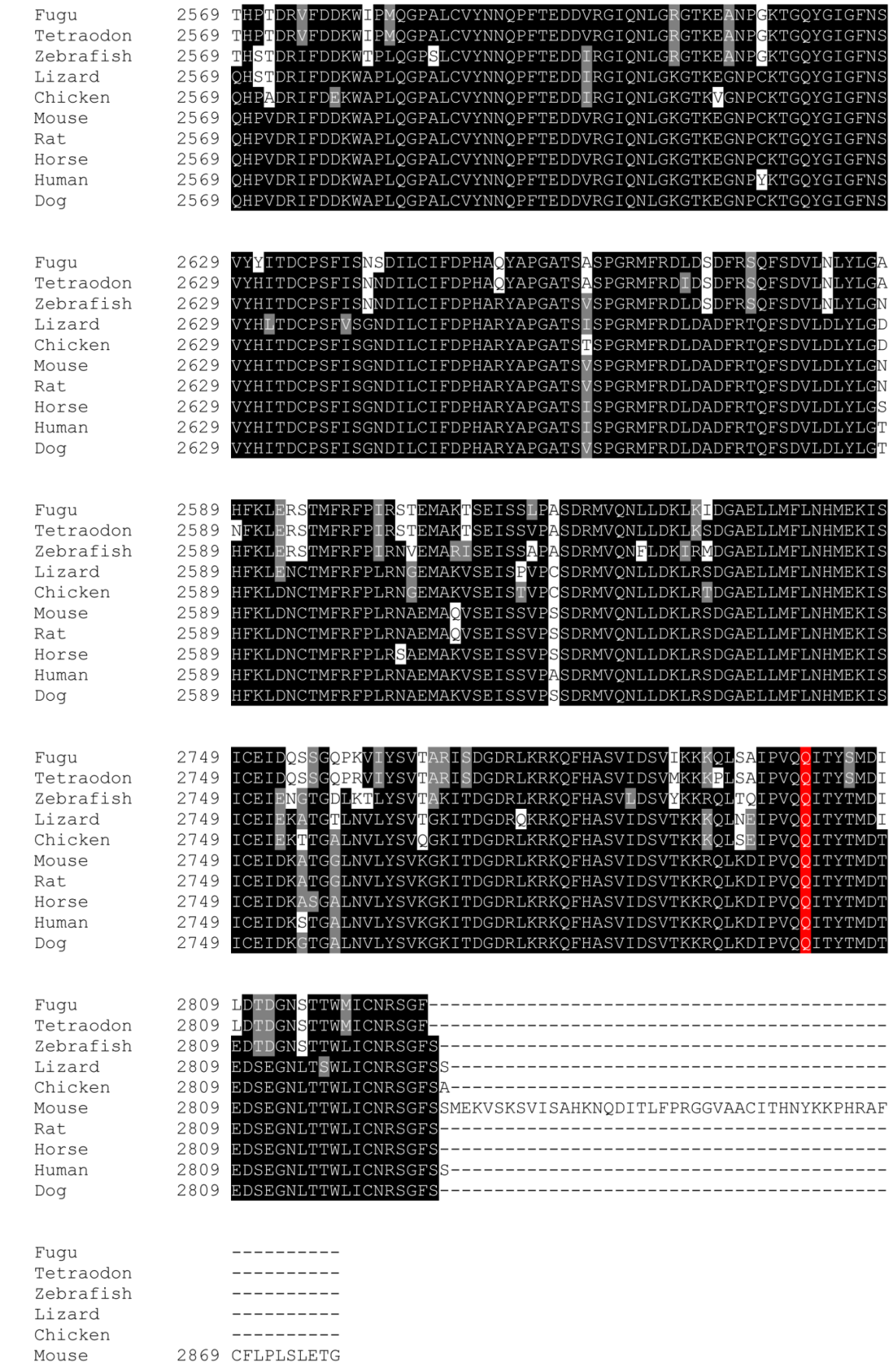
Fugu 2569 THPTDRVFDDKWIPMQGPALCVYNNQPFTEDDVRGIQNLGRGTKEANPGKTGQYGIGFNS
Tetraodon 2569 THPTDRVFDDKWIPMQGPALCVYNNQPFTEDDVRGIQNLGRGTKEANPGKTGQYGIGFNS
Zebrafish 2569 THSTDRIFDDKWTPLQGPSLCVYNNQPFTEDDIRGIQNLGRGTKEANPGKTGQYGIGFNS
Lizard 2569 QHSTDRIFDDKWAPLQGPALCVYNNQPFTEDDIRGIQNLGKGTKEGNPCKTGQYGIGFNS
Chicken 2569 QHPADRIFDEKWAPLQGPALCVYNNQPFTEDDIRGIQNLGKGTKVGNPCKTGQYGIGFNS
Mouse 2569 QHPVDRIFDDKWAPLQGPALCVYNNQPFTEDDVRGIQNLGKGTKEGNPCKTGQYGIGFNS
Rat 2569 QHPVDRIFDDKWAPLQGPALCVYNNQPFTEDDVRGIQNLGKGTKEGNPCKTGQYGIGFNS
Horse 2569 QHPVDRIFDDKWAPLQGPALCVYNNQPFTEDDVRGIQNLGKGTKEGNPCKTGQYGIGFNS
Human 2569 QHPVDRIFDDKWAPLQGPALCVYNNQPFTEDDVRGIQNLGKGTKEGNPYKTGQYGIGFNS
Dog 2569 QHPVDRIFDDKWAPLQGPALCVYNNQPFTEDDVRGIQNLGKGTKEGNPCKTGQYGIGFNS
Fugu 2629 VYYITDCPSFISNSDILCIFDPHAQYAPGATSASPGRMFRDLDSDFRSQFSDVLNLYLGA
Tetraodon 2629 VYHITDCPSFISNNDILCIFDPHAQYAPGATSASPGRMFRDIDSDFRSQFSDVLNLYLGA
Zebrafish 2629 VYHITDCPSFISNNDILCIFDPHARYAPGATSVSPGRMFRDLDSDFRSQFSDVLNLYLGN
Lizard 2629 VYHLTDCPSFVSGNDILCIFDPHARYAPGATSISPGRMFRDLDADFRTQFSDVLDLYLGD
Chicken 2629 VYHITDCPSFISGNDILCIFDPHARYAPGATSTSPGRMFRDLDADFRTQFSDVLDLYLGD
Mouse 2629 VYHITDCPSFISGNDILCIFDPHARYAPGATSVSPGRMFRDLDADFRTQFSDVLDLYLGN
Rat 2629 VYHITDCPSFISGNDILCIFDPHARYAPGATSVSPGRMFRDLDADFRTQFSDVLDLYLGN
Horse 2629 VYHITDCPSFISGNDILCIFDPHARYAPGATSISPGRMFRDLDADFRTQFSDVLDLYLGS
Human 2629 VYHITDCPSFISGNDILCIFDPHARYAPGATSISPGRMFRDLDADFRTQFSDVLDLYLGT
Dog 2629 VYHITDCPSFISGNDILCIFDPHARYAPGATSVSPGRMFRDLDADFRTQFSDVLDLYLGT
Fugu 2589 HFKLERSTMFRFPIRSTEMAKTSEISSLPASDRMVQNLLDKLKIDGAELLMFLNHMEKIS
Tetraodon 2589 NFKLERSTMFRFPIRSTEMAKTSEISSVPASDRMVQNLLDKLKSDGAELLMFLNHMEKIS
Zebrafish 2589 HFKLERSTMFRFPIRNVEMARISEISSAPASDRMVQNFLDKIRMDGAELLMFLNHMEKIS
Lizard 2589 HFKLENCTMFRFPLRNGEMAKVSEISPVPCSDRMVQNLLDKLRSDGAELLMFLNHMEKIS
Chicken 2589 HFKLDNCTMFRFPLRNGEMAKVSEISTVPCSDRMVQNLLDKLRTDGAELLMFLNHMEKIS
Mouse 2589 HFKLDNCTMFRFPLRNAEMAQVSEISSVPSSDRMVQNLLDKLRSDGAELLMFLNHMEKIS
Rat 2589 HFKLDNCTMFRFPLRNAEMAQVSEISSVPSSDRMVQNLLDKLRSDGAELLMFLNHMEKIS
Horse 2589 HFKLDNCTMFRFPLRSAEMAKVSEISSVPSSDRMVQNLLDKLRSDGAELLMFLNHMEKIS
Human 2589 HFKLDNCTMFRFPLRNAEMAKVSEISSVPASDRMVQNLLDKLRSDGAELLMFLNHMEKIS
Dog 2589 HFKLDNCTMFRFPLRNAEMAKVSEISSVPSSDRMVQNLLDKLRSDGAELLMFLNHMEKIS
Fugu 2749 ICEIDQSSGQPKVIYSVTARISDGDRLKRKQFHASVIDSVIKKKQLSAIPVQQITYSMDI
Tetraodon 2749 ICEIDQSSGQPRVIYSVTARISDGDRLKRKQFHASVIDSVMKKKPLSAIPVQQITYSMDI
Zebrafish 2749 ICEIENGTGDLKTLYSVTAKITDGDRLKRKQFHASVLDSVYKKRQLTQIPVQQITYTMDI
Lizard 2749 ICEIEKATGTLNVLYSVTGKITDGDRQKRKQFHASVIDSVTKKKQLNEIPVQQITYTMDI
Chicken 2749 ICEIEKTTGALNVLYSVQGKITDGDRLKRKQFHASVIDSVTKKKQLSEIPVQQITYTMDT
Mouse 2749 ICEIDKATGGLNVLYSVKGKITDGDRLKRKQFHASVIDSVTKKRQLKDIPVQQITYTMDT
Rat 2749 ICEIDKATGGLNVLYSVKGKITDGDRLKRKQFHASVIDSVTKKRQLKDIPVQQITYTMDT
Horse 2749 ICEIDKASGALNVLYSVKGKITDGDRLKRKQFHASVIDSVTKKRQLKDIPVQQITYTMDT
Human 2749 ICEIDKSTGALNVLYSVKGKITDGDRLKRKQFHASVIDSVTKKRQLKDIPVQQITYTMDT
Dog 2749 ICEIDKGTGALNVLYSVKGKITDGDRLKRKQFHASVIDSVTKKRQLKDIPVQQITYTMDT
Fugu 2809 LDTDGNSTTWMICNRSGF----------
Tetraodon 2809 LDTDGNSTTWMICNRSGF----------
Zebrafish 2809 EDTDGNSTTWLICNRSGFS----------
Lizard 2809 EDSEGNLTSWLICNRSGFSS----------
Chicken 2809 EDSEGNLTTWLICNRSGFSA----------
Mouse 2809 EDSEGNLTTWLICNRSGFSSMEKVSKSVISAHKNQDITLFPRGGVAACITHNYKKPHRAF
Rat 2809 EDSEGNLTTWLICNRSGFS----------
Horse 2809 EDSEGNLTTWLICNRSGFS----------
Human 2809 EDSEGNLTTWLICNRSGFSS----------
Dog 2809 EDSEGNLTTWLICNRSGFS----------
Fugu ----------
Tetraodon ----------
Zebrafish ----------
Lizard ----------
Chicken ----------
Mouse 2869 CFLPLSLETG

E

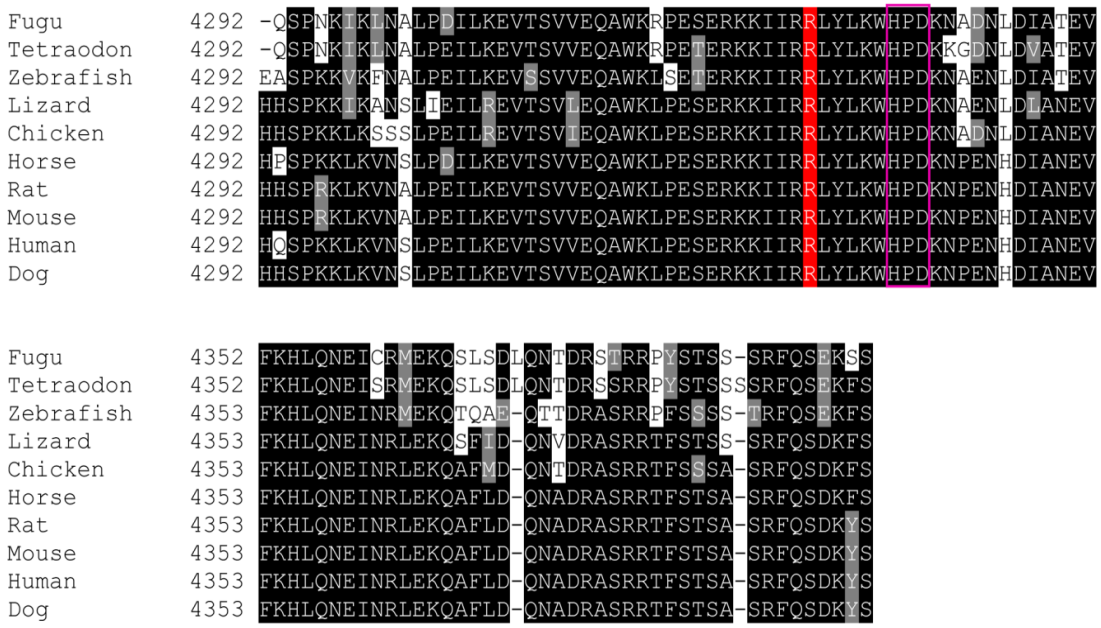

Figure 3. 8 continued Predicted consequences of patient SACS mutations.

D) Sequence alignment of HSP90 like region 1 of sacsin, amino acids 2509-2828. Conserved residue Q2801 is shaded in red E) Sequence Alignment of highly conserved sacsin J-Domain, amino acids 4293-4393. Amino Acid R4331Q, mutated in ARSACS is highly conserved, depicted by red shading. The highly conserved histidine-proline-aspartic acid (HPD) motif is denoted by Pink box.

3.4 Mitochondrial morphology of ARSACS Patients

ARSACS patients and control fibroblasts were stained with anti- Tom20 (Translocase of Outer Membrane 20) for mitochondria and nuclear stain, 4',6-diamidino-2-phenylindole (DAPI). Morphological phenotypes counted, were blind to experimental status and scored following confocal imaging (Figure 3. 9). Cells where the majority of the mitochondrial network was situated in close proximity to the nucleus and where remote cytoplasmic regions were mostly devoid of mitochondria, were classified as collapsed (Figure 3. 3) (Wang et al., 2008). ARSACS patients' fibroblasts displayed a more interconnected, perinuclear collapsed mitochondrial network than controls ($p \leq 0.0001$) (Figure 3. 9B). Patient K1715*/R4331Q had the most severe collapsed phenotype with collapsed network being the predominant mitochondrial phenotype (Figure 3. 9A-B). Although the bulbous, hyperfused phenotype observed in Canadian ARSACS patients as well as in the knockdowns was absent in these patients the compact, interconnected network was similar to that described in sacsin knockdown fibroblasts above.

3.4.1 Volumetric and Numerical Analysis in ARSACS Fibroblasts

Morphometric analysis of ARSACS fibroblasts were carried out similarly to *SACS* fibroblasts. To analyse the mitochondrial morphology, fibroblasts were incubated with 100nM MitoTracker for 30 minutes. Live confocal Z-stack images of the mitochondria were subsequently taken and used to generate maximum intensity projections. Imaris was used to generate surface rendered, 3D images and to calculate the number of the mitochondria and volume. MitoTracker is capable of passive diffusion through the cell membrane and into active mitochondria, thereby staining the mitochondria. Using this probe for live cell imaging ensured that changes in mitochondrial shape were not due to artefacts caused by fixation methods prior to immunocytochemistry.

There was a significant decrease ($p \leq 0.01$) in the number of mitochondria in patient 2801delQ ($57.18 \pm 4.11 \mu m^3$) when compared to control ($80.42 \pm 5.79 \mu m^3$). There were

small differences in the number of mitochondria in patients c.2094-2A>C/Q4054* (76.60 ± 5.80µm^3), K1715*/R4331Q (69.34 ± 9.84 µm^3), R2002fs/Q4054* (81.20 ± 4.11µm^3) however these differences were not statistically significant (Figure 3. 10B). All of the patient fibroblasts had an increase in their average mitochondrial volume compared to control (Figure 3. 10). The largest average mitochondrial volume of 162 ± 32.31µm^3 was recorded in patient R2002fs/Q4054*, significantly (p≤0.0001) more than the average volume of 52.3µm^3 ± 6.81µm^3 observed in the controls (Figure 3. 10C). The increase in the average mitochondrial volume observed in the other patients did not reach statistical significance. The smallest average mitochondrial volume of the patients was seen in patient 2801delQ 92.13µm^3 ± 17.77µm^3 and the average mitochondrial volumes in patient K1715*/R4331Q and patient c.2094-2A>C/Q4054* were 97.53µm^3 ± 18.48µm^3 and 97.13µm^3 ± 15.60µm^3 respectively. Following on from these measurements, the mean total volume of the entire mitochondrial network was calculated. A significant (p≤0.0001) increase in the volume of the mitochondrial network was observed in patient R2002fs/Q4054* (623.24 ± 61.01 µm^3) and 2801delQ 480.16 ± 45.92 µm^3) when compared to control (257.78 ± 19.97 µm^3). No statistical difference in the total mitochondrial network volume was observed between the control and patients c.2094-2A>C/Q4054* (341.57 ± 27.03 µm^3) and K1715*/R4331Q (370.78 ± 32.79 µm^3) (Figure 3. 10D). In addition there was an increase in the frequency of larger mitochondria observed in all patients when compared to control fibroblast (Figure 3. 10E). This increase was particularly highlighted in the frequency of mitochondria with volumes between 100-199 µm^3 and with the larger volumes of 500-599 µm^3. There was a higher frequency of mitochondria with volumes between 100-199 µm^3 in patient fibroblasts (Figure 3. 10F). Of note there were no mitochondria with volumes over 400µm^3 in control fibroblasts.

The increased interconnectivity of the mitochondria in the ARSACS patient fibroblasts was indicated by the decrease in number of discrete mitochondria as well as an increase in frequency of mitochondria with larger volumes (Figure 3. 10E). This is in keeping with the inverse relationship between mitochondrial volume and number in *SACS* null cells presented earlier, as well as previous data where an increase in

mitochondrial volume and decrease in mitochondrial number was described (Girard et al., 2012).

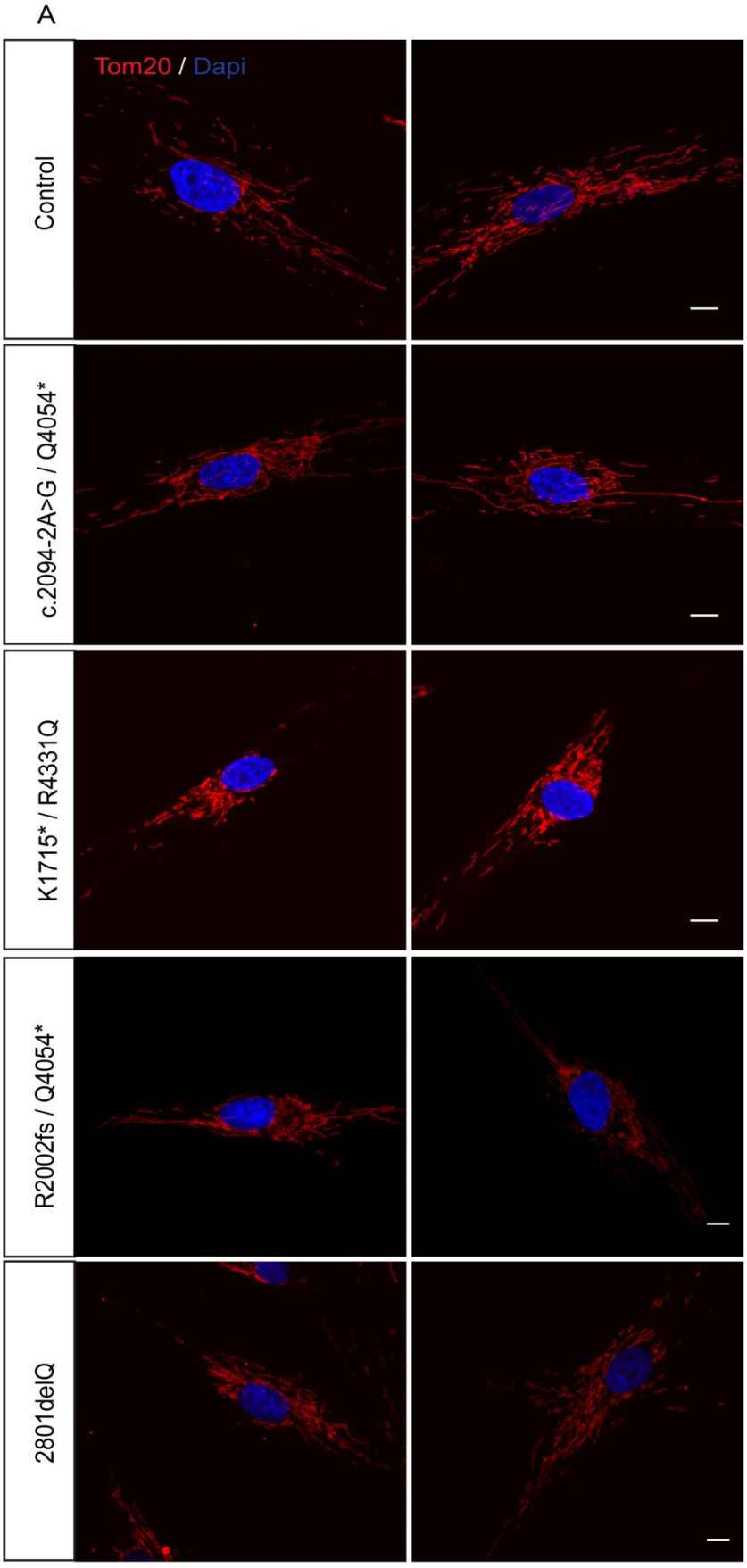
A
Tom20 / Dapi
Control
c.2094-2A>G / Q4054*
K1715* / R4331Q
R2002fs / Q4054*
2801delQ

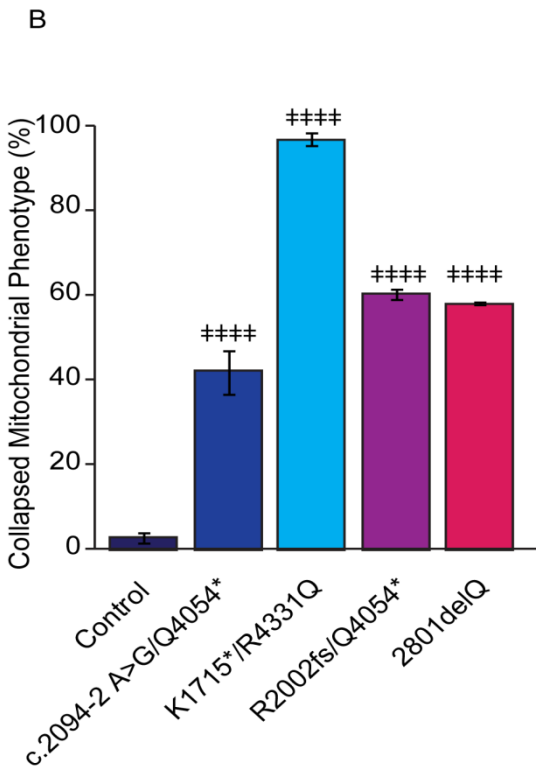

Figure 3. 9 Mitochondrial morphology differs in ARSACS patients compared to control.

Confocal immunofluorescent images of ARSACS patients and control dermal fibroblasts. Cells were immunostained with Tom20 (red) and DAPI (blue) to visualise the mitochondria and nucleus respectively. B) Quantification of the percentage of fibroblasts with collapsed mitochondrial networks was performed. (mean ±SEM, n=3 30 cells counted per experiment) Scale bars represent 10µm ‡‡‡‡ p≤0.0001

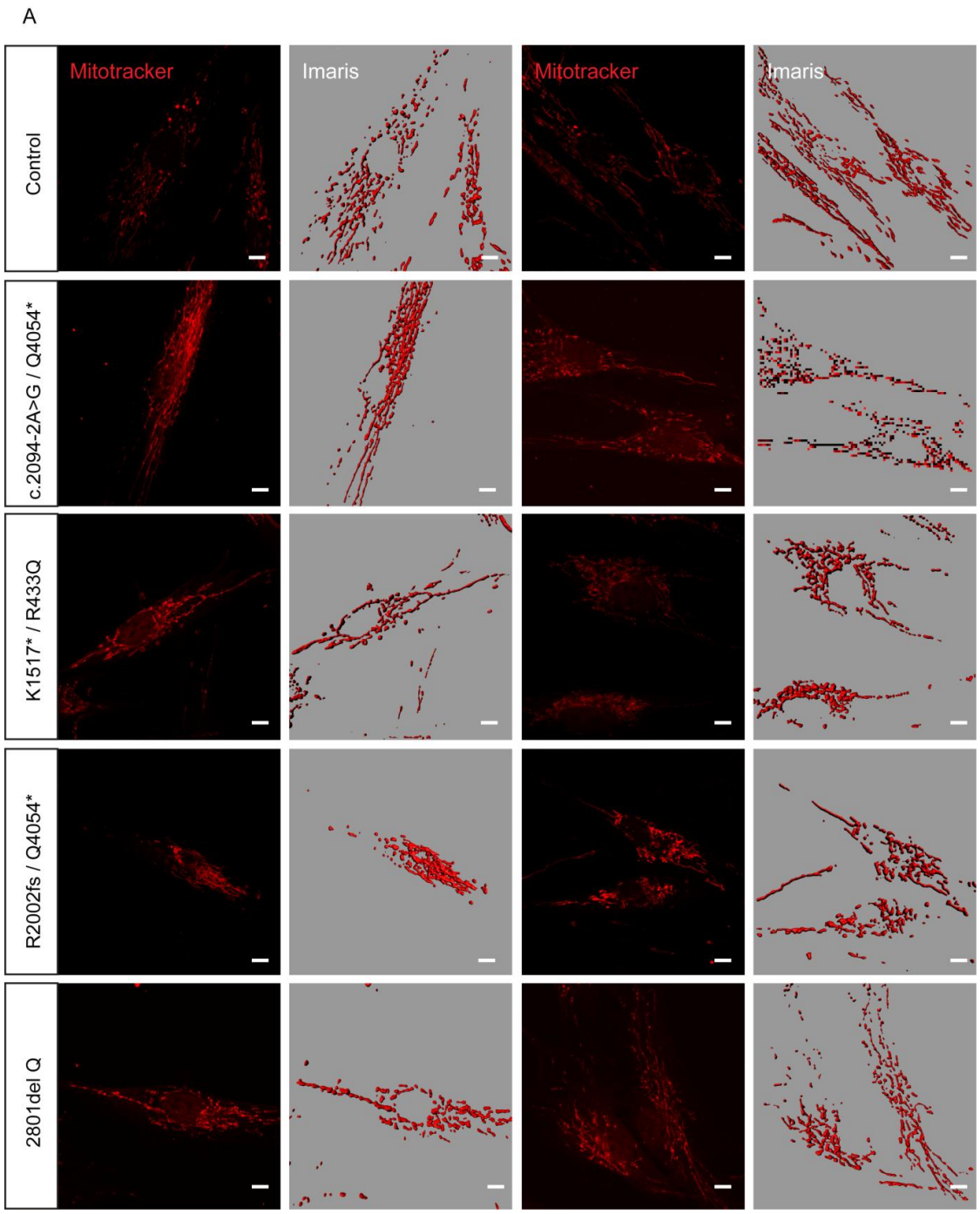

Figure 3. 10 Mitochondrial morphology of ARSACS patients.

Representative images of ARSACS patients and control fibroblasts incubated with 100nm of MitoTracker for 30mins at 37°C. Confocal Z-stacks were subsequently taken. Imaris image analysis software was used to surface render the mitochondrial network for morphometric analysis as described earlier.

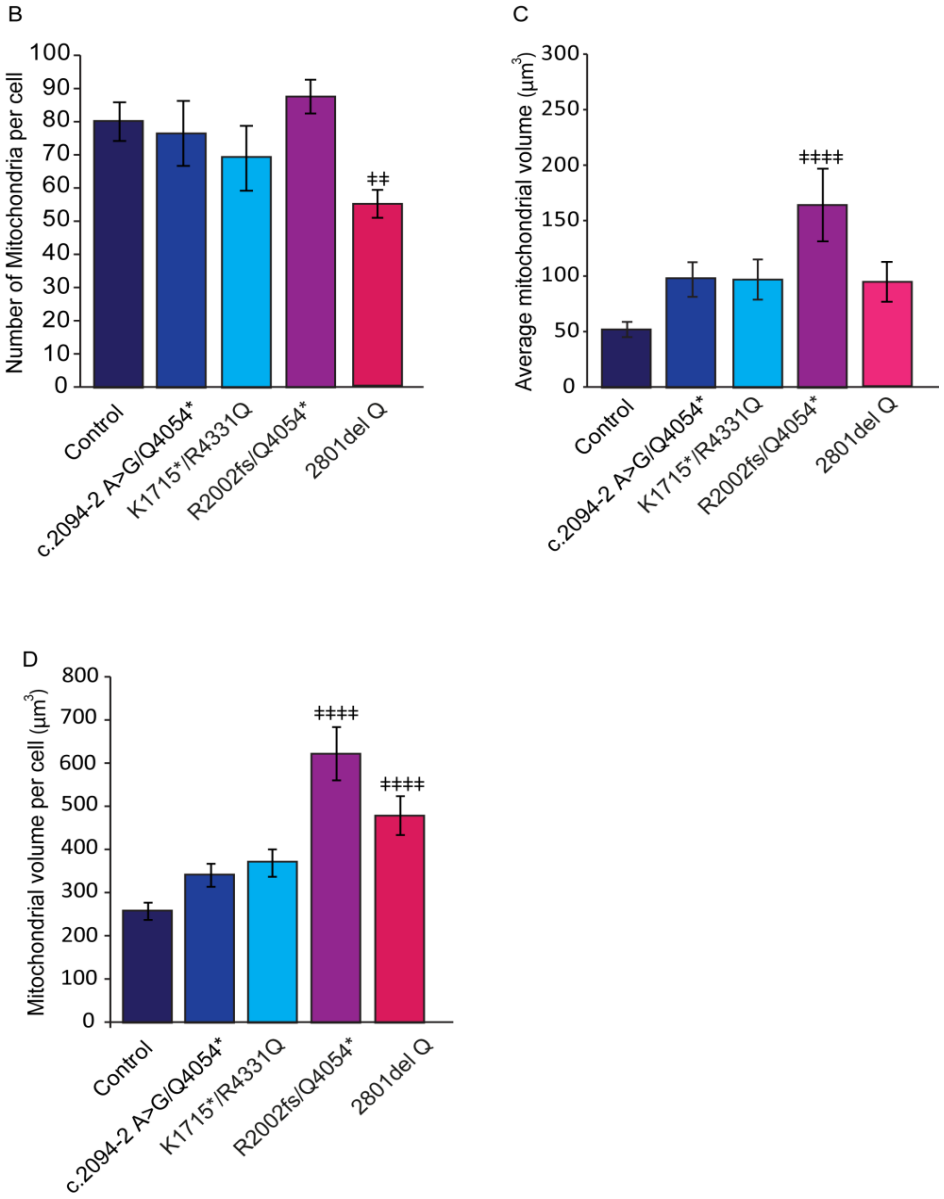

Figure 3. 10 continued Mitochondrial morphology of ARSACS patients.

B) The mean number of mitochondria per cell. C) The average mitochondrial volume per cell. D) The mean global (entire network) mitochondrial volume.

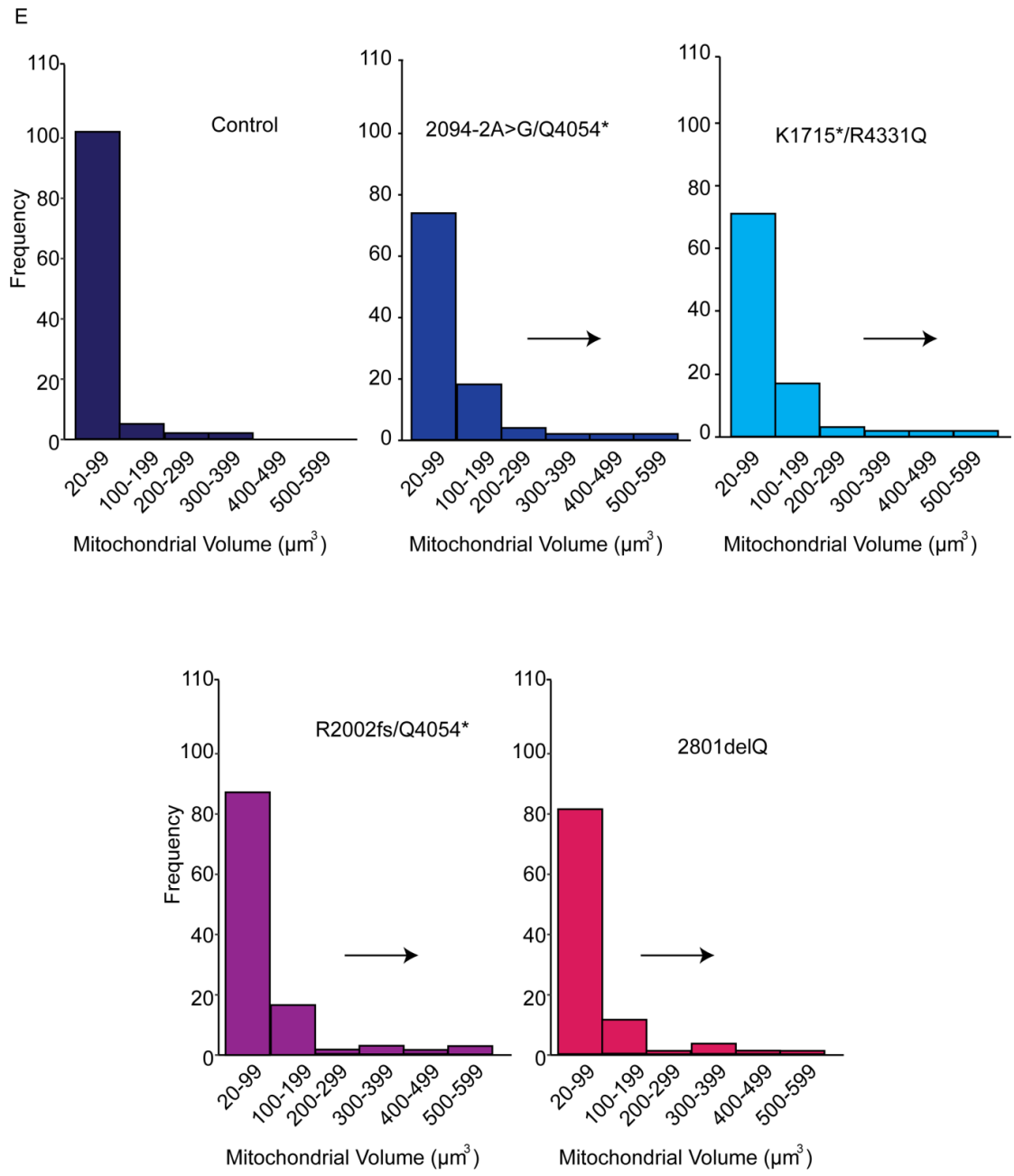
E
Control
2094-2A>G/Q4054*
K1715*/R4331Q
R2002fs/Q4054*
2801delQ
Frequency
0
20
40
60
80
100
110
20-99
100-199
200-299
300-399
400-499
500-599
Mitochondrial Volume (µm3)

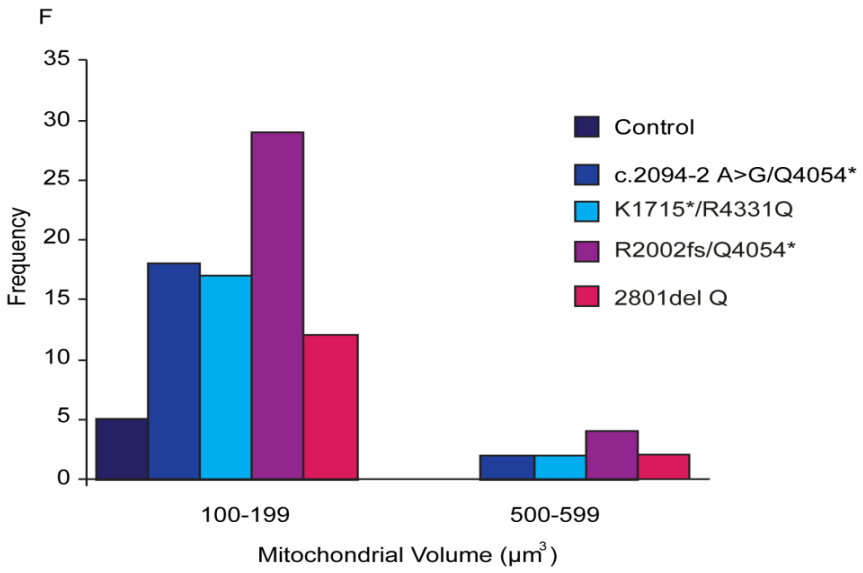

Figure 3. 10 continued Mitochondrial morphology of ARSACS patients.

E) Distribution histogram of mitochondrial volume. Arrows highlight the change in distribution to the right. F) Frequency of mitochondria with volumes between 100-199 μm^3 and 500-599μm^3. Scale bars represent 10µm. ‡‡p < 0.01 ‡‡‡‡p < 0.0001. Error bars are presented as ± SEM.

3.5 Cytoskeletal Structure in Sacsin Knockdown and ARSACS Fibroblasts.

The cytoskeleton can influence mitochondrial network organisation and distribution. Capable of both retrograde and anterograde transport along microfilaments and microtubules, mitochondrial trafficking is important for biogenesis and distribution of mitochondria (Morris and Hollenbeck, 1995, Ligon and Steward, 2000, Davis and Clayton, 1996). As semi-autonomous organelles it is hypothesised that mitochondrial biogenesis happens at close proximity to the nucleus, due to the requirement of nuclear-encoded gene products for mtDNA replication and expression with mitochondria then migrating to other cellular locations (Davis and Clayton, 1996). Trafficking is also responsible for transportation of mitochondria to areas with high energy requirements.

Disruption of cytoskeletal structure can lead to the redistribution of mitochondria, shifting the transport toward anterograde transport (Morris and Hollenbeck, 1995). Depolymerisation of the microtubules by anti mitotic agent nocodazole or colcemid was shown to cause the collapse of the mitochondrial network toward the nucleus by disrupting the filamentous structure (Koutsopoulos et al., 2010, Heggeness et al., 1978). Interestingly, a similar mitochondrial phenotype was observed in cultured hippocampal neurons transduced with lentiviral encoded *SACS* shRNA and now, in ARSACS patient fibroblasts (Girard et al., 2012).

The collapsed cellular phenotype observed in the patient fibroblasts as well as previously reported observations mentioned above by Girard et al, led to the examination on the cytoskeletal structure in sacsin knockdown and the ARSACS patient fibroblasts. This was to determine whether the mitochondrial collapsed phenotype observed was due to a defect in microtubule structure rather than an inherent problem in mitochondrial dynamics. Using fibroblasts prevented the exploration of association of intermediate filaments with mitochondrial distribution and shape, as previous studies have suggested that mitochondria are associated with microtubules in

conjunction with their motor proteins and not with intermediate filaments in cultured fibroblasts (Ball and Singer, 1982, Heggeness et al., 1978, Lackner, 2013).

3.5.1 Microtubule Structure in Sacsin Knockdown Fibroblasts.

Fibroblasts were transiently transfected with siRNAs targeting *SACS* mRNA (*SACS*) along with a plasmid expressing green fluorescent protein (GFP). A scrambled non-targeting siRNA was also transiently transfected as a control (*SCRM*) again with GFP. In these experiments, it was assumed that cells expressing GFP were successfully transfected with the siRNAs. Fibroblasts were fixed and stained for β-tubulin 48 hours post transfection.

There was, visually, no significant difference observed in the microtubule structure of *SACS* fibroblasts when compared to *SCRM* fibroblasts (Figure 3. 11). The microtubule network in *SACS* fibroblasts appeared to be organised and very similar to that of *SCRM* fibroblasts. Therefore the hypothesis that the mitochondrial phenotype observed in sacsin knockdown fibroblasts was due to microtubule disruption, was not pursued further.

3.5.2 Microtubule Structure in ARSACS Fibroblasts.

Patient and control fibroblasts were grown until they were 70% confluent. After which they were fixed and stained with β-tubulin to visualise the microtubule structure within the fibroblasts. 20 cells were imaged for each patient and control.

The microtubule structure observed in the patients was very similar to those observed in the controls (Figure 3. 12). Like in the *SACS* fibroblasts, there were no striking differences between the patients and the controls to be reported. The microtubules appeared relatively organised with a filamentous network which extended to the periphery of the cell.

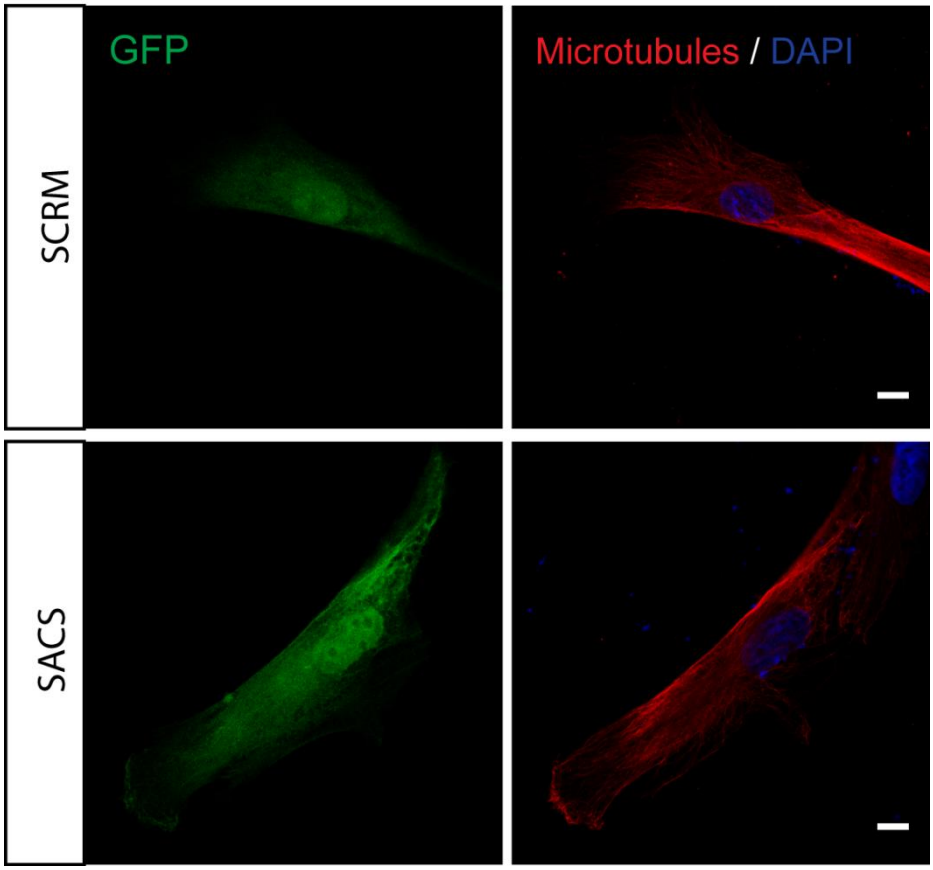

Figure 3. 11 Representative images of microtubules (red) and GFP

Fibroblast were transfected with GFP and either *SCRM* or *SACS* siRNAs. Confocal images were taken 48 hours post transfection. Cells were fixed and stained with β-Tubulin.

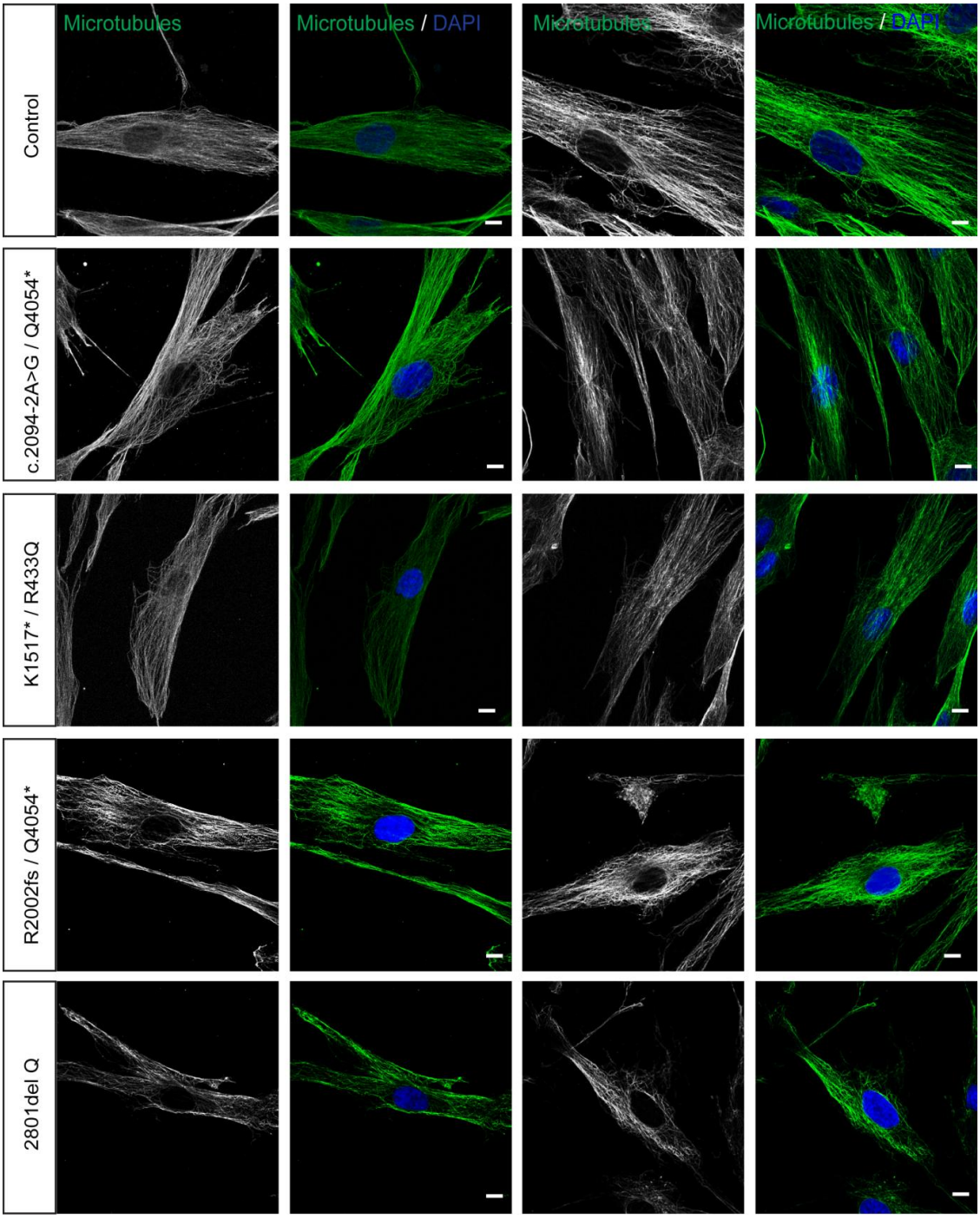

Figure 3. 12 Microtubule structure was similar in ARSACS patients and control. Confocal immunofluorescent images of ARSACS patients and control dermal fibroblasts. Cells were immunostained with β-Tubulin (green) and DAPI (blue) to visualise the microtubules and nucleus respectively.

3.6 Discussion

Mitochondrial fusion and fission are important regulators of mitochondrial function. Perturbations of mitochondrial dynamics can greatly impact the regulation of other cellular processes as well as mitochondrial function.

The mitochondrial phenotype in fibroblasts with reduced levels of sacsin protein or loss of sacsin function due to mutations in *SACS,* is similar to that of the mitochondrial network in cells with knockdown of mitochondrial fission proteins or over expression of mitochondrial fusion proteins. As the microtubule network in the *SACS* and ARSACS fibroblasts tend to resemble that of the controls, supports that this phenotype is likely due to a defect in mitochondrial dynamics. Sacsin, like Drp1 and fission adapters, is possibly indirectly involved in mitochondrial distribution. The collapsed morphology in ARSACS fibroblasts is similar to the morphology noted in patient carrying embryonic lethal Drp1 mutation (Chen and Chan, 2009, Waterham et al., 2007). Furthermore both phenotypes observed in the *SACS* and ARSACS fibroblasts have been observed in cells transfected with dominant negative Drp1 or Drp1 RNAi (Wang et al., 2008, Li et al., 2004, Smirnova et al., 1998). The hyperfused and collapsed mitochondrial network phenotypes were shown to be indicative of a loss of Drp1 function (Smirnova et al., 1998, Wang et al., 2008).

The subtle differences in the mitochondrial volume and number for the patients may be due to sacsin's role in mitochondrial dynamics. The severity of the mitochondrial phenotypes due to loss of mitochondrial dynamic proteins has been shown to vary depending on the protein and the pathway effected. For example, reduction in the levels of mitochondrial fission protein Fis 1 results in the mitochondria having a more elongated shape. It has been demonstrated that this effect on mitochondrial morphology is somewhat subtle in mammalian cells when compared to controls. Moreover the change in morphology caused by reduced Fis 1 has also been shown to be less dramatic than the changes in morphology brought about by reduction in Mff or Drp1 (Otera et al., 2010).

Of interest, the global mitochondrial volume did not vary greatly between *SACS* and *SCRM* fibroblasts. This would suggest that mitophagy and biogenesis are continuing to occur in the absence of sacsin. If this were not the case the cells would not be viable. This data is similar to that of mitochondrial fission proteins MFF, MiD51/49 and hFIS (Gandre-Babbe and van der Bliek, 2008, Losón et al., 2013, Palmer et al., 2013). Moreover this data is particularly interesting as mitochondrial turnover heavily relies on the fission process. Both mitochondrial biogenesis and mitophagy occur through pathways involving the fragmentation of the mitochondrial network. Loss of sacsin may therefore decrease the rate of fission. Further investigation on the rate of fission/fusion is needed to establish this hypothesis. Although this finding was similar in 2 of the patients compared to control, a significant reduction in the number of mitochondria was evident in patient 2801delQ and both patients 2801delQ and R2002fs/Q4054* showed a significant increase in mitochondrial network volume therefore it is important not to disregard problems in mitochondrial biogenesis and clearance.

Controversially, increasing mitochondrial fusion events have been postulated to be potentially beneficial in treating Parkinson's and Alzheimer's disease, as delayed apoptosis may allow time for the mitochondria to share contents with the network, potentially "healing" repairable mitochondria (Cereghetti et al., 2010, Lutz et al., 2009, Qi et al., 2013, Bonda et al., 2011). However, it is well established that the disruption of mitophagy can lead to the accumulation of toxic by-products within the mitochondria. Consequently, these toxins can damage the mitochondria and lead to cell death (Uo et al., 2009). These and previous results may find a possible role for sacsin in indirect regulation of cell death through regulation of mitochondrial morphology.

The results imply that the observed interconnected, collapsed mitochondrial network is in some way linked to the loss of sacsin function. Further examination of the fission process as well as the effects of this change in morphology will be addressed. As novel pathways and proteins involved in regulation of mitochondrial dynamics are being

investigated, more standardized tests are needed. Moreover the development of a systematic quantitative classification that can be applied to multiple studies would facilitate comparison between studies from different groups on different components of the machinery that regulates mitochondrial dynamics.

Chapter 4

Dynamin related protein 1 in ARSACS Patients and Sacsin Knockdown Fibroblasts

4.1 Introduction

The morphological phenotype of the mitochondrial network in sacsin knockdown and ARSACS patient fibroblasts is consistent with increased fusion or reduced fission. Importantly, our lab along with our Canadian collaborators, established a link between sacsin and the essential mitochondrial fission protein Drp1. Immunofluorescence analysis revealed that sacsin partial overlaps with Drp1 foci at mitochondria. Moreover, an interaction between the N-terminus of sacsin (residues 1-1368) and Drp1 was identified through co-immunoprecipitation (Girard et al., 2012). These results, coupled with the mitochondrial phenotype observed in *SACS* knockdown cells and ARSACS patients (Chapter 3 of this thesis) suggest a role for sacsin in mitochondrial fission.

Drp1 is crucial for normal mitochondrial fission and subsequently for mitochondrial distribution, shape and function (Waterham et al., 2007, Wang et al., 2008, Chen and Chan, 2005, Hemach et al., 2011, Wakabayashi et al., 2009). Drp1 is localised throughout the cytosol and at foci on mitochondria – with approximately 3% of the protein reported to be at mitochondria under normal physiological conditions (Smirnova et al., 2001). For fission to occur Drp1 monomers/dimers in the cytosol are recruited to mitochondria, where they form higher order scission complexes that undergo conformational change driven by GTP-hydrolysis, which is believed to constrict mitochondria (Figure 4. 1). Although better understood in yeast, the process of Drp1 recruitment is still enigmatic in mammalian cells.

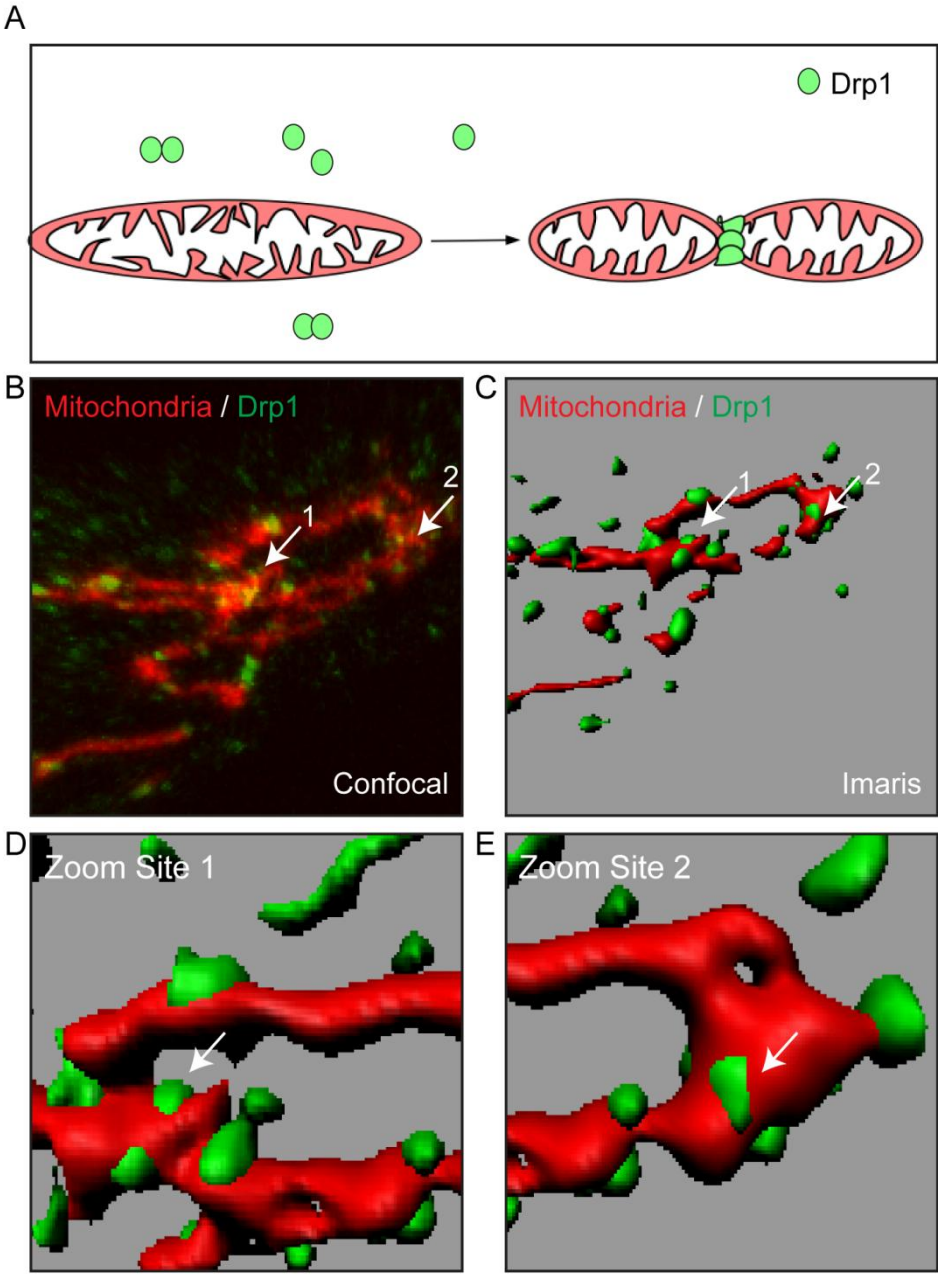
A
Drp1
B
Mitochondria / Drp1
1
2
Confocal
C
Mitochondria / Drp1
1
2
Imaris
D
Zoom Site 1
E
Zoom Site 2

Figure 4. 1 Schematic and images of Drp1 recruitment to mitochondria.

Drp1 is recruited from the cytosol to sites of potential fission. The protein forms oligomeric ring-like structures where scission can occur. B) Representative confocal image showing mitochondria (red) with associated Drp1 foci (green). The majority of Drp1 foci are found in the cytsol with a small percent localised to the mitochondria. Once localized to the mitochondria, Drp1 can form oligomeric spirals. C) 3D surface rendering of confocal image. Arrows 1 and 2 clearly show the Drp1 “wrapped” around the mitochondria. D) Zoomed in image of site 1 shown in C. Arrow highlights the Drp1 ring like Drp1 foci E) Zoomed in image of site 2 shown in C. Arrow highlights the ring like Drp1 foci.

In Yeast, mitochondrial fission adaptors Mdv1 and Caf4 are as much essential components of the mitochondrial division machinery as Dmn1, the yeast Drp1 orthologue. During fission Dmn1 is recruited to the mitochondria via Mdv1 to Fis1 at the outer mitochondrial membrane. Once bound to Fis1, Mdv1 co-assembles with Dnm1 to form oligomeric spirals around mitochondria (Naylor et al., 2006, Bhar et al., 2006, Bui et al., 2012). These oligomers then undergo conformational change, causing scission of the mitochondria and ultimately fission occurs. The loss of Drp1 oligomers and/or protein involved in the recruitment of Drp1 prevents fission.

Mammalian cells lack orthologues of the yeast mitochondrial fission adaptors Mdv1 or Caf4 (Palmer et al., 2011c) and are capable of undergoing hFis 1 independent Drp1 mediated fission (Koch et al., 2005, Chang and Blackstone, 2010a, Suzuki et al., 2003). It is therefore postulated that identified mammalian mitochondrial fission proteins Mff, hFis1, MiD49 and MiD51 bind and sequester Drp1 to the outer mitochondrial membrane facilitating oligomerisation and subsequent scission and may therefore act as an alternate mechanism for Drp1 recruitment in mammalian cells (Figure 4. 1) (Palmer et al., 2011a, Palmer et al., 2011c, Palmer et al., 2013). Moreover, although mechanisms regulating oligomeric assembly and stabilisation of Drp1 in mammalian cells remains unclear, it is postulated that Mff, hFis1, MiD49 and MiD51 have a role similar to that of Mdv1 in yeast (Palmer et al., 2013). It is important to note that these proteins are not wholly essential for mitochondrial fragmentation as loss or reduced expression does not obliterate fission (Palmer et al., 2011a, Gandre-Babbe and van der Bliek, 2008, Zhao et al., 2011, Losón et al., 2013). This phenomenon suggests a complex recruitment mechanism for Drp1 in mammalian cells with the possibility of additional unidentified accessory proteins (Koirala et al., 2013, Chen and Chan, 2005, Wilson et al., 2012).

In this chapter, the effect of loss of sacsin function on mitochondria associated Drp1 recruitment was investigated to further establish cellular pathogenic mechanisms of ARSACS.

4.2 Localisation of mitochondrial fission protein Drp1 in Sacsin Knockdown Fibroblast

Fibroblasts were transfected with mitoDsRed along with either SACS or SCRM siRNA. Cells were fixed and stained with anti-Drp1 (green) and DAPI (blue). Confocal imaging was performed and two methods were employed to quantify Drp1 localisation.

4.2.1 Quantification of Drp1 Localised to the Mitochondria in Sacsin Knockdown Fibroblasts

Firstly, the number of Drp1 foci per micrometer of mitochondrial length was determined using the line trace function of the LSM510 confocal software (Zeiss). Line trace measured the intensity of both the red and green channel along individual mitochondria (Figure 4. 2A). Peaks in green intensity along this line represented Drp1 foci (Figure 4. 2A-B). The number of Drp1 foci along the measured length of mitochondria was then collated from the graphical and tabular output. Six individual mitochondria were measured in twenty fibroblasts from three separate experiments and the number of Drp1 foci was quantified. This gave an n of 120 mitochondria measured for each treatment in three experimental replicates.

The Surpass and Co-loc, co-localisation module of Imaris, were used in conjunction with this analysis to quantify the degree of overlap between Drp1 foci and mitochondria in the fibroblasts. Surpass was used to define the mitochondria as regions of interest for analysis. The creation and subsequent application of the masking channel in Coloc excluded areas that were attributed to non specific background staining and areas of no signal (Figure 4. 2C). Following this, the thresholds were automatically calculated and statistical data exported (Figure 4. 2C).

Manders' coefficient was used to measure the colocalized overlap of Drp1 (green) and mitochondria (red). This method was chosen due to its properties as a good method of analysis for proteins with diffuse localisation patterns (Costes et al., 2004). Manders'

coefficient is based on the Pearson's coefficient, however unlike Pearson's, the Manders' equation does not take the intensity of the signal being analysed into consideration again making it suited for proteins like Drp1 which is primarily diffuse throughout the cytoplasm (Equation 1) (Costes et al., 2004, Manders et al., 1996). Manders' coefficient is sensitive to thresholding therefore outputs heavily rely on the thresholds set to distinguish real signal from background. The coefficient ranges in values from 0 (corresponding to no overlapping) to 1 (representing 100% overlap).

$$M_{Red} = \frac{\sum_i R_i coloc}{\sum_i R_i} \qquad M_{Green} = \frac{\sum_i G_i coloc}{\sum_i G_i}$$

Equation 1 Manders' Coefficient.

R_i =grey voxel (*i*) values of Red Ichannel. G_i = grey voxel of Green (G) channel

Imaris Coloc automatic threshold was used to remove any researcher bias as the software uses the Costes algorithm. This algorithm is based on the two-dimensional histogram of both channels which is then used to compute the overall fraction of each protein being colocalized. This computation calculates the probability that a given area will have a p –value of <95% and identifies colocalized pixels based on the overall fraction of overlapping proteins (Costes et al., 2004).

For the colocalization analysis, Z-stacks were collected from five fibroblasts in three experiments from each condition. The difference in the amount of Drp1 colocalization with mitochondria was insignificant with Manders' coefficient for *SCRM* and *SACS* siRNA treated fibroblasts being 0.092 ± 0.005 and 0.061 ± 0.004 respectively (Fig 4.3C). However, measuring the number of Drp1 foci localised to the mitochondria showed reduction in Drp1 foci per micrometer of mitochondria in SACS fibroblasts (Fig 4.3B). On average, fibroblasts transfected with SACS siRNA had 0.68 ± 0.039 Drp1 foci per µm of mitochondria compared to 0.81 ± 0.047 Drp1 foci per µm of mitochondria for scrambled controls. This reduction in Drp1 foci associated with mitochondria in SACS knockdown cells was significant (p=0.02) (Figure 4. 3B).

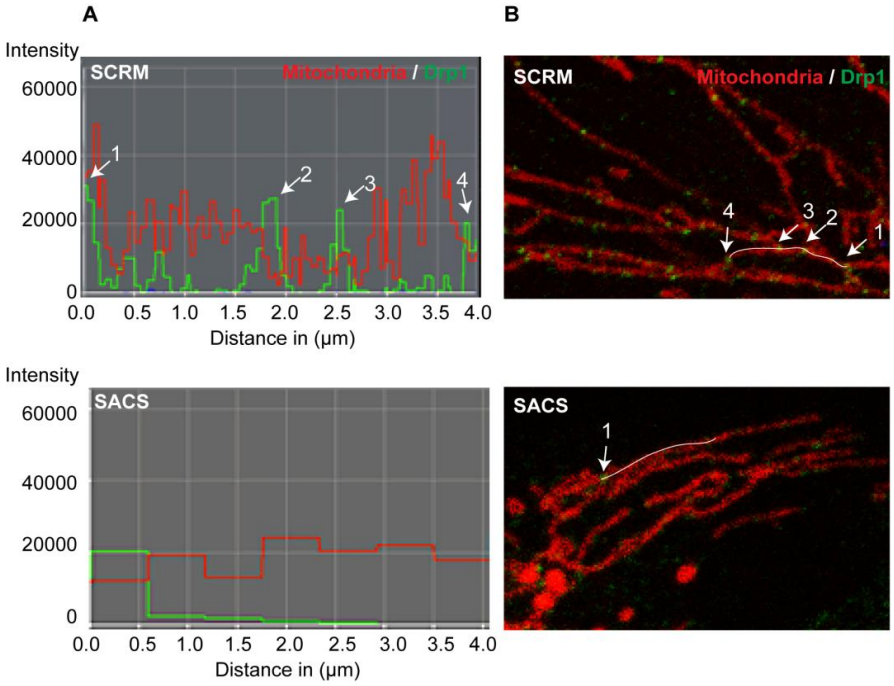

C

Confocal Z-stacks uploaded to Imaris

Surpass Module
Channel Mask built using the following:
[Algorithm]
Enable Region of Interest = false
Enable Region Growing = false
Enable Tracking = false
[Source Channel]
Source Channel Index = 4
Enable Smooth = true
Surface Grain SIze =0.279µm
Enable Eliminate Background = false
Diameter of largest Sphere = 1.05µm
[Threshold]
Enable Automatic Threshold = false
Manual Threshold Value = 1.55605
Active Threshold = true
Enable Automatic Threshold B = true
Manual Treshold Value B = 232.465
Active Threshold B = false
[Classify Surfaces]
Number of Voxels above 3.07e5
[Apply Mask]
Inside suface voxels = 4095
Outside surface voxels = 0

Coloc Module
Open newly masked image in the new module
[Define Region of Interest]
Apply Mask Channel
[Thresholding]
Calculate thresholdings
Enable PSF Width = true
Enable P-Value = true
P-Value =1
% of random image with a larger correlation = 0.000%

Build Coloc Channel

Export Channel Statistics

Figure 4. 2 Quantification methods used for analyses of Drp1 mitochondrial localisation.

Fibroblasts were transfected with mitoDsRed along with either SACS or SCRM siRNA. Cells were fixed and stained for Drp1 (green) 48hours post transfection. Line traces were performed along the length of the mitochondria (red) and the number Drp1 foci (green peaks) were counted. A-B) Representative, zoomed images and their corresponding line traces for each condition. Line traces are indicated by white line and arrows on the confocal image. C) Imaris workflow for quantifying Drp1 colocalization with mitochondria in SCRM and SACS fibroblasts.

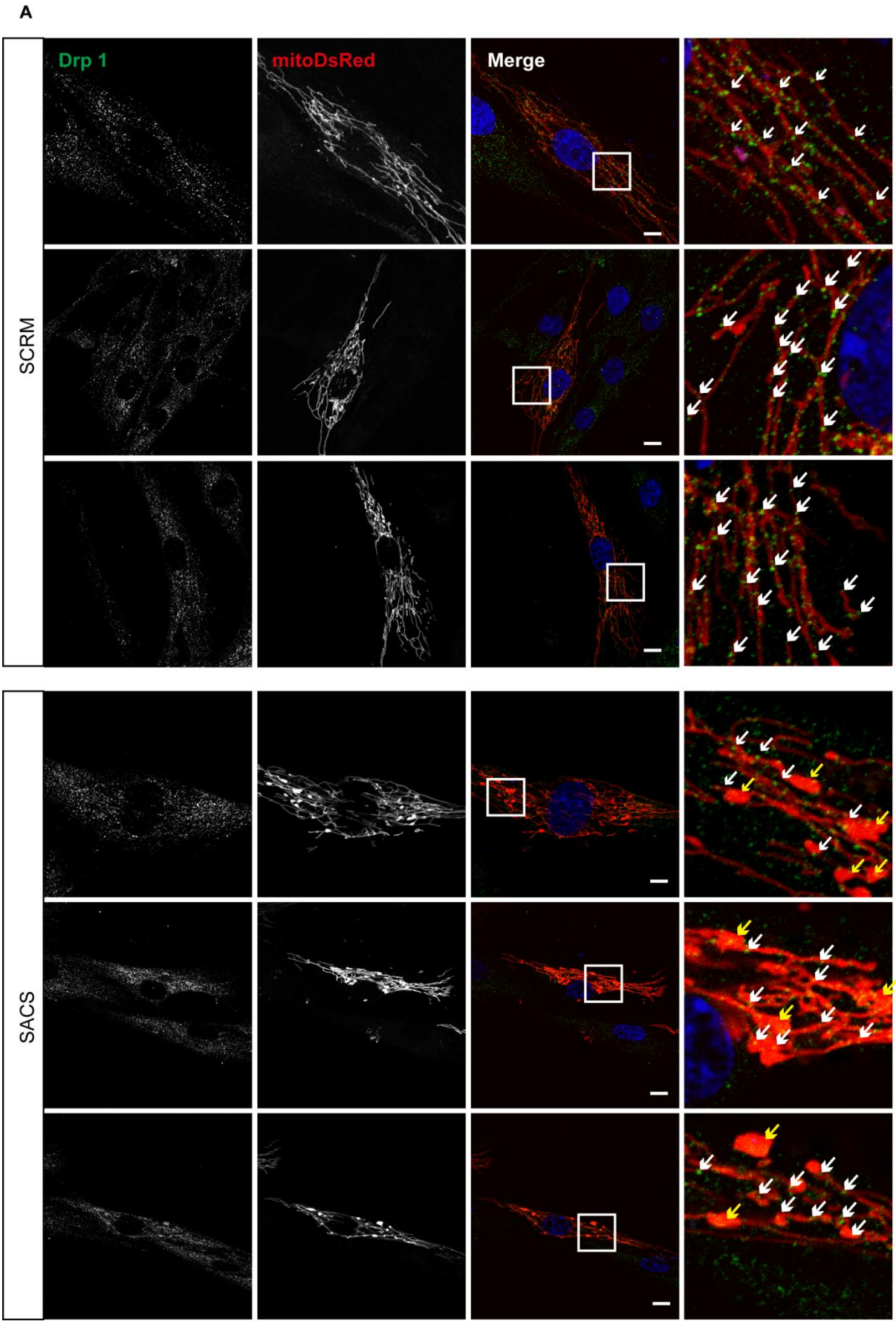
A
Drp 1
mitoDsRed
Merge
SCRM
SACS

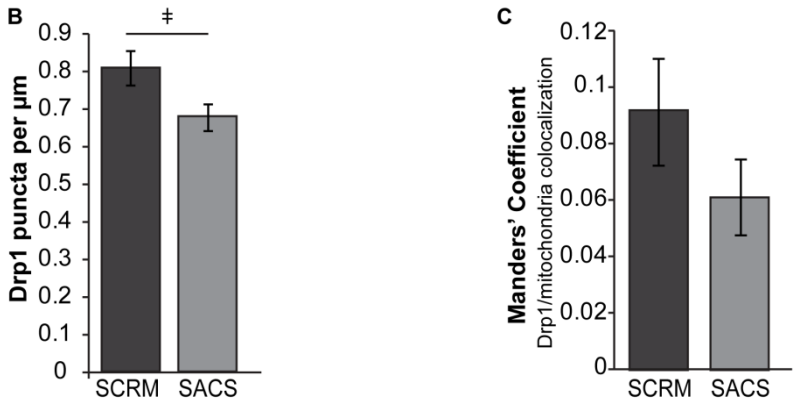

Figure 4. 3 Reduced localisation of Drp1 foci to mitochondria was observed in SACS fibroblasts

Representative confocal images of SACS and SCRM fibroblasts. Fibroblasts were transfected with mitoDsRed along with either SACS or SCRM siRNA. Cells were fixed and stained for Drp1 (green) 48 hours post transfection. The white box in the merged panel is shown zoomed in the panel on the far right. White arrows indicate Drp1 foci in close proximity to mitochondria. Yellow arrows show areas of hyperfusion in SACS fibroblasts. B) Quantification of the mean number of Drp1 in SACS and SCRM fibroblasts, showed reduced Drp1 foci per µm of mitochondria. Line traces were performed along the length of mitochondria (red) and the number Drp1 foci (green peaks) were counted. 6 mitochondria were analysed per cell in 20 fibroblasts per experiment. 3 experiments for each condition were analysed. C) Drp1 colocalisation with mitochondria was analysed using the Coloc module of Imaris in 15 cells (5 x 3 experiments) from each condition. Z-stacks were collected and used to establish the degree of colocalisation. This was expressed as Manders coefficient of Drp1/mitochondria. Error bars represent SEM, ‡ p=0.02 Scale bar = 10µm

4.2.2 Effect of Induced Fission on Drp1 Localisation in Sacsin Knockdown Fibroblasts

The previous results showing a reduction of Drp1 foci at mitochondria would suggest that there is a defect in the Drp1 recruitment in sacsin null cells. To investigate if knockdown fibroblasts were fully fission competent, cells were exposed to 20µM carbonyl cyanide *m*-chlorophenyl hydrazone (CCCP) for 1hr before mitochondrial morphological analysis. Carbonyl cyanide *m*-chlorophenyl hydrazone inhibits oxidative phosphorylation leading to uncoupling of the proton gradient and resulting in mitochondrial fragmentation through unopposed Drp1 mediated fission (Legros et al., 2002).

Fibroblasts were transfected with mitoDsRed and either SACS or SCRM siRNA. The fibroblasts were fixed and stained for Drp1 (green) and DAPI (blue) 48 hours post transfection. Confocal Z-stacks were taken and Imaris was used to surface render mitochondria, enabling quantification of the number of mitochondria in each cell as previously described. In this instance, for each condition, six mitochondria were measured in fourteen cells from three separate experiments. In these experiments, successful fission was quantitatively verified by an increase in the number of mitochondria. Complete fission appears to occur in SCRM siRNA transfected fibroblasts. Small fragmented mitochondria were seen after 1 hour of CCCP treatment (Figure 4. 4A). This observation was further validated by quantification using the Imaris software. A large increase in number of mitochondria in SCRM fibroblasts occurred after treatment with CCCP ($p=0.0002$). Untreated SCRM fibroblasts had an average of 55.89 ± 6.70 mitochondria compared to 95.13 ± 5.60 mitochondria in CCCP treated SCRM fibroblasts (Figure 4. 4). CCCP appeared to also induce fission in SACS knockdown fibroblasts as there was a small increase in mitochondrial number, however this was not significant at the $p<0.05$ level of significance (Figure 4. 4B). The average number of mitochondria went from 34.07 ± 3.22 in untreated cells to 46.88 ± 5.07 in treated cells. While some degree of fragmentation was observed, in parts, hyperfused mitochondrial networks remained (Figure 4. 4A). This was not the case in SCRM siRNA transfected fibroblasts (Figure 4. 4A).

Interestingly, a small but insignificant increase in Drp1 recruitment was observed after treatment with CCCP in SACS knockdown fibroblasts (Figure 4. 4B) 0.42 ± 0.025 Drp1 foci per µm of mitochondria were recorded in untreated cells whilst 0.52 ± 0.018 Drp1 foci per µm of mitochondria were present after CCCP. In contrast there was a significant increase in Drp1 localisation at the mitochondria after CCCP treatment in SCRM controls (Figure 4. 4C). The 1.02 ± 0.028 Drp1 foci per µm of mitochondria in untreated rose to 1.41 ± 0.038 Drp1 foci per µm of mitochondria in CCCP treated fibroblasts.

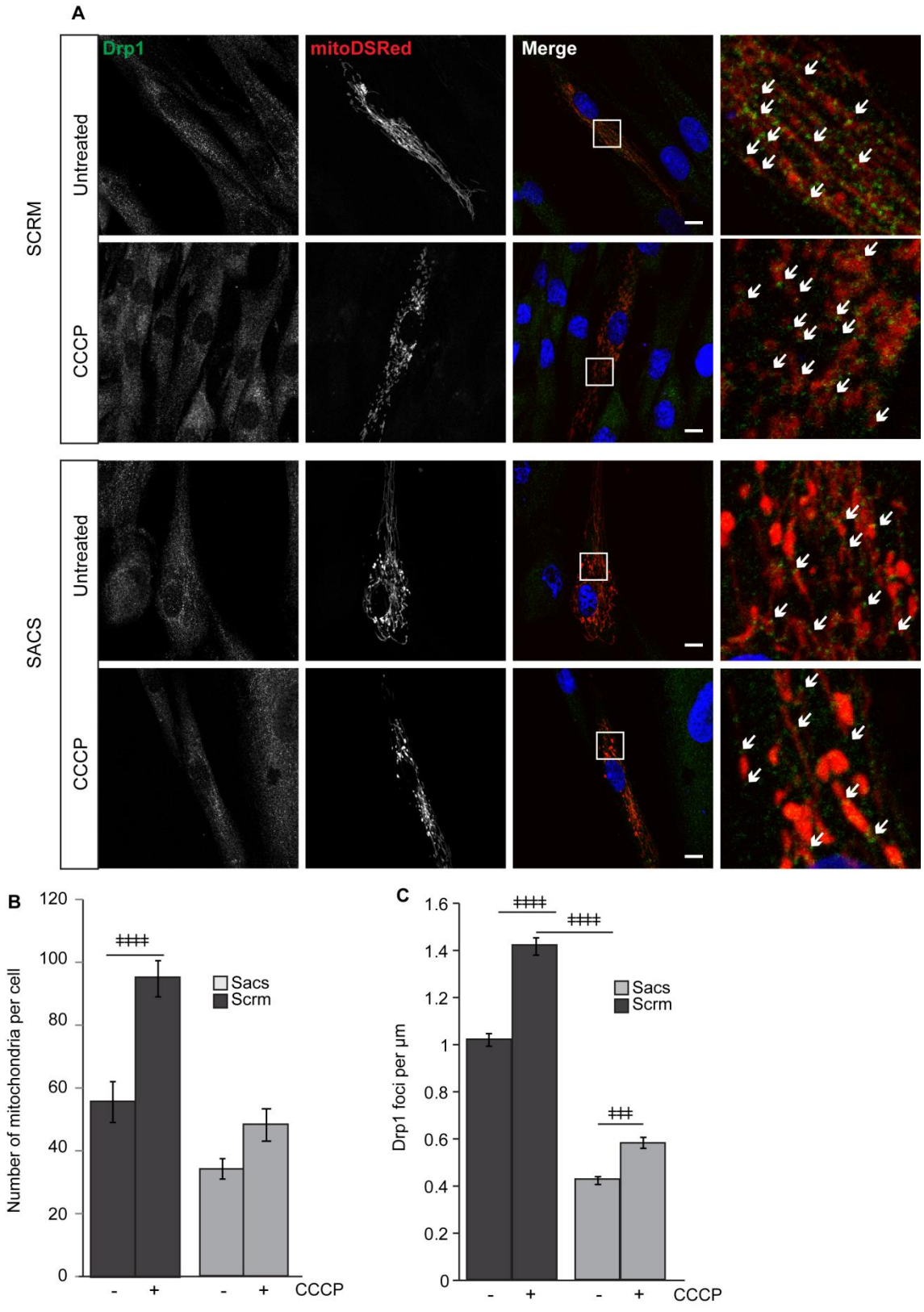
A
Drp1
mitoDSRed
Merge
SCRM
Untreated
CCCP
SACS
Untreated
CCCP
B
Number of mitochondria per cell
120
100
80
60
40
20
0
###
Sacs
Scrm
- + - + CCCP
C
Drp1 foci per µm
1.6
1.4
1.2
1
0.8
0.6
0.4
0.2
0
###
###
##
Sacs
Scrm
- + - + CCCP

Figure 4. 4 Drp1 recruitment to mitochondria was reduced in *SACS* knockdown fibroblasts following CCCP treatment. Fibroblasts were transfected with mitoDsRed along with either SACS or SCRM siRNA. 48 hours post transfection, cells were incubated for 60 mins with 20µM of mitochondrial uncoupler CCCP to induce fission. Fibroblasts were then fixed and stained for Drp1 (green). A) Representative confocal images showing an increase in mitochondrial fragmentation in control fibroblasts after treatment with CCCP. The white box in the merged panel is shown zoomed in the panel on the far right. Zoomed panel clearly show hyperfused mitochondria in SACS fibroblasts. White arrows indicate Drp1 foci in close proximity to mitochondria. B) Imaris image analysis software was used to 3D surface render the mitochondrial network and to quantify the number of mitochondria. C) The number of Drp1 foci per µm of mitochondria was quantified from confocal images. Scale bars represent 10µm ‡‡‡‡ p≤0.0001 ‡‡‡p≤0.001

4.3 Localisation of Mitochondrial Fission Protein Drp1in ARSACS Fibroblast

4.3.1 Quantification of Total Drp1 Protein

Immunoblotting and subsequent quantification of total Drp1 in sacsin fibroblasts was difficult due to low transfection efficiency with siRNA. This analysis was however possible in ARSACS fibroblasts. The immunoblot and densitometry analysis show that the total Drp1 protein levels were similar in 4 ARSACS patients and 4 control lines (Figure 4. 5A). Fibroblasts were labelled with Tom20 antibody for mitochondria (red), Drp1 (green) and nuclear stain DAPI (blue). Confocal images were taken and the number of Drp1 foci per µm of the mitochondria was quantified as previously described. Six mitochondria were measured in twenty-five fibroblasts from three separate experiments and the number of Drp1 foci was quantified.

4.3.2 Quantification of Drp1 Localised to the Mitochondria in ARSACS fibroblasts

In this instance, five cultured control fibroblasts lines from five healthy individuals were compared with the ARSACS patient cell lines (Figure 4. 6). A significant reduction ($p \leq 0.0001$) of Drp1 foci localised to the mitochondria was observed in all of the ARSACS patients when compared to controls (Figure 4. 6A-B). An average of 0.84 ± 0.028 Drp1 foci per µm of mitochondria was observed in the controls while interestingly, patient K1715*/R4331Q which displayed the most collapsed mitochondrial network described in chapter 3, had 0.19 ± 0.020 Drp1 foci per µm of mitochondria. (Figure 4. 6B). Patients R2002fs/Q4054* and 2801delG had 0.58 ± 0.023 Drp1 foci per µm of mitochondria and 0.62 ± 0.023 Drp1 foci per µm of mitochondria respectively (Figure 4. 6B). Lastly fewer Drp1 foci per µm mitochondria were found to be localised to the mitochondria in patient c.2094-2A>G/ Q4054*, with 0.39 ± 0.031 Drp1 foci per µm of mitochondria recorded (Figure 4. 6B).

The degree of overlap between Drp1 (green) and mitochondria (red) was also investigated using Imaris image analysis. For these analyses, cells were stained with Tom20 red, and Drp1 green. For the colocalization analyses, confocal Z-stacks of 25 cells were acquired from each of three separate experiments. The colocalization highlighted the reduced Drp1 foci localised to the mitochondria in patient K1715*/R4331Q with the Manders' coefficient of 0.08 ± 0.003, the lowest of all of the patients (Figure 4. 6C). This was significantly ($p \leq 0.0001$) less than the controls and agreed with earlier quantification of Drp1 foci per µm of mitochondria. Patients R2002fs/Q4054* and patient 2801delG Manders' results also showed significantly less Drp1 localised to the mitochondria than in the controls fibroblasts with values of 0.13 ± 0.005 ($p \leq 0.05$) and 0.10 ± 0.12 ($p \leq 0.001$) respectively (Figure 4. 6C). In contrast to the results obtained from quantifying the number of Drp1 foci localised to the mitochondria, these colocalisation results did not show any statistical difference (>0.05) in Drp1 localisation between control at 0.17 ± 0.005 and patient c.2094-2A>G/ Q4054* 0.15 ± 0.009 (Figure 4. 6C).

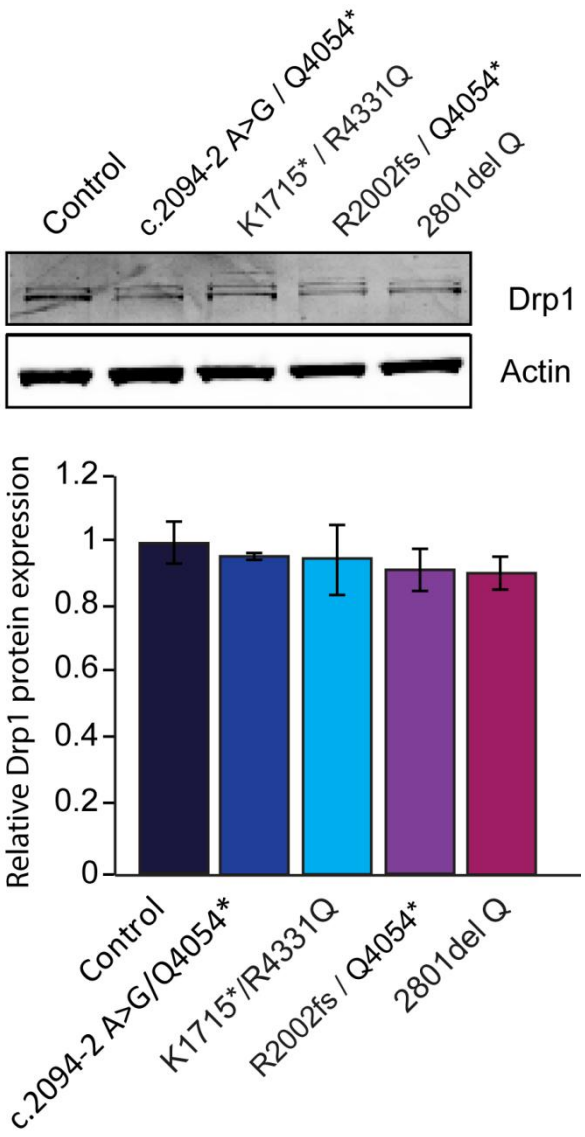

Figure 4. 5 Western Blot analysis of Drp1 expression in control and ARSACS patients' fibroblasts

Densitometric analysis of the western blot revealed similar levels of Drp1 expression in patients and controls. Levels were normalised to β-Actin and then to the control. Error bars represent SEM. N=3

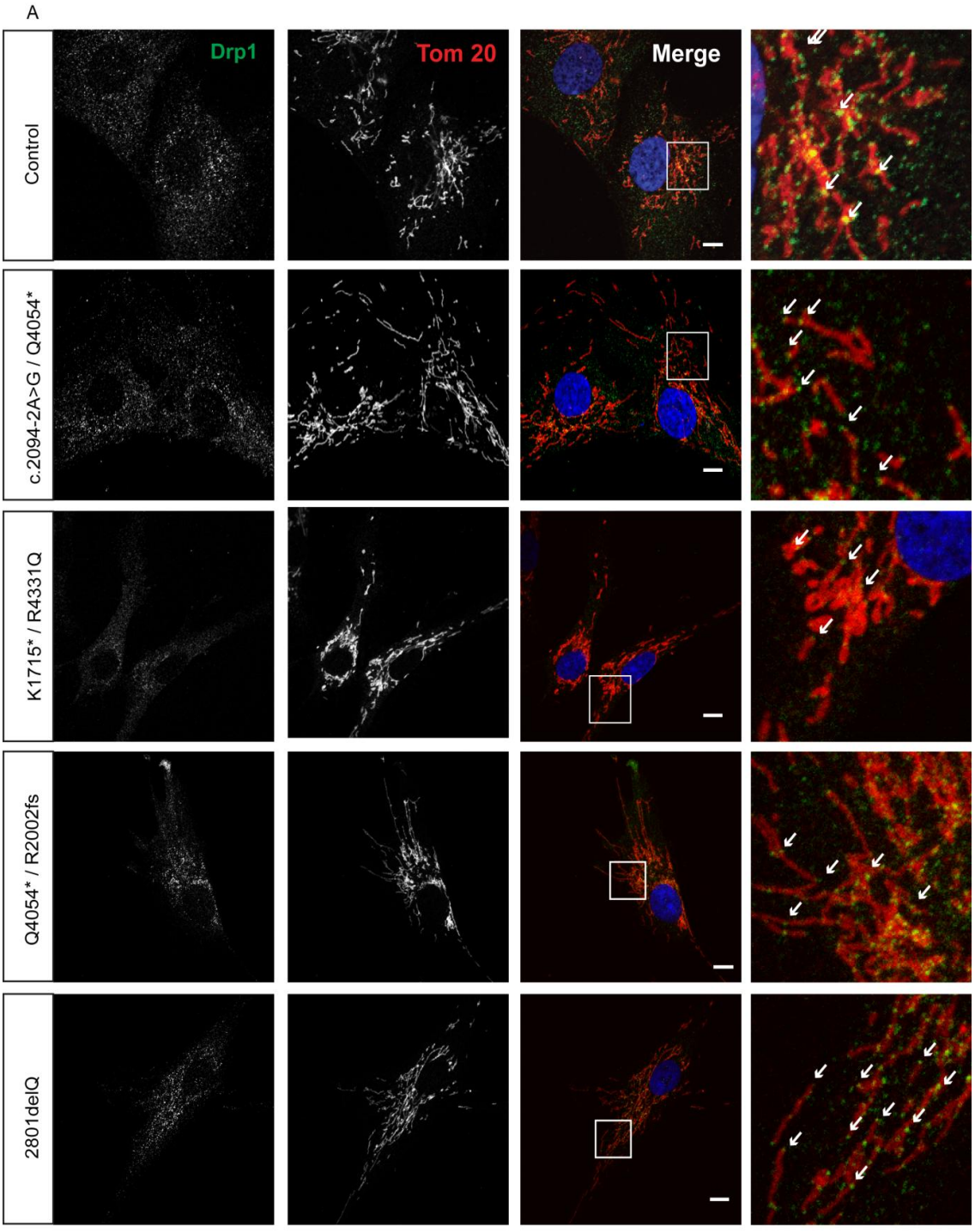
A
Drp1
Tom 20
Merge
Control
c.2094-2A>G / Q4054*
K1715* / R4331Q
Q4054* / R2002fs
2801delQ

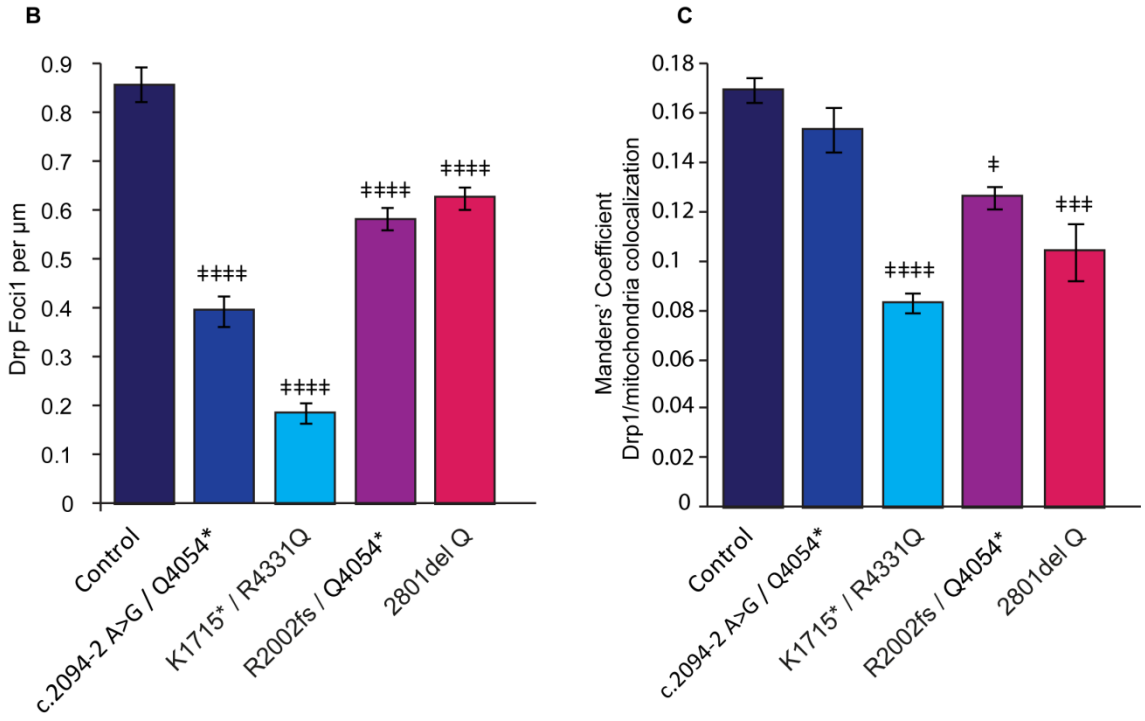

Figure 4. 6 Mutation in *SACS* impairs Drp1 recruitment to prospective sites of fission.

Fibroblasts were fixed and stained with Tom20 (red) and Drp1 (green). Confocal images were taken and line traces were used to quantify the number Drp1 foci localised to the mitochondria. Arrows indicate Drp1 foci localised to the mitochondria. B) Quantification of Drp1 foci localised to the mitochondria. C) Colocalization of Drp1 and the mitochondria was quantified in the patients represented by Manders' coefficient. Error bars represent SEM. Scale bar=10µm. ‡ $p<0.05$ ‡‡‡ $p\leq0.001$ ‡‡‡‡ $p\leq0.0001$

4.3.3 Effect of Induced Fission on Drp1 Localisation in ARSACS Fibroblasts

To investigate if patient fibroblasts were fully fission competent, cells were exposed to 20µM carbonyl cyanide *m*-chlorophenyl hydrazone (CCCP) for 1hr before the analysis of mitochondrial morphology. Fibroblasts were fixed and stained with Tom20 (red) for the mitochondria, Drp1 (green) and DAPI (blue). Confocal images and Z-stacks were collected and analysed as previously described. In these patients and controls, six mitochondria where measured in fifteen cells from three separate experiments, for each condition.

Small fragmented mitochondria were seen after 1 hour of CCCP treatment in control cells. This was accompanied by an increase in Drp1 localised to the mitochondria. A less fragmented mitochondrial network was observed in ARSACS patient cells after treatment with the uncoupler. This suggests a partial inhibition of CCCP induced mitochondrial fission due to the observed reduction in Drp1 foci localised to the mitochondria (Figure 4. 7A).

Quantification of confocal images of fibroblasts from patients and controls demonstrated there was significantly ($p \leq 0.0001$) more Drp1 localised to the mitochondria after CCCP treatment in control fibroblasts than in patient fibroblasts. The amount of Drp1 foci per micrometer of mitochondria in the controls increased from 0.89 ± 0.039 to 1.27 ± 0.064 Drp1 foci per µm of mitochondria after treatment with CCCP (Figure 4. 7B). Interestingly, a small but insignificant increase in Drp1 localisation at mitochondria was observed after treatment with CCCP in all of the ARSACS fibroblasts (Figure 4. 7B). In patient c.2094-2A>G/ Q4054*, 0.49 ± 0.034 of Drp1 foci per µm of mitochondria was recorded in untreated cells whilst 0.61 ± 0.06 Drp1 foci per µm of mitochondria counted after CCCP. As well as having more Drp1 recruitment than in the other patients, more mitochondrial fragmentation than the other patients was also observed. Patient K1715*/R4331Q which had the most interconnected mitochondrial phenotype exhibited the least amount of fragmentation

as well as a very small increase in Drp1 foci associated with mitochondria after CCCP treatment. Untreated K1715*/R4331Q fibroblasts had 0.34 ± 0.034 Drp1 foci per µm of mitochondria which after treatment rose to 0.43 ± 0.048 Drp1 foci per µm of mitochondria. Patient R2002fs /Q4054* and 2801delG had 0.48 ± 0.017 and 0.59 ± 0.044 Drp1 foci per µm of mitochondria respectively, when untreated (Figure 4. 7). In these two cases, the amount of Drp1 foci per µm of mitochondria after CCCP again increased, however the increases were not at a statistically significant level ($p \geq 0.05$) with 0.51 ± 0.046 and 0.62 ± 0.038 Drp1 foci per µm of mitochondria respectively (Figure 4. 7B).

To assess the levels of CCCP induced fission, the average number of mitochondria per cell was quantified in patient K1715*/R4331Q, as it exhibited the most extreme, collapsed mitochondrial phenotype compared to controls cell lines (chapter 3.4) and also showed a reduction in Drp1 foci per micrometer of the mitochondria. The quantification of the average number of mitochondria after CCCP treatment was also performed in patient c.2094-2A>G/ Q4054*. This patient had a less severe mitochondrial phenotype (chapter 3 section 3.4) when compared to the controls and also displayed the largest increase in Drp1 foci per micrometer of the mitochondria when compared to the other patients.

An increase in the number of mitochondria was seen in both patients and controls after CCCP treatment. This increase however was not of the same magnitude as in the controls. The controls had a significant ($p \leq 0.0001$) increase in the average number of mitochondria from 92.20 ± 30.84 when untreated to 260.9 ± 13.00 when treated with CCCP. A significant ($p \leq 0.05$) increase was also observed in patient c.2094-2 A>G /Q4054*. The average number of mitochondria increased from 63.70 ± 22.94 when untreated to 144.7 ± 15.57 mitochondria when treated with CCCP. An increase in the number of mitochondria in patient K1715*/ R4331Q from 46.38 ± 27.03 to 112.5 ± 9.93 however this increase was deemed statistically insignificant by ANOVA testing. This result suggests partial inhibition of fission occurs due to reduced Drp1 recruitment (Figure 4. 7C).

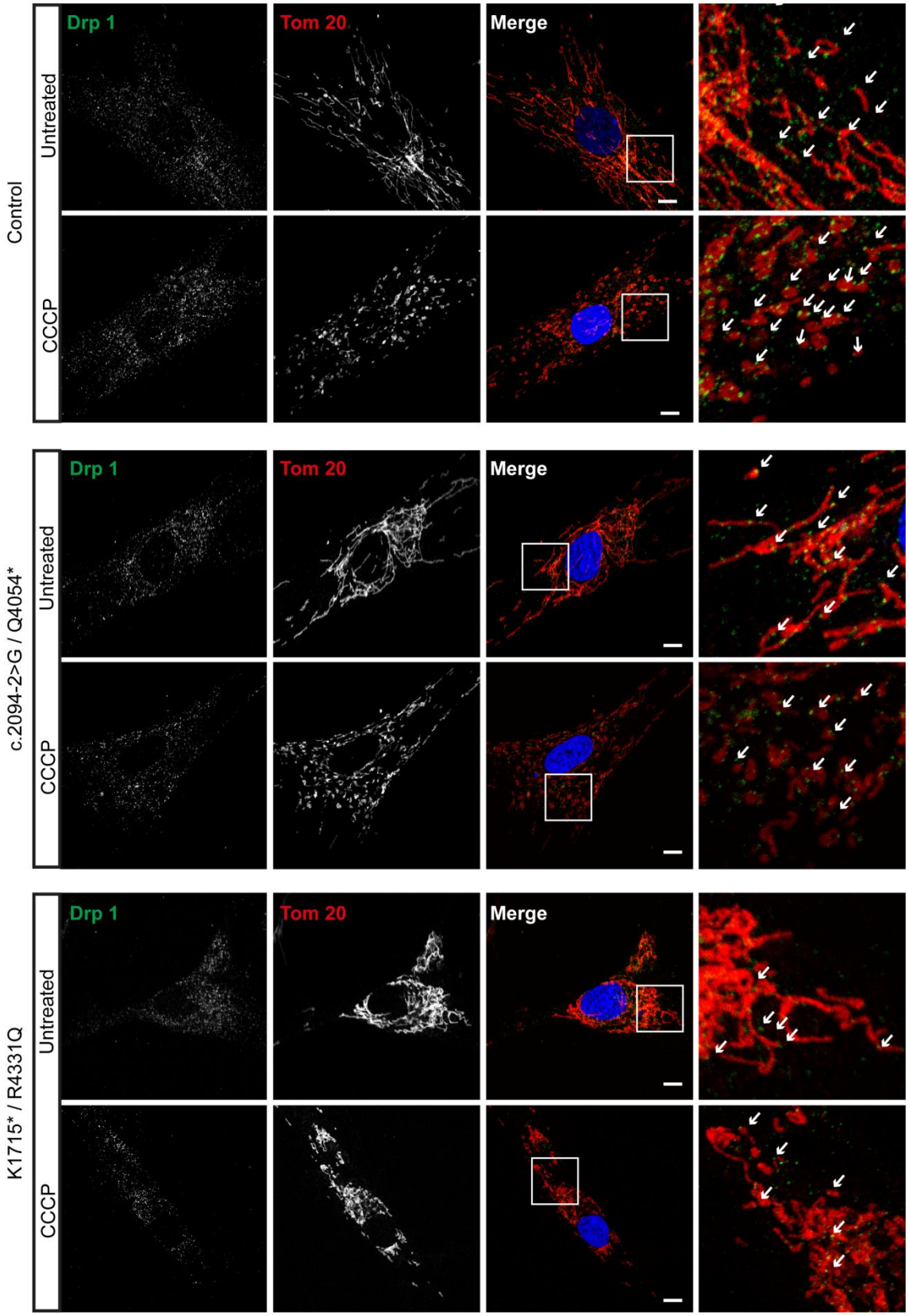
Control
Untreated
CCCP
Drp 1
Tom 20
Merge
c.2094-2>G / Q4054*
Untreated
CCCP
Drp 1
Tom 20
Merge
K1715* / R4331Q
Untreated
CCCP
Drp 1
Tom 20
Merge

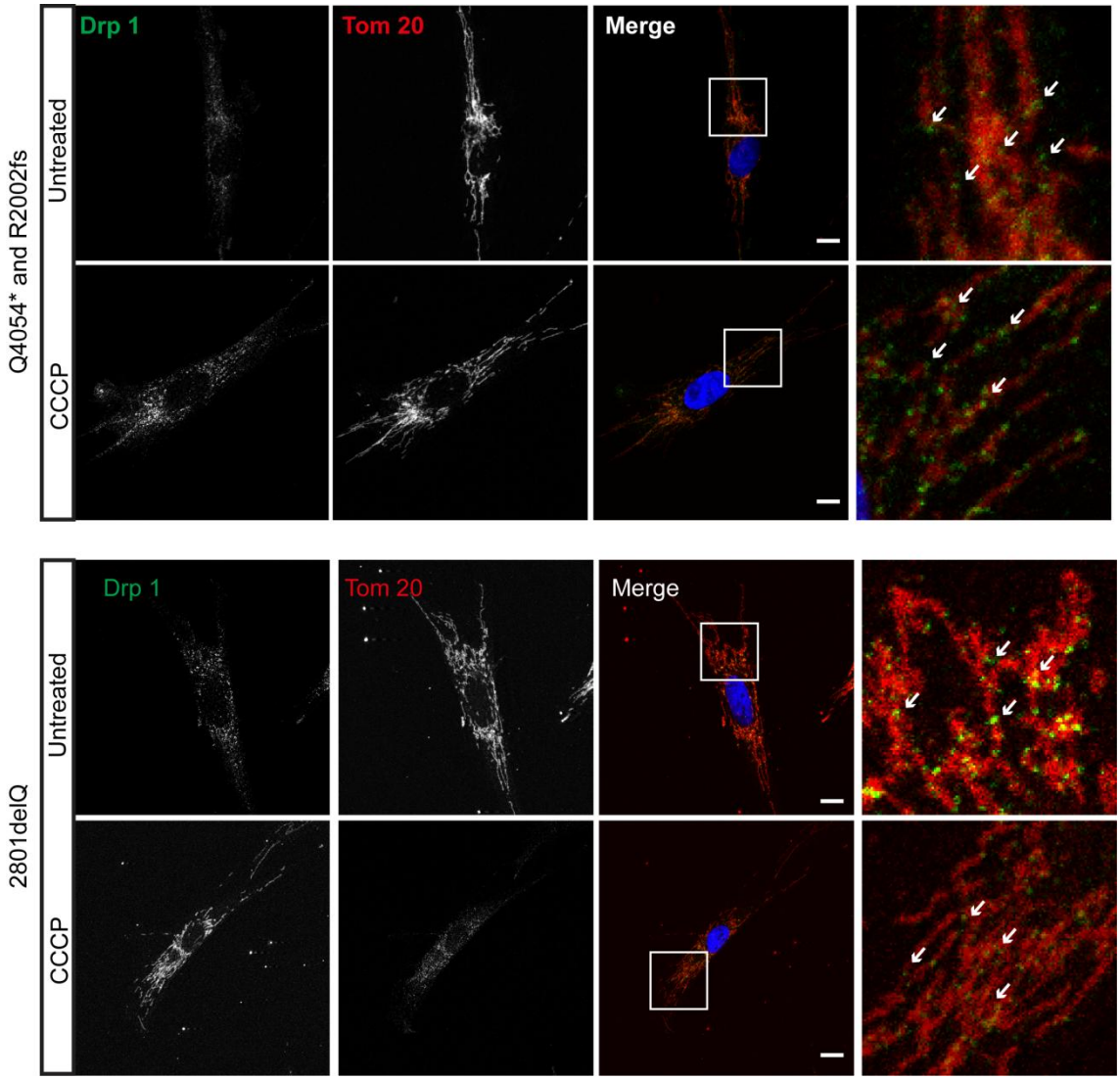
Drp 1
Tom 20
Merge
Untreated
CCCP
Q4054* and R2002fs
Drp 1
Tom 20
Merge
Untreated
CCCP
2801delQ

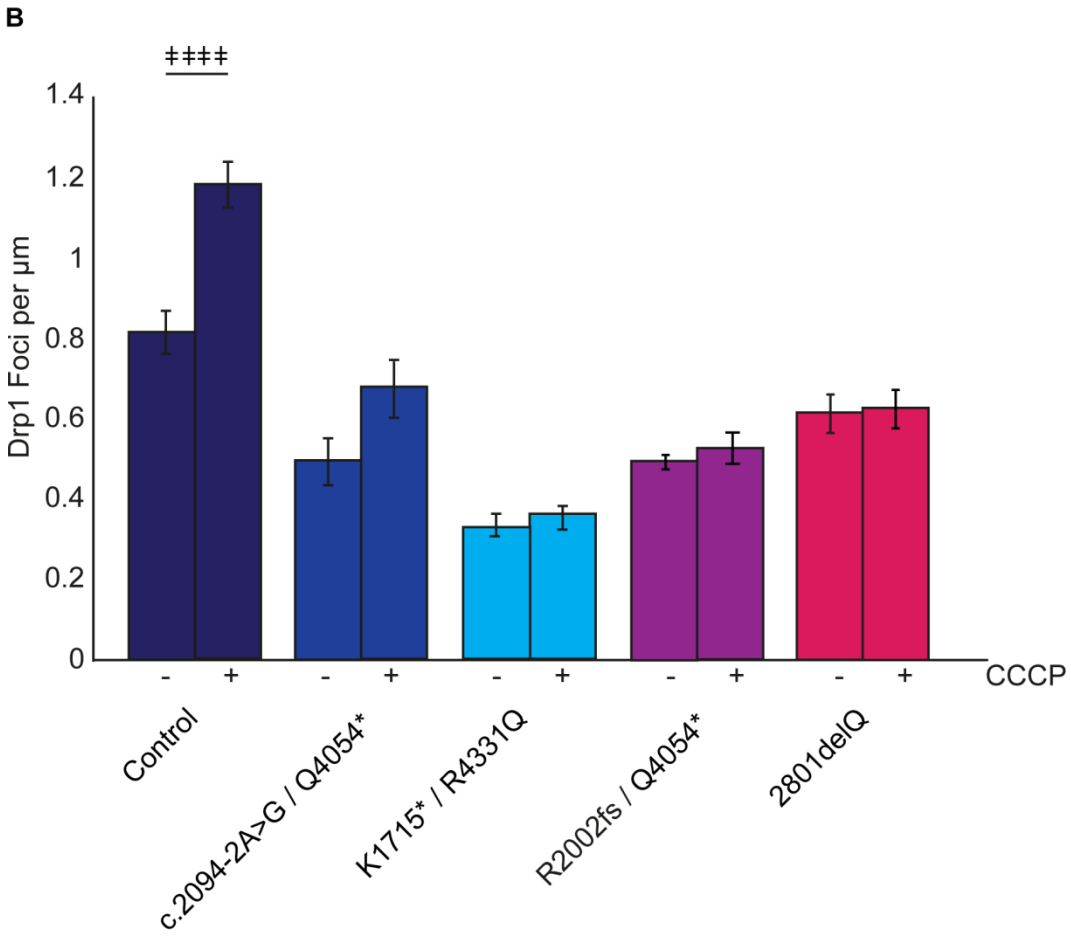
B
‡‡‡‡
1.4
1.2
1
0.8
0.6
0.4
0.2
0
Drp1 Foci per µm
- + - + - + - + - +
CCCP
Control
c.2094-2A>G / Q4054*
K1715* / R4331Q
R2002fs / Q4054*
2801delQ

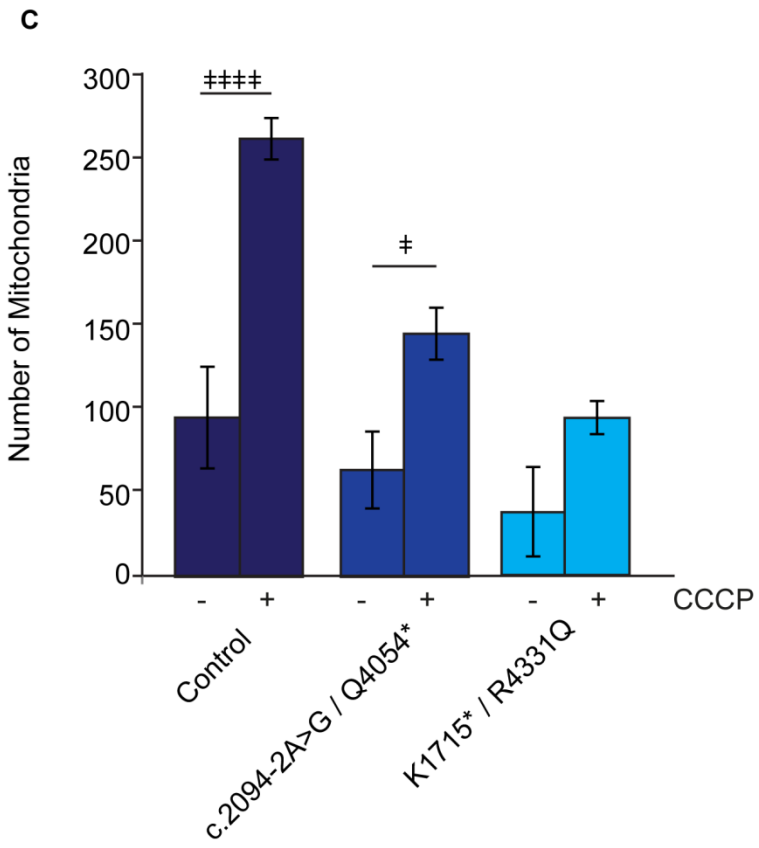
C
‡‡‡‡
‡
300
250
200
150
100
50
0
Number of Mitochondria
- + - + - +
CCCP
Control
c.2094-2A>G / Q4054*
K1715* / R4331Q

Figure 4. 7 Drp1 recruitment to the mitochondria was not significantly increased after fission was induced in ARSACS fibroblasts

Fibroblasts were incubated for 60mins with 20µM of CCCP prior to fixation and staining with Tom20 for mitochondria (red), Drp1 (green) and DAPI. B) The number of Drp1 foci per µm of mitochondria was quantified from confocal images using ZEN software. Confocal Z stacks were taken and cell images were rendered using Imaris. Scale bars represent 10µm.

To summarise the data so far in this chapter, there are significantly fewer Drp1 foci localised to the mitochondria in both sacsin knockdown and in ARSACS patient fibroblasts than in the control cells. Importantly, cells without sacsin showed a reduction in the recruitment of Drp1 to mitochondria after the induction of mitochondrial fission by the addition of uncoupler, CCCP. These localisation results strengthen the hypothesis that loss of sacsin function impairs Drp1 recruitment and it is by this mechanism that mitochondrial dynamics is impaired in ARSACS.

4.4 Drp1 Foci Diameter and Intensity in Sacsin Knockdown and ARSACS Fibroblasts

Further evaluation of sacsin's role in Drp1 recruitment and stabilisation was addressed by measuring the size and intensity of mitochondria associated Drp1 foci and cytosolic Drp1 foci. This was of interest as loss of mitochondrial fission proteins lead to a reduction of the size and intensity of Drp1 foci associated with mitochondria (Losón et al., 2013). As sacsin is in close proximity with Drp1 (Girard et al., 2012) and appears to be involved in the recruitment of Drp1 foci to the mitochondria, the effect of sacsin knockdown and SACS mutations on the size and intensity of Drp1 was investigated.

Fibroblasts were transfected with mitoDsRed along with either SACS or SCRM siRNA. Cells were fixed and stained with anti-Drp1 (green) and DAPI (blue) and confocal images were taken. To avoid variability related to image acquisition and or immunocytochemistry methodology, all samples were stained simultaneously. Confocal imaging of the samples was also performed on the same day using the same acquisition settings (16 bit confocal Z-stack images through the cell were acquired at 0.45µm Z intervals for quantification). Imaris modules Surface and Measurement Pro were used to measure the intensity and diameter of five Drp1 foci on five randomly chosen mitochondria and in five cytosolic regions (Figure 4. 8A). This was carried out for six cells in three experiments, giving a total n number of 450 measurements of Drp1 foci in the cytosol and 450 measurements of mitochondria associated Drp1 foci.

The diameters of cytosolic Drp1 foci were similar in cells transfected with sacsin targeting and scrambled siRNAs. The average diameters of cytosolic Drp1 foci in SCRM and SACS were 0.38 ± 0.005µm and 0.36 ± 0.009µm respectively. Mitochondria associated Drp1 foci in control cells were 0.52 ±0.0094µm in diameter. This was 17.5% larger than that observed in sacsin knockdown fibroblasts, which had mitochondrial foci with an average diameter of 0.44 ± 0.008µm ($p \leq 0.01$) (Figure 4. 8B).

The fluorescence intensity of mitochondrial Drp1 foci relative to cytosolic Drp1 fluorescence intensity was used as a method of further characterising Drp1 recruitment. The mean intensity of Drp1 foci was collected, using the Measurement

Pro and Surface modules of Imaris. Once collected, the mean mitochondrial Drp1 foci fluorescence intensity was divided by the mean intensity of cytosolic Drp1 foci within the same cell generating a ratio used to define the relative Drp1 foci fluorescence. This analysis was similar to work carried out by Losón et al 2013 and Zunino et al 2009 where the relative fluorescence intensity of mitochondria associated Drp1 foci compared to cytosolic Drp1 foci was presented as a means of measuring for Drp1 recruitment and the formation of oligomers at the outer mitochondrial membrane. The relative intensity of Drp1 foci was significantly less ($p \leq 0.01$) in the sacsin knockdown fibroblasts than in the SCRM controls (Figure 4. 8). The relative Drp1 foci intensity in sacsin knockdown was 6.97 ± 0.196 AU (arbitrary units for fluorescence intensity) compared to 8.09 ± 0.284 AU recorded in the control cells. These analyses indicated a potential decrease in Drp1 levels in mitochondria associated foci and may suggest a possible problem with Drp1 oligomerisation.

The relative fluorescence intensity of Drp1 foci was further compared ARSACS patient K1715*/R4331Q and control fibroblasts. The results showed that patient K1715*/R4331Q had significantly ($p<0.001$) smaller mitochondrial associated Drp1 foci than the control. In this instance, Drp1 foci in patient K1715*/R4331Q were on average 0.54µm ± 0.008µm, 11.5% less than in the controls where foci averaged 0.61µm ± 0.010µm. Additionally, the relative mean Drp1 intensity was 2.83 ± 0.052AU in ARSACS patient K1715*/R4331Q lower than control 3.48 ± 0.063AU ($p \geq 0.0001$) (Figure 4. 9).

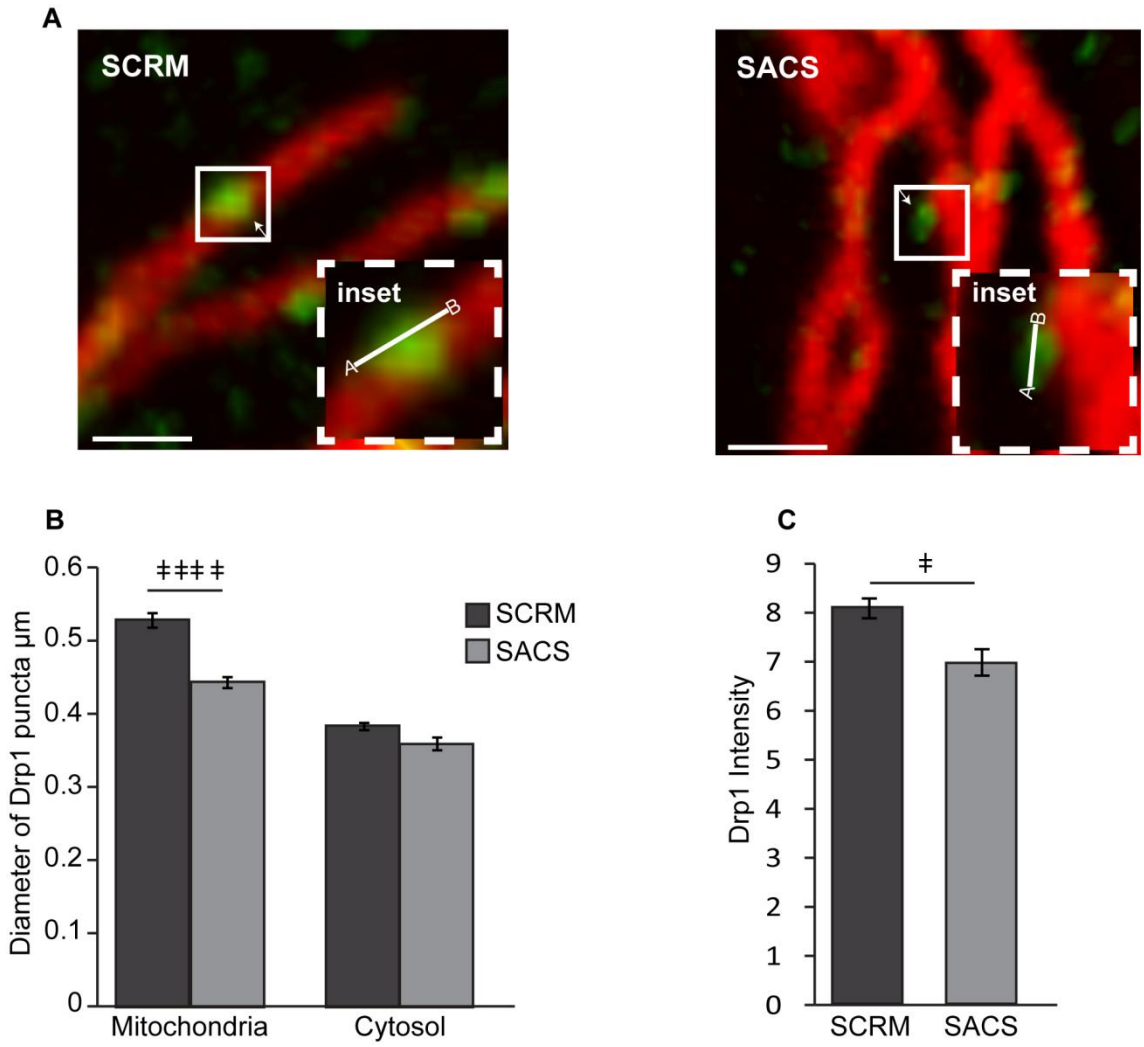

Figure 4. 8 Drp1 foci in SACS knockdown fibroblasts were significantly smaller and less intense than controls.

Fibroblasts were transfected with mitoDsRed along with SCRM or SACS siRNA. Cells were fixed and stained with Drp1 (green). Z-Stacks were collected and analysed using IMARIS image analysis software. Representative zoomed images and insets show examples of how Drp1 foci were measured. B) The diameter and intensity of 5 Drp1 foci on 5 different mitochondria and in 5 cytosolic regions in each cell were measured. Analysis was carried out in 3 experiments consisting of 6 cells per experiment. SACS knockdown fibroblasts had on average smaller Drp1 foci. C) The relative ratio of mitochondrial Drp1/cytosolic Drp1 was less in SACS fibroblasts. ‡‡ $p \leq 0.01$ ‡‡‡‡ $p \leq 0.0001$ Error bars ± SEM Scale bars represent 1µm.

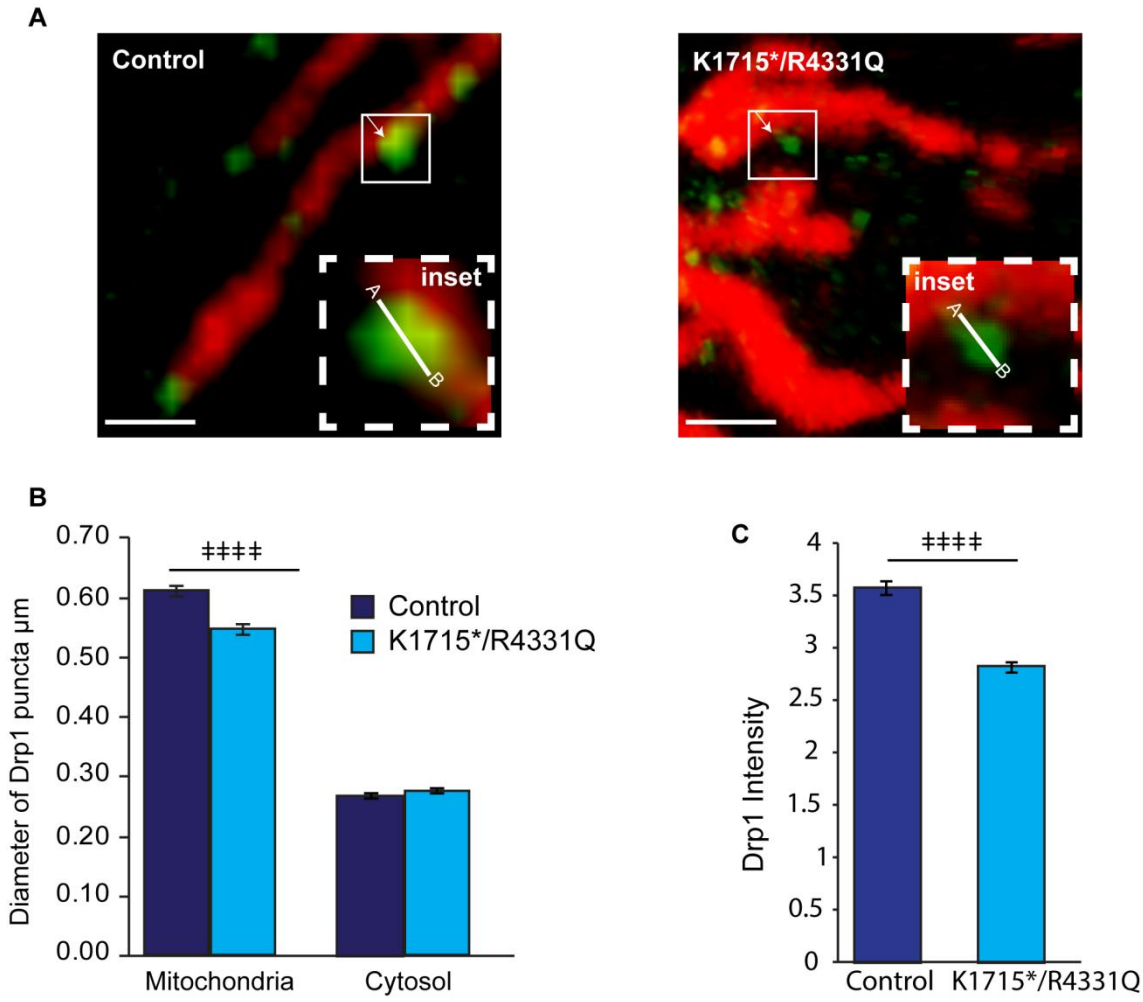

Figure 4. 9 Drp1 foci in patient fibroblasts were significantly smaller and less intense than control

Fibroblasts were fixed and stained with Tom20 (red), Drp1 (green) and DAPI (blue). Representative zoomed images for each condition. B) Drp1 foci were measured and quantified as previously described. Drp1 foci were on average significantly smaller than controls. C) Drp1 foci intensity was ascertained using Imaris surface and measure modules. Error bars ± SEM. ‡‡‡‡ p≤0.0001 Scale bars represent 1µm.

4.5 Discussion

There were significantly fewer Drp1 foci associated with the mitochondria in sacsin knockdown and patient fibroblasts.

We hypothesize that this decrease in Drp1 recruitment to mitochondria accounts for the altered mitochondrial morphology discussed in Chapter 3. Concordantly, similar results have been published in cells where levels of mitochondrial fission accessory proteins MiD49/51, Fis1 and Mff were reduced (Palmer et al., 2011b, Gandre-Babbe and van der Bliek, 2008,(Losón et al., 2013). In these reports, reduction of the aforementioned proteins significantly decreased the number of Drp1 foci localized to the mitochondria, and this was accompanied by an increasingly fused mitochondrial network (Gandre-Babbe and van der Bliek, 2008).

Of importance, the Drp1 localization phenotype observed in SACS and patient fibroblasts did not significantly improve upon inducing fission. These continued to have significantly fewer Drp1 foci per µm of mitochondria when compared to controls. This finding was similar to that reported on MiD49/51 by Palmer et al who observed MiD49/51 knockdown cells had a fourfold decrease in CCCP-induced mitochondrial fragmentation (Palmer et al., 2011a). Similar observations were also made when Mff knockdown cells were treated with the uncoupler CCCP (Gandre-Babbe and van der Bliek, 2008). These results suggest that sacsin, like the MiD and Mff proteins, may be involved in regulating mitochondrial fission. It is however important to note that loss of these proteins did not obliterate fission (Palmer et al., 2011a, Gandre-Babbe and van der Bliek, 2008). Unlike Drp1, loss of the MiD and Mff proteins were non-lethal, emphasizing multiple steps and the involvement of other accessory proteins in the facilitation of the fission process. The complex mechanism which brings about mitochondrial fragmentation along with the low expression of sacsin in skin would suggest that sacsin is not vital in dermal fibroblasts and may in fact only be essential in certain neuronal populations. As neurons have high metabolic demands, they are therefore more sensitive to changes in mitochondrial morphology. Therefore this

decrease in recruitment to the mitochondria and change in morphology may contribute to neurodegenerative aspects of ARSACS pathology.

Strikingly, there is a reduction of intensity and diameter of mitochondria-associated Drp1 in SACS and patient fibroblasts. Again these results are consistent with that of prior studies of known mitochondrial fission proteins. In 2013, Loson et al reported a significant decrease in size and intensity of mitochondria-associated Drp1 in Fis1, Mff and Fis1/Mff knockdown cells (Losón et al., 2013). In theory, as Drp1 forms an oligomeric structure at potential sites of fission, there should be an increase in both the diameter and intensity of Drp1 (green foci) on the mitochondria. The reduction in intensity and diameter suggests that there is either a problem with the recruitment of Drp1 (not going to the mitochondria) or in the stabilization of the oligomeric structure preventing the scission/ fission process.

Drp1 mediated mitochondrial fission consists of several vital stages. It is yet to be determined whether sacsin's role in recruitment of Drp1 to the mitochondria is mainly to assist in sequestering, or if it is also involved in stabilization of Drp1 oligomers involved in scission. Further experiments that analyze and quantify Drp1 oligomers, kinetics and regulation in ARSACS patients or sacsin knockdown cells would contribute towards further defining sacsin's involvement in the fission process. Quantification of cytosolic and mitochondria associated Drp1 protein can be performed by subcellular fractionation and immunoblotting in sacsin knockdown and patients cells. Similar biochemical analyses have been performed in MiD49/51 and Mff studies. A significant reduction of mitochondria associated Drp1 was found in MiD, Fis and Mff null cells whilst there was no difference in total Drp1 protein levels (Losón et al., 2013, Palmer et al., 2011a). Total Drp1 levels were found to be similar in the ARSACS patients and controls, although reduced localization of Drp1 to the mitochondria was observed by confocal imaging and imaging analysis. Therefore further investigation via subcellular fractionation will be useful in validating the reduction of Drp1 recruited to the mitochondria in cells with reduced or no sacsin.

In addition, it is important to note that fission heavily depends on Drp1 cycling dynamics. It is important that Drp1 is able to translocate to the mitochondria, associate and then disassociate rapidly in response to cellular stresses or inducers of mitochondrial depolarization. Wasiak et al established that Drp1 sequestration was delayed in HeLa cells upon the induction of apoptosis (Wasiak et al., 2007). Using FRAP experiments, they postulated that the retarded turnover of yellow fluorescently tagged Drp1 was due to the stabilization and accumulation of Drp1 at the mitochondria preventing it from cycling back to the cytosol (Wasiak et al., 2007). Merrill et al also demonstrated that unopposed fusion led to "slow recycling" of Drp1 and reduced disassembly of oligomers in their neuroprotective cell model (Merrill et al., 2011).

In answering whether the effect of a loss of sacsin on mitochondrial morphology and Drp1 recruitment is related to Drp1 turnover, Drp1 cycling dynamics needs to be examined in control fibroblasts and compared to ARSACS patients and sacsin knockdown cells. Replacing endogenous Drp1 with a GFP-tagged Drp1 plasmid which also co-expresses Drp1 shRNA as described by Cribbs and Strack will allow for more accurate quantification of Drp1 dynamics (Cribbs and Strack, 2007). Time lapsed imaging coupled with observed image analysis software such as Imaris will enable particle tracking via its ImarisTrack and MeasurementPro modules. These modules use a customized algorithm which incorporates Brownian and autoregression motion models as well as other advanced models which assist in tracking and tracing the particles and their migration pathways (Coleri et al., 2013). Comparing the cycling dynamics of the Drp1 protein under normal and fission inducing conditions in patients, controls and knockdown cells will assist in determining the effects of loss of sacsin on Drp1 cycling.

It is also important to take into account the extensive post translational modifications that regulate Drp1 function and recruitment. Therefore there is a need to address the relationship between loss of sacsin and key regulatory modifications. Primarily, determining the phosphorylation status of Drp1 in ARSACS patients and sacsin knockdown cells is important. Phosphorylation of serine 637 is known to inhibit Drp1

activation leading to retention of the protein in the cytosol while dephosphorylation of serine 637 promotes translocation of Drp1 to the mitochondria from the cytosol and subsequently leads to an accumulation of Drp1 at the mitochondria (Knott et al., 2008, Cereghetti et al., 2008). In order to further examine the phosphorylation status of Drp1, the levels of expression and activation of proteins which regulate phosphorylation such as protein kinase A (PKA) and calcineurin possibly needs to be considered. Such investigations will explore sacsin's role in the regulation of Drp1 activity as well as help in understanding sacsin's position in the fission pathway. Defining whether sacsin has a more upstream or indeed downstream role.

Moreover, an investigation on the loss of sacsin and its effect on Drp1 regulation by SUMOylation is yet to be reported. SUMOylation stabilizes Drp1 and enhances fission via E3 ligases such as MAPL (mitochondrial anchored protein ligase) or proteases such as SENP5 (Harder et al., 2004, Wasiak et al., 2007, Zunino et al., 2009, Schauss et al., 2010). Further work to investigate the mitochondrial SUMOylation targets in ARSACS and sacsin knockdown cells will enhance the understanding of loss of sacsin Drp1 regulation and activation.

Taken together, these results support a role for sacsin in Drp1 recruitment, explaining the fission defect suggested by morphometric analyses. Disruptions in mitochondrial dynamics will likely lead to dysfunctional mitochondria. This is investigated in Chapter 6.

Chapter 5

Consequences of Loss of Sacsin Function on Endoplasmic Reticulum and Peroxisomes Morphology

5.1 Introduction

Reduced levels of sacsin correlated with a reduction in the amount of Drp1 recruited to mitochondria. Proteins involved in mitochondrial dynamics have been demonstrated to have roles that go beyond regulation of mitochondrial dynamics. Some mitochondrial fission proteins have been shown to also have a role in regulating the dynamics of other organelles, including peroxisomes and lysosomes. Moreover, mitochondrial fusion proteins have been reported to additionally be involved in the regulation of mitochondrial contact sites with the endoplasmic reticulum. The interactions between the mitochondria and other organelles can also influence mitochondrial dynamics. The dynamic nature of those interactions along with, in some instances, shared components of the fission machinery, reinforces the notion of cross talk occurring between these subcellular compartments (Schrader et al., 2013, Beach et al., 2012, Cheville, 2013, Zampese et al., 2011).

5.2 Endoplasmic Reticulum and the Mitochondria Associated Membrane

The endoplasmic reticulum (ER) is responsible for the synthesis and trafficking of membrane components, including luminal and secretory proteins as well as the synthesis of cellular lipids. Additionally, the ER has a significant role in Ca^{2+} homeostasis and storage within the cell (Franzini-Armstrong, 1963, Henkart, 1980, Weber et al., 2001, Kim et al., 2014).

A physical association between the ER and the mitochondria, termed mitochondria associated membranes (MAM), was experimentally identified in the 1990s (Vance, 1990, de Brito and Scorrano, 2008, Rizzuto et al., 1998). Close contact sites between ER and mitochondrial membranes are tethered by proteins including phosphofurin acid cluster sorting protein 2 (PACS-2) and mitofusin 2 (Mfn2), on the respective membranes (de Brito and Scorrano, 2008, Iwasawa et al., 2010, Kornmann, 2013).

PACS-2 is a multifunctional sorting protein which localizes to both the ER and mitochondria (Simmen et al., 2005). It has been demonstrated to be essential in the maintenance and association of ER with mitochondria by stabilizing and regulating contact (Simmen et al., 2005). The importance of PACS-2 was demonstrated in cells treated with PACS-2 siRNA. The knockdown of this protein resulted in the uncoupling of the ER from the mitochondria and increased mitochondrial fragmentation (Simmen et al., 2005).

Mitochondrial fusion protein, Mfn2 has been found to be essential in ER tethering to the mitochondria (Friedman et al., 2011, de Brito and Scorrano, 2008). Loss of this protein resulted in decreased tethering of the mitochondrial and ER membranes as well as mitochondrial fragmentation (de Brito and Scorrano, 2008, Friedman et al., 2011).

MAMs are enriched with enzymes required in the lipid biosynthetic pathways, phospholipid metabolism and transport (Stone and Vance, 2000, van Meer et al., 2008). One example is Phosphatidylserine synthase 2 (PTDSS2), an enzyme which was primarily found to be present in MAMs and is involved in the biosynthesis of

mammalian cell membrane constituents; phosphatidylserine (PtSer), phosphatidylcholine (PtdCho) and phosphatidylethanolamine (PtEt) (Bergo et al., 2002, Fujimoto et al., 2012, Stone and Vance, 2000). The synthesis of PtSer, facilitated by PTDSS2 and PtdCho, by phosphatidylethonalamine methyltransferase (PEMT) occur in the MAMs (Schon and Area-Gomez, 2013).

The ER releases Ca^{2+} at the mitochondrial contact sites, providing an accumulation of Ca^{2+} required for mitochondrial metabolism (Filippin et al., 2003, Duchen, 2004b, Rizzuto et al., 2004). The close contact with mitochondria facilitates the mitochondrial uptake of Ca^{2+} released from the ER. This is important as the Ca^{2+} imported to the mitochondria increased the efficiency of vital enzymes such as ATP synthase and TCA dehydrogenases (Calì et al., 2012, McCormack et al., 1990).

MAMs are also implicated in the regulation of cell death (Høyer-Hansen and Jäättelä, 2007, Iwasawa et al., 2010, Hamasaki et al., 2013). One proposed mechanism is that apoptosis can be stimulated by the local influx of Ca^{2+}. This arises from the opening of mitochondrial permeability transition pores (mPTP) causing release of cytochrome c and initiating the apoptotic cascade (Pinton et al., 2001, Szalai et al., 1999).

Notably, a number of proteins that play a role in regulating Ca^{2+} and apoptosis are found localized to MAMS (Rizzuto et al., 1998, Lasorsa et al., 2008). These include inositol 1,4,5-trisphophate receptor (IP_3R), the principle intracellular Ca^{2+} release channel, which facilitates the uptake of Ca^{2+} by mitochondria enabling the mediation of apoptosis and the metabolic flow of Ca^{2+} via the voltage dependant anion channel (VDAC) (Szabadkai et al., 2006, Mendes et al., 2005).

The disruption of MAMs may also play a role in neurological disorder such as Alzheimer's disease. Evidence for this includes the observation of an increase in MAMs in hippocampal neurons exposed to oligomeric Aβ (Hedskog et al., 2013). Moreover, an increase in the number and size of MAMs in presenilin 1 and 2 double knockout mouse embryonic fibroblasts (MEF) and human sporadic (SAD) and familial (FAD) Alzheimer's patient fibroblasts has been observed. Electron microscopy and quantitative analysis revealed a significant increase in the incidence of very long and

long MAMs in double knockout MEFs as well as in SAD and FAD patient fibroblasts (Area-Gomez et al., 2012).

Of particular interest, in the context of my work on Drp1 recruitment to mitochondria, the ER has also been implicated in regulating mitochondrial fission as the contact points have been shown to mark sites of prospective fission. Time lapse imaging of Cos-7 cells expressing mitochondrial marker mitoDsRed and ER protein GFP-Sec61β showed that mitochondrial division mostly occurred at sites of mitochondria and ER contacts. As well as this, ER contacts were also observed to be located adjacent to Drp1 puncta and Mff. Imaging of Cos-7 cells expressing fluorescently tagged Drp1, KDEL (ER marker) and mito-EGFP or fluorescently tagged Mff, KDEL and mtDsRed showed that these ER/mitochondrial sites are associated (Friedman et al., 2011). Moreover, three dimensional electron microscope tomograms of wild type yeast cells showed constriction of the mitochondrion tubule at sites of ER contact. The tomograms show that ER tubules wrapped around the mitochondria at these sites (Friedman et al., 2011). It is postulated that the constriction of the mitochondrial tubules is first caused by ER tubules therefore enabling the assembly of Drp1 oligomers along with other mitochondrial fission proteins (Kornmann, 2013, Friedman et al., 2011). Although this theory of ER constriction being upstream of Drp1 oligomerisation is widely accepted, it has also been suggested that in fact, the ER preferentially tethers to the already altered, constricted mitochondria (Rowland and Voeltz, 2012).

The first aim of the work described in this chapter was to identify if loss of sacsin affected the incidence of ER/mitochondrial contact sites. The rationale was that MAM formation represents a step in mitochondrial division that is upstream of Drp1 recruitment. Using the hypothesis that ER mediated mitochondrial constriction initiates Drp1 recruitment, we explored whether the reduced localisation of Drp1 and increased network interconnectivity was due to an earlier defect in the fission pathway. This was analysed through the quantification of ER/mitochondrial contacts by immunofluorescent analysis.

5.2.1 Endoplasmic Reticulum and Mitochondrial Membrane contacts in Sacsin Knockdown Fibroblasts

Fibroblasts were transfected with GFP-Sec61β, an ER marker, along with either SACS or SCRM siRNA. After 48 hours, the fibroblasts were incubated with 100nM MitoTracker for 30 minutes then fixed and stained with DAPI (blue). Confocal stacks in the Z-axis were collected and used for co-localisation analysis. Each stack had a thickness of 0.85µm and 15 cells were imaged for each condition. The confocal acquisition settings remained constant throughout imaging and for each condition.

The Surpass and Co-loc, co-localisation modules of Imaris were used in conjunction with this analysis to quantify the degree of overlap between the ER (green) and mitochondria (red) in the fibroblasts. As before, Manders' coefficient was used to measure the colocalized overlap of ER and mitochondria. The method of analysis and Imaris workflow was similar to that described in Chapter 4 of this thesis (where the colocalisation of Drp1 to the mitochondria was quantified). This method was also similar to that performed by de Brito et al where colocalisation analysis of ER to mitochondria was performed on confocal images in Mfn knockout MEF or HELA cells and analysed using Manders' coefficient (de Brito and Scorrano, 2008).

In this Chapter, the analysis of the co-localisation of the ER to mitochondria was used as a means of quantifying ER/mitochondrial contacts. The results showed that there was no significant difference in ER/mitochondrial contacts in the sacsin knockdown fibroblasts compared to the controls (Figure 5. 1A-B). Control fibroblasts had a Manders' coefficient of 0.25 ± 0.060 while the sacsin knockdown fibroblasts had a Manders' coefficient of 0.32 ± 0.051. Although the value in sacsin knockdown fibroblasts was higher than the controls, a student's t-test revealed an insignificant p value of 0.38 (Figure 5. 1A-B).

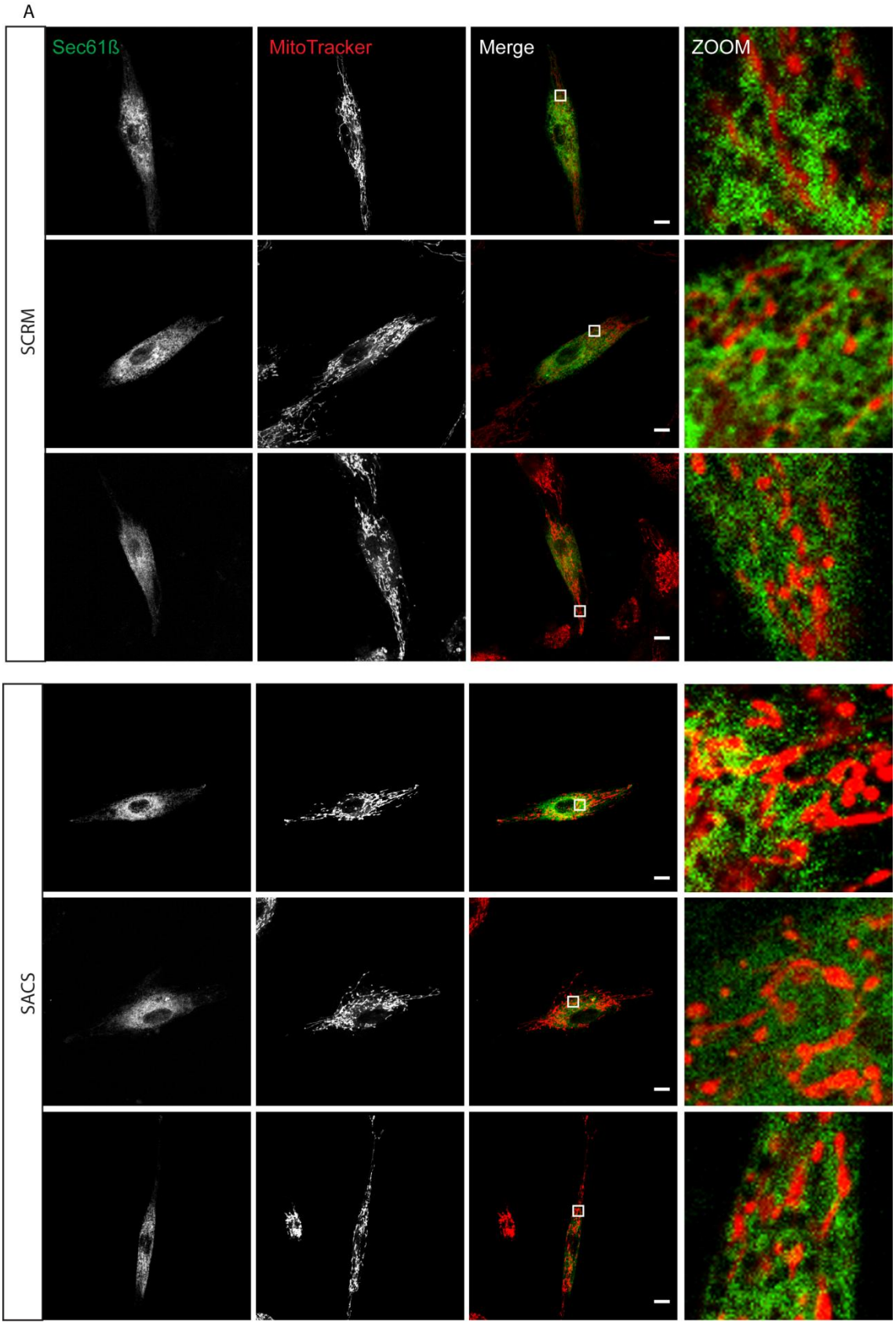
A
Sec61ß
MitoTracker
Merge
ZOOM
SCRM
SACS

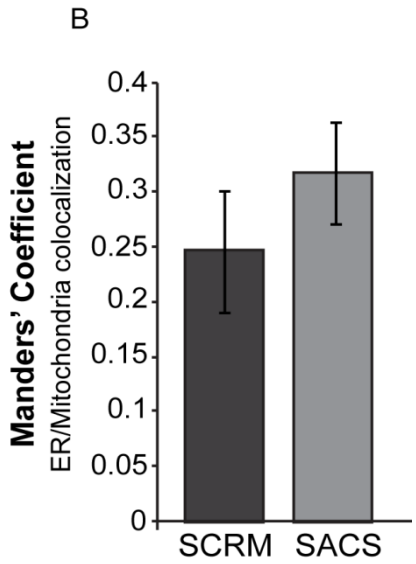

Figure 5. 1 No statistical difference in the colocalisation of ER with mitochondria was observed between sacsin knockdown cells and controls.

Fibroblasts were transfected with either SACS or SCRM siRNA along with GFP tagged, ER protein, Sec61β (green). Cells were incubated with 100nm of MitoTracker for 30mins, 48 hours after transfection. Cells were then fixed and confocal Z-stacks were acquired. Surface and Coloc modules of Imaris were used for Manders' analysis. A) Representative images of ER morphology and mitochondria. B) There was no statistical difference in the Manders' coefficient of sacsin knockdown and control fibroblasts. Error bars represent ± SEM. Scale bars represent 10µm.

5.2.2 Endoplasmic Reticulum and Mitochondrial Membrane Contacts in ARSACS Fibroblasts

Following on from the previous experiment, ER/mitochondrial contacts were quantified in 4 ARSACS patients and 2 controls fibroblast cell lines. Cells were first transfected with GFP tagged Sec61β. After 48 hours, cells were incubated with 100mM of MitoTracker for 30mins. Live cell imaging involving the collection of confocal images taken at 0.85µm Z-axis intervals was performed. As before, the confocal settings remained constant throughout the experiment and 15 cells for each cell type were imaged. Surpass and Co-loc was used to measure co-localisation which here is defined by Manders' coefficient.

As in the fibroblasts transfected with *SACS* siRNA, no observable difference in the amount of overlap of the mitochondria and the ER was observed (Figure 5. 2A-B). The Manders' coefficient was lowest in patient 2801delQ with a value of 0.135 ± 0.017. The control and patients c.2094-2 A>G/Q4054*, K1715*/R4331Q, R2002fs/ Q4054* had very similar Manders' coefficient values of; 0.20 ± 0.045, 0.245 ±0.044, 0.230 ± 0.032 and 0.241± 0.040 respectively. ANOVA statistical analysis showed that these values were statistically insignificant with p values greater than 0.5 (Figure 5. 2A-B).

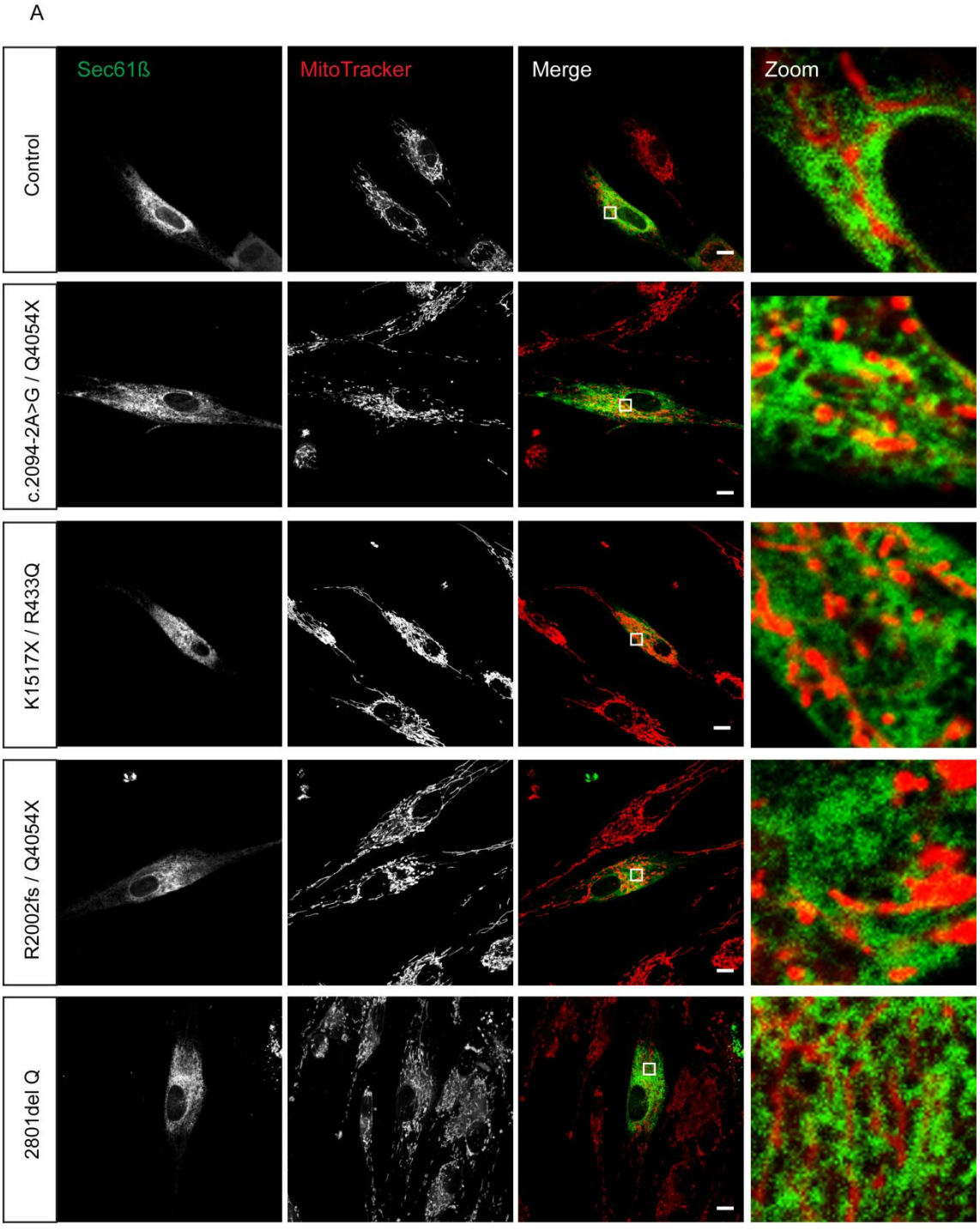
A
Sec61ß
MitoTracker
Merge
Zoom
Control
c.2094-2A>G / Q4054X
K1517X / R433Q
R2002fs / Q4054X
2801del Q

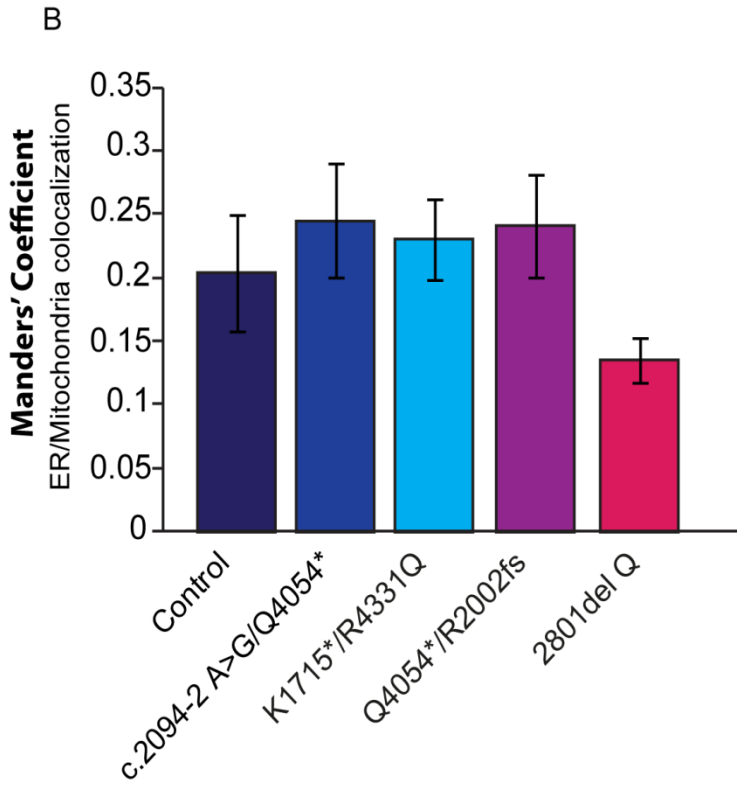

Figure 5. 2 No statistical difference in the colocalisation of ER to mitochondria was observed between patients and controls.

Fibroblasts were transfected with GFP tagged, ER protein, Sec61β (green) once a confluence of 70% was achieved. Cells were incubated with 100nM of MitoTracker for 30mins, 48 hours after transfection. Cells were then fixed and confocal Z-stacks were acquired. Surface and Co-Loc modules of Imaris were used for Manders' analysis. A) Representative images of ER morphology and mitochondria. B) There was no statistical difference in the Manders' coefficient of sacsin knockdown and control fibroblasts. Error bars represent ± SEM. Scale bars represent 10µm.

5.3 Peroxisome Morphology

Proteins involved in mitochondrial fission and in the regulation of Drp1 have also been demonstrated to have a role in regulating peroxisome dynamics. This includes evidence that Drp1 is required for peroxisome division (Waterham et al., 2007). Thus the effect of *SACS* mutations or reduced levels of sacsin on peroxisome morphology was analyzed.

Peroxisomes are single membrane organelles involved in essential catabolic and anabolic functions such as lipid metabolism, β-oxidation of fatty acids as well as synthesis of other lipids some of which are vital for myelin sheath formation (van den Bosch et al., 1992). Peroxisomes both produce and scavenge for reactive oxygen species (ROS) in the cell (Ivashchenko et al., 2011, Boveris et al., 1972, De Duve and Baudhuin, 1966). The process of β-oxidation of fatty acids is the main contributor of hydrogen peroxide (H_2O_2) generation in these organelles (Schrader and Fahimi, 2006). The antioxidant enzyme catalase, found in the peroxisomes catalyses the decomposition of H_2O_2 to water and oxygen (Schrader and Fahimi, 2006). As with mitochondria, dysfunction of peroxisomes leads to an increase in ROS and oxidative stress. The importance of peroxisome function was also shown to be essential in brain development (Li et al., 2002, Janssen et al., 2003). For example, a delay in neocortical neuronal migration was observed in knockout mouse pups lacking PEX5 which encodes the essential peroxisome targeting signaling 1 receptor (Janssen et al., 2003). This change in neuronal migration was accompanied by an accumulation of very long chain fatty acids (VLCFA) as well as an increase in neocortical neural cell death (Janssen et al., 2003).

Furthermore, changes in peroxisome morphology have been identified in neurodegeneration. Alterations in peroxisome regulation were linked to Alzheimer's disease progression in mouse disease models (Cimini et al., 2009, Fanelli et al., 2013). A significant induction of peroxisome membrane protein of 70kDa (PMP70) was observed by immunoblotting of hippocampal protein extracts and the immunostaining of pyramidal cell layer in 3 month old male and female transgenic Alzheimer's disease

model mice (Tg2576) (Cimini et al., 2009, Fanelli et al., 2013). A dramatic decrease in PMP70 protein levels was observed via the same methods in 6 month old Tg2576 mice (Fanelli et al., 2013). Both the induction of PMP70 and decrease in PMP70 protein level were significantly different from their wild-type littermates (Fanelli et al., 2013). Finally, an increase in PMP70 levels was observed in the AD model mice at 18 months. This was postulated to signify an increase in the number of peroxisomes. The authors suggest that the increase in PMP70 recorded at 18 months was most likely due to astrogliosis caused by disease progression (Fanelli et al., 2013).

An increase in total peroxisomal volume per cell was described in Parkinson disease patient fibroblasts. While there was a significant decrease in catalase, up to a 5 fold increase in the volume of peroxisomes were recorded in these patients, both of whom carry mutations in *parkin* gene PARK2 (Pacelli et al., 2011). Of interest the mitochondrial network in these fibroblasts were notably more fragmented than in the control. The authors made no mention of peroxisome number but state that the decrease in catalase may contribute to the imbalance of intracellular ROS indentified (Pacelli et al., 2011).

The relationship between peroxisomes and mitochondria is evident through their functional and morphological similarities. Like mitochondria, peroxisomes are dynamic organelles which change morphology and abundance in response to cellular environment. Additionally, the Drp1 fission complex has been shown to be conserved between the two organelles (Schrader et al., 2012). The regulation of peroxisome dynamics is crucial to both peroxisome function and biogenesis. During peroxisome proliferation, existing peroxisomes import newly synthesized proteins from the cytosol. The peroxisome then elongates with the assistance of protein Pex11p, this elongation is subsequently followed by fission (Lazarow and Fujiki, 1985, Li and Gould, 2003, Motley and Hettema, 2007). Importantly, division is caused by GTPase activity associated with Drp1, Mff and Fis1 (Gandre-Babbe and van der Bliek, 2008, Koch et al., 2003, Koch et al., 2005).

Mitochondrial fission proteins Mff and Fis1 have all been found to localize to the peroxisomes and inhibition or loss of these proteins lead to elongated peroxisomes (Koch et al., 2003, Koch et al., 2005, Koch and Brocard, 2012). Furthermore, while not directly localised to the peroxisomes, the regulation of Drp1 activity by MiD49/51 also led to a change in peroxisome morphology. Over expression of MiD49/51 was found to result in the elongation of peroxisomes due to the deactivation of Drp1 (Palmer et al., 2013). Notably in 2007 an elongated peroxisome morphology was also described in a patient carrying Drp1 mutation (Waterham et al., 2007). As well as this, increased lactate and very long chains fatty acids were measured in the plasma of this patient, suggestive of a probable defect in fatty acid oxidation and peroxisome function (Waterham et al., 2007).

5.3.1 Peroxisome morphology in sacsin knockdown fibroblasts.

Fibroblasts were transfected with GFP along with either *SACS* or SCRM siRNA. The fibroblasts were then fixed and stained with anti-PMP70 (red) and DAPI (blue) 48 hours after transfection. Confocal stacks of 0.44µm in the z dimension were collected and used for surface rendering and volumetric analysis using the Surpass module of Imaris. A total of 15 cells were imaged for this experiment. PMP70 has been described as a good marker for morphometric analysis of peroxisomal population and was therefore used in this experiment (Fanelli et al., 2013).

Volumetric analysis of the peroxisomes was based on Imaris defined thresholding which discarded objects brought about by non specific staining and ensured that calculations were performed on discernible peroxisomes. The analysis and Imaris workflow was similar to that described in Chapter 3 of this thesis (where the mitochondrial volume was analyzed).

There was a significant decrease in the number of peroxisomes in the sacsin knockdown fibroblasts ($p = 0.049$) (Figure 5. 3A-B). The mean number of peroxisomes in the control fibroblasts was found to be 209.69 ± 25.01 peroxisomes per cell. Conversely the mean number of peroxisomes in sacsin knockdown fibroblasts was found to be in 147.77 ± 14.44 peroxisomes per cell (Figure 5. 3B).

The total combined volume of peroxisomes in sacsin knockdown fibroblasts was not statistically different to the volume in the controls. A mean total volume of 246.71 ± 14.89µm^3 per cell was recorded in control fibroblasts while the mean total volume of peroxisomes in sacsin knockdown fibroblasts was 209.77 ± 28.57µm^3 (Figure 5. 3C).

An obvious morphological change in sacsin knockdown fibroblasts was not observed (Figure 5. 3A). The sphericity of the peroxisomes was measured in order to capture any subtle differences in peroxisome shape. This measurement was performed using the Surface module of Imaris image analysis software. Sphericity is the measure of how spherical an object is. The sphericity is usually measured from 0 to 1 with 1 representing a completely spherical object. This measurement was based on the

hypothesis that like other mitochondrial fission proteins, loss of sacsin will result in an elongation of the peroxisome, resulting in knockdown cells having more peroxisomes with a sphericity of less than 1 when compared to controls.

The sphericity of peroxisomes was similar in sacsin knockdown and control fibroblasts. The controls had a higher frequency of peroxisomes with values between 0 and 0.8, than sacsin knockdown cells (Figure 5. 3D). This indicated that the controls had a higher frequency of less spherical objects.

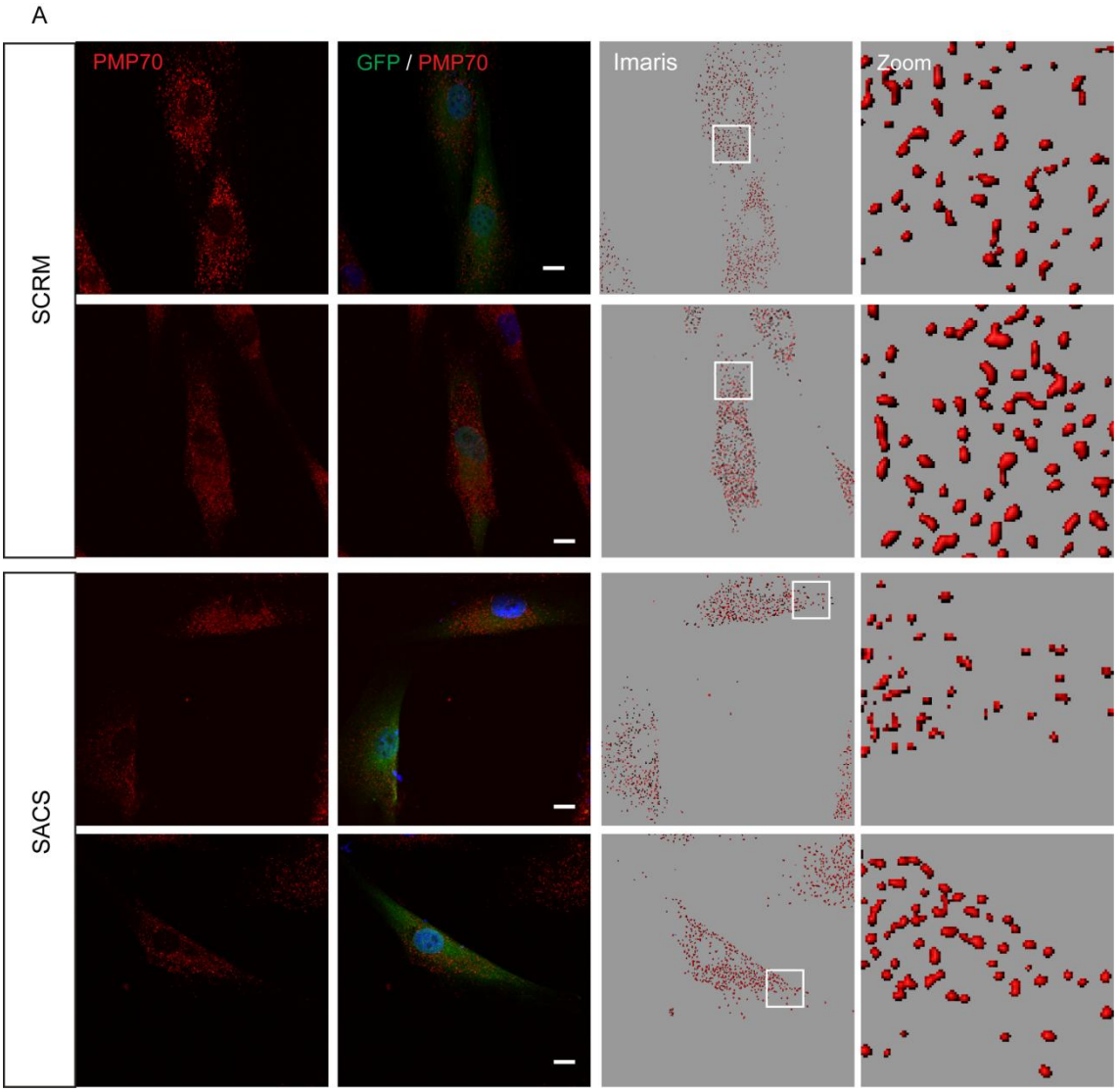

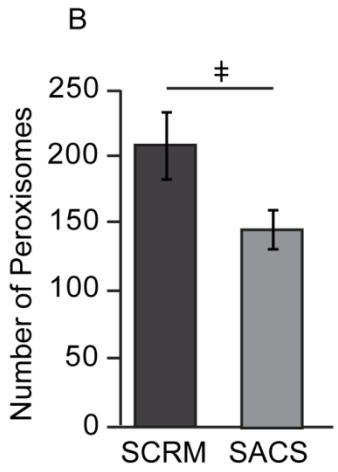
B
‡
Number of Peroxisomes
250
200
150
100
50
0
SCRM
SACS

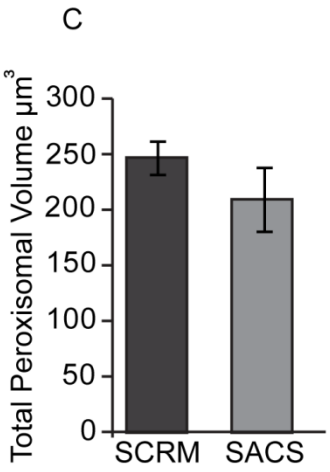
C
Total Peroxisomal Volume µm³
300
250
200
150
100
50
0
SCRM
SACS

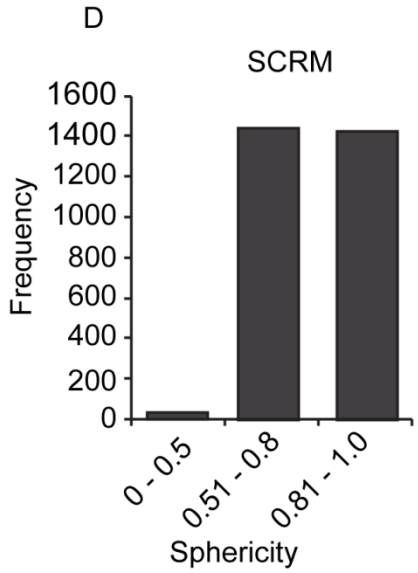
D
SCRM
Frequency
1600
1400
1200
1000
800
600
400
200
0
0 - 0.5
0.51 - 0.8
0.81 - 1.0
Sphericity

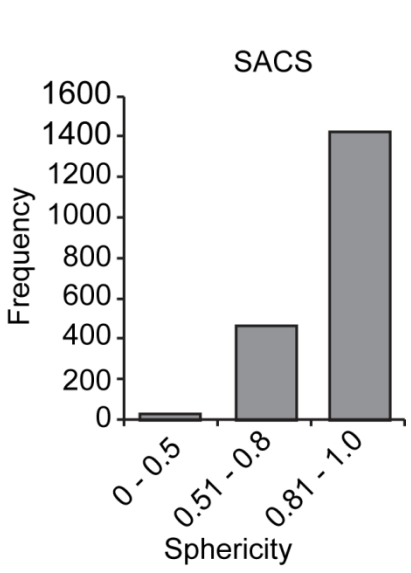
SACS
Frequency
1600
1400
1200
1000
800
600
400
200
0
0 - 0.5
0.51 - 0.8
0.81 - 1.0
Sphericity

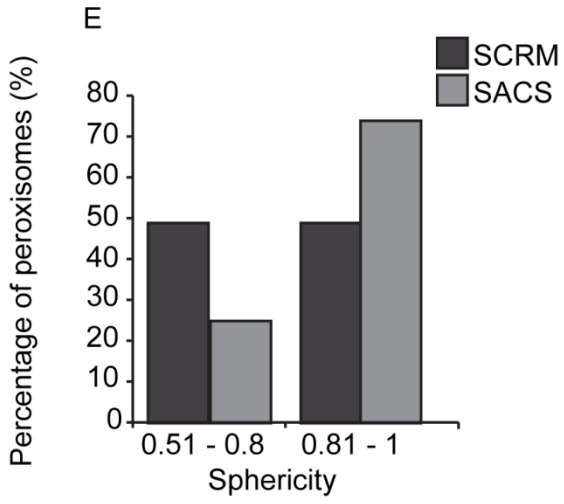
E
SCRM
SACS
Percentage of peroxisomes (%)
80
70
60
50
40
30
20
10
0
0.51 - 0.8
0.81 - 1
Sphericity

Figure 5. 3 A significant decrease in the number of peroxisome were observed in sacsin fibroblasts.

Fibroblasts were transfected with GFP along with either *SACS* or SCRM siRNA. Cells were then fixed and stained for PMP70 (red) and DAPI (blue). Confocal Z-stacks were acquired. Surface module of Imaris was used for analysis. A) Representative images of peroxisomes B) Average number of peroxisomes per cell. Peroxisome numbers were quantified using the Surface module of Imaris. C) Average total peroxisomal volume per cell. D) Distribution histogram of peroxisomal volume. E) Percentages of peroxisomes which had sphericity values between 0.51-0.8 and 0.81-1. Error bars represent ± SEM. Scale bars represent 10µm. ‡p≤0.05

5.3.2 Peroxisome morphology in ARSACS fibroblasts

Fibroblasts were grown until a confluence of 70% was reached. Cells were then fixed and stained with anti-PMP70 (red) and DAPI (blue). Confocal Z-stacks of 0.44µm thick sections were collected and used for surface rendering and volumetric analysis using the Surface module of Imaris. Volumetric analysis was performed on 15 cells for each cell line. The experiment was repeated 3 times giving a total n of 45 for each cell line.

The analyses show that there was a decrease in both the number of peroxisomes and total volume per cell in the patient fibroblasts (Figure 5. 4A-C). However, this decrease was only statistically significant in two of the patients. Control fibroblasts had a mean of 316 ± 36.09 peroxisomes per cell. Patient 2801delQ had the lowest mean number of peroxisomes with 155.8 ± 7.52 peroxisomes per cell. This decrease in peroxisome number was significant with a $p \leq 0.001$. There were also significantly less peroxisomes in patient K1715*/R4331Q ($p \leq 0.05$), this patient had a mean of 220.7 ± 18.58 peroxisomes per cell, 30.16% less than the number of peroxisomes in the control fibroblasts. Patient c.2094-2 A > G/Q4054* and R2002fs/ Q4054* had similar amounts of peroxisomes with 292 ± 33.94 and 295 ± 36.55 peroxisomes per cell respectively (Figure 5. 4B).

Patient 2801delQ had the lowest total peroxisomal volume with a mean of 207.5 ± 18.75 μm^3. This volume was significantly less ($p \leq 0.01$) than control fibroblasts which had a mean volume of 631.9 ± 108.14μm^3 per cell (Figure 5. 4C). Patient K1715*/R4331Q, although having significantly less peroxisomes, had the highest peroxisomal volume relative to the patients with a mean volume of 517 ± 49.26μm^3 per cell. Similarly patient c.2094-2 A > G / Q4054* had a mean total peroxisomal volume of 507.3 ± 84.74μm^3 per cell. Lastly patient R2002fs/ Q4054* had a mean peroxisomal volume of 441 ± 62.47 μm^3 per cell (Figure 5. 4C).

Densitometric analysis of immunoblots performed using cell lysates showed a significant decrease in the levels of PMP70 in these cells (fig 5.4D). PMP70 levels appeared to be most significantly ($p \leq 0.001$) decreased in patient K1715*/R4331Q compared to the controls than any of the other patients. All of the other patients also

had significantly less PMP70 than in the control ($p \leq 0.01$). This seems to confirm the results showing a decrease in peroxisome number.

When analysing these results it was important to note that the patients had fewer peroxisomes then the controls. The majority of peroxisomes had spherecity values of between 0.51- 0.8 and 0.81 – 1 in controls and patient fibroblasts (Figure 5. 4E-F). In the controls 61% of peroxisomes had sphericity values between 0.51-0.8 and 38% of peroxisomes had values between 0.81-1. Patient c.2095-2A>G had a higher frequency of peroxisomes with sphericity values between 0.51 -0.8. The histogram therefore had a slight shift to the left with 73% of the peroxisomes having values within this range and 26% had values of 0.81-1. There was also a slight shift of the sphericity histogram to the left in patient K1715*/R4331Q as 76% of peroxisomes had sphericity values of 0.51-8 while 23% had values between 0.81 -1 (Figure 5. 4E-F). Patients 2801delQ and R2002fs/Q4054* had roughly equal amounts of peroxisomes in both groups. Patient 2801delQ had 55% of peroxisomes with sphericity values of 0.51-0.8 and 44% of peroxisomes with sphericity values of 0.81-1. Lastly, patient R2002fs/Q4054* had 52% and 47% of peroxisome within 0.51- 0.8 and 0.81-1 respectively. In all, patients K1715*/R4331Q and c.2095-2A>G had a higher frequency of peroxisomes which were less spherical than the controls (Figure 5. 4F). This may suggest a subtle change in peroxisomal morphology however this was not observed in patients 2801delQ and R2002fs/Q4054*.

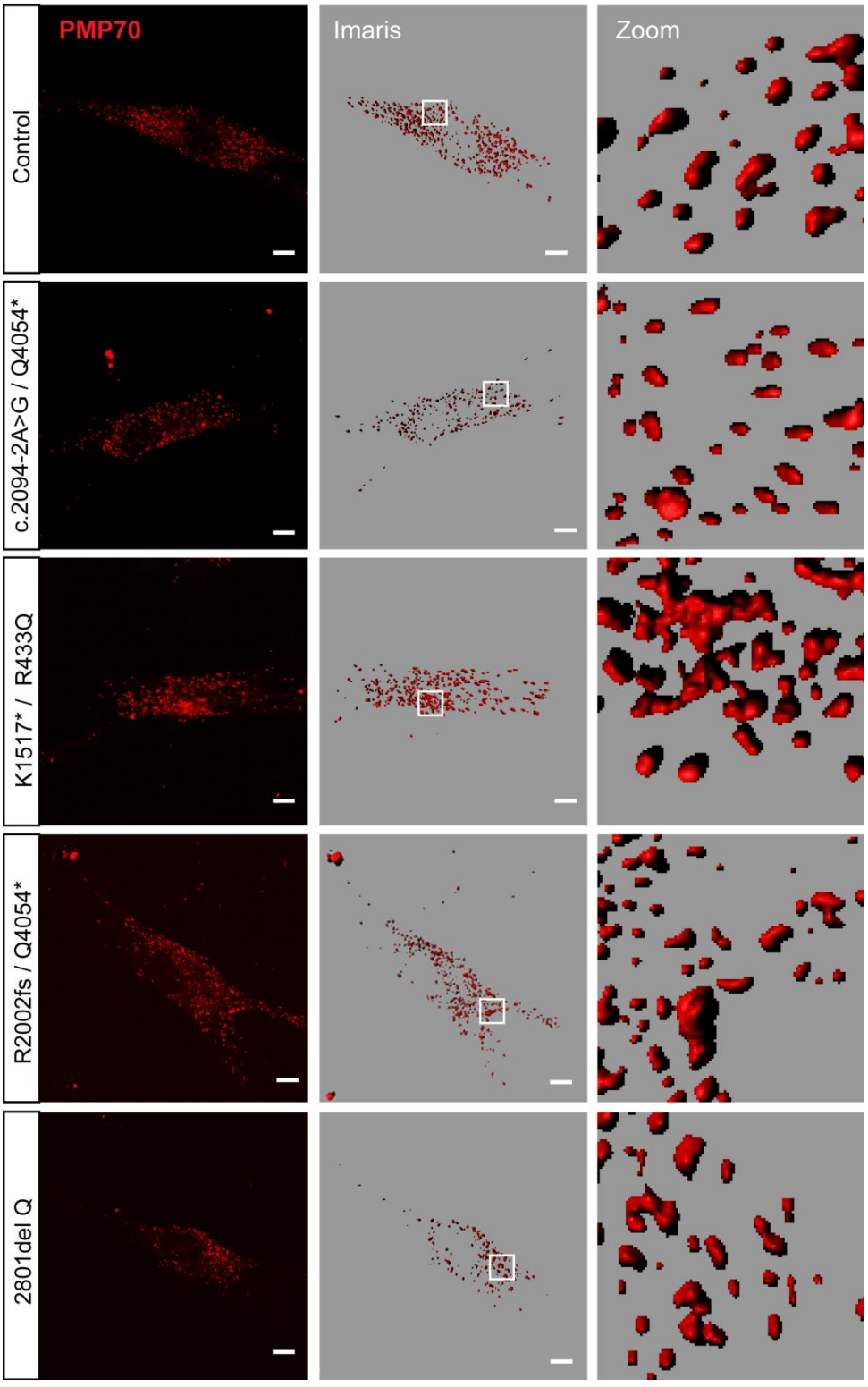
PMP70
Imaris
Zoom
Control
c.2094-2A>G / Q4054*
K1517* / R433Q
R2002fs / Q4054*
2801del Q

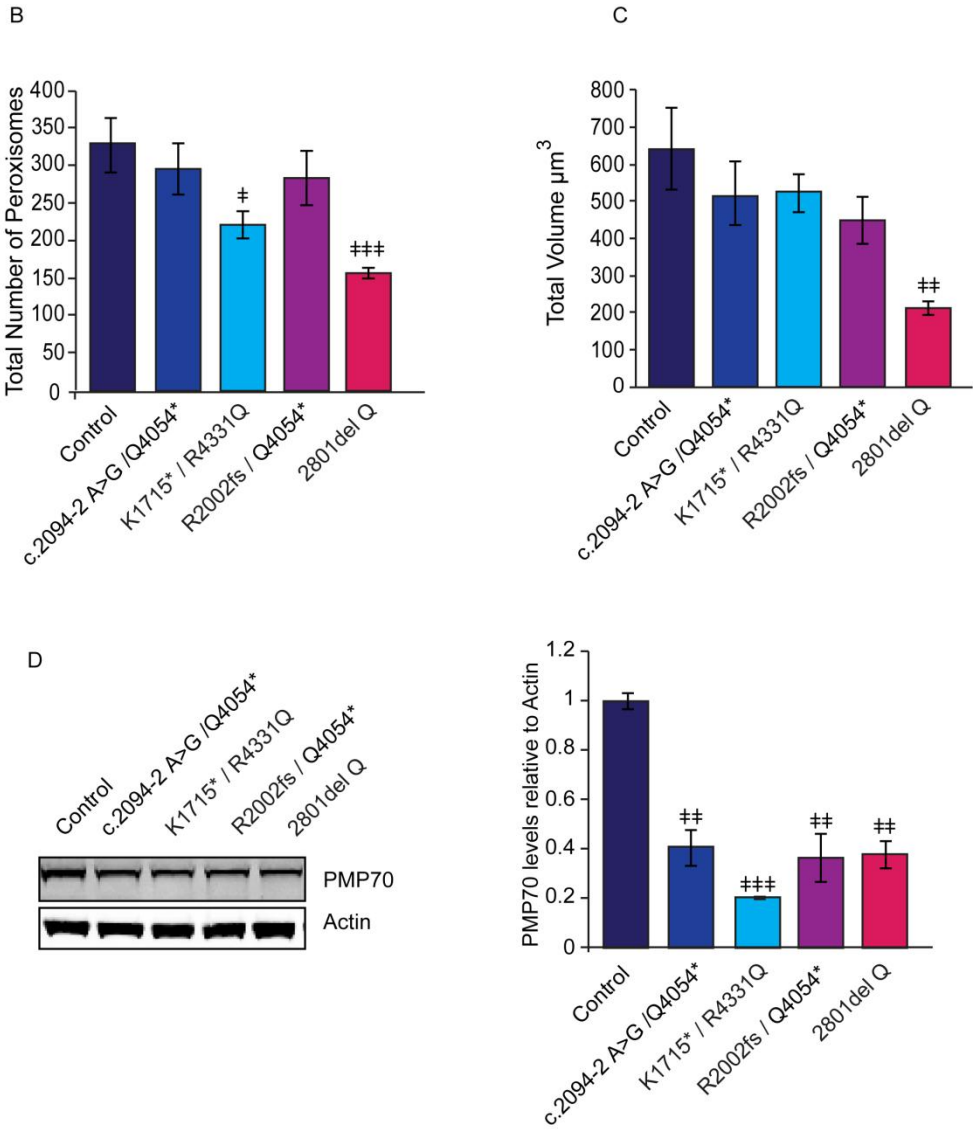
B
Total Number of Peroxisomes
400
350
300
250
200
150
100
50
0
‡
‡‡‡
Control
c.2094-2 A>G /Q4054*
K1715* / R4331Q
R2002fs / Q4054*
2801del Q
C
Total Volume µm3
800
700
600
500
400
300
200
100
0
‡‡
Control
c.2094-2 A>G /Q4054*
K1715* / R4331Q
R2002fs / Q4054*
2801del Q
D
Control
c.2094-2 A>G /Q4054*
K1715* / R4331Q
R2002fs / Q4054*
2801del Q
PMP70
Actin
PMP70 levels relative to Actin
1.2
1
0.8
0.6
0.4
0.2
0
‡‡
‡‡‡
‡‡
‡‡
Control
c.2094-2 A>G /Q4054*
K1715* / R4331Q
R2002fs / Q4054*
2801del Q

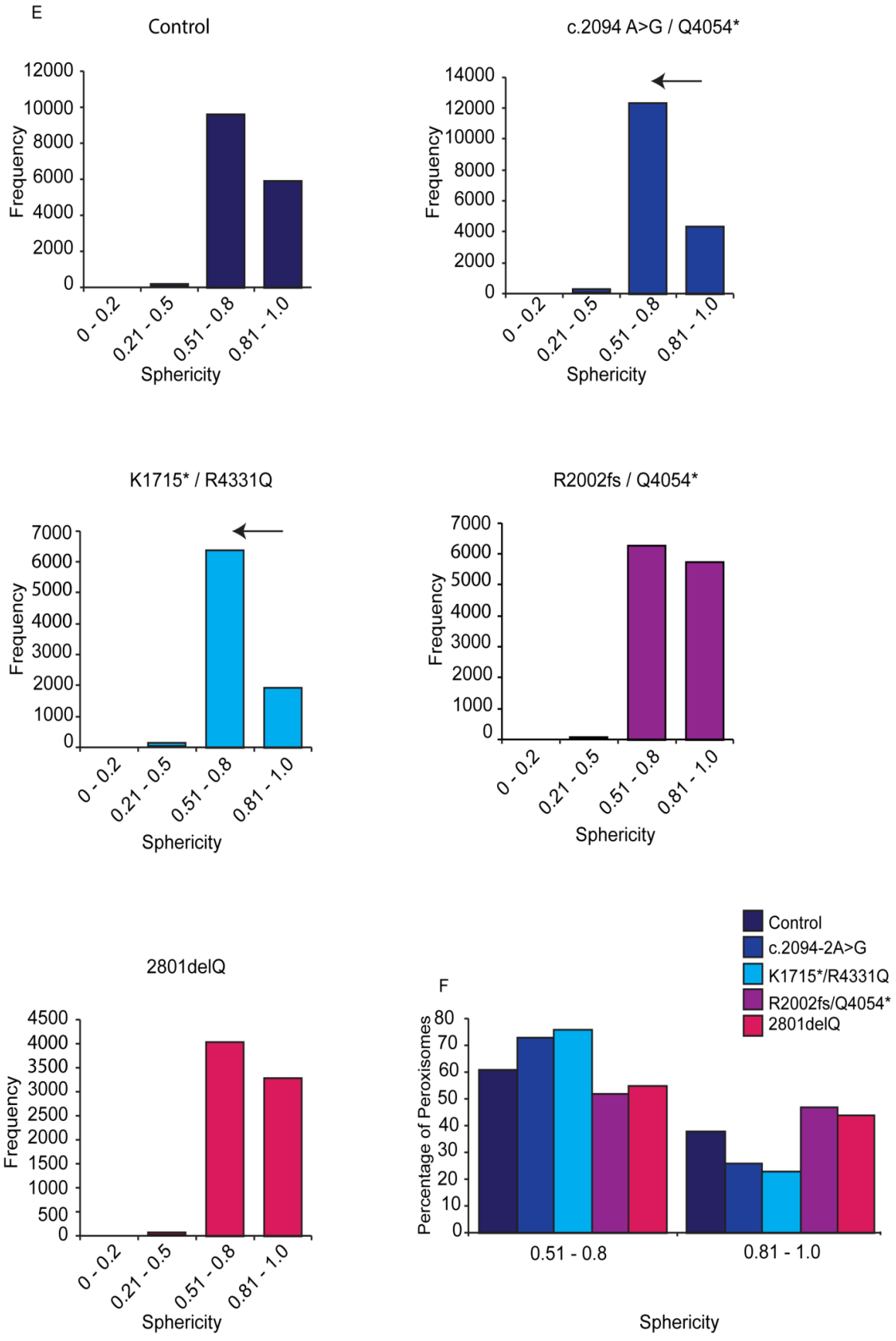
E
Control
c.2094 A>G / Q4054*
K1715* / R4331Q
R2002fs / Q4054*
2801delQ
Frequency
Sphericity
0 - 0.2
0.21 - 0.5
0.51 - 0.8
0.81 - 1.0
F
Control
c.2094-2A>G
K1715*/R4331Q
R2002fs/Q4054*
2801delQ
Percentage of Peroxisomes
0.51 - 0.8
0.81 - 1.0
Sphericity

Figure 5. 4 A decrease in the number of peroxisomes was observed in ARSACS fibroblasts.

Cells were fixed and stained for PMP70 (red) after a confluence of 70% had been obtained. Confocal Z-stacks were acquired and the Surface module of Imaris was used for analysis. A) Representative images of peroxisomes and Imaris surface rendered images. B) Average number of peroxisomes per cell. Peroxisome numbers were quantified using the surface module of Imaris. C) Average total peroxisomal volume per cell. D) Distribution histogram of peroxisomal volume. E) Percentages of peroxisomes which had sphericity values between 0.51-0.8 and 0.81-1. Error bars represent ± SEM. Scale bars represent 10µm. ‡p≤0.05 ‡‡ p≤0.01 ‡‡‡p≤0.001.

5.4 Discussion

The investigation of ER/mitochondria co-localisation was based on the model of fission which suggests that constriction of the mitochondria as a result of the ER and mitochondrial tethering is an important initiator of Drp1 recruitment (Friedman et al., 2011). Quantification of the ER/mitochondria co-localisation showed no statistical difference in the amount of ER /mitochondria contact sites between sacsin knockdown and control or between patient and control fibroblasts. The morphology of the ER also appeared normal in the patients and in fibroblasts transfected with SACS siRNA. From these results we can infer that the reduction of Drp1 recruitment to the mitochondria in sacsin knockdown and patient fibroblasts reported in Chapter 4 is unlikely to be due to a reduction in ER/mitochondrial contacts.

Confocal imagery and Imaris image analysis software were utilised in this study. More recently super resolution imagery has become available. The developments in super resolution microscopy will further resolve the definition of the contact regions in these cells. It can lead to a better understanding of the structure and tethering of the ER to the mitochondria. For instance, the maintenance of these contacts and ultimate mitochondrial constriction depends on the correct function and expression of the tethering proteins Mfn and PACS2, which were not explored on this occasion and should be investigated. Exploration of PACS2 may be preferential as it is not directly involved in mitochondrial dynamics and therefore conclusion made regarding ER tethering may be more specific to tethering and less dependent on mitochondrial morphology. Super resolution images and analysis on the localisation of PACS2 as well as the effects of overexpression of the protein on the Drp1 recruitment phenotype in sacsin knockdown and patient fibroblasts will not only further clarify the role of MAMs in Drp1 sequestration but may also uncover a method of rescuing the phenotype in these cells. In addition qPCR and immunoblotting of PACS2 expression in sacsin knockdown and patient fibroblasts will also be useful in understanding MAMs in ARSACS.

Further approaches to look at MAM function in ARSACS would be beneficial. The synthesis of phospholipids PtSer, PtdCho and PtEt depend on optimal MAM function (Schumacher et al., 2002). Measuring the abundance of these phospholipids has been used as a measure for the biochemical activity of MAMs. A 1.5 to 2 fold increase in PtSer and PtEt biosynthesis was reported in these cells (Area-Gomez et al., 2012). The exploration of MAM function in patient and sacsin knockdown fibroblasts will give biochemical information of MAM mechanism in these cells.

Moving on from this, a putative function for sacsin function in the regulation of organelle dynamics beyond the mitochondria remains unclear. Although a decrease in the number of peroxisomes was observed in both sacsin knockdown and patient fibroblasts a significant difference in the mean total peroxisomal volume per cell was only recorded in patients K1715*/R4331Q and 2801delQ. Interestingly both of these patients had significantly impaired recruitment of Drp1 to the mitochondria reported in Chapter 4. The immunoblot and densitometric analysis showed a marked decrease in the level of PMP70 in ARSACS fibroblasts. This blot further confirms the decrease in the number of peroxisomes in patient fibroblast. The results show that there is a reduction of peroxisomes in patient fibroblasts. There was also a decrease in the frequency of spherical peroxisomes in sacsin knockdown and patient fibroblasts relative to the number of peroxisomes. This would suggest that *SACS* mutations or reduced levels of sacsin may in fact have an effect on peroxisome morphology, however the effect is very subtle. It is possible that sacsin may not have a direct role in peroxisome dynamics and the effects observed may be due to its effect on Drp1 regulation.

A decrease in the number of peroxisomes was observed in cells with reduced levels of Fis1 and in cells where MiD49/51 had been over expressed, however these changes were accompanied by an obvious change in peroxisome morphology (Kobayashi et al., 2007). A decrease in peroxisomes was also reported in Alzheimer's disease mouse model (Kou et al., 2011). This loss of peroxisomes was observed in the neuronal processes where there was an abnormal phosphorylation of tau that was accompanied by accumulation of substrates of peroxisomal β oxidation (Kou et al., 2011).

The results reported in Alzheimer's disease model demonstrated that a loss of peroxisomes led to a decrease in peroxisomal function. Therefore a more comprehensive investigation into the effect of these subtle changes on the function of peroxisomes could be important for understanding the consequences of reduced Drp1 recruitment in cells with reduced sacsin function. Investigations of the levels of VLCFA and ROS production in neurodegeneration have been referred to in section 5.2 of this chapter. It will be beneficially to examine the impact of reduced sacsin on the function of peroxisomes.

It is important to note that the impairment of peroxisome function may also lead to an increase in cellular oxidative stress. Although the changes in peroxisome may be subtle these may still provide an enhanced effect in the brain which is sensitive to oxidative insult. Measuring the expression, abundance and efficiency of catalase will address whether there is an increase in cellular ROS as a result of reduced sacsin or *SACS* mutations. In addition to using the fibroblasts models, it will be beneficial to immunostain neurons and brain sections from the ARSACS mouse model to examine whether the effect of the loss of sacsin on peroxisome function is enhanced in the brain.

Whether sacsin localises to peroxisomes should be investigated by either immunofluorescence or immunoblotting of a peroxisome fraction. In addition, peroxisome biogenesis and clearance has not been explored in ARSACS. The decrease in peroxisome number may be due to a deregulation of peroxisome biogenesis and or pexophagy (peroxisome autophagy). Therefore these must be examined in sacsin knockdown and patient cells. The regulation of peroxisome turnover is a relatively new field. However, investigating the expression levels of PpAtg30, a protein which has been described to selectively target peroxisomes and initiate autophagy and investigating PEX proteins; Pex3p and Pex19p and Pex11β which are involved in peroxisome biogenesis will resolve sacsin's role in the regulation of peroxisomes (Farré et al., 2008, Eckert and Erdmann, 2003, Kunau, 2005).

In addition to this, the monitoring of the peroxisome may give insight into its regulation and turnover. Live cell imaging of peroxisome dynamics using Halo-Tag technology and pulse imaging or CellLight® Peroxisome-GFP, BacMam 2.0 have been successfully used in studies to examine peroxisome dynamics and trafficking in mammalian cells and in hereditary spastic paraplegia patient derived cells (Fan et al., 2014, Huybrechts et al., 2009). These methods can also be employed in sacsin knockdown and patient fibroblasts.

The results in this chapter have led to the conclusion that sacsin's involvement in Drp1 recruitment is downstream of the ER's role in mitochondrial fission. The findings also suggests that sacsin's role in Drp1 recruitment may also affect peroxisomes.

Chapter 6

Mitochondrial function in sacsin knockdown and ARSACS fibroblasts

6.1 Introduction

The disruption of Drp1 recruitment to mitochondria in ARSACS patients and sacsin knockdown fibroblasts, potentially explains the morphological phenotype of the mitochondrial network. As discussed previously, impairment in mitochondrial fission is known to be detrimental to cells. In particular, impaired fission can prevent the elimination of damaged mitochondria (Seo et al., 2010, Mammucari and Rizzuto, 2010). Moreover, mitochondrial dysfunction has been found to be a contributing factor of many neurological, and ARCA disorders. This chapter focuses on examining mitochondrial function through measuring respiration rate and mitochondrial superoxide production, focusing on the hypothesis that reduced recruitment of Drp1 and associated changes in mitochondrial network morphology will be linked to impaired mitochondrial function in sacsin knockdown and ARSACS patient fibroblasts.

The main function of the mitochondria is the generation of adenosine triphosphate (ATP) via the process of cellular respiration. This complex process leads to the production of toxic by-products, which are then cleared by other pathways within the organelle. Before considering the measurement of mitochondrial function it is necessary to expand on the role of the mitochondrion in cellular respiration.

Briefly, the end products of glycolysis and fatty acid oxidation, namely pyruvate and fatty acids are transported from the cytosol into the matrix of the mitochondria where they are converted into Acetyl CoA by Coenzyme A (Figure 6. 1). Acetyl CoA is then utilised by the tricarboxylic cycle (TCA) to generate the electron carrier molecules nicotinamide adenine dinucleotide (NADH) or flavin adenine dinucleotide ($FADH_2$), needed for the electron transport chain (ETC). The production of ATP in a series of reactions is known collectively as oxidative phosphorylation (OXPHOS). Mainly, the ETC reduces consumed molecular oxygen (O_2) to water, creating a proton gradient across the inner mitochondrial membrane (Figure 6. 1). This gradient is then used in the synthesis of ATP from ADP by the enzyme ATP synthase (Figure 6. 1) (Brand and Murphy, 1987, Baldwin and Krebs, 1981, Hatefi, 1985, Ernster and Schatz, 1981).

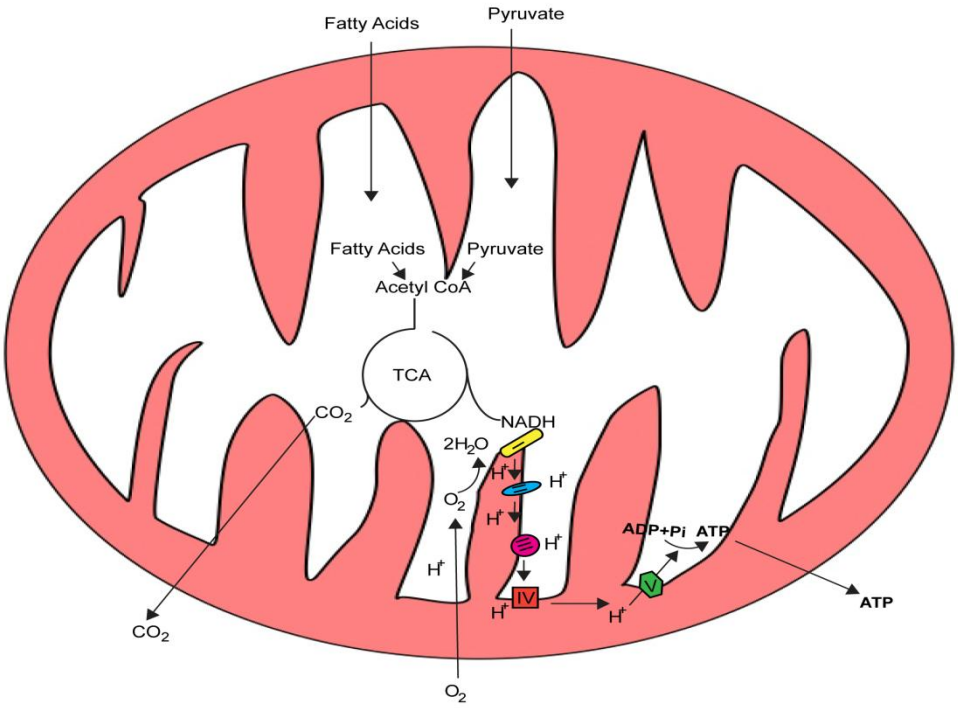

Figure 6. 1 Schematic representation of cellular respiration.

Products of glycolysis and fatty acid oxidation, namely pyruvate and fatty acids are transported from the cytosol to the mitochondria where they are converted to NADH and $FADH_2$ through the citric acid (TCA) cycle. Electrons are donated to the electron transport chain (ETC) from NADH and $FADH_2$ to produce adenosine triphosphate (ATP) through a series of reactions.

As well as ATP and CO_2, OXPHOS produces reactive oxygen species (ROS) as a potentially cytotoxic by-product. ROS arise as a consequence of unpaired electrons from the ETC interacting with O_2 and subsequently generating superoxide ions. These superoxide ions can then be converted into other species such as hydrogen peroxide (H_2O_2) and hydroxyl radicals (OH^-) (Duchen, 2004a). The mitochondria are a major source and target of ROS. Mitochondria and subsequently cells are usually protected from ROS induced damage by antioxidant enzymes such as superoxide dismutase (SOD) and catalase (Duchen, 2004a). Although ROS may be damaging, there are emerging reports showing there is also a beneficial role for ROS in signalling several physiological processes (Balaban et al., 2005). For example, H_2O_2 was found to be required for TGF-β signalling in primary lung fibroblasts. Treatment of these fibroblasts with mitochondria targeted antioxidants like mitochondria-vitamin E led to the attenuation of TGF-β mediated gene expression (Jain et al., 2013). Interestingly TNF induced c-Jun NH2-terminal kinase (JNK)/p38 activation pathway, which is important in regulation of apoptosis, was found to be dependent on H_2O_2 in mouse embryonic fibroblasts. This pathway was inhibited by treatment of these cells with chemical antioxidant N-acetyl-L-cysteine (Nac) (Tobiume et al., 2001). Moreover both epidermal growth factor and platelet derived growth factor have been demonstrated to be mediated by H_2O_2 (Bae et al., 1997, Sundaresan et al., 1995). In addition superoxide was demonstrated to be essential for the activation of $CD4^+$ T-Cells and treatment with mitochondria-vitamin E attenuated interlukin-2 induction and hence T-Cell activation (Sena et al., 2013).

Mostly, ROS are damaging to cells and disrupt cellular function when they are at sustained elevated levels. In homeostasis, the equilibrium between ROS production and antioxidant detoxifying effects, maintains the cell in a healthy state. Oxidative stress occurs once there is a disequilbrium created by elevated ROS which overwhelms the antioxidant capacity of the cell. This increase in ROS is usually indicative of mitochondrial dysfunction.

The brain is particularly susceptible to the damaging effects of ROS and oxidative stress, probably due to the consequences of high metabolic demands of neurons which

are non-dividing cells. Accordingly, increased oxidative stress and mitochondrial dysfunction plays a role in the pathologies of neurodegenerative disorders including Huntington's, Parkinson's and Alzheimer's disease. Elevated ROS was seen in Huntington's disease post-mortem cortex and striatum. Moreover, marked neuronal cell death, as well as increased mitochondrial ROS was recorded in the Huntington's disease mouse models (Valencia et al., 2013). Likewise analysis conducted on post mortem brain tissue showed oxidative damage caused by elevated ROS results in the degradation of dopaminergic cells in the substantia nigra of Parkinson's disease (Jenner et al., 1992). In addition, elevated ROS has been described as being an early event in Alzheimer's, preceding the formation of amyloid-β plaques (Nunomura et al., 2001, Praticò et al., 2001).

Oxidative stress is also involved in autosomal cerebellar ataxias. This includes that oxidative stress and impaired OXPHOS has been observed in Friedreich's Ataxia patients (Lodi et al., 1999, Bradley et al., 2000). Additionally, oxidative stress and elevated ROS were present in the Ataxia-Telangiectasia, ATM-deficient mouse model (Kamsler et al., 2001).

Mitochondrial function can be more directly analysed by measuring the efficiency of respiration. Mitochondrial bioenergetics analyzers like the Seahorse Extracellular flux (XF) analyser have been developed to assess OXPHOS by measuring the rate of oxygen consumption (OCR) and glycolysis by determining the extracellular acidification rate (ECAR) of cultured cells. These systems are capable of sensitively analysing mitochondria bioenergetics in real time and can be used to detect relatively subtle impairment of mitochondrial function.

The Seahorse XF analyser has been used in investigating neurodegenerative disorders. A study revealed a deficit in mitochondrial bioenergetics directly preceding the development of amyloid pathology in Alzheimers disease mouse models, agreeing with the increase of ROS at this time (Yao et al., 2009). In cells treated with Parkinson's disease mimetic compounds, there was a significant decrease in OCR and increase in

ECAR leading to increased cell death, suggesting a role for mitochondrial dysfunction in the disease (Giordano et al., 2012).

6.2 Superoxide production in sacsin knockdown and ARSACS fibroblasts

The MitoSOX fluorogenic dye and fluorescent imaging technology allows for the quantitative analysis of mitochondrial superoxide production in individual cells and has been used as an indicator of impaired mitochondrial function in numerous studies (Mukhopadhyay et al., 2007, Meimaridou et al., 2012, Mezencev et al., 2011). Fibroblasts were transfected with GFP along with either SACS or SCRM siRNA. After 48hrs, cells were washed once with PBS and incubated with MitoSOX for 10 minutes in a 37°C, 5% CO_2 incubator, followed by a further wash and imaging. Cells which expressed GFP were assumed to have been successfully transfected with siRNA. GFP in this instance was also useful in defining the cell boundaries for MitoSOX analysis (Figure 6. 2).

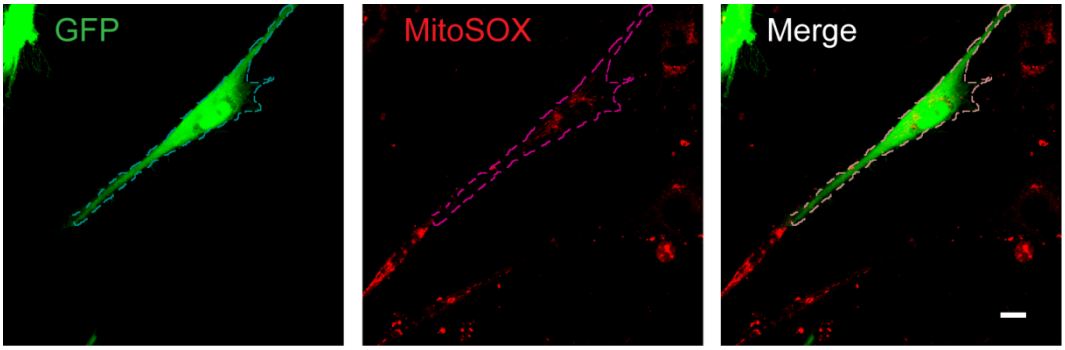

Figure 6. 2 Representative maximum intensity projections of MitSOX fluorescence.

Fibroblasts were transfected with SCRM siRNA along with GFP. After 48 hours, cells were washed with PBS and incubated with MitoSOX for 10mins. Region of interest (ROI) were selected by drawing around the cell boundary visualised by GFP, using the line tool in the Zeiss software. The mean MitoSOX fluorescence within each ROI was measured using the software.

For this analysis confocal Z-stacks of 0.55µm each over an average of 7µm were acquired in 35 cells for each condition. MitoSOX fluorescence occurs through oxidisation of the reagent by superoxide, therefore the intensity of MitoSOX fluorescence was used to indicate the levels of mitochondrial superoxide present within the mitochondria. Intensity was measured using the Zeiss confocal software which allowed for the measurement of intensity within a selected region of interest (ROI). The line tool in the software was used to draw around the cell boundary (ROI) and measurement tool to measure mean red (MitoSOX) fluorescence (Figure 6. 2). Confocal conditions were maintained for each sample throughout the experiment.

The sacsin knockdown fibroblasts had a higher level of MitoSOX fluorescence than then controls. A fluorescence of 469.61 ± 40.01AU was recorded in SCRM fibroblasts, significantly lower ($p \leq 0.05$) than the 708.99 ± 91.77AU recorded in *SACS* fibroblasts. This indicated the presence of more mitochondrial superoxide in the sacsin knockdown than in control fibroblasts (Figure 6. 3B).

Following on from the results obtained in sacsin knockdown fibroblasts, the mitochondrial superoxide production was examined in patient fibroblasts using MitoSOX. The cells were grown until a confluence of 70% was reached. Cells were washed in PBS and incubated with MitoSOX for 10 minutes as previously described. Phase images were used instead of GFP in this instance to define the cell boundary. Confocal Z-stacks were collected at 0.5 µm Z-intervals for 75 cells from 3 control and 4 patient fibroblasts cell lines.

A higher MitoSOX fluorescence was observed in all of the patients when compared to control fibroblasts (Figure 6. 3B). Control fibroblasts had a mean fluorescence of 235.53 ± 8.66 AU. Patient c.2094-A>G/Q4054*(296.17 ± 12.44 AU), and patient 2801Q (300.35 ± 20.49 au) had similar levels of MitoSOX fluorescence and both were significantly ($p \leq 0.01$) higher than controls. Similarly, significantly ($p \leq 0.0001$) higher levels of fluorescence was observed in patient R2002fs/Q4054*, which had the highest fluorescence of 436.69 ± 23.33 AU and patient K1715*/R4331Q, the second highest MitoSOX fluorescence (418.37 ± 14.99 AU) recorded (Figure 6. 4B).

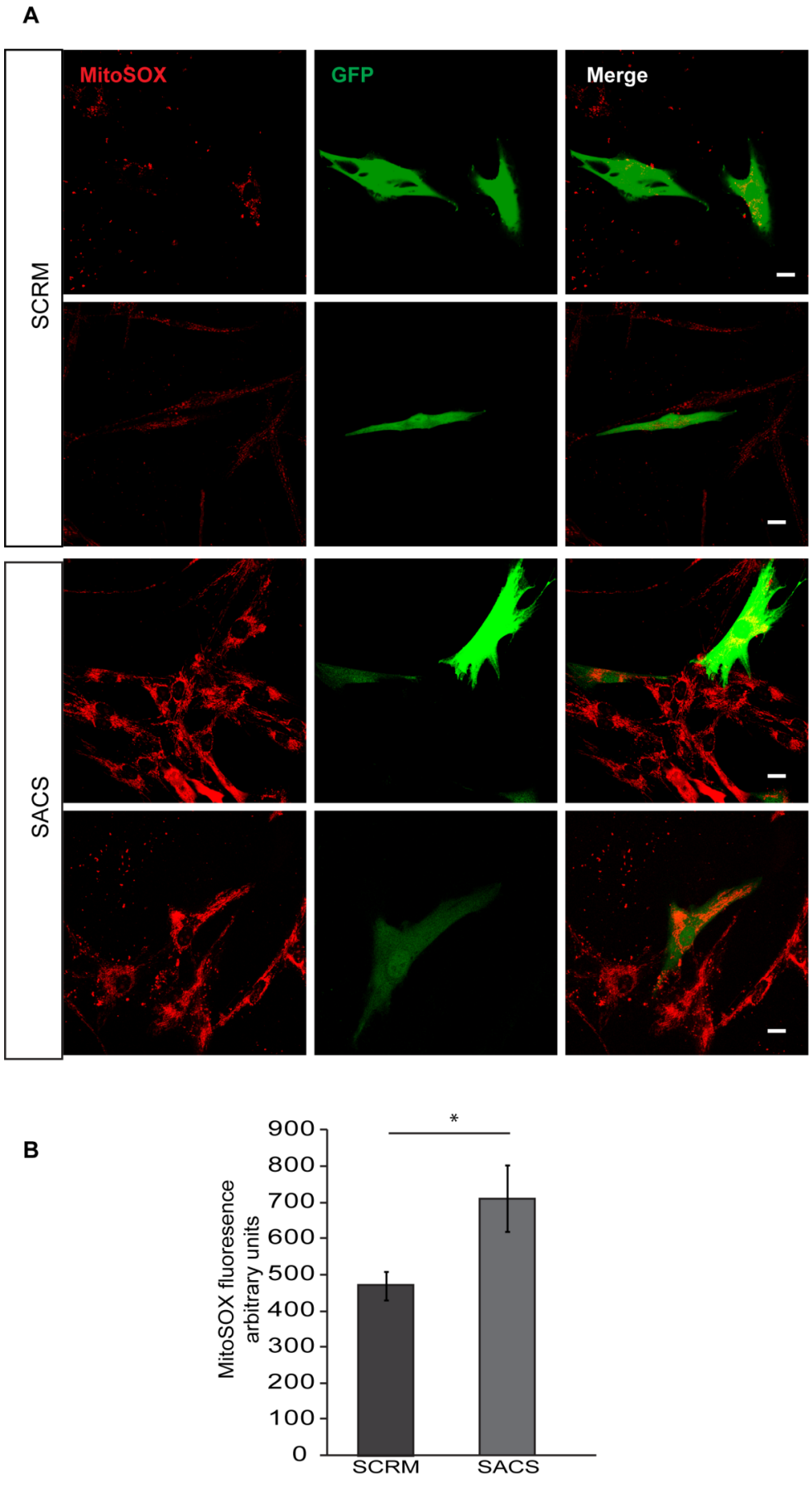
A
MitoSOX
GFP
Merge
SCRM
SACS
B
MitoSOX fluoresence arbitrary units
900
800
700
600
500
400
300
200
100
0
*
SCRM
SACS

Figure 6. 3 Sacsin knockdown fibroblasts have significantly higher levels of mitochondrial superoxide than scrambled control fibroblasts.

Fibroblasts were transfected with either SACS or SCRM siRNA along with GFP. Fibroblasts were washed and loaded with MitoSox 48 hours post transfection. Confocal Z-stacks were taken and images were analysed using the Zeiss confocal software. A) Representative images of MitoSox fluorescence in *SACS* and *SCRM* fibroblasts. B) Quantification of MitoSOX was performed using Zeiss confocal software. Data represents mean values. Error bars represent ± SEM. Scale bars represent 10µm. n=35 ‡p≤0.05.

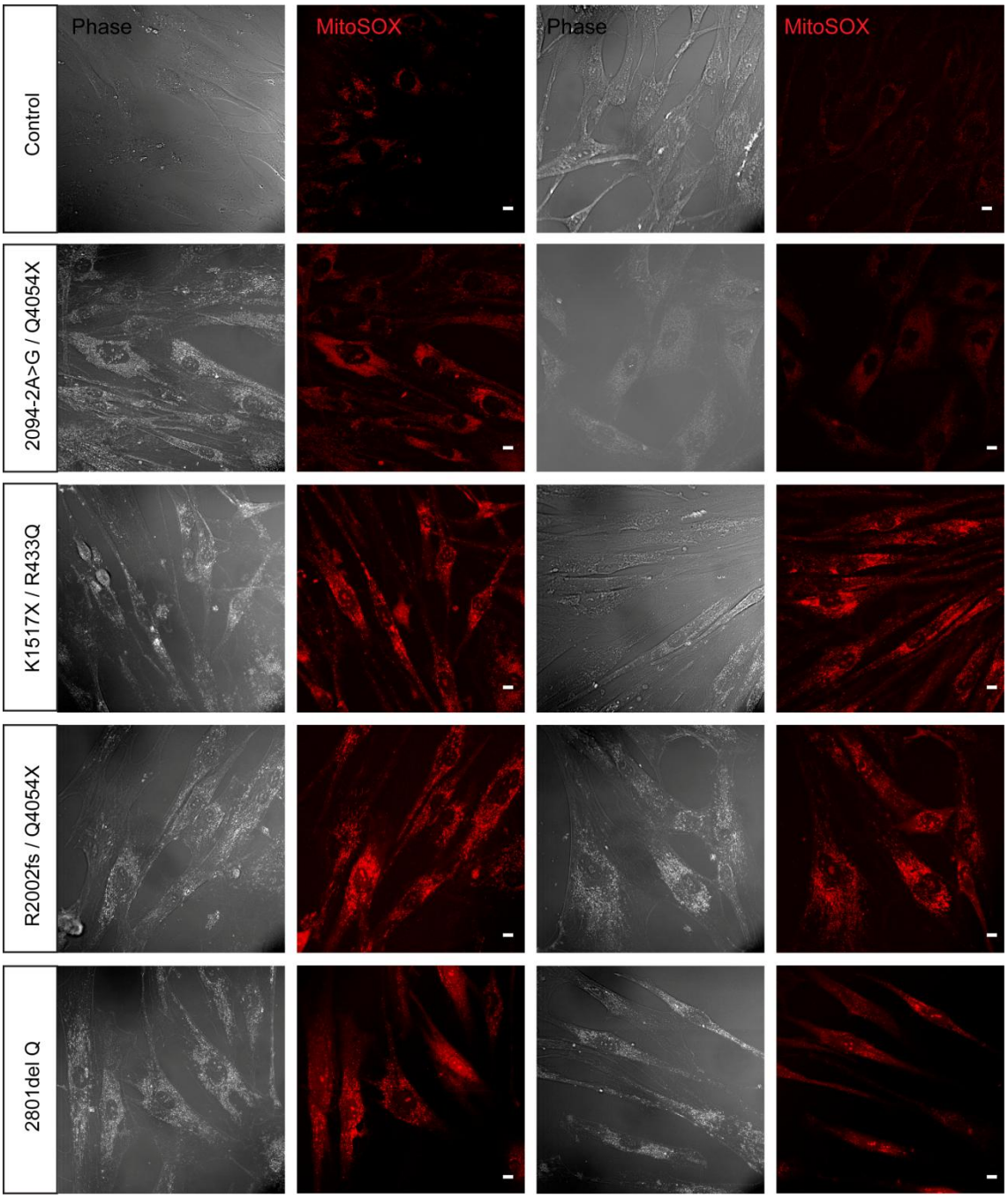
Phase
MitoSOX
Phase
MitoSOX
Control
2094-2A>G / Q4054X
K1517X / R433Q
R2002fs / Q4054X
2801del Q

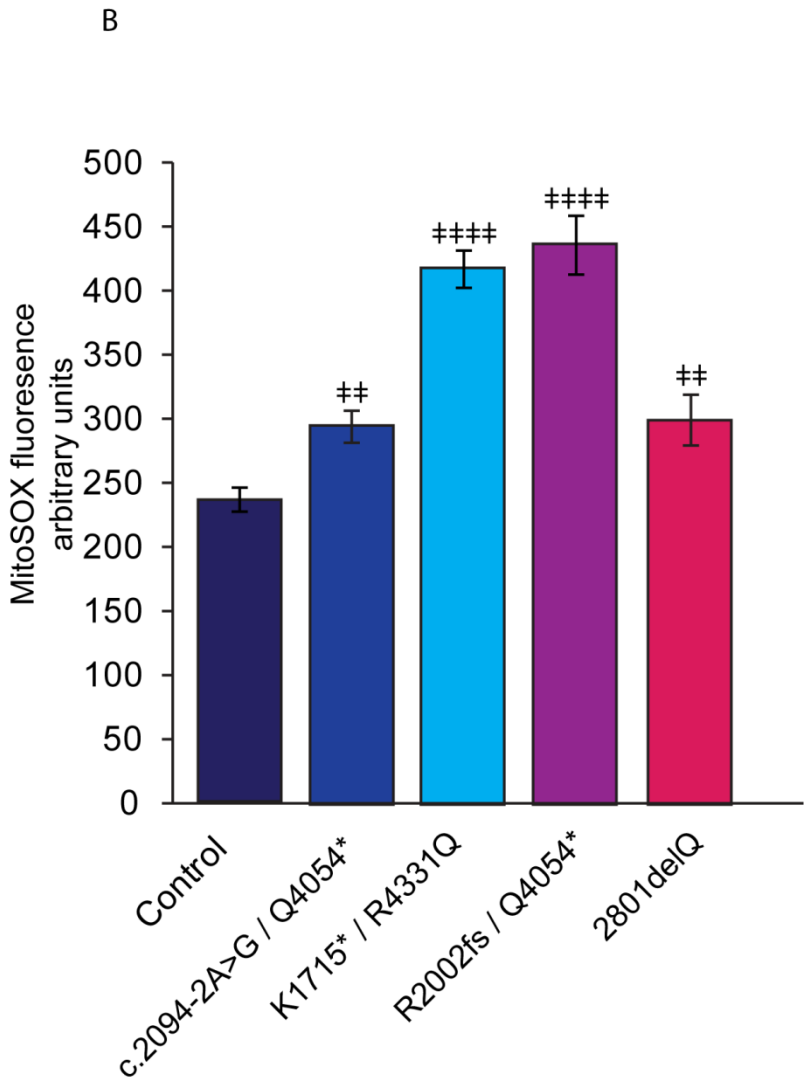

Figure 6. 4 ARSACS patient fibroblasts have significantly higher levels of mitochondrial superoxide than control fibroblasts.

Fibroblasts were washed and loaded with MitoSOX for 10mins prior to imaging. Confocal Z-stacks were taken and images were analysed using the Zeiss confocal software. A) Representative images of MitoSOX fluorescence in patient and control fibroblasts. B) Quantification of MitoSOX was performed using Zeiss confocal software. Data represents mean values. Error bars represent ± SEM. N=75 Scale bars represent 10µm

6.3 Mitochondrial respiration in ARSACS patient fibroblasts

The bioenergic profile of the controls and patient fibroblasts were analysed using XF^e96 flux analyser along with XF Cell MitoStress kit (Seahorse Bioscience). These allowed the accurate measurement of the basal respiration as well as the response to mitochondrial insult by the introduction of reagents known to induce mitochondrial stress. siRNA treated fibroblasts were not used for this analysis due to the low transfection efficiency making measurements on populations of cells difficult. The OCR was measured in 3 control and 4 patient fibroblasts lines.

In the first instance, 4 OCR measurements were recorded to establish the basal OCR of the fibroblasts. After these measurements were taken, 4 reagents (Oligomycin, carbonyl cyanide-p-trifluoromethoxyphenyl analyser, Rotenone and Antimycin A) were added sequentially to the culture plate and OCR readings were recorded. All measurements were in quadruplet in 10-12 replicates for each sample.

Oligomycin, an ATP coupler, was the first reagent added at a concentration of 5 µM. Oligomycin inhibits ATP synthesis by blocking ADP phosphorylation. The reduction in OCR after the introduction of Oligomycin indicates the oxygen consumption required for ATP synthesis as well as the percentage of oxygen consumption necessary to overcome the proton leak across the inner membrane (Figure 6. 5).

The second reagent added was 0.5µM of carbonyl cyanide-p-trifluoromethoxyphenyl analyser (FCCP), which causes an increase in OCR (Figure 6. 5). FCCP is an uncoupler which disrupts mitochondrial membrane potential allowing hydrogen ions across the mitochondrial membrane bypassing complex V. This in turn disrupts ATP synthesis and therefore accelerates the ETC. The increase in OCR is indicative of the maximal respiration of the fibroblasts (Figure 6. 5).

1µM of rotenone, a complex I inhibitor and Antimycin A, a complex III inhibitor were the final reagents added. These reagents inhibit the production of ATP resulting in a decrease in OCR measurements. OCRs recorded after the addition of these reagents indicate non-mitochondrial respiration (Figure 6. 5).

The basal OCRs were calculated as the OCRs recorded prior to the addition of mitochondrial inhibitors minus non-mitochondrial respiration (Figure 6. 5). These readings were carried out in the presence of 10mM glucose. The basal OCRs of the patient fibroblasts were significantly ($p \leq 0.0001$) reduced when compared to control (Figure 6. 6, Figure 6. 7) Control fibroblasts had an OCR of 116.71 ± 9.98 pmol/min while patient 2801delQ had the lowest basal OCR at 20.49 ± 0.73 pmol/min. Patient K1715*/R4331Q had the highest basal OCR of 72.68 ± 3.23 pmol/min despite having a more collapsed mitochondrial phenotype described in chapter 3. Patients c.2094-2 A>G/Q4054* and R2002fs/Q4054*had OCRs of 52.17 ± 3.18 pmol/min and 36.55 ± 1.38 pmol/min respectively.

The amount of proton leak was calculated as OCR after oligomycin treatment minus non-mitochondrial respiration (Figure 6. 5). The results gathered showed that patient fibroblasts had a marked decrease in proton leak. The lowest proton leak, 4.04 ± 0.32 pmol/min, was recorded in patient 2801delQ which was significantly ($p \leq 0.0001$) less than recorded in control, (21.78 ± 3.84 pmol/min). Similarly, a significant ($p \leq 0.001$) decrease in proton leak was found in patient R2002fs/Q4054* with an OCR reading of 9.35 ± 0.40 pmol/min. Patients K1715*/R4331Q and c.2094-2 A>G/Q4054* had similar measurements of 12.12 ± 0.14 pmol/min and 12.84 ± 0.83 pmol/min which again was notably different from the controls ($p \leq 0.01$).

A significant ($p \leq 0.0001$) reduction in ATP production was observed in ARSACS patients. Here, the ATP production was defined as the difference between basal OCR and proton leak (Figure 6. 5). Control fibroblasts had an OCR of 94.93 ± 6.43pmol/min (Figure 6. 7). This OCR was over 2x higher than that observed in patient c.2094-2 A>G/Q4054* (39.34 ± 2.07 pmol/min) and over 3.5 x higher than patient R2002fs/Q4054* (27.19 ± 0.65 pmol/min). Patient K1715*/R4331Q and had a higher ATP production than the other patients which was reflected by OCR of 60.56 ± 2.83 pmol/min. Contrastingly, ATP production was lowest in patient 2801delQ indicated by an OCR of 16.45 ± 0.23 pmol/min (**Figure 6. 7**).

Interestingly, maximal respiration was significantly ($p \leq 0.0001$) reduced in the patients. Maximal respiration was calculated as the difference between the OCR recorded after FCCP injection minus non-mitochondrial respiration (Figure 6. 7). OCR readings recorded show that the mitochondria did not appear to effectively respond to FCCP treatment as it did in the controls. While control maximal respiration OCR reading was 126.49 ± 6.23 pmol/min, patient c.2094-2 A>G/Q4054* and K1715*/R4331Q had OCRs of 25.35 ± 1.43 and 56.50 ± 2.35 pmol/min respectively(Figure 6. 6, Figure 6. 7). Patient 2801delQ had the lowest OCR at 4.00 ± 0.35 pmol/min and did not recover from ATP synthesis inhibition after treatment with oligomycin (Figure 6. 6). Lastly patient R2002fs /Q4054* also showed reduced recovery following oligomycin treatment and had a mean maximal respiration of 6.98 ± 0.23 pmol/min Figure 6. 6,Figure 6. 7).

Spare capacity was defined as the difference between maximum and basal respiration (Figure 6. 5). A reduction in the spare respiratory capacity was observed in patients (Figure 6. 6, Figure 6. 7). These results were significant with $p \leq 0.0001$. Strikingly, none of the patients appeared to have sufficient spare respiratory capacity and on average yielded negative readings. In the control fibroblasts, the increase in OCRs after treatment with FCCP showed that the mitochondrial uncoupling had occurred and mitochondria recovered after oligomycin treatment. The same appeared to be true for patients c.2094-2A>G/Q4054* and K1715*/R4331Q, however the OCRs obtained after FCCP treatment were lower that the basal OCRs recorded. As expected, based on very low values for maximum respiration, patient 2801delQ and R2002fs /Q4054* had the worse recorded values for spare capacity -16.49 ± 0.44 and -29.57 ± 1.22 pmol/min.

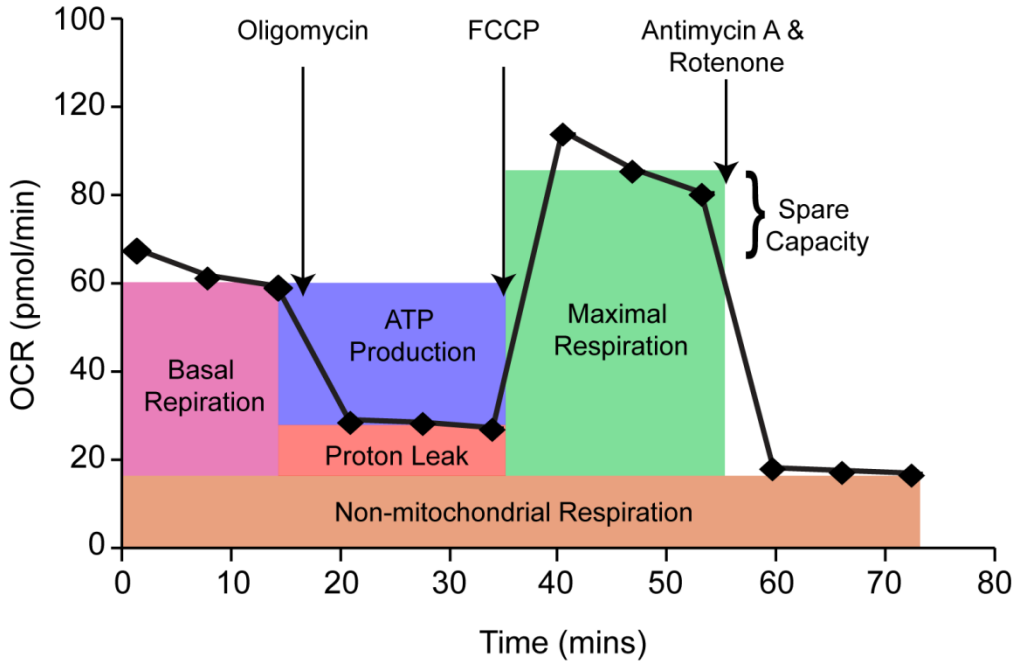

Figure 6. 5 Representative respiratory profile of human dermal fibroblasts.

450 x10^3 Dermal fibroblasts were seeded into the XF^{e}96 microculture plate 24 hours prior to analysis. Cells were then washed and incubated with supplemented XF Assay media for 1 hour in a non CO_2 incubator. Cells were placed into the analyser and 3 initial OCR readings were taken. This was followed by sequential injections of 25µl of 5µM Oligomycin, 25µl of 0.5 µM FCCP and 25µl of 1µM Antimycin A/Rotenone. Concentrations represent final concentrations in the well. This profile represents 12 replicates. Three measurements were taken after each injection.

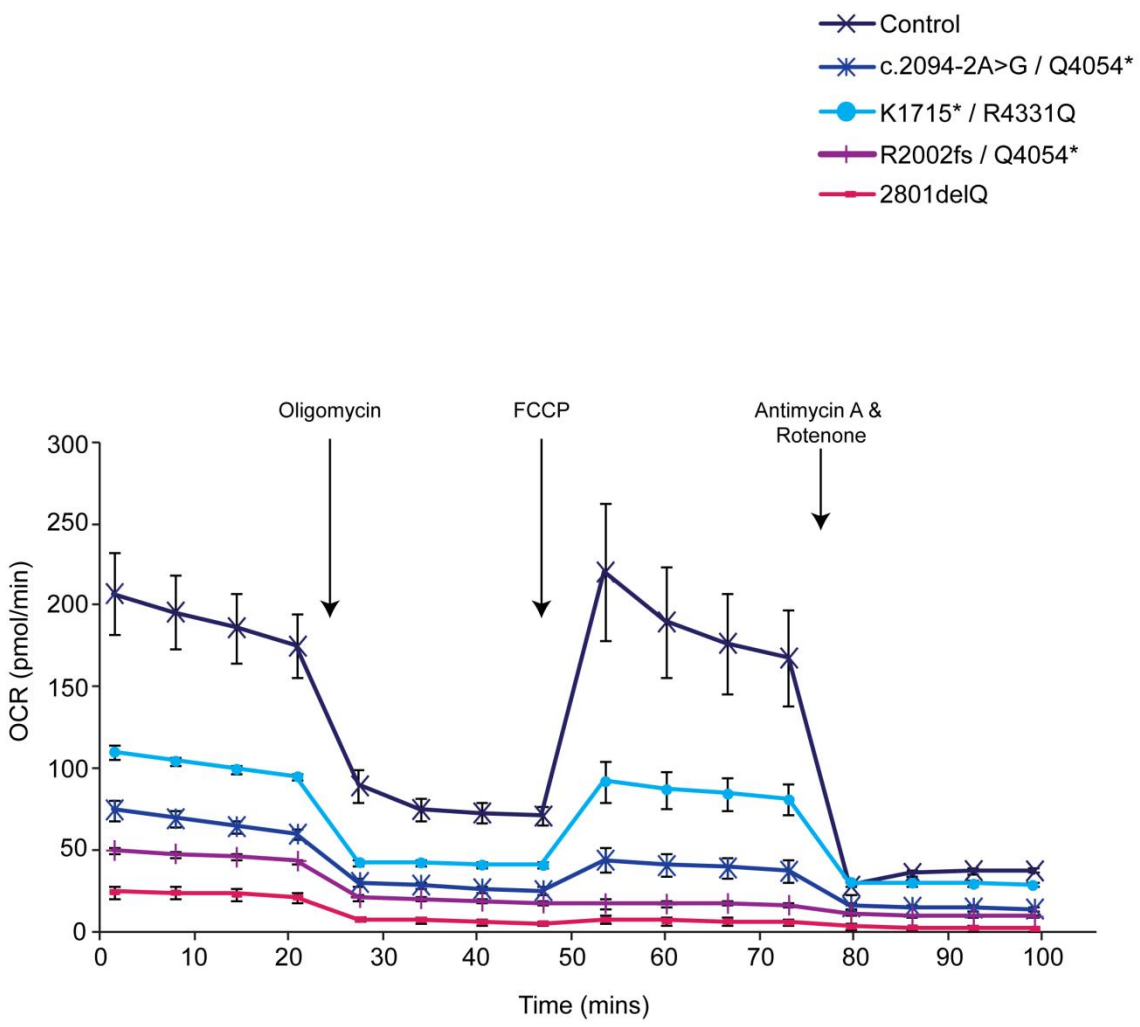

Figure 6. 6 Reduced mitochondrial respiration was observed in ARSACS patients.

Respiratory profile of 3 control and 4 patient fibroblasts. 390 x10^3 cells were seeded into the XF^{e}96 microculture plate 24 hours prior to analysis. Cells were then washed and incubated with XF Assay media for 1 hour in a non CO_2 incubator. Cells were placed into the analyser and 4 initial OCR readings were taken. This was followed by sequential injections of 25µl of 5µM Oligomycin, 25µl of 0.5 µM FCCP and 25µl of 1µM Antimycin A/Rotenone. This profile represents 10-12 replicates. Four measurements were taken after each injection. Error bars represent ±SEM.

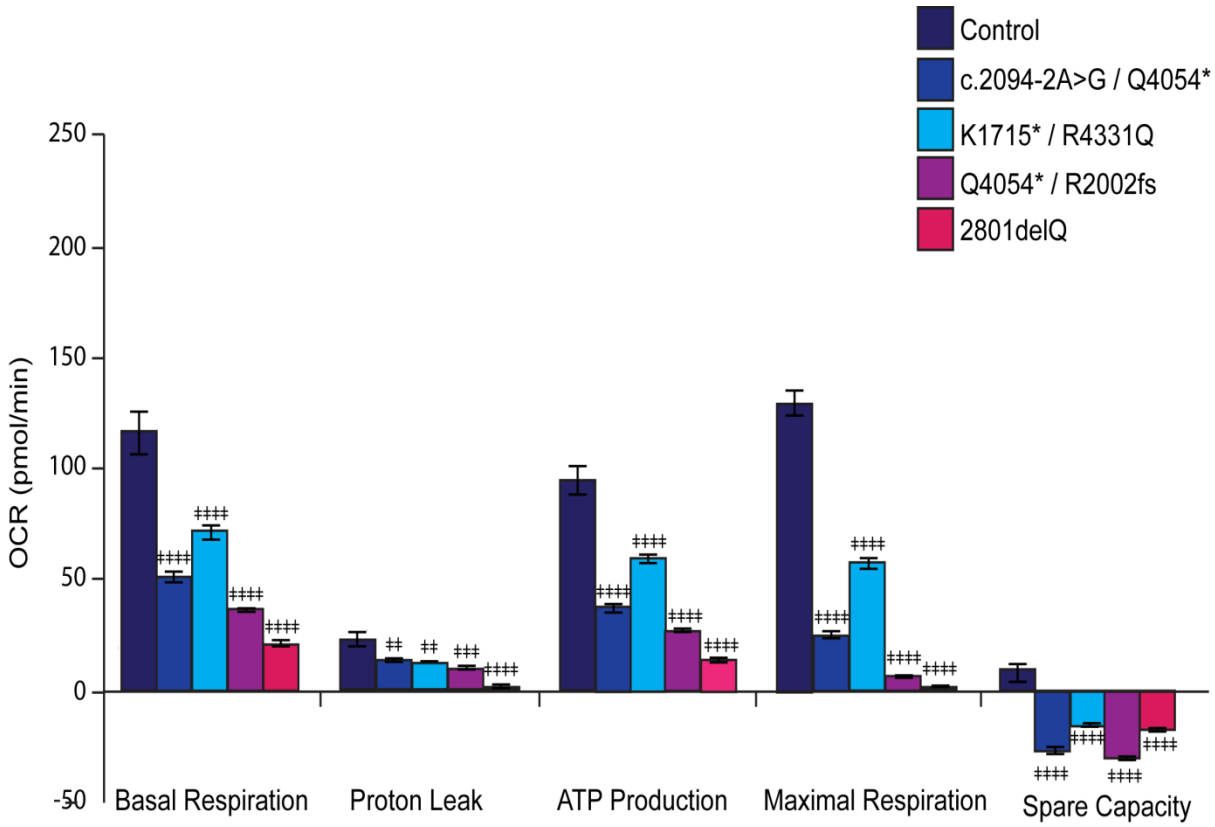

Figure 6. 7 Reduced mitochondrial efficiency was observed in ARSACS patients.

A reduction in maximum respiratory capacity as well as ATP production was recorded in patient fibroblasts. Each bar in the chart represents the mean of four readings in 10-12 replicates. The OCR measurements were normalised to 390 x 10^3 cells Error bars represent ± SEM. ‡‡ p≤0.01 ‡‡‡p≤0.001 ‡‡‡‡p≤0.0001

6.4 Glycolytic Function in ARSACS fibroblasts

The glycolytic profile of the controls and patient fibroblasts were analysed using the XF^{e}96 flux analyser along with XF Cell Glycolysis Stress kit. Cells are capable of dynamically shifting energy production between oxidative phosphorylation and glycolysis, in order to maintain the balance of energy in response to changes in environment. Being able to adapt mechanism of energy production is vital. OXPHOS occurs under aerobic conditions, where pyruvate produced in the glycolysis process enters the TCA cycle initiating the process described earlier (Figure 6. 1). Under anaerobic conditions pyruvate is reduced to lactate (lactic acid) by lactate dehydrogenase A (Pfeiffer et al., 2001). This process occurs in the cytoplasm and the lactic acid produced is excreted into the extracellular environment.

The production and excretion of lactic acid allowed for the measurement of the change in pH of the fibroblasts' extracellular medium. Lactic acid excreted into the extracellular medium leads to acidification of the medium. The change in pH can then be measured by the XF^{e}96 flux analyser.

The Glycolysis Stress kit allowed for the measurement of glycolysis, maximal glycolytic capacity and glycolytic reserve in the patient and control fibroblasts by examining the cells response to glycolytic stress. After the initial basal ECAR measurements were taken, 3 reagents (Glucose, Oligomycin and 2-Deoxy-D-Glucose) were added sequentially to the culture plate and ECAR readings were recorded. All measurements were in quadruplet in 10-12 replicates for 3 control and 4 patient fibroblasts lines.

A high concentration of 10mM of glucose was the first reagent added after the four basal ECAR readings were recorded. Cells at this stage, have been deprived of pyruvate and glucose for an hour, therefore this injection of glucose results in the uptake of glucose by the cells so that it can be utilised to produce ATP through the process of glycolysis as described earlier. This sudden uptake leads to release of protons into surrounding media and hence an increase in ECAR. The response induced by the introduction of glucose is measured as the rate of glycolysis (Figure 6. 8).

The second reagent was ATP synthase inhibitor oligomycin (5µM). Oligomycin inhibits ATP production and therefore shifts the production of energy toward glycolysis. The increase in ECAR is due to the cells attempting to maintain ATP production through this alternate process and gives us the maximum glycolytic capacity of the cell (Figure 6. 8).

The addition of 100mM 2-Deoxy-D-Glucose (2DG) results in the decrease of ECAR and 2DG inhibits glycolysis through competitive binding to glucose hexokinase. 2DG is an analogue of glucose which cannot undergo glycolysis due to a change in the hydroxyl group of the inhibitor. Once bound to glucose hexokinase it suppresses the action of the hexokinase preventing the initiation of glycolysis. The use of this molecule ensures that the ECARs recorded during the experiment were the result of glycolysis (Figure 6. 8).

Glycolysis in this case was calculated as the ECAR recorded after glucose injection minus the non-glycolytic acidification. Glycolysis was highest in patient 2801delQ at 42.89 8.32 mpH/min. This was higher than all of the patients and significantly ($p \leq 0.01$) higher than control. Glycolysis measurements were similar in the control and the other 3 patients. The control fibroblasts had a value of 12.96 ± 3.00 mpH/min, while patient c. 2094-2 A>G/Q4054*, K1715*/R4331Q and R2002fs / Q4054* had values of 14.63 ± 1.97 mpH/min, 13.19 ± 7.09 mpH/min and 15.42 ± 2.27 mpH/min respectively. These results were not deemed statistical different from the controls.

The glycolytic capacity was defined as the difference between the ECAR recorded after the oligomycin injection and non-glycotic acidification. Glycolytic capacity was highest in patient 2801delQ with a mean ECAR measurement of 55.53 ± 7.78mpH/min, superseding measurements recorded in the controls and other patient fibroblasts. The increase in ECAR was statistical different with a p value ≤0.001. The control had a mean ECAR of 20.30 ± 2.55 mpH/min representing the glycolytic capacity. These measurements were comparable to those observed in the patients c.2094-2 A>G/Q4054*, K1715*/R4331Q and R2002fs/Q4054* in which glycolytic capacity was represented by mean ECARs of 18.25 ± 2.19 mpH/min, 16.10 ± 6.73 mpH/min and

14.96 ± 1.25 mpH/min respectively. ANOVA statistical testing did not find the difference to be statistically significant.

The results for glycolytic capacity in the patients were quite varied. A significant ($p \leq 0.01$) decrease in glycolytic capacity was found in patient R2002fs/Q4054* (-0.46 ± 1.81) (Figure 6. 9,Figure 6. 10). The glycolytic profile for this patient clearly shows a lack of response to oligomycin treatment in these cells, therefore these results are in keeping with the profile obtained (Figure 6. 9, Figure 6. 10). Contrastingly, patient 2801delQ had a significant ($p \leq 0.05$) increase in glycolytic capacity(12.65 ± 1.73) when compared to control (7.35 ± 0.46 mpH/min). The differences in the glycolytic reserve between patient c.2094-2>AG/Q4054* and control and patient K1715*/R331Q and control did not obtain statistical significance ($p > 0.05$).

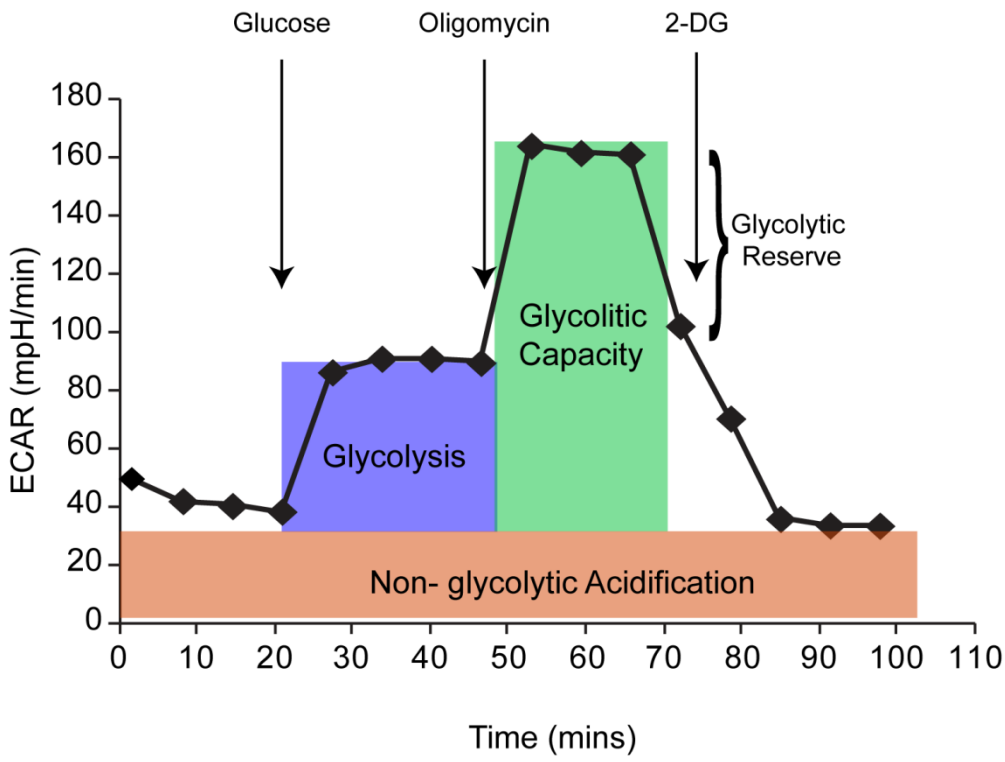

Figure 6. 8 Representative glycolytic profile of human dermal fibroblasts.

390 x10^3 dermal fibroblasts were seeded into the XF^{e}96 microculture plate 24 hours prior to analysis. Cells were then washed and incubated with XF Assay media without glucose for 1 hour in a non CO_2 incubator. Cells were placed into the analyser and 4 initial ECAR readings were taken. This was followed by sequential injections of 25µl of 10mM Glucose, 25µl of 5µM Oligomycin and 25µl of 100mM 2-DG. Concentrations represent final concentrations in the well. This profile represents 12 replicates. Three measurements were taken after each injection.

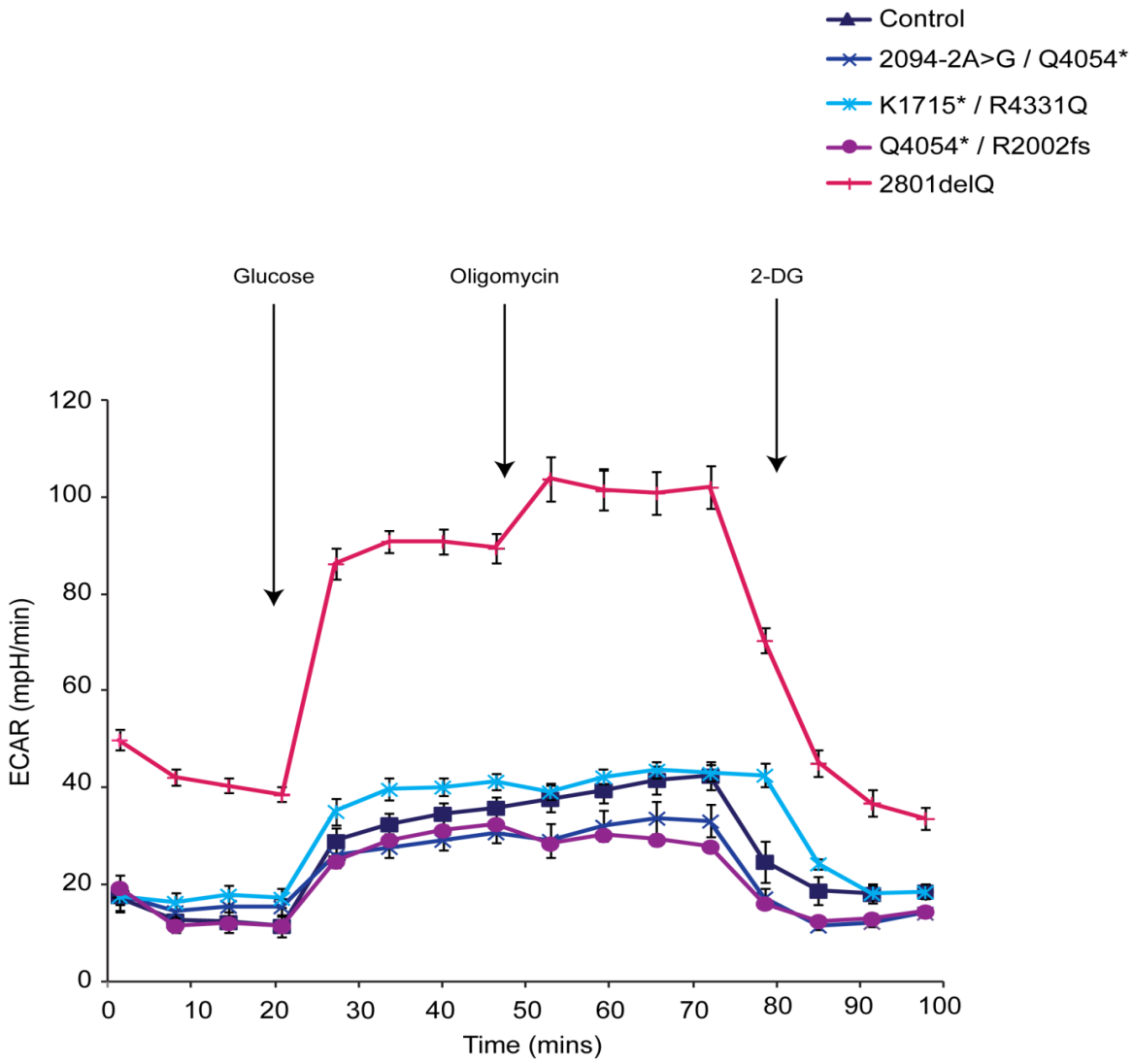

Figure 6. 9 An increased basal ECAR and maximum ECAR was observed in patient 2801delQ.

Glycolytic profile of 3 control and 4 patient fibroblasts. 390 x10^3 cells were seeded into the XF^{e}96 microculture plate 24 hours prior to analysis. Cells were then washed and incubated with XF Assay media for 1 hour in a non CO_2 incubator. Cells were placed into the analyser and 4 initial OCR readings were taken. This was followed by sequential injections of 25µl of 5µM Oligomycin, 25µl of 0.5 µM FCCP and 25µl of 1µM Antimycin A/Rotenone. This profile represents 10-12 replicates. Four measurements were taken after each injection. Error bars represent ±SEM.

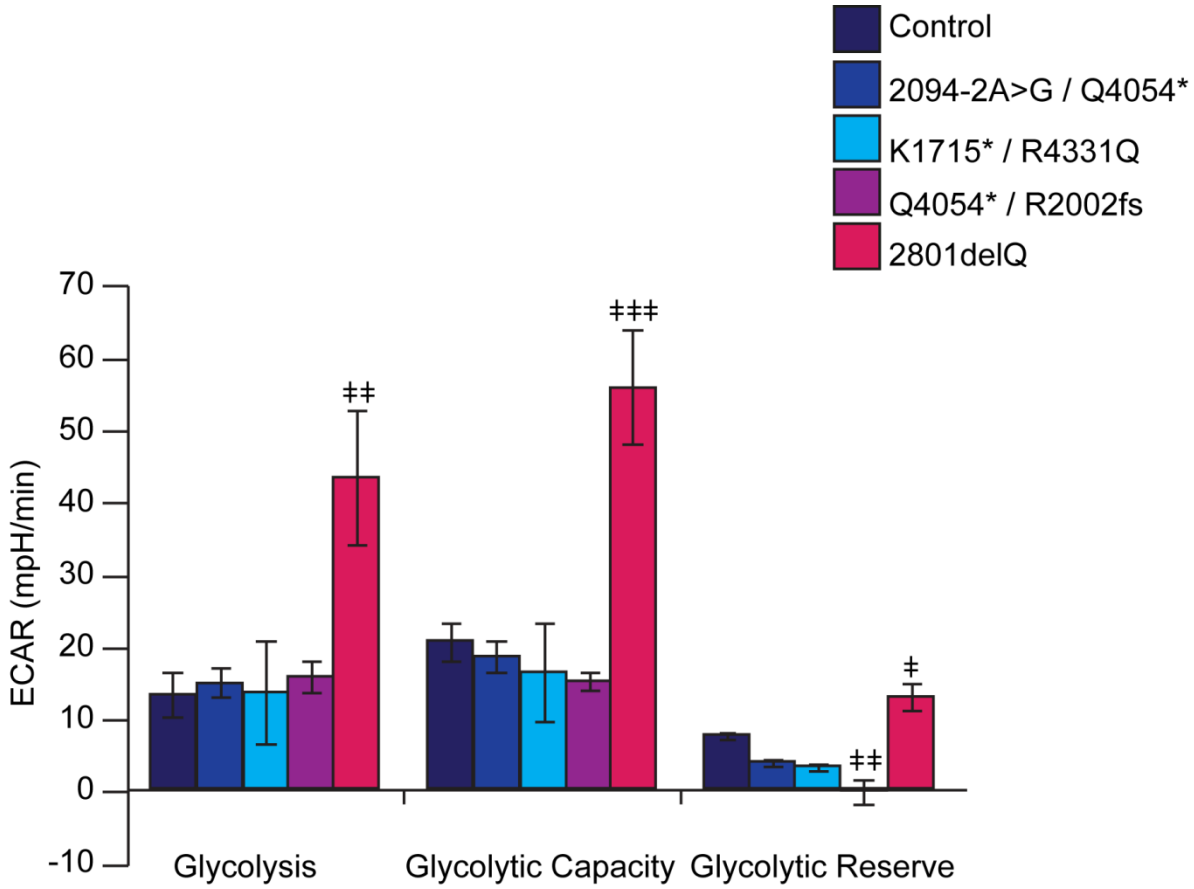

Figure 6. 10 Increased glycolytic efficiency was observed in patient 2801delQ.

Each bar in the chart represents the mean of four readings in 10-12 replicates. The ECAR measurements were normalised to 390 x 10^3 cells. Error bars represent ± SEM. ‡p≤0.05 ‡‡p≤0.01 ‡‡‡p≤0.001.

6.5 Discussion

An increased level of mitochondrial superoxide was measured in sacsin knockdown and patient fibroblasts. MitoSOX fluorescence observed in sacsin knockdown fibroblasts was 1.5 x greater than in controls. This relative difference varied between 1.25 – ~1.9x in the patients (Table 6. 1). Mitochondrial superoxide is produced by components of the ETC like complex I and III (Brand et al., 2004, Turrens, 2003). The superoxide anion (O_2^{-}.) is the precursor of reactive oxygen species (ROS) produced through the reduction of oxygen by 1- electron and is a potential source of cellular damage if it accumulates (Brand et al., 2004, Li et al., 1995). This reactive molecule is usually converted to hydrogen peroxide (H_2O_2), which can occur spontaneously or through a reaction catalysed by superoxide dismutases. H_2O_2 can then be reduced to water and oxygen by catalase and glutathione peroxidase enzymes through a series of reactions (Turrens, 2003). The imbalance between superoxide production and it's clearance by antioxidant enzymes or scavengers, result in oxidative stress.

	MitoSOX fluorescence (relative to control)
Sacsin knockdown	1.5
c.2094-2 A>G/ Q4054*	1.25
K1715*/R4331Q	1.77
R2002fs/Q4054*	1.86
2801delQ	1.27

Table 6. 1 Summary of the MitoSOX fluorescence relative to control fibroblasts.

While these results are interesting, further analysis of the regulation of mitochondrial antioxidant enzymes will provide a more comprehensive ROS profile in patient cells and in cells with reduced sacsin.

Prior studies have demonstrated the importance of understanding the regulation of mitochondrial antioxidants in the pathology of neurodegenerative diseases. Increased ROS/superoxide production has been described as a feature of neurodegenerative disorders. High, sustained levels of superoxide was observed when frataxin was knocked down in SH-SY5Y cells (Bolinches-Amorós et al., 2014). These cells also exhibited a fused mitochondrial network and reduction in mitochondrial number (Bolinches-Amorós et al., 2014). Developing neurons from Alzheimer's mouse model were shown to have increased mitochondrial manganese superoxide dismutase (MnSOD) activity as well as an increase in the levels of MnSOD protein. However these levels decreased in mature neurons of the Alzheimer's disease mouse model, which was suggested to result in an impairment of the neurons to respond to oxidative insult and hence contributing to disease pathology (Sompol et al., 2008). Increased levels of ROS, MnSOD activity and a decrease in antioxidant enzyme, glutathione peroxidase (GPX1) were found in the cerebellum of ATM null mice (Kamsler et al., 2001, Okuno et al., 2012). In addition, an increase in mitochondrial manganese superoxide dismustase and mitochondrial glutathione peroxidase was reported in the brain of a Parkinson's disease mouse model (Andres-Mateos et al., 2007). The analysis of gene and protein expression of MnSOD and GPX1, via quantitative real time PCR and immunoblotting, as well as the assessment of their enzymatic activity by colourimetric assays, can be carried out using patient fibroblasts or sacsin knockdown SH-SY5Y cells. Such an undertaking will be beneficial in understanding the consequence of a loss of sacsin on the ROS status of mitochondria.

Similar to results obtained in this thesis, sustained mitochondrial fusion, caused by the reduction of hFis1 in HeLa cells led to an increase in ROS production and a decrease in membrane potential (Lee et al., 2007).

An increase in ROS and ROS damage is postulated to be an upstream activator of mitophagy (Wang et al., 2012). As mentioned earlier in this thesis, damaged mitochondria are removed by this selective process to limit the damage to the entire mitochondrial network and to protect the cell from damage and ultimately apoptosis (Mammucari and Rizzuto, 2010). Most importantly however, in order for mitophagy to occur, damaged sections of the mitochondrial network are removed by mitochondrial fission. Therefore loss of this mechanism impairs mitopagy and can potentially result in the cell death observed in neurodegeneration (Mammucari and Rizzuto, 2010, Youle and Narendra, 2011).

Interestingly the relative difference in MitoSOX fluorescence was highest in patient R2002fs/Q4054* with 1.86 times more fluorescence recorded than controls. Morphometric analysis of the mitochondrial network, reported in Chapter 3 of thesis, showed this patient to have a significantly larger total mitochondrial volume than controls. The studies linking mitophagy, oxidative stress and regulation of mitochondrial dynamics, in conjuction with results presented here and in chapters 3-4, have provoked questions of whether the cellular death reported in ARSACS is a consequence of the increased ROS brought about by impaired fission and cellular damage or attenuated mitophagy. It is therefore important to explore the regulation of mitophagy in sacsin knockdown and patient cells as well as cell viability.

Examining the cellular localisation of markers involved in mitophagy like PINK1 and parkin in sacsin null cells will give a better understanding of sacsin's role in mitophagy. PINK1 is known to accumulate on the surface of damaged mitochondria thereby recruiting parkin and initiating the mitophagy cascade. Quantification of the cellular localisation of these proteins in *SACS* null cells will address whether mitophagy is impared in ARSACS.

Results in this chapter highlights the extent of mitochondrial dysfunction in ARSACS fibroblasts. Patients had low basal respiration which may be due to the damaged mitochondria caused by elevated ROS. The main function of mitochondria is the production of ATP. Optimal function is especially important in neuronal cells, which

have high demands for energy. A decrease in maximal respiration was observed in the ARSACS patient cells indicating decrease in efficiency of mitochondrial respiration. Reduced ATP production has been linked with other neurodegenerative diseases. For example, hippocampal neurons in an Alzhiemer's disease mouse model displayed significantly lower basal OCR than controls (Yao et al., 2009). Moreover a significant reduction in maximal OCR was also observed in the hipocampal neurons of the same mice (Yao et al., 2009). In fibroblasts with reduced levels of parkin, a decrease in basal respiration was described. This was significantly lower than their scrambled siRNA controls (Ferretta et al., 2014).

A decrease in mitochondrial respiration was observed in cells where fission had been impaired. Furthermore, a low basal respiration as well as low ATP production was observed in cells where Drp1 had been reduced (Benard et al., 2007a). A recent paper published in 2013 showed that supressor of cytokine sigalling 6 (SOCS6), may be involved in the translocation of Drp1 to the mitochondria (Lin et al., 2013). An increase in mitochondrial elongation was observed in cells with reduced levels of SOCS6. As well as this, a reduction in basal respiration, spare capacity and ATP production was also measured in the SOCS6 knockdown cells (Lin et al., 2013).

Finally, an increase in glycolytic capacity and glycolysis was observed in patient 2801delQ. A shift toward glycolysis tends to be a sign of dyfunctional OXPHOS. This shift is in keeping with the reduction of ATP production observed patient in 2801delQ cellular respiratory profile. An increase in ECAR accompanied a decrease in OCR was observed in cells with hyperfused mitochondria where Drp1 had been reduced (Qian et al., 2012). Glycolysis and glycolytic capacity was lower in the other ARSACS patients compared to the controls. Similar results were also observed in SOCS6 knockdown cells. These cells also had a lower basal OCR than in controls as well as reduced glycolytic capacity (Lin et al., 2013).

Of note, the delay in the recovery of oxidative metabolism and membrane potential in sacsin knockdown cells following CCCP washout experiment was suggested by Girad et al, to be attributed to either reduced proton pumping or increased proton leakage

(Girard et al., 2012). Conversely, a significant decrease in proton leak was observed in the patients. The process of oxidative phosphorylation is not 100% efficient. This is a result of the ability of some protons to leak across the membrane, returning to the mitochondrial matrix without the ATP synthase complex, therefore no ATP is generated from this process (Divakaruni and Brand, 2011). Nonetheless, proton leak pathways are important in other functions such as nonshivering thermogenesis (Jastroch et al., 2005). Controversially, it was suggested that proton leak can function to protect ROS damage, this hypothesis is fascinating in relation to data obtained in the patient fibroblasts. However, this has not been conclusively demonstrated (Brand, 2000). These results could mean that the observations regarding oxidative metabolism are due to decreased proton pumping and not increased proton leakage. Whilst this is alluring, an exploration of proton cycling in sacsin knockdown cells is required to address this hypothesis.

It will be of some interest to investigate whether the increased mitochondrial ROS observed in sacsin knockdown cells is the result of dysfunctional OXPHOS or visa versa. Overexpression of mitochondrial antioxidants such as mitochondrial superoxide dimutase in the sacsin knockdown cells or treatment with mitochondria targeted antioxidant like MitoQ may reduce ROS and improve function.

The results in this chapter demonstrates the mitochondrial bioenergetic profile and mitochondrial superoxide production in patient fibroblasts and in cells where sacsin has been reduced. Further discussions regarding the implications of these findings will continue in the subsequent chapter.

Chapter 7

Discussions

This thesis set out to explore sacsin's role in the regulation of mitochondrial dynamics and thus further understand the molecular pathology of ARSACS. Morphometric analysis established that an overly interconnected mitochondrial network is a phenotype in Non-Quebec ARSACS patients. This was consistent with a similar phenotype observed in fibroblasts from patients with the common Canadian mutation (Girard et al., 2012). Furthermore, this study went on to show that a loss of sacsin directly impacted the mitochondrial fission machinery, potentially explaining the mitochondrial morphology phenotype. Expanding on the work published by our group along with our collaborators, my PhD supports sacsin's involvement in the recruitment of Drp1 to the mitochondria and further describes the effect of loss of sacsin on mitochondrial function.

To date, four mammalian mitochondrial fission accessory proteins (MiD49, MiD51, Mff and hFis1) have been identified and characterised. Loss of function of these proteins results in cells having a mitochondrial phenotype similar to that described in ARSACS patients and sacsin knockdown fibroblasts (see chapters 3 of this thesis) (Table 7. 2) (Palmer et al., 2011b, Gandre-Babbe and van der Bliek, 2008, Palmer et al., 2013, Otera et al., 2010, Koch et al., 2005). Loss of function of Mff and MiD 49/51 reportedly leads to a more extreme mitochondrial network phenotype than loss of hFis 1 alone (Table 7.) (Losón et al., 2013, Gandre-Babbe and van der Bliek, 2008). It has been suggested that the more moderate phenotype observed in hFis1 knockdown cells may be due to this protein being dispensable in the fission process implying that the other proteins are therefore more essential (Otera et al., 2010, Losón et al., 2013). Moreover, it is suggested that the relative severity of the mitochondrial phenotype and significance of these proteins in regulating fission can be largely due to the pathway(s) (e.g. apoptosis and mitophagy) mostly affected by its loss of function (Losón et al., 2013, Bui and Shaw, 2013). The severity of the mitochondrial phenotype in SACS and patient cells shown in chapter 3 are more akin to that observed in Mff and MiD49/51 knockdown cells than that observed in hFis 1 knockdown cells. This suggests that sacsin too is essential for the normal regulation of mitochondrial dynamics in neurons.

Mutation Status	Mitochondrial Morphology	Drp1 Localisation to mitochondria and Recruitment
Control	Mixed Tubular Phenotype	Average Drp1 foci per µm of mitochondria was 0.84 ± 0.028 Drp1 foci per µm of mitochondria. Which significantly increased after treatment with CCCP.
2094-2 A>G / Q4054*	Moderate/severe phenotype Fused, interconnected mitochondria with Mixture of Collapsed and Tubular Phenotype (*Increased mitochondrial volume)*	Significant less Drp1 foci per µm of mitochondria than control. No significant change after inducing mitochondrial fission.
K1715* / R4331Q	Moderate/severe phenotype Fused, interconnected mitochondria with Collapsed Phenotype (most severe) (*Increased mitochondrial volume)*	Significant less Drp1 foci per µm of mitochondria than control. No significant change after inducing mitochondrial fission.
R2002fs / Q4054*	Moderate/severe phenotype Fused, interconnected mitochondria with Collapsed Phenotype (*Increased mitochondrial volume)*	Significant less Drp1 foci per µm of mitochondria than control. No significant change after inducing mitochondrial fission.
2801delQ	Collapsed Phenotype (*Increased mitochondrial volume)*	Significant less Drp1 foci per µm of mitochondria than control. No significant change after inducing mitochondrial fission.

.Table 7. 1 Summary of Results and phenotypes measure/observed in ARSACS patient

Mutation Status	MitoSOX	Mitochondrial Function
Control	Average mean intensity – 235.53±8.66 AU	"Normal"
2094-2 A>G / Q4054*	Increased Average mean intensity 296.17±12.44 AU. Indicating increased Superoxide Levels	Decreased: Basal Respiration, Proton Leak, ATP production, Maximum Respiration, Spare capacity.
K1715* / R4331Q	Increased Average mean intensity 418.37±14.99 AU Indicating increased Superoxide Levels	Decreased: Basal Respiration, Proton Leak, ATP production, Maximum Respiration, Spare capacity.
R2002fs / Q4054*	Increased Average mean intensity 436.69±23.33 AU Indicating increased Superoxide Levels	Decreased: Basal Respiration, Proton Leak, ATP production, Maximum Respiration, Spare capacity.
2801delQ	Increased Average mean intensity 300.35±20.49 AU Indicating increased Superoxide Levels	Decreased: Basal Respiration, Proton Leak, ATP production, Maximum Respiration, Spare capacity. This patient has the most severe phenotype and has an increase in glycolytic capacity and glycolytic reserve.

Table 7. 2 continued, Summary of Results and phenotypes measure/observed in ARSACS patient

Protein	Reduction of Protein by RNAi		
	Mitochondrial Phenotype	**Drp1 recruitment**	**Reference**
Drp1	**Severe phenotype** Fused networks, showing both hyperfused and collapsed mitochondrial networks.	No recruitment of Drp1 to the mitochondria.	(Smirnova et al., 2001, Gandre-Babbe and van der Bliek, 2008)
Mff	**Moderate/severe phenotype** Fused mitochondrial phenotype with increased branching of the mitochondrial network.	Reduced recruitment of Drp1 to the mitochondria.	(Gandre-Babbe and van der Bliek, 2008)
MiD49/51	**Moderate/severe phenotype** Fused mitochondrial phenotype with collapsed/irregular distribution of the network.	Reduced recruitment of Drp1 to the mitochondria.	(Palmer et al., 2011b, Losón et al., 2013)
hFis1	**Mild/moderate phenotype** Elongation of mitochondria with some increased branching observed.	Slight reduction of recruitment of Drp1 to the mitochondria.	(Koch et al., 2005, Losón et al., 2013)
Sacsin	Moderate/severe phenotype Fused, interconnected mitochondria with a more compact mitochondrial network.	Reduced recruitment of Drp1 to the mitochondria.	(Girard et al., 2012),This thesis.

Table 7. 2 Summary of mitochondrial phenotypes observed in published mitochondrial fission accessory proteins and sacsin.

Data presented in chapter 4 suggests the effect of sacsin loss on mitochondrial network morphology is through impaired recruitment of Drp1 to the mitochondria. This impairment was observed both in patients and in fibroblasts with reduced levels of sacsin. The regulation of Drp1 recruitment to the mitochondria is the canonical function of accessory proteins MiD49, MiD51 and Mff (Losón et al., 2013, Palmer et al., 2013, Gandre-Babbe and van der Bliek, 2008). Reduction of these proteins by RNAi in MEFs led to a reduction in Drp1 recruitment. The findings obtained in sacsin knockdown and patient cells give similar results to studies on loss of function of mitochondrial accessory proteins, Mff and MiD49/51. This suggests that sacsin may function in the same pathway as these proteins.

During mitochondrial fragmentation, several processes including mitochondrial constriction, Drp1 recruitment, assembly of a scission complex, scission and subsequent dissasembly of the complex must occur. The endoplasmic reticulum has been postulated to initiate the fission process by constricting mitochondria. This process was suggested to occur prior to Drp1 sequestration (Friedman et al., 2011). It was therefore important to estabish whether the decrease in Drp1 recruitment observed in my experiments, was a consequent of regulation of the protein or merely a downstream occurrence. As there was no observable difference in the number of contacts between mitochondria and the endoplasmic reticulm, it would appear that sacsin's involvement in mitochondrial fission is downstream of the endoplasmic reticulum.

Sacsin, like Fis1 and Mff, seems also to be involved in the regulation of peroxisome dynamics. However, the peroxisome phenotype observed in SACS and patient fibroblasts was distinct from that found in patient fibroblasts harbouring Drp1 mutation or cells with reduced levels of Fis1 or Mff. Knockdown of Drp1 or these accessory proteins led to an elongated peroxisome phenotype and a reduction in the number of peroxisomes (Palmer et al., 2013, Gandre-Babbe and van der Bliek, 2008, Waterham et al., 2007). Conversley, MiD 49/51 proteins were not found to be targeted to the peroxisome and while a loss of MiD proteins had no effect of peroxisome morphology, overexpression of the proteins led to an increase in peroxisome length

and a decrease in peroxisome number (Palmer et al., 2013). This was attributted to the proposed mechanism of MiD function in which Drp1 is inactivated by phosphorylation at serine resiude 637 and the inactive form is recruited to proposed sites of fisson. This therefore impairs peroxisome dynamics and results in the elongated morphology observed (Palmer et al., 2013). From these results, MiD 49/51 were shown to be primarily involved in mitochondrial fission. Loss of sacsin did not result in peroxisomes having an elongated phenotype. However, a reduction in the number of peroxisomes was oberved in patient and sacsin knockdown fibroblasts. Moreover a reduction in the total cellular peroxisome volume was evident in *SACS* and patient cells. Further investigation is required to asertain whether this change in the number of peroxisomes is directly linked to sacsin modulating Drp1 activity.

Mitochondria associated Drp1 foci are smaller in sacsin knockdown and ARSACS patient fibroblasts when compared to controls. This finding could suggest that sacsin has a role in the stabilization/assembly of the Drp1 complex. Similarly, loss of Mff and/or Fis1 led to a decrease in the size and intensity of Drp1 foci (Losón et al., 2013). The mitochondrial Drp1 foci in Fis1, Mff and Fis1-Mff null MEFs were ~ 30%, ~50% and ~70% smaller than Drp1 foci measured in wild type. Likewise, the mitochondrial Drp1 foci in Fis1, Mff and Fis1-Mff null MEFs had 30%, ~50% and ~70% less fluorescence intensity than the foci in wild type cells (Losón et al., 2013). In comparison, the diameter of the mitochondrial Drp1 foci in sacsin knockdown fibroblasts and in patient K1715*/R4331Q were 11.5% and 17.5% respectively, smaller than Drp1 foci in the controls. Moreover the mitochondrial Drp1 foci in cells had 20% and 14% less fluorescence intensity than the mitochondrial Drp1 foci in the controls. The magnitude of percentage difference in Drp1 foci size and intensity observed in sacsin knockdown and patient fibroblasts were lower than those observed in Fis1, Mff and Fis1-Mff null MEFs. A possible explanation for this is that sacsin may not be as vital as Fis1 or Mff in the stabilisation/assembly of the Drp1 oligomers. However, it is important to bear in mind that various factors such as different cell types and methods used in my work and in studies by Losòn et al 2013 and Palmer et al 2013, can also account for this apparent difference in magnitude. Importantly, the decrease in intensity and diameter

of Drp1 foci in patients and sacsin knockdown cells is in accordance with the Losòn et al study. Summarily, loss of sacsin resulted in a decrease of recruitment and/assembly of the Drp 1 scission complex, correlating with a decrease in mitochondrial fission.

Although reduced levels of Mff and MiD49/51 in HeLa and COS-7 cells affected mitochondrial morphology, fission was not completely obliterated. This appears to also be the case in *SACS* knockdown and patient fibroblasts as the cells are viable and mitochondrial function is only partially impaired. This highlights the complexity of the fission mechanism. One explanation for the impaired, but not complete ablation of fission, is that Mff, hFis 1, MiD 49 and MiD 51 have a degree of functional redundancy and are capable of functioning independently of one another (Losón et al., 2013, Palmer et al., 2013). Therefore loss of one of these proteins would still allow for mitochondrial fission, all be it that regulation of the process is not optimal. This is consistent with our observations in ARSACS patient cells and cells where levels of sacsin had been reduced by RNAi.

We speculate that the mitochondrial dysfunction we observed in sacsin null cells (chapter 6) is downstream of the disequilibrium of mitochondrial network dynamics reported in this thesis (chapter 3). Bioenergetic decline observed in cells with an imbalance in mitochondrial dynamics has been hypothesised to be due to a number of reasons, including mitochondrial quality control. Increased fusion influences mitochondrial biogenesis and mitochondrial clearance and can result in the accumulation of toxins, which in turn damages the mitochondria (Twig et al., 2008a, Twig et al., 2008b, Benard, 2011). Mitochondrial network morphology and dynamics change in response to the energy state of the cell as well as to mitochondrial energy production. In addition, mitochondrial energy production is reliant on mitochondrial network morphology (Benard et al., 2007b, Benard, 2011). These two process are not mutually exclusive and in fact have been described as being bidirectional (Benard, 2011). Therefore altered mitochondrial dynamics also disrupts this quality control cycle and can hamper the energy production of a mitochondrion.

There is still some way to go in understanding the complexity of mitochondrial fission in mammalian cells. Although capable of independent function, a reduction in more than one accessory protein increases the severity of the mitochondrial phenotype as was the case in Mff and Fis1 double knockdown mouse embryonic fibroblasts (Losón et al., 2013). Further work needs to be conducted in order to examine whether loss of sacsin has an effect on other proteins regulating mitochondrial dynamics.

New structural reports on MiD51 have given more insight into the regulation of this protein and its subsequent role in mitochondrial fission. These studies show that MiD51 belongs to the nucleotidyltransferase fold superfamily of proteins (Richter et al., 2014, Losón et al., 2014). This is of interest in the context of sacsin as it processes a HEPN domain and HEPN domains are hypothesised to form a complex with adjacent nucleotidyltransferase and facilitate nucleotide binding (Grynberg et al., 2003, Kozlov et al., 2011).

To recap, a cleft nucleotidyltransferases bind nucleotide trisphophates catalysing the polymerisation of the nucleic acids (Kristiansen et al., 2011, Kuchta et al., 2009). Interestingly, as MiD51 binds to GDP and ADP instead of nucleotide trisphophates, it was suggested that it may not support nucleotide hydrolysis and transfer (Richter et al., 2014). In addition to the partial conservation of the nucleotidyltransferase binding domain, MiD51 crystallised as a dimer (Losón et al., 2014). Sacsin's HEPN domain is also suggested to form a dimer and was found to bind ATP and GTP with low affinity, a process thought to be important for sacsin function (Kozlov et al., 2011). Taking the findings of these studies together with the information on sacsin structure, it is possible that sacsin may have a further role in the fission complex and may be associated with the MiD49/51 proteins.

Important to mitochondrial fission, severe disruption of nucleotidyltransferase domain reduced Drp1 recruitment (Richter et al., 2014, Losón et al., 2014). Sedimentation experiments using recombinant Drp1 and recombinant MiD51 showed that MiD51 was capable of basally promoting the assembly of Drp1 oligomers which was enhanced upon binding of ADP to the protein (Losón et al., 2014, Richter et al., 2014). These

findings raise the question as to whether sacsin may interact with MiD51 and thereby also have a role in MiD51 mediated regulation of Drp1. Further investigation is required to examine; 1. whether there is an interaction between sacsin and MiD51 and 2. the effect of a loss of sacsin function on the localisation and regulation or expression of MiD proteins.

Loss of sacsin does not prevent fission completely, hence it is possible that there may be an upregulation of another accessory protein which enables fission to occur. Futhermore the increased fused state of the mitochondria may also affect the regulation and or activation of Mfn 1/2 and OPA 1 proteins. The effect of reduced Drp1 recruitment on the regulation and expression of these proteins should also be looked at.

The interconnected, fused mitochondrial phenotype seems to be common to sacsin null cells, however the severity of the phenotype appears to vary between our patients. This may be due to the specific SACS mutations harboured by the patient. The characterisation of mitochondrial morphology from more ARSACS patients with a range of different mutations may allow for the establishment of a genotype-cellular phenotype correlation. Results from this genotype-cellular phenotype correlation could also be combined with clinical phenotype data to further develop our understanding of ARSACS. Well defined genotype-phenotype correlation data may also be useful in the development of strategies for screening of potential therapeutic reagents.

Such analysis would need a high throughput, standardised method of scoring the mitochondria phenotypes. This could be based on methods developed for this thesis, along with more sophisticated computer algorithms. This throughput should be capable of attributing a numerical score to different categories of mitochondrial network morphology. Westrate et al recently developed a new way of classifying shape and dynamics through computer algorithm and high resolution imagery. Their approach used geometeric parameters such as perimeter and solidity to place mitochondria into a fused, branched or fragmented classification. Fused or branched

mitochondria have a higher perimeter because of the change in shape and would therefore also have a lower solidity than smaller compact mitochondria. In this algorithm solidity measures the amount of pixels contained within a defined region, selected by the program. This is then given a score between 0-1, where 0 represents a more irregular shaped mitochondrion and 1 represents a more compact mitochondrion (Westrate et al., 2014).

Mitochondrial dysfunction is a feature of multiple neurodegenerative diseases. For example reduced mitochondrial function and increased cell death have been described in primary neurons from a mouse model of Parkinson's disease (Wood-Kaczmar et al., 2008). Wood-Kaczamar et al went on to validate this finding by creating a PINK1 loss of function model in human neuronal stem cells which were capable of differentiating into functional dopaminergic neurons. A significant increase in mitochondrial ROS production and cell death were observed in these cells (Wood-Kaczmar et al., 2008). Mitochondrial dysfunction was also found to be a feature of Huntington's. Impaired mitochondrial respiration, ATP production and increased mitochondrial superoxide were recorded in the clonal striatal cells from the embryos of a Huntington's disease mouse (Milakovic and Johnson, 2005, Siddiqui et al., 2012). It is important to note that Parkinson's, Alzheimer's and Huntington's disease are mostly late age of onset disorders which have similar features, while ARSACS has an early age of onset and lacks the accumulation of misfolded proteins which are characteristic of the aforementioned disorders. These studies however do highlight the importance of the regulation of mitochondrial dynamics and function in neuronal survival and possible disease progression, which is a vital feature of ARSACS. Taking these studies into account, the brain's high demand for energy makes it particularly sensitive to reduced ATP production and cellular damage resulting in cell death. Potentially the decrease in ATP and increased ROS production in ARSACS patients reported in the previous chapter likely contributes to the pathogenesis of ARSACS including a loss of Purkinje cells and dendrites. In relation to the modulation of Drp1, reduced levels of Drp1 protein or over expression of dominant negative Drp1 resulted in a significant increase in cell death of cultured cortical neurons (Uo et al., 2009). Loss of sacsin may also be

linked to programmed cell death through the disruption of mitochondrial dynamics and hence function. However further examination on the cell viability will be required before any such conclusions can be made.

Rescuing the mitochondrial phenotype of ARSACS and reducing ROS production represents a potential therapeutic target for ARSACS. We have been unable to heterologously express sacsin in cells, most likely due to its large size. Hence rescue of the sacsin null phenotype by overexpression has not been possible the cellular models, therefore ultimately, other methods will have to be employed. Precision editng techniques such as transcription activator-like effector nuleases (TALEN) and the clustered regularly interspaced short palindromic repeats/Cas9 systems (CRISPR/Cas9) have been sucessful used to correct genetic mutations in primary fibroblasts of Epidermolysis Bullosa and Duchen's Muscular Dystrophy patients (Ousterout et al., 2013, Osborn et al., 2013). The cells were either reprogrammed into inducible pluripotent cells or into myoblasts (Ousterout et al., 2013, Osborn et al., 2013). Both systems have been shown to be very effective and have distinct mechansims of action. TALEN induces site specific double stranded break in DNA. Following this, an exogenous donor template is used in order for homology directed repair to occur (Ding et al., 2013). In the CRISPR /Cas 9 RNA guided system, Cas9, a bacterial nuclease, induces a break in double stranded DNA. In this instance a RNA guide is also used to ensure site speicificity. The cleaved DNA strands can be repaired by either nonhomologous end joining or by oligo-mediated homology repair (Gaj et al., 2013, Cong et al., 2013). Such approaches are likely to prove to be good tools when exploring sacsin function as they would allow us to generate isogenic control lines for the ARSACS patient fibroblasts.

The overexpression of Drp1 signficantly rescued the perinuclear mitochondrial network observed in Alzheimers fibroblasts and the overexpression of Mff in Fis 1 knockdown cells rescued the mitochondrial phenotype observed in those cells (Losón et al., 2013, Wang et al., 2008). Markedly enhanced recruitment of Drp1 was observed when MiD proteins were overexpressed in Mff/Fis1 knockdown cells (Losón et al., 2013). Therefore the overexpression of Drp1 or a mitochondrial fission accessory

protein in the sacsin knockdown and patient fibroblasts could lead to an increase in mitochondrial fragmentation and a decrease in mitochondrial dysfunction.

Mitochondrial ATP production has been used to assess mitochondrial function in our ARSACS cell models. However mitochondria are also involved in Calcium (Ca^{2+}) homeostasis (Duchen, 2004a, Chen et al., 2007) it would also be of interest to explore calcium regulation in ARSACS. As mentioned in Chapter 5, the ER is the major source of Ca^{2+} and Ca^{2+} signalling of the ER and mitochondria is facilitated by mitochondrial-ER contacts (MAMs) (Rizzuto et al., 2004, de Brito and Scorrano, 2008).

Calcium is very important in regulating mitochondrial function and energy production by stimulating OXPHOS and regulating many of the enzymes involved in the citric acid cycle, glycolysis and the ETC complexes (McCormack et al., 1990, Brookes et al., 2004, Duchen, 2004a, Rizzuto et al., 2004). An increase in the uptake of Ca^{2+} results in an upregulation of enzymes involved in OXPHOS and ultimately an increase in ATP production (Jouaville et al., 1995). Likewise a decrease in ATP production was found to be accompanied by an intracellular imbalance of ions like Ca^{2+}, an increase in ROS and cell death (Duchen, 2004a, Brookes et al., 2004, Chen and Chan, 2009).

Futhermore calcium overload has been observed in disorders such as Alzheimer's and Parkinson's (Gibson et al., 2010). Mammalian neurons, deficient in PINK1 were found to have an increase in ROS production, calcium overload and decreased mitochondrial function (Gandhi et al., 2009) Alzheimer's preslin-1 mutations in PC12 cells were also shown to disrupt calcium homeostaisis leading to an increase in Ca^{2+} resulting in an increase in amyloid formation and ultimately cell death (Guo et al., 1996). Conversely, decreased calcium uptake has been observed in fibroblasts from patients with Alzheimer's (Kumar et al., 1994)

Investigating the calcium homeostasis in patient and sacsin knockdown fibroblasts is required to examine the Ca^{2+} status of ARSACS patient cells. Fluorescent indicators of Ca^{2+} such as voltage sensitive dye rhodamine 123 (Rh123) and fura-2 or proteins like Cameleon, will allow for the quantification of Ca^{2+}using confocal imaging and analysis software or by flow cytometery (Kovács et al., 2005, Gandhi et al., 2009, Whitaker,

2010). These experiments will assist in further defining the role of the ER in ARSACS as well as provide a calcium profile and more understanding of mitochondrial function in this disorder.

In conclusion, this thesis has shown that sacsin is nessecary for the regulation of mitochondrial dynamics. We propose that this is through the regulation and recruitment of Drp1 from the cytosol to prospective sites of fission (Figure 7. 1), making sacsin one of the accessory proteins involved in mitochondrial fission. Futhermore we provided evidence that a loss of sacsin results in mitochondrial dysfunction and an increase in the reactive oxygen species. We postulate that this dysfunction will contribute to the cellular pathology of ARSACS.

Proposed Model of Sacsin Function in Mitochondrial Dynamics.

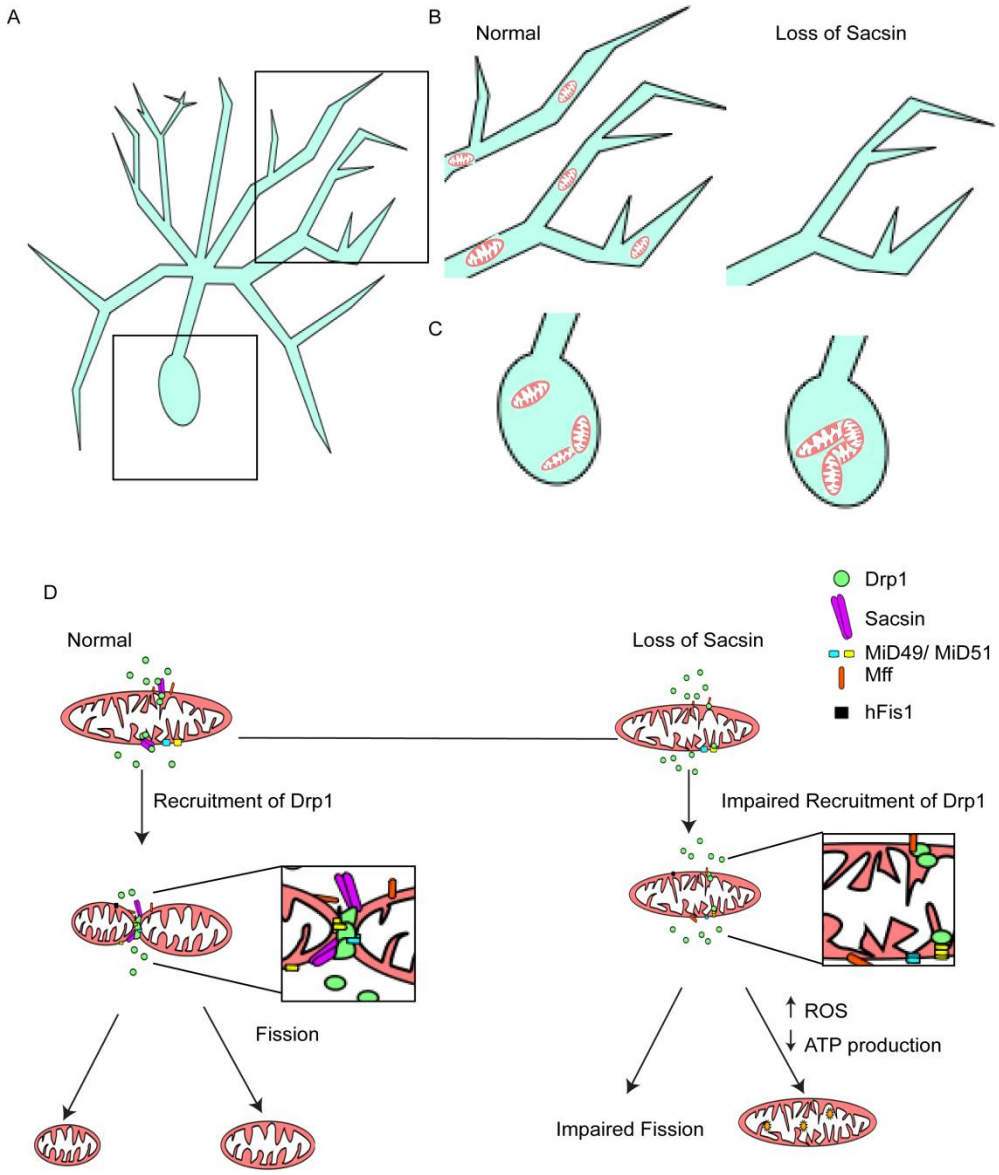

Figure 7. 1 Sacsin functions as a mitochondrial fission accessory protein.

A) Schematic of Purkinje cell. B-C) Loss of sacsin leads to accumulation of mitochondria in the cell body due to reduced fission. This alters the distribution of mitochondria and resulting in loss of dendrites. D) Sacsin is involved in the regulation and recruitment of Drp1 from the cytosol to prospective sites of fission. Loss of sacsin results in a decrease of Drp1 foci recruited to the mitochondria and therefore leads to impaired mitochondrial fission and mitochondrial dysfunction.

References

ALBIN, R. L. 2003. Dominant ataxias and Friedreich ataxia: an update. *Curr Opin Neurol,* 16**,** 507-14.

ANDERSON, J. F., SILLER, E. & BARRAL, J. M. 2010. The Sacsin Repeating Region (SRR): A Novel Hsp90-Related Supra-Domain Associated with Neurodegeneration. *Journal of Molecular Biology,* 400**,** 665-674.

ANDERSON, J. F., SILLER, E. & BARRAL, J. M. 2011. The Neurodegenerative-Disease-Related Protein Sacsin Is a Molecular Chaperone. *Journal of Molecular Biology,* 411**,** 870-880.

ANDRES-MATEOS, E., PERIER, C., ZHANG, L., BLANCHARD-FILLION, B., GRECO, T. M., THOMAS, B., KO, H. S., SASAKI, M., ISCHIROPOULOS, H., PRZEDBORSKI, S., DAWSON, T. M. & DAWSON, V. L. 2007. DJ-1 gene deletion reveals that DJ-1 is an atypical peroxiredoxin-like peroxidase. *Proc Natl Acad Sci U S A,* 104**,** 14807-12.

ANESI, L., DE GEMMIS, P., PANDOLFO, M. & HLADNIK, U. 2011. Two novel homozygous SACS mutations in unrelated patients including the first reported case of paternal UPD as an etiologic cause of ARSACS. *J Mol Neurosci,* 43**,** 346-9.

ANHEIM, M., FLEURY, M., MONGA, B., LAUGEL, V., CHAIGNE, D., RODIER, G., GINGLINGER, E., BOULAY, C., COURTOIS, S., DROUOT, N., FRITSCH, M., DELAUNOY, J. P., STOPPA-LYONNET, D., TRANCHANT, C. & KOENIG, M. 2010. Epidemiological, clinical, paraclinical and molecular study of a cohort of 102 patients affected with autosomal recessive progressive cerebellar ataxia from Alsace, Eastern France: implications for clinical management. *Neurogenetics,* 11**,** 1-12.

AREA-GOMEZ, E., DEL CARMEN LARA CASTILLO, M., TAMBINI, M. D., GUARDIA-LAGUARTA, C., DE GROOF, A. J., MADRA, M., IKENOUCHI, J., UMEDA, M., BIRD, T. D., STURLEY, S. L. & SCHON, E. A. 2012. Upregulated function of mitochondria-associated ER membranes in Alzheimer disease. *EMBO J,* 31**,** 4106-23.

ARTHUR, C. R., MORTON, S. L., DUNHAM, L. D., KEENEY, P. M. & BENNETT, J. P. 2009. Parkinson's disease brain mitochondria have impaired respirasome assembly, age-related increases in distribution of oxidative damage to mtDNA and no differences in heteroplasmic mtDNA mutation abundance. *Mol Neurodegener,* 4**,** 37.

ATTARDI, G. & SCHATZ, G. 1988. Biogenesis of mitochondria. *Annu Rev Cell Biol,* 4**,** 289-333.

BABCOCK, M., DE SILVA, D., OAKS, R., DAVIS-KAPLAN, S., JIRALERSPONG, S., MONTERMINI, L., PANDOLFO, M. & KAPLAN, J. 1997. Regulation of mitochondrial iron accumulation by Yfh1p, a putative homolog of frataxin. *Science,* 276**,** 1709-12.

BAE, Y. S., KANG, S. W., SEO, M. S., BAINES, I. C., TEKLE, E., CHOCK, P. B. & RHEE, S. G. 1997. Epidermal growth factor (EGF)-induced generation of hydrogen peroxide. Role in EGF receptor-mediated tyrosine phosphorylation. *J Biol Chem,* 272**,** 217-21.

BAETS, J., DECONINCK, T., SMETS, K., GOOSSENS, D., VAN DEN BERGH, P., DAHAN, K., SCHMEDDING, E., SANTENS, P., RASIC, V. M., VAN DAMME, P., ROBBERECHT, W., DE MEIRLEIR, L., MICHIELSENS, B., DEL-FAVERO, J., JORDANOVA, A. & DE JONGHE, P. 2010. Mutations in SACS cause atypical and late-onset forms of ARSACS. *Neurology,* 75**,** 1181-8.

BALABAN, R. S., NEMOTO, S. & FINKEL, T. 2005. Mitochondria, oxidants, and aging. *Cell,* 120**,** 483-95.

BALDWIN, J. E. & KREBS, H. 1981. The evolution of metabolic cycles. *Nature,* 291**,** 381-2.

BALL, E. H. & SINGER, S. J. 1982. Mitochondria are associated with microtubules and not with intermediate filaments in cultured fibroblasts. *Proc Natl Acad Sci U S A,* 79**,** 123-6.

BALOH, R. H., SCHMIDT, R. E., PESTRONK, A. & MILBRANDT, J. 2007. Altered axonal mitochondrial transport in the pathogenesis of Charcot-Marie-Tooth disease from mitofusin 2 mutations. *J Neurosci,* 27**,** 422-30.

BEACH, A., BURSTEIN, M. T., RICHARD, V. R., LEONOV, A., LEVY, S. & TITORENKO, V. I. 2012. Integration of peroxisomes into an endomembrane system that governs cellular aging. *Front Physiol,* 3**,** 283.

BEASLEY, S. A., SAFADI, S. S., BARBER, K. R. & SHAW, G. S. 2012. Solution structure of the E3 ligase HOIL-1 Ubl domain. *Protein Sci,* 21**,** 1085-92.

BENARD, G., BELLANCE, N., JAMES, D., PARRONE, P., FERNANDEZ, H., LETELLIER, T. & ROSSIGNOL, R. 2007a. Mitochondrial bioenergetics and structural network organization. *J Cell Sci,* 120**,** 838-48.

BENARD, G., BELLANCE, N., JAMES, D., PARRONE, P., FERNANDEZ, H., LETELLIER, T. & ROSSIGNOL, R. 2007b. Mitochondrial bioenergetics and structural network organization. *Journal of Cell Science,* 120**,** 838-848.

BENARD, G. B., NADEGE. JOSE, CAROLINE. ROSSIGNOL, RODRIGUE. 2011. Relationships Between Mitochondrial Dynamics and Bioenergetics - Springer. *In:* LU, B. (ed.) *Mitochondrial Dynamics and Neurodegeneration.* Springer Netherlands.

BERCIANO, J., INFANTE, J., GARCÍA, A., POLO, J. M., VOLPINI, V. & COMBARROS, O. 2005. Very late-onset Friedreich's ataxia with minimal GAA1 expansion mimicking multiple system atrophy of cerebellar type. *Mov Disord,* 20**,** 1643-5.

BERGO, M. O., GAVINO, B. J., STEENBERGEN, R., STURBOIS, B., PARLOW, A. F., SANAN, D. A., SKARNES, W. C., VANCE, J. E. & YOUNG, S. G. 2002. Defining the importance of phosphatidylserine synthase 2 in mice. *J Biol Chem,* 277**,** 47701-8.

BERMAN, S. B., PINEDA, F. J. & HARDWICK, J. M. 2008. Mitochondrial fission and fusion dynamics: the long and short of it. *Cell Death and Differentiation,* 15**,** 1147-1152.

BERRY-KRAVIS, E., ABRAMS, L., COFFEY, S. M., HALL, D. A., GRECO, C., GANE, L. W., GRIGSBY, J., BOURGEOIS, J. A., FINUCANE, B., JACQUEMONT, S., BRUNBERG, J. A., ZHANG, L., LIN, J., TASSONE, F., HAGERMAN, P. J., HAGERMAN, R. J. & LEEHEY, M. A. 2007. Fragile X-associated tremor/ataxia syndrome: clinical features, genetics, and testing guidelines. *Mov Disord,* 22**,** 2018-30, quiz 2140.

BHAR, D., KARREN, M. A., BABST, M. & SHAW, J. M. 2006. Dimeric Dnm1-G385D interacts with Mdv1 on mitochondria and can be stimulated to assemble into fission complexes containing Mdv1 and Fis1. *J Biol Chem,* 281**,** 17312-20.

BIRD, T. 2014. *Hereditary Ataxia Overview* [Online]. GeneReviews® [Internet]. Seattle (WA): University of Washington, Seattle; 1993-2015.: Available from: http://www.ncbi.nlm.nih.gov/books/NBK1138/. [Accessed 28th December 2014 2014].

BLOCH-ZUPAN, A., JAMET, X., ETARD, C., LAUGEL, V., MULLER, J., GEOFFROY, V., STRAUSS, J. P., PELLETIER, V., MARION, V., POCH, O., STRAHLE, U., STOETZEL, C. & DOLLFUS, H. 2011. Homozygosity mapping and candidate prioritization identify mutations, missed by whole-exome sequencing, in SMOC2, causing major dental developmental defects. *Am J Hum Genet,* 89**,** 773-81.

BOLINCHES-AMORÓS, A., MOLLÁ, B., PLA-MARTÍN, D., PALAU, F. & GONZÁLEZ-CABO, P. 2014. Mitochondrial dysfunction induced by frataxin deficiency is associated with cellular senescence and abnormal calcium metabolism. *Front Cell Neurosci,* 8**,** 124.

BONDA, D. J., SMITH, M. A., PERRY, G., LEE, H. G., WANG, X. & ZHU, X. 2011. The mitochondrial dynamics of Alzheimer's disease and Parkinson's disease offer important opportunities for therapeutic intervention. *Curr Pharm Des,* 17**,** 3374-80.

BOUCHARD, J. P. 1991. ***Recessive spastic ataxia of Charlevoix-Saguenay***, *Amsterdam: Elsevier*.

BOUCHARD, J. P., BARBEAU, A., BOUCHARD, R. & BOUCHARD, R. W. 1978. Autosomal recessive spastic ataxia of Charlevoix-Saguenay. *Can J Neurol Sci,* 5**,** 61-9.

BOUCHARD, J. P., BARBEAU, A., BOUCHARD, R. & BOUCHARD, R. W. 1979a. Electromyography and nerve conduction studies in Friedreich's ataxia and autosomal recessive spastic ataxia of Charlevoix-Saguenay (ARSACS). *Can J Neurol Sci,* 6**,** 185-9.

BOUCHARD, J. P., RICHTER, A., MATHIEU, J., BRUNET, D., HUDSON, T. J., MORGAN, K. & MELANÇON, S. B. 1998. Autosomal recessive spastic ataxia of Charlevoix-Saguenay. *Neuromuscul Disord,* 8**,** 474-9.

BOUCHARD, R. W., BOUCHARD, J. P., BOUCHARD, R. & BARBEAU, A. 1979b. Electroencephalographic findings in Friedreich's ataxia and autosomal recessive spastic ataxia of Charlevoix-Saguenay (ARSACS). *Can J Neurol Sci,* 6**,** 191-4.

BOUHLAL, Y., AMOURI, R., EL EUCH-FAYECHE, G. & HENTATI, F. 2011. Autosomal recessive spastic ataxia of Charlevoix-Saguenay: An overview. *Parkinsonism Relat Disord*.

BOUHLAL, Y., EL EUCH-FAYECHE, G., HENTATI, F. & AMOURI, R. 2009. A novel SACS gene mutation in a Tunisian family. *J Mol Neurosci,* 39**,** 333-6.

BOUHLAL, Y., ZOUARI, M., KEFI, M., BEN HAMIDA, C., HENTATI, F. & AMOURI, R. 2008. Autosomal recessive ataxia caused by three distinct gene defects in a single consanguineous family. *J Neurogenet,* 22**,** 139-48.

BOVERIS, A., OSHINO, N. & CHANCE, B. 1972. The cellular production of hydrogen peroxide. *Biochem J,* 128**,** 617-30.

BRADLEY, J. L., BLAKE, J. C., CHAMBERLAIN, S., THOMAS, P. K., COOPER, J. M. & SCHAPIRA, A. H. 2000. Clinical, biochemical and molecular genetic correlations in Friedreich's ataxia. *Hum Mol Genet,* 9**,** 275-82.

BRAND, M. D. 2000. Uncoupling to survive? The role of mitochondrial inefficiency in ageing. *Exp Gerontol,* 35**,** 811-20.

BRAND, M. D., AFFOURTIT, C., ESTEVES, T. C., GREEN, K., LAMBERT, A. J., MIWA, S., PAKAY, J. L. & PARKER, N. 2004. Mitochondrial superoxide: production, biological effects, and activation of uncoupling proteins. *Free Radic Biol Med,* 37**,** 755-67.

BRAND, M. D. & MURPHY, M. P. 1987. Control of electron flux through the respiratory chain in mitochondria and cells. *Biol Rev Camb Philos Soc,* 62**,** 141-93.

BRECKPOT, J., TAKIYAMA, Y., THIENPONT, B., VAN VOOREN, S., VERMEESCH, J. R., ORTIBUS, E. & DEVRIENDT, K. 2008. A novel genomic disorder: a deletion of the SACS gene leading to spastic ataxia of Charlevoix-Saguenay. *Eur J Hum Genet,* 16**,** 1050-4.

BROOKES, P. S., YOON, Y., ROBOTHAM, J. L., ANDERS, M. W. & SHEU, S. S. 2004. Calcium, ATP, and ROS: a mitochondrial love-hate triangle. *Am J Physiol Cell Physiol,* 287**,** C817-33.

BRUSSE, E., DE KONING, I., MAAT-KIEVIT, A., OOSTRA, B. A., HEUTINK, P. & VAN SWIETEN, J. C. 2006. Spinocerebellar ataxia associated with a mutation in the fibroblast growth factor 14 gene (SCA27): A new phenotype. *Mov Disord,* 21**,** 396-401.

BUI, H. T., KARREN, M. A., BHAR, D. & SHAW, J. M. 2012. A novel motif in the yeast mitochondrial dynamin Dnm1 is essential for adaptor binding and membrane recruitment. *J Cell Biol,* 199**,** 613-22.

BUI, H. T. & SHAW, J. M. 2013. Dynamin assembly strategies and adaptor proteins in mitochondrial fission. *Curr Biol,* 23**,** R891-9.

BULTEAU, A. L., O'NEILL, H. A., KENNEDY, M. C., IKEDA-SAITO, M., ISAYA, G. & SZWEDA, L. I. 2004. Frataxin acts as an iron chaperone protein to modulate mitochondrial aconitase activity. *Science,* 305**,** 242-5.

BURRIGHT, E. N., CLARK, H. B., SERVADIO, A., MATILLA, T., FEDDERSEN, R. M., YUNIS, W. S., DUVICK, L. A., ZOGHBI, H. Y. & ORR, H. T. 1995. SCA1 transgenic mice: a model for neurodegeneration caused by an expanded CAG trinucleotide repeat. *Cell,* 82**,** 937-48.

CALÌ, T., OTTOLINI, D. & BRINI, M. 2012. Mitochondrial Ca(2+) as a key regulator of mitochondrial activities. *Adv Exp Med Biol,* 942**,** 53-73.

CAMPUZANO, V., MONTERMINI, L., MOLTÒ, M. D., PIANESE, L., COSSÉE, M., CAVALCANTI, F., MONROS, E., RODIUS, F., DUCLOS, F., MONTICELLI, A., ZARA, F., CAÑIZARES, J.,

KOUTNIKOVA, H., BIDICHANDANI, S. I., GELLERA, C., BRICE, A., TROUILLAS, P., DE MICHELE, G., FILLA, A., DE FRUTOS, R., PALAU, F., PATEL, P. I., DI DONATO, S., MANDEL, J. L., COCOZZA, S., KOENIG, M. & PANDOLFO, M. 1996. Friedreich's ataxia: autosomal recessive disease caused by an intronic GAA triplet repeat expansion. *Science,* 271**,** 1423-7.

CEREGHETTI, G. M., COSTA, V. & SCORRANO, L. 2010. Inhibition of Drp1-dependent mitochondrial fragmentation and apoptosis by a polypeptide antagonist of calcineurin. *Cell Death and Differentiation,* 17**,** 1785-1794.

CEREGHETTI, G. M., STANGHERLIN, A., MARTINS DE BRITO, O., CHANG, C. R., BLACKSTONE, C., BERNARDI, P. & SCORRANO, L. 2008. Dephosphorylation by calcineurin regulates translocation of Drp1 to mitochondria. *Proc Natl Acad Sci U S A,* 105**,** 15803-8.

CERVENY, K. L., TAMURA, Y., ZHANG, Z., JENSEN, R. E. & SESAKI, H. 2007. Regulation of mitochondrial fusion and division. *Trends Cell Biol,* 17**,** 563-9.

CHANG, C.-R. & BLACKSTONE, C. 2010a. Dynamic regulation of mitochondrial fission through modification of the dynamin-related protein Drp1. *Annals of the New York Academy of Sciences,* 1201**,** 34-39.

CHANG, C. R. & BLACKSTONE, C. 2010b. Dynamic regulation of mitochondrial fission through modification of the dynamin-related protein Drp1. *Ann N Y Acad Sci,* 1201**,** 34-9.

CHARBONNEAU, H. & ROBERT, N. 1987. *The French origins of the Canadian population*

1608–1759, Toronto, University of Toronto Press.

CHEETHAM, M. E. & CAPLAN, A. J. 1998. Structure, function and evolution of DnaJ: conservation and adaptation of chaperone function. *Cell Stress Chaperones,* 3**,** 28-36.

CHEN, D. H., BRKANAC, Z., VERLINDE, C. L., TAN, X. J., BYLENOK, L., NOCHLIN, D., MATSUSHITA, M., LIPE, H., WOLFF, J., FERNANDEZ, M., CIMINO, P. J., BIRD, T. D. & RASKIND, W. H. 2003a. Missense mutations in the regulatory domain of PKC gamma: a new mechanism for dominant nonepisodic cerebellar ataxia. *Am J Hum Genet,* 72**,** 839-49.

CHEN, H. & CHAN, D. C. 2005. Emerging functions of mammalian mitochondrial fusion and fission. *Hum Mol Genet,* 14 Spec No. 2**,** R283-9.

CHEN, H. & CHAN, D. C. 2009. Mitochondrial dynamics-fusion, fission, movement, and mitophagy-in neurodegenerative diseases. *Human Molecular Genetics,* 18**,** R169-R176.

CHEN, H., DETMER, S. A., EWALD, A. J., GRIFFIN, E. E., FRASER, S. E. & CHAN, D. C. 2003b. Mitofusins Mfn1 and Mfn2 coordinately regulate mitochondrial fusion and are essential for embryonic development. *J Cell Biol,* 160**,** 189-200.

CHEN, H., MCCAFFERY, J. M. & CHAN, D. C. 2007. Mitochondrial fusion protects against neurodegeneration in the cerebellum. *Cell,* 130**,** 548-62.

CHEN, H., VERMULST, M., WANG, Y. E., CHOMYN, A., PROLLA, T. A., MCCAFFERY, J. M. & CHAN, D. C. 2010. Mitochondrial fusion is required for mtDNA stability in skeletal muscle and tolerance of mtDNA mutations. *Cell,* 141**,** 280-9.

CHEVILLE, N. F. 2013. Ultrastructural pathology and interorganelle cross talk in hepatotoxicity. *Toxicol Pathol,* 41**,** 210-26.

CHEVROLLIER, A., CASSEREAU, J., FERRÉ, M., ALBAN, J., DESQUIRET-DUMAS, V., GUEGUEN, N., AMATI-BONNEAU, P., PROCACCIO, V., BONNEAU, D. & REYNIER, P. 2012. Standardized mitochondrial analysis gives new insights into mitochondrial dynamics and OPA1 function. *Int J Biochem Cell Biol,* 44**,** 980-8.

CHO, B., CHOI, S. Y., CHO, H. M., KIM, H. J. & SUN, W. 2013. Physiological and Pathological Significance of Dynamin-Related Protein 1 (Drp1)-Dependent Mitochondrial Fission in the Nervous System. *Exp Neurobiol,* 22**,** 149-157.

CHO, D. H., NAKAMURA, T. & LIPTON, S. A. 2010. Mitochondrial dynamics in cell death and neurodegeneration. *Cell Mol Life Sci,* 67**,** 3435-47.

CHUN, H. H. & GATTI, R. A. 2004. Ataxia-telangiectasia, an evolving phenotype. *DNA Repair (Amst),* 3**,** 1187-96.

CIMINI, A., MORENO, S., D'AMELIO, M., CRISTIANO, L., D'ANGELO, B., FALONE, S., BENEDETTI, E., CARRARA, P., FANELLI, F., CECCONI, F., AMICARELLI, F. & CERÙ, M. P. 2009. Early biochemical and morphological modifications in the brain of a transgenic mouse model of Alzheimer's disease: a role for peroxisomes. *J Alzheimers Dis,* 18**,** 935-52.

CIPOLAT, S., MARTINS DE BRITO, O., DAL ZILIO, B. & SCORRANO, L. 2004. OPA1 requires mitofusin 1 to promote mitochondrial fusion. *Proc Natl Acad Sci U S A,* 101**,** 15927-32.

COLERI, E., KAYHANIAN, M., HARVEY, J. T., YANG, K. & BOONE, J. M. 2013. Clogging evaluation of open graded friction course pavements tested under rainfall and heavy vehicle simulators. *J Environ Manage,* 129**,** 164-72.

CONG, L., RAN, F. A., COX, D., LIN, S., BARRETTO, R., HABIB, N., HSU, P. D., WU, X., JIANG, W., MARRAFFINI, L. A. & ZHANG, F. 2013. Multiplex genome engineering using CRISPR/Cas systems. *Science,* 339**,** 819-23.

CONTI, E., FRANKS, N. P. & BRICK, P. 1996. Crystal structure of firefly luciferase throws light on a superfamily of adenylate-forming enzymes. *Structure,* 4**,** 287-98.

COSSÉE, M., DÜRR, A., SCHMITT, M., DAHL, N., TROUILLAS, P., ALLINSON, P., KOSTRZEWA, M., NIVELON-CHEVALLIER, A., GUSTAVSON, K. H., KOHLSCHÜTTER, A., MÜLLER, U., MANDEL, J. L., BRICE, A., KOENIG, M., CAVALCANTI, F., TAMMARO, A., DE MICHELE, G., FILLA, A., COCOZZA, S., LABUDA, M., MONTERMINI, L., POIRIER, J. & PANDOLFO, M. 1999. Friedreich's ataxia: point mutations and clinical presentation of compound heterozygotes. *Ann Neurol,* 45**,** 200-6.

COSTES, S. V., DAELEMANS, D., CHO, E. H., DOBBIN, Z., PAVLAKIS, G. & LOCKETT, S. 2004. Automatic and quantitative measurement of protein-protein colocalization in live cells. *Biophys J,* 86**,** 3993-4003.

CRIBBS, J. T. & STRACK, S. 2007. Reversible phosphorylation of Drp1 by cyclic AMP-dependent protein kinase and calcineurin regulates mitochondrial fission and cell death. *EMBO Rep,* 8**,** 939-44.

CRISCUOLO, C., BANFI, S., ORIO, M., GASPARINI, P., MONTICELLI, A., SCARANO, SANTORELLI, F. M., PERRETTI, A., SANTORO, L. & MICHELE, G. 2004a. A novel mutation in SACS gene in a family from southern Italy. *Neurology,* 62**,** 100-102.

CRISCUOLO, C., BANFI, S., ORIO, M., GASPARINI, P., MONTICELLI, A., SCARANO, V., SANTORELLI, F. M., PERRETTI, A., SANTORO, L., DE MICHELE, G. & FILLA, A. 2004b. A novel mutation in SACS gene in a family from southern Italy. *Neurology,* 62**,** 100-2.

CRISCUOLO, C., SACCÀ, F., DE MICHELE, G., MANCINI, P., COMBARROS, O., INFANTE, J., GARCIA, A., BANFI, S., FILLA, A. & BERCIANO, J. 2005. Novel mutation of SACS gene in a Spanish family with autosomal recessive spastic ataxia. *Mov Disord,* 20**,** 1358-61.

CUMMINGS, C. J., MANCINI, M. A., ANTALFFY, B., DEFRANCO, D. B., ORR, H. T. & ZOGHBI, H. Y. 1998. Chaperone suppression of aggregation and altered subcellular proteasome localization imply protein misfolding in SCA1. *Nat Genet,* 19**,** 148-54.

DAGDA, R. K., GUSDON, A. M., PIEN, I., STRACK, S., GREEN, S., LI, C., VAN HOUTEN, B., CHERRA, S. J. & CHU, C. T. 2011. Mitochondrially localized PKA reverses mitochondrial pathology and dysfunction in a cellular model of Parkinson's disease. *Cell Death Differ,* 18**,** 1914-23.

DAGDA, R. K., ZAUCHA, J. A., WADZINSKI, B. E. & STRACK, S. 2003. A developmentally regulated, neuron-specific splice variant of the variable subunit Bbeta targets protein phosphatase 2A to mitochondria and modulates apoptosis. *J Biol Chem,* 278**,** 24976-85.

DARIN, N., KADHOM, N., BRIÈRE, J. J., CHRETIEN, D., BÉBÉAR, C. M., RÖTIG, A., MUNNICH, A. & RUSTIN, P. 2003. Mitochondrial activities in human cultured skin fibroblasts contaminated by Mycoplasma hyorhinis. *BMC Biochem,* 4**,** 15.

DAVID, C. L., SMITH, H. E., RAYNES, D. A., PULCINI, E. J. & WHITESELL, L. 2003. Expression of a unique drug-resistant Hsp90 ortholog by the nematode Caenorhabditis elegans. *Cell Stress Chaperones,* 8**,** 93-104.

DAVID, D. C., HAUPTMANN, S., SCHERPING, I., SCHUESSEL, K., KEIL, U., RIZZU, P., RAVID, R., DRÖSE, S., BRANDT, U., MÜLLER, W. E., ECKERT, A. & GÖTZ, J. 2005. Proteomic and functional analyses reveal a mitochondrial dysfunction in P301L tau transgenic mice. *J Biol Chem,* 280**,** 23802-14.

DAVIS, A. F. & CLAYTON, D. A. 1996. In situ localization of mitochondrial DNA replication in intact mammalian cells. *J Cell Biol,* 135**,** 883-93.

DE BRAEKELEER, M., GIASSON, F., MATHIEU, J., ROY, M., BOUCHARD, J. P. & MORGAN, K. 1993. Genetic epidemiology of autosomal recessive spastic ataxia of Charlevoix-Saguenay in northeastern Quebec. *Genet Epidemiol,* 10**,** 17-25.

DE BRITO, O. M. & SCORRANO, L. 2008. Mitofusin 2 tethers endoplasmic reticulum to mitochondria. *Nature,* 456**,** 605-10.

DE CASTRO, M., CRUZ-MARTÍNEZ, A., VÍLCHEZ, J. J., SEVILLA, T., PINEDA, M., BERCIANO, J. & PALAU, F. 1999. Early onset cerebellar ataxia and preservation of tendon reflexes: clinical phenotypes associated with GAA trinucleotide repeat expanded and non-expanded genotypes. *J Peripher Nerv Syst,* 4**,** 58-62.

DE DUVE, C. & BAUDHUIN, P. 1966. Peroxisomes (microbodies and related particles). *Physiol Rev,* 46**,** 323-57.

DE PAEPE, B., SMET, J., VANLANDER, A., SENECA, S., LISSENS, W., DE MEIRLEIR, L., VANDEWOESTYNE, M., DEFORCE, D., RODENBURG, R. J. & VAN COSTER, R. 2012. Fluorescence imaging of mitochondria in cultured skin fibroblasts: a useful method for the detection of oxidative phosphorylation defects. *Pediatr Res,* 72**,** 232-40.

DE RASMO, D., PANELLI, D., SARDANELLI, A. M. & PAPA, S. 2008. cAMP-dependent protein kinase regulates the mitochondrial import of the nuclear encoded NDUFS4 subunit of complex I. *Cell Signal,* 20**,** 989-97.

DESSERRE, J., DEVOS, D., SAUTIÈRE, B. G., DEBRUYNE, P., SANTORELLI, F. M., VUILLAUME, I. & DEFOORT-DHELLEMMES, S. 2011. Thickening of peripapillar retinal fibers for the diagnosis of autosomal recessive spastic ataxia of charlevoix-saguenay. *Cerebellum,* 10**,** 758-62.

DIAS-SANTAGATA, D., FULGA, T. A., DUTTAROY, A. & FEANY, M. B. 2007. Oxidative stress mediates tau-induced neurodegeneration in Drosophila. *J Clin Invest,* 117**,** 236-45.

DIMAURO, S. 2004. Mitochondrial diseases. *Biochim Biophys Acta,* 1658**,** 80-8.

DIMAURO, S. & DAVIDZON, G. 2005. Mitochondrial DNA and disease. *Ann Med,* 37**,** 222-32.

DING, Q., LEE, Y. K., SCHAEFER, E. A., PETERS, D. T., VERES, A., KIM, K., KUPERWASSER, N., MOTOLA, D. L., MEISSNER, T. B., HENDRIKS, W. T., TREVISAN, M., GUPTA, R. M., MOISAN, A., BANKS, E., FRIESEN, M., SCHINZEL, R. T., XIA, F., TANG, A., XIA, Y., FIGUEROA, E., WANN, A., AHFELDT, T., DAHERON, L., ZHANG, F., RUBIN, L. L., PENG, L. F., CHUNG, R. T., MUSUNURU, K. & COWAN, C. A. 2013. A TALEN genome-editing system for generating human stem cell-based disease models. *Cell Stem Cell,* 12**,** 238-51.

DING, W. X. & YIN, X. M. 2012. Mitophagy: mechanisms, pathophysiological roles, and analysis. *Biol Chem,* 393**,** 547-64.

DIVAKARUNI, A. S. & BRAND, M. D. 2011. The regulation and physiology of mitochondrial proton leak. *Physiology (Bethesda),* 26**,** 192-205.

DRAICCHIO, M. S., FRANCESCO, P., ALBERTO, R., FRANCESCO, SERRAO, M., PIERELLI, F., RANAVOLO, A., DRAICCHIO, F., CONTE, C., DON, R., FABIO, R., LEROSE, M., PADUA, L., SANDRINI, G. & CASALI, C. 2012. Gait Pattern in Inherited Cerebellar Ataxias. *The Cerebellum,* 11**,** 194-211.

DUBOFF, B., GÖTZ, J. & FEANY, M. B. 2012. Tau promotes neurodegeneration via DRP1 mislocalization in vivo. *Neuron,* 75**,** 618-32.

DUCHEN, M. R. 2004a. Mitochondria in health and disease: perspectives on a new mitochondrial biology. *Molecular Aspects of Medicine,* 25**,** 365-451.

DUCHEN, M. R. 2004b. Roles of mitochondria in health and disease. *Diabetes,* 53 Suppl 1**,** S96-102.

DURR, A. 2010. Autosomal dominant cerebellar ataxias: polyglutamine expansions and beyond. *Lancet Neurol,* 9**,** 885-94.

DÜRR, A., COSSEE, M., AGID, Y., CAMPUZANO, V., MIGNARD, C., PENET, C., MANDEL, J. L., BRICE, A. & KOENIG, M. 1996. Clinical and genetic abnormalities in patients with Friedreich's ataxia. *N Engl J Med,* 335**,** 1169-75.

EATON, J. S., LIN, Z. P., SARTORELLI, A. C., BONAWITZ, N. D. & SHADEL, G. S. 2007. Ataxia-telangiectasia mutated kinase regulates ribonucleotide reductase and mitochondrial homeostasis. *J Clin Invest,* 117**,** 2723-34.

ECKERT, J. H. & ERDMANN, R. 2003. Peroxisome biogenesis. *Rev Physiol Biochem Pharmacol,* 147**,** 75-121.

EL EUCH-FAYACHE, G., LALANI, I., AMOURI, R., TURKI, I., OUAHCHI, K., HUNG, W. Y., BELAL, S., SIDDIQUE, T. & HENTATI, F. 2003. Phenotypic features and genetic findings in sacsin-related autosomal recessive ataxia in Tunisia. *Arch Neurol,* 60**,** 982-8.

ENGERT, J. C., BÉRUBÉ, P., MERCIER, J., DORÉ, C., LEPAGE, P., GE, B., BOUCHARD, J. P., MATHIEU, J., MELANÇON, S. B., SCHALLING, M., LANDER, E. S., MORGAN, K., HUDSON, T. J. & RICHTER, A. 2000. ARSACS, a spastic ataxia common in northeastern Québec, is caused by mutations in a new gene encoding an 11.5-kb ORF. *Nat Genet,* 24**,** 120-5.

ERNSTER, L. & SCHATZ, G. 1981. Mitochondria: a historical review. *J Cell Biol,* 91**,** 227s-255s.

ESTAQUIER, J. & ARNOULT, D. 2007. Inhibiting Drp1-mediated mitochondrial fission selectively prevents the release of cytochrome c during apoptosis. *Cell Death Differ,* 14**,** 1086-94.

EVANS, M. J. & SCARPULLA, R. C. 1990. NRF-1: a trans-activator of nuclear-encoded respiratory genes in animal cells. *Genes Dev,* 4**,** 1023-34.

FAELBER, K., POSOR, Y., GAO, S., HELD, M., ROSKE, Y., SCHULZE, D., HAUCKE, V., NOÉ, F. & DAUMKE, O. 2011. Crystal structure of nucleotide-free dynamin. *Nature,* 477**,** 556-60.

FAN, Y., WALI, G., SUTHARSAN, R., BELLETTE, B., CRANE, D. I., SUE, C. M. & MACKAY-SIM, A. 2014. Low dose tubulin-binding drugs rescue peroxisome trafficking deficit in patient-derived stem cells in Hereditary Spastic Paraplegia. *Biol Open,* 3**,** 494-502.

FANELLI, F., SEPE, S., D'AMELIO, M., BERNARDI, C., CRISTIANO, L., CIMINI, A., CECCONI, F., CERU', M. P. & MORENO, S. 2013. Age-dependent roles of peroxisomes in the hippocampus of a transgenic mouse model of Alzheimer's disease. *Mol Neurodegener,* 8**,** 8.

FARRÉ, J. C., MANJITHAYA, R., MATHEWSON, R. D. & SUBRAMANI, S. 2008. PpAtg30 tags peroxisomes for turnover by selective autophagy. *Dev Cell,* 14**,** 365-76.

FERRETTA, A., GABALLO, A., TANZARELLA, P., PICCOLI, C., CAPITANIO, N., NICO, B., ANNESE, T., DI PAOLA, M., DELL'AQUILA, C., DE MARI, M., FERRANINI, E., BONIFATI, V., PACELLI, C. & COCCO, T. 2014. Effect of resveratrol on mitochondrial function: implications in parkin-associated familiar Parkinson's disease. *Biochim Biophys Acta,* 1842**,** 902-15.

FIGUEROA-ROMERO, C., IÑIGUEZ-LLUHÍ, J. A., STADLER, J., CHANG, C. R., ARNOULT, D., KELLER, P. J., HONG, Y., BLACKSTONE, C. & FELDMAN, E. L. 2009. SUMOylation of the mitochondrial fission protein Drp1 occurs at multiple nonconsensus sites within the B domain and is linked to its activity cycle. *FASEB J,* 23**,** 3917-27.

FILIPPIN, L., MAGALHÃES, P. J., DI BENEDETTO, G., COLELLA, M. & POZZAN, T. 2003. Stable interactions between mitochondria and endoplasmic reticulum allow rapid accumulation of calcium in a subpopulation of mitochondria. *J Biol Chem,* 278**,** 39224-34.

FORD, M. G., JENNI, S. & NUNNARI, J. 2011. The crystal structure of dynamin. *Nature,* 477**,** 561-6.

FRANZINI-ARMSTRONG, C. 1963. PORES IN THE SARCOPLASMIC RETICULUM. *J Cell Biol,* 19**,** 637-41.

FRIEDMAN, J. R., LACKNER, L. L., WEST, M., DIBENEDETTO, J. R., NUNNARI, J. & VOELTZ, G. K. 2011. ER Tubules Mark Sites of Mitochondrial Division. 1-8.

FUJIMOTO, M., HAYASHI, T. & SU, T. P. 2012. The role of cholesterol in the association of endoplasmic reticulum membranes with mitochondria. *Biochem Biophys Res Commun,* 417**,** 635-9.

GAJ, T., GERSBACH, C. A. & BARBAS, C. F. 2013. ZFN, TALEN, and CRISPR/Cas-based methods for genome engineering. *Trends Biotechnol,* 31**,** 397-405.

GANDHI, S., WOOD-KACZMAR, A., YAO, Z., PLUN-FAVREAU, H., DEAS, E., KLUPSCH, K., DOWNWARD, J., LATCHMAN, D. S., TABRIZI, S. J., WOOD, N. W., DUCHEN, M. R. & ABRAMOV, A. Y. 2009. PINK1-associated Parkinson's disease is caused by neuronal vulnerability to calcium-induced cell death. *Mol Cell,* 33**,** 627-38.

GANDRE-BABBE, S. & VAN DER BLIEK, A. M. 2008. The Novel Tail-anchored Membrane Protein Mff Controls Mitochondrial and Peroxisomal Fission in Mammalian Cells. *Molecular Biology of the Cell,* 19**,** 2402-2412.

GARCIA-MARTIN, E., BAMBO, M. P., GAZULLA, J., LARROSA, J. M., POLO, V., FUERTES, M. I., FUENTES, J. L., FERRERAS, A. & PABLO, L. E. 2013a. Finding of retinal nerve fiber layer hypertrophy in ataxia of Charlevoix-Saguenay patients. *Arch Soc Esp Oftalmol*.

GARCIA-MARTIN, E., PABLO, L. E., GAZULLA, J., POLO, V., FERRERAS, A. & LARROSA, J. M. 2013b. Retinal nerve fibre layer thickness in ARSACS: myelination or hypertrophy? *Br J Ophthalmol,* 97**,** 238-41.

GERWIG, M., KRUGER, S., KREUZ, F. R., KREIS, S., GIZEWSKI, E. R. & TIMMANN, D. 2010. Characteristic MRI and funduscopic findings help diagnose ARSACS outside Quebec. *Neurology,* 75**,** 2133-2133.

GESCHWIND, D. H., PERLMAN, S., FIGUEROA, C. P., TREIMAN, L. J. & PULST, S. M. 1997. The prevalence and wide clinical spectrum of the spinocerebellar ataxia type 2 trinucleotide repeat in patients with autosomal dominant cerebellar ataxia. *Am J Hum Genet,* 60**,** 842-50.

GIBSON, G. E., STARKOV, A., BLASS, J. P., RATAN, R. R. & BEAL, M. F. 2010. Cause and consequence: mitochondrial dysfunction initiates and propagates neuronal dysfunction, neuronal death and behavioral abnormalities in age-associated neurodegenerative diseases. *Biochim Biophys Acta,* 1802**,** 122-34.

GILISSEN, C., HOISCHEN, A., BRUNNER, H. G. & VELTMAN, J. A. 2012. Disease gene identification strategies for exome sequencing. *Eur J Hum Genet,* 20**,** 490-7.

GIORDANO, S., LEE, J., DARLEY-USMAR, V. M. & ZHANG, J. 2012. Distinct effects of rotenone, 1-methyl-4-phenylpyridinium and 6-hydroxydopamine on cellular bioenergetics and cell death. *PLoS One,* 7**,** e44610.

GIRARD, M., LARIVIÈRE, R., PARFITT, D. A., DEANE, E. C., GAUDET, R., NOSSOVA, N., BLONDEAU, F., PRENOSIL, G., VERMEULEN, E. G., DUCHEN, M. R., RICHTER, A., SHOUBRIDGE, E. A., GEHRING, K., MCKINNEY, R. A., BRAIS, B., CHAPPLE, J. P. & MCPHERSON, P. S. 2012. Mitochondrial dysfunction and Purkinje cell loss in autosomal recessive spastic ataxia of Charlevoix-Saguenay (ARSACS). *Proc Natl Acad Sci U S A,* 109**,** 1661-6.

GOTTLIEB, E., ARMOUR, S. M., HARRIS, M. H. & THOMPSON, C. B. 2003. Mitochondrial membrane potential regulates matrix configuration and cytochrome c release during apoptosis. *Cell Death Differ,* 10**,** 709-17.

GREER, P. L., HANAYAMA, R., BLOODGOOD, B. L., MARDINLY, A. R., LIPTON, D. M., FLAVELL, S. W., KIM, T.-K., GRIFFITH, E. C., WALDON, Z., MAEHR, R., PLOEGH, H. L., CHOWDHURY,

S., WORLEY, P. F., STEEN, J. & GREENBERG, M. E. 2010. The Angelman Syndrome Protein Ube3A Regulates Synapse Development by Ubiquitinating Arc. *Cell,* 140**,** 704-716.

GRENERT, J. P., SULLIVAN, W. P., FADDEN, P., HAYSTEAD, T. A., CLARK, J., MIMNAUGH, E., KRUTZSCH, H., OCHEL, H. J., SCHULTE, T. W., SAUSVILLE, E., NECKERS, L. M. & TOFT, D. O. 1997. The amino-terminal domain of heat shock protein 90 (hsp90) that binds geldanamycin is an ATP/ADP switch domain that regulates hsp90 conformation. *J Biol Chem,* 272**,** 23843-50.

GRIECO, G. S., MALANDRINI, A., COMANDUCCI, G., LEUZZI, VALOPPI, M., TESSA, A., PALMERI, S., BENEDETTI, L., PIERALLINI, A. & GAMBELLI, S. 2004. Novel SACS mutations in autosomal recessive spastic ataxia of Charlevoix-Saguenay type. *Neurology,* 62**,** 103-106.

GRYNBERG, M., ERLANDSEN, H. & GODZIK, A. 2003. HEPN: a common domain in bacterial drug resistance and human neurodegenerative proteins. *Trends Biochem Sci,* 28**,** 224-6.

GUERNSEY, D. L., DUBÉ, M. P., JIANG, H., ASSELIN, G., BLOWERS, S., EVANS, S., FERGUSON, M., MACGILLIVRAY, C., MATSUOKA, M., NIGHTINGALE, M., RIDEOUT, A., DELATYCKI, M., ORR, A., LUDMAN, M., DOOLEY, J., RIDDELL, C. & SAMUELS, M. E. 2010. Novel mutations in the sacsin gene in ataxia patients from Maritime Canada. *Journal of the Neurological Sciences,* 288**,** 79-87.

GUILLERY, O., MALKA, F., FRACHON, P., MILEA, D., ROJO, M. & LOMBÈS, A. 2008. Modulation of mitochondrial morphology by bioenergetics defects in primary human fibroblasts. *Neuromuscul Disord,* 18**,** 319-30.

GUILLON, B., BULTEAU, A. L., WATTENHOFER-DONZÉ, M., SCHMUCKER, S., FRIGUET, B., PUCCIO, H., DRAPIER, J. C. & BOUTON, C. 2009. Frataxin deficiency causes upregulation of mitochondrial Lon and ClpP proteases and severe loss of mitochondrial Fe-S proteins. *FEBS J,* 276**,** 1036-47.

GUO, Q., FURUKAWA, K., SOPHER, B. L., PHAM, D. G., XIE, J., ROBINSON, N., MARTIN, G. M. & MATTSON, M. P. 1996. Alzheimer's PS-1 mutation perturbs calcium homeostasis and sensitizes PC12 cells to death induced by amyloid beta-peptide. *Neuroreport,* 8**,** 379-83.

H'MIDA-BEN BRAHIM, D., M'ZAHEM, A., ASSOUM, M., BOUHLAL, Y., FATTORI, F., ANHEIM, M., ALI-PACHA, L., FERRAT, F., CHAOUCH, M., LAGIER-TOURENNE, C., DROUOT, N., THIBAUT, C., BENHASSINE, T., SIFI, Y., STOPPA-LYONNET, D., N'GUYEN, K., POUJET, J., HAMRI, A., HENTATI, F., AMOURI, R., SANTORELLI, F. M., TAZIR, M. & KOENIG, M. 2011. Molecular diagnosis of known recessive ataxias by homozygosity mapping with SNP arrays. *J Neurol,* 258**,** 56-67.

HAMASAKI, M., FURUTA, N., MATSUDA, A., NEZU, A., YAMAMOTO, A., FUJITA, N., OOMORI, H., NODA, T., HARAGUCHI, T., HIRAOKA, Y., AMANO, A. & YOSHIMORI, T. 2013. Autophagosomes form at ER-mitochondria contact sites. *Nature,* 495**,** 389-93.

HARA, K., ONODERA, O., ENDO, M., KONDO, H., SHIOTA, H., MIKI, K., TANIMOTO, N., KIMURA, T. & NISHIZAWA, M. 2005a. Sacsin-related autosomal recessive ataxia without prominent retinal myelinated fibers in Japan. *Movement Disorders,* 20**,** 380-382.

HARA, K., ONODERA, O., ENDO, M., KONDO, H., SHIOTA, H., MIKI, K., TANIMOTO, N., KIMURA, T. & NISHIZAWA, M. 2005b. Sacsin-related autosomal recessive ataxia without prominent retinal myelinated fibers in Japan. *Mov Disord,* 20**,** 380-2.

HARA, K., SHIMBO, J., NOZAKI, H., KIKUGAWA, K., ONODERA, O. & NISHIZAWA, M. 2007. Sacsin-related ataxia with neither retinal hypermyelination nor spasticity. *Mov Disord,* 22**,** 1362-3.

HARDER, Z., ZUNINO, R. & MCBRIDE, H. 2004. Sumo1 conjugates mitochondrial substrates and participates in mitochondrial fission. *Curr Biol,* 14**,** 340-5.

HARDING, A. E. 1981. Genetic aspects of autosomal dominant late onset cerebellar ataxia. *J Med Genet,* 18**,** 436-41.

HARDING, A. E. 1982. The clinical features and classification of the late onset autosomal dominant cerebellar ataxias. A study of 11 families, including descendants of the 'the Drew family of Walworth'. *Brain,* 105**,** 1-28.

HARDING, A. E. 1983. Classification of the hereditary ataxias and paraplegias. *Lancet,* 1**,** 1151-5.

HARTMANN-PETERSEN, R. & GORDON, C. 2004. Integral UBL domain proteins: a family of proteasome interacting proteins. *Semin Cell Dev Biol,* 15**,** 247-59.

HATEFI, Y. 1985. The mitochondrial electron transport and oxidative phosphorylation system. *Annu Rev Biochem,* 54**,** 1015-69.

HECHT, F. & HECHT, B. K. 1990. Cancer in ataxia-telangiectasia patients. *Cancer Genet Cytogenet,* 46**,** 9-19.

HEDSKOG, L., PINHO, C. M., FILADI, R., RÖNNBÄCK, A., HERTWIG, L., WIEHAGER, B., LARSSEN, P., GELLHAAR, S., SANDEBRING, A., WESTERLUND, M., GRAFF, C., WINBLAD, B., GALTER, D., BEHBAHANI, H., PIZZO, P., GLASER, E. & ANKARCRONA, M. 2013. Modulation of the endoplasmic reticulum-mitochondria interface in Alzheimer's disease and related models. *Proc Natl Acad Sci U S A,* 110**,** 7916-21.

HEGGENESS, M. H., SIMON, M. & SINGER, S. J. 1978. Association of mitochondria with microtubules in cultured cells. *Proc Natl Acad Sci U S A,* 75**,** 3863-6.

HEMACH, P., REDDY, P. H., REDDY, R., REDDY, T. P., MANCZAK, M., CALKINS, M. J., SHIRENDEB, U. & MAO, P. 2011. Dynamin-related protein 1 and mitochondrial fragmentation in neurodegenerative diseases. *Brain Research Reviews,* 67**,** 103-118.

HENKART, M. 1980. Identification and function of intracellular calcium stores in axons and cell bodies of neurons. *Fed Proc,* 39**,** 2783-9.

HERMAN-BERT, A., STEVANIN, G., NETTER, J. C., RASCOL, O., BRASSAT, D., CALVAS, P., CAMUZAT, A., YUAN, Q., SCHALLING, M., DÜRR, A. & BRICE, A. 2000. Mapping of spinocerebellar ataxia 13 to chromosome 19q13.3-q13.4 in a family with autosomal dominant cerebellar ataxia and mental retardation. *Am J Hum Genet,* 67**,** 229-35.

HERMANN, G. J. & SHAW, J. M. 1998. Mitochondrial dynamics in yeast. *Annu Rev Cell Dev Biol,* 14**,** 265-303.

HOLMES, G. 1939. The Cerebellum of Man. *Brain,* 62.

HOLMES, S. E., O'HEARN, E. E., MCINNIS, M. G., GORELICK-FELDMAN, D. A., KLEIDERLEIN, J. J., CALLAHAN, C., KWAK, N. G., INGERSOLL-ASHWORTH, R. G., SHERR, M., SUMNER, A. J., SHARP, A. H., ANANTH, U., SELTZER, W. K., BOSS, M. A., VIERIA-SAECKER, A. M., EPPLEN, J. T., RIESS, O., ROSS, C. A. & MARGOLIS, R. L. 1999. Expansion of a novel CAG trinucleotide repeat in the 5' region of PPP2R2B is associated with SCA12. *Nat Genet,* 23**,** 391-2.

HOM, J., YU, T., YOON, Y., PORTER, G. & SHEU, S. S. 2010. Regulation of mitochondrial fission by intracellular Ca2+ in rat ventricular myocytes. *Biochim Biophys Acta,* 1797**,** 913-21.

HOULDEN, H., JOHNSON, J., GARDNER-THORPE, C., LASHLEY, T., HERNANDEZ, D., WORTH, P., SINGLETON, A. B., HILTON, D. A., HOLTON, J., REVESZ, T., DAVIS, M. B., GIUNTI, P. & WOOD, N. W. 2007. Mutations in TTBK2, encoding a kinase implicated in tau phosphorylation, segregate with spinocerebellar ataxia type 11. *Nat Genet,* 39**,** 1434-6.

HUANG, H. M., FOWLER, C., XU, H., ZHANG, H. & GIBSON, G. E. 2005. Mitochondrial function in fibroblasts with aging in culture and/or Alzheimer's disease. *Neurobiol Aging,* 26**,** 839-48.

HUYBRECHTS, S. J., VAN VELDHOVEN, P. P., BREES, C., MANNAERTS, G. P., LOS, G. V. & FRANSEN, M. 2009. Peroxisome dynamics in cultured mammalian cells. *Traffic,* 10**,** 1722-33.

HØYER-HANSEN, M. & JÄÄTTELÄ, M. 2007. Connecting endoplasmic reticulum stress to autophagy by unfolded protein response and calcium. *Cell Death Differ,* 14**,** 1576-82.

IKEDA, H., YAMAGUCHI, M., SUGAI, S., AZE, Y., NARUMIYA, S. & KAKIZUKA, A. 1996. Expanded polyglutamine in the Machado-Joseph disease protein induces cell death in vitro and in vivo. *Nat Genet,* 13**,** 196-202.

IKEDA, Y., DICK, K. A., WEATHERSPOON, M. R., GINCEL, D., ARMBRUST, K. R., DALTON, J. C., STEVANIN, G., DÜRR, A., ZÜHLKE, C., BÜRK, K., CLARK, H. B., BRICE, A., ROTHSTEIN, J. D., SCHUT, L. J., DAY, J. W. & RANUM, L. P. 2006. Spectrin mutations cause spinocerebellar ataxia type 5. *Nat Genet,* 38**,** 184-90.

INVERNIZZI, F., ZEVIANI, M., TIRANTI, V. & JENSEN, P. B. *Measuring mitochondrial defects in human skin fibroblasts* [Online]. 2004].

IRWIN, S., VANDELFT, M., PINCHEV, D., HOWELL, J. L., GRACZYK, J., ORR, H. T. & TRUANT, R. 2005. RNA association and nucleocytoplasmic shuttling by ataxin-1. *J Cell Sci,* 118**,** 233-42.

IVASHCHENKO, O., VAN VELDHOVEN, P. P., BREES, C., HO, Y. S., TERLECKY, S. R. & FRANSEN, M. 2011. Intraperoxisomal redox balance in mammalian cells: oxidative stress and interorganellar cross-talk. *Mol Biol Cell,* 22**,** 1440-51.

IWANAMI, H., TANAKA, M., IWAKAWA, H., TAKIGUTI, Y. & INUKAI, T. 2011. [A case presenting with ataxic gait and dementia due to vitamin B_{12} deficiency without megaloblastic anemia or subacute combined degeneration of the spinal cord]. *Brain Nerve,* 63**,** 267-9.

IWASAWA, R., MAHUL-MELLIER, A.-L., DATLER, C., PAZARENTZOS, E. & GRIMM, S. 2010. Fis1 and Bap31 bridge the mitochondria–ER interface to establish a platform for apoptosis induction. *The EMBO Journal,* 30**,** 556-568.

JAIN, M., RIVERA, S., MONCLUS, E. A., SYNENKI, L., ZIRK, A., EISENBART, J., FEGHALI-BOSTWICK, C., MUTLU, G. M., BUDINGER, G. R. & CHANDEL, N. S. 2013. Mitochondrial reactive oxygen species regulate transforming growth factor-β signaling. *J Biol Chem,* 288**,** 770-7.

JANSSEN, A., GRESSENS, P., GRABENBAUER, M., BAUMGART, E., SCHAD, A., VANHOREBEEK, I., BROUWERS, A., DECLERCQ, P. E., FAHIMI, D., EVRARD, P., SCHOONJANS, L., COLLEN, D., CARMELIET, P., MANNAERTS, G., VAN VELDHOVEN, P. & BAES, M. 2003. Neuronal migration depends on intact peroxisomal function in brain and in extraneuronal tissues. *J Neurosci,* 23**,** 9732-41.

JASTROCH, M., WUERTZ, S., KLOAS, W. & KLINGENSPOR, M. 2005. Uncoupling protein 1 in fish uncovers an ancient evolutionary history of mammalian nonshivering thermogenesis. *Physiol Genomics,* 22**,** 150-6.

JENNER, P., DEXTER, D. T., SIAN, J., SCHAPIRA, A. H. & MARSDEN, C. D. 1992. Oxidative stress as a cause of nigral cell death in Parkinson's disease and incidental Lewy body disease. The Royal Kings and Queens Parkinson's Disease Research Group. *Ann Neurol,* 32 Suppl**,** S82-7.

JONCKHEERE, A. I., HUIGSLOOT, M., JANSSEN, A. J., KAPPEN, A. J., SMEITINK, J. A. & RODENBURG, R. J. 2010. High-throughput assay to measure oxygen consumption in digitonin-permeabilized cells of patients with mitochondrial disorders. *Clin Chem,* 56**,** 424-31.

JORGENSEN, N. D., ANDRESEN, J. M., PITT, J. E., SWENSON, M. A., ZOGHBI, H. Y. & ORR, H. T. 2007. Hsp70/Hsc70 regulates the effect phosphorylation has on stabilizing ataxin-1. *J Neurochem,* 102**,** 2040-8.

JOUAVILLE, L. S., ICHAS, F., HOLMUHAMEDOV, E. L., CAMACHO, P. & LECHLEITER, J. D. 1995. Synchronization of calcium waves by mitochondrial substrates in Xenopus laevis oocytes. *Nature,* 377**,** 438-41.

KAMADA, S., OKAWA, S., IMOTA, T., SUGAWARA, M. & TOYOSHIMA, I. 2008a. Autosomal recessive spastic ataxia of Charlevoix-Saguenay (ARSACS). *Journal of Neurology,* 255**,** 803-806.

KAMADA, S., OKAWA, S., IMOTA, T., SUGAWARA, M. & TOYOSHIMA, I. 2008b. Autosomal recessive spastic ataxia of Charlevoix-Saguenay (ARSACS): novel compound heterozygous mutations in the SACS gene. *J Neurol,* 255**,** 803-6.

KAMIONKA, M. & FEIGON, J. 2004. Structure of the XPC binding domain of hHR23A reveals hydrophobic patches for protein interaction. *Protein Science,* 13**,** 2370-2377.

KAMPINGA, H. H., HAGEMAN, J., VOS, M. J., KUBOTA, H., TANGUAY, R. M., BRUFORD, E. A., CHEETHAM, M. E., CHEN, B. & HIGHTOWER, L. E. 2009. Guidelines for the nomenclature of the human heat shock proteins. *Cell Stress Chaperones,* 14**,** 105-11.

KAMSLER, A., DAILY, D., HOCHMAN, A., STERN, N., SHILOH, Y., ROTMAN, G. & BARZILAI, A. 2001. Increased oxidative stress in ataxia telangiectasia evidenced by alterations in redox state of brains from Atm-deficient mice. *Cancer Res,* 61**,** 1849-54.

KANABUS, M., HEALES, S. J. & RAHMAN, S. 2014. Development of pharmacological strategies for mitochondrial disorders. *Br J Pharmacol,* 171**,** 1798-817.

KARBOWSKI, M., ARNOULT, D., CHEN, H., CHAN, D. C., SMITH, C. L. & YOULE, R. J. 2004. Quantitation of mitochondrial dynamics by photolabeling of individual organelles shows that mitochondrial fusion is blocked during the Bax activation phase of apoptosis. *J Cell Biol,* 164**,** 493-9.

KELLEY, W. L. 1999. Molecular chaperones: How J domains turn on Hsp70s. *Current Biology,* 9**,** R305-R308.

KIM, B., ZHANG, X., KAN, R., COHEN, R., MUKAI, C. & TRAVIS, A. J. 2014. The role of MATER in endoplasmic reticulum distribution and calcium homeostasis in mouse oocytes. 386**,** 331–339.

KIM, I., RODRIGUEZ-ENRIQUEZ, S. & LEMASTERS, J. J. 2007. Selective degradation of mitochondria by mitophagy. *Arch Biochem Biophys,* 462**,** 245-53.

KLEMENT, I. A., SKINNER, P. J., KAYTOR, M. D., YI, H., HERSCH, S. M., CLARK, H. B., ZOGHBI, H. Y. & ORR, H. T. 1998. Ataxin-1 nuclear localization and aggregation: role in polyglutamine-induced disease in SCA1 transgenic mice. *Cell,* 95**,** 41-53.

KLOCKGETHER, T. 2010. Sporadic ataxia with adult onset: classification and diagnostic criteria. *Lancet Neurol,* 9**,** 94-104.

KNOTT, A. B., PERKINS, G., SCHWARZENBACHER, R. & BOSSY-WETZEL, E. 2008. Mitochondrial fragmentation in neurodegeneration. *Nat Rev Neurosci,* 9**,** 505-18.

KOBAYASHI, S., TANAKA, A. & FUJIKI, Y. 2007. Fis1, DLP1, and Pex11p coordinately regulate peroxisome morphogenesis. *Exp Cell Res,* 313**,** 1675-86.

KOCH, A., THIEMANN, M., GRABENBAUER, M., YOON, Y., MCNIVEN, M. A. & SCHRADER, M. 2003. Dynamin-like protein 1 is involved in peroxisomal fission. *J Biol Chem,* 278**,** 8597-605.

KOCH, A., YOON, Y., BONEKAMP, N. A., MCNIVEN, M. A. & SCHRADER, M. 2005. A role for Fis1 in both mitochondrial and peroxisomal fission in mammalian cells. *Mol Biol Cell,* 16**,** 5077-86.

KOCH, J. & BROCARD, C. 2012. PEX11 proteins attract Mff and human Fis1 to coordinate peroxisomal fission. *J Cell Sci,* 125**,** 3813-26.

KOIRALA, S., GUO, Q., KALIA, R., BUI, H. T., ECKERT, D. M., FROST, A. & SHAW, J. M. 2013. Interchangeable adaptors regulate mitochondrial dynamin assembly for membrane scission. *Proc Natl Acad Sci U S A,* 110**,** E1342-51.

KORNMANN, B. 2013. The molecular hug between the ER and the mitochondria. *Curr Opin Cell Biol,* 25**,** 443-8.

KOSHIBA, T., DETMER, S. A., KAISER, J. T., CHEN, H., MCCAFFERY, J. M. & CHAN, D. C. 2004. Structural basis of mitochondrial tethering by mitofusin complexes. *Science,* 305**,** 858-62.

KOU, J., KOVACS, G. G., HÖFTBERGER, R., KULIK, W., BRODDE, A., FORSS-PETTER, S., HÖNIGSCHNABL, S., GLEISS, A., BRÜGGER, B., WANDERS, R., JUST, W., BUDKA, H., JUNGWIRTH, S., FISCHER, P. & BERGER, J. 2011. Peroxisomal alterations in Alzheimer's disease. *Acta Neuropathol,* 122**,** 271-83.

KOUTSOPOULOS, O. S., LAINE, D., OSELLAME, L., CHUDAKOV, D. M., PARTON, R. G., FRAZIER, A. E. & RYAN, M. T. 2010. Human Miltons associate with mitochondria and induce microtubule-dependent remodeling of mitochondrial networks. *Biochim Biophys Acta,* 1803**,** 564-74.

KOVÁCS, R., KARDOS, J., HEINEMANN, U. & KANN, O. 2005. Mitochondrial calcium ion and membrane potential transients follow the pattern of epileptiform discharges in hippocampal slice cultures. *J Neurosci,* 25**,** 4260-9.

KOZLOV, G., DENISOV, A. Y., GIRARD, M., DICAIRE, M. J., HAMLIN, J., MCPHERSON, P. S., BRAIS, B. & GEHRING, K. 2011. Structural basis of defects in the sacsin HEPN domain responsible for autosomal recessive spastic ataxia of Charlevoix-Saguenay (ARSACS). *J Biol Chem,* 286**,** 20407-12.

KRISTIANSEN, H., GAD, H. H., ESKILDSEN-LARSEN, S., DESPRES, P. & HARTMANN, R. 2011. The oligoadenylate synthetase family: an ancient protein family with multiple antiviral activities. *J Interferon Cytokine Res,* 31**,** 41-7.

KUCHTA, K., KNIZEWSKI, L., WYRWICZ, L. S., RYCHLEWSKI, L. & GINALSKI, K. 2009. Comprehensive classification of nucleotidyltransferase fold proteins: identification of novel families and their representatives in human. *Nucleic Acids Res,* 37**,** 7701-14.

KUMAR, U., DUNLOP, D. M. & RICHARDSON, J. S. 1994. Mitochondria from Alzheimer's fibroblasts show decreased uptake of calcium and increased sensitivity to free radicals. *Life Sci,* 54**,** 1855-60.

KUNAU, W. H. 2005. Peroxisome biogenesis: end of the debate. *Curr Biol,* 15**,** R774-6.

LACKNER, L. L. 2013. Determining the shape and cellular distribution of mitochondria: the integration of multiple activities. *Curr Opin Cell Biol,* 25**,** 471-6.

LASORSA, F. M., PINTON, P., PALMIERI, L., SCARCIA, P., ROTTENSTEINER, H., RIZZUTO, R. & PALMIERI, F. 2008. Peroxisomes as novel players in cell calcium homeostasis. *J Biol Chem,* 283**,** 15300-8.

LATONEN, L. 2011. Nucleolar aggresomes as counterparts of cytoplasmic aggresomes in proteotoxic stress. Proteasome inhibitors induce nuclear ribonucleoprotein inclusions that accumulate several key factors of neurodegenerative diseases and cancer. *Bioessays,* 33**,** 386-95.

LAVIN, M. F. & SHILOH, Y. 1997. The genetic defect in ataxia-telangiectasia. *Annu Rev Immunol,* 15**,** 177-202.

LAZAROW, P. B. & FUJIKI, Y. 1985. Biogenesis of peroxisomes. *Annu Rev Cell Biol,* 1**,** 489-530.

LAÇO, M. N., OLIVEIRA, C. R., PAULSON, H. L. & REGO, A. C. 2012. Compromised mitochondrial complex II in models of Machado-Joseph disease. *Biochim Biophys Acta,* 1822**,** 139-49.

LEE, H. C. & WEI, Y. H. 2005. Mitochondrial biogenesis and mitochondrial DNA maintenance of mammalian cells under oxidative stress. *Int J Biochem Cell Biol,* 37**,** 822-34.

LEE, S., JEONG, S. Y., LIM, W. C., KIM, S., PARK, Y. Y., SUN, X., YOULE, R. J. & CHO, H. 2007. Mitochondrial fission and fusion mediators, hFis1 and OPA1, modulate cellular senescence. *J Biol Chem,* 282**,** 22977-83.

LEE, Y. J., JEONG, S. Y., KARBOWSKI, M., SMITH, C. L. & YOULE, R. J. 2004. Roles of the mammalian mitochondrial fission and fusion mediators Fis1, Drp1, and Opa1 in apoptosis. *Mol Biol Cell,* 15**,** 5001-11.

LEGROS, F., LOMBÈS, A., FRACHON, P. & ROJO, M. 2002. Mitochondrial fusion in human cells is efficient, requires the inner membrane potential, and is mediated by mitofusins. *Mol Biol Cell,* 13**,** 4343-54.

LI, X., BAUMGART, E., MORRELL, J. C., JIMENEZ-SANCHEZ, G., VALLE, D. & GOULD, S. J. 2002. PEX11 beta deficiency is lethal and impairs neuronal migration but does not abrogate peroxisome function. *Mol Cell Biol,* 22**,** 4358-65.

LI, X. & GOULD, S. J. 2003. The dynamin-like GTPase DLP1 is essential for peroxisome division and is recruited to peroxisomes in part by PEX11. *J Biol Chem,* 278**,** 17012-20.

LI, Y., HUANG, T. T., CARLSON, E. J., MELOV, S., URSELL, P. C., OLSON, J. L., NOBLE, L. J., YOSHIMURA, M. P., BERGER, C., CHAN, P. H., WALLACE, D. C. & EPSTEIN, C. J. 1995. Dilated cardiomyopathy and neonatal lethality in mutant mice lacking manganese superoxide dismutase. *Nat Genet,* 11**,** 376-81.

LI, Z., OKAMOTO, K., HAYASHI, Y. & SHENG, M. 2004. The importance of dendritic mitochondria in the morphogenesis and plasticity of spines and synapses. *Cell,* 119**,** 873-87.

LIEBERMAN, A. P., TROJANOWSKI, J. Q., LEONARD, D. G., CHEN, K. L., BARNETT, J. L., LEVERENZ, J. B., BIRD, T. D., ROBITAILLE, Y., MALANDRINI, A. & FISCHBECK, K. H. 1999. Ataxin 1 and ataxin 3 in neuronal intranuclear inclusion disease. *Ann Neurol,* 46**,** 271-3.

LIGON, L. A. & STEWARD, O. 2000. Role of microtubules and actin filaments in the movement of mitochondria in the axons and dendrites of cultured hippocampal neurons. *J Comp Neurol,* 427**,** 351-61.

LILL, R., HOFFMANN, B., MOLIK, S., PIERIK, A. J., RIETZSCHEL, N., STEHLING, O., UZARSKA, M. A., WEBERT, H., WILBRECHT, C. & MÜHLENHOFF, U. 2012. The role of mitochondria in cellular iron-sulfur protein biogenesis and iron metabolism. *Biochim Biophys Acta*.

LIM, J., HAO, T., SHAW, C., PATEL, A. J., SZABÓ, G. & RUAL, J. F. 2006. A protein–protein interaction network for human inherited ataxias and disorders of Purkinje cell degeneration. *Cell*.

LIN, H. Y., LAI, R. H., LIN, S. T., LIN, R. C., WANG, M. J., LIN, C. C., LEE, H. C., WANG, F. F. & CHEN, J. Y. 2013. Suppressor of cytokine signaling 6 (SOCS6) promotes mitochondrial fission via regulating DRP1 translocation. *Cell Death Differ,* 20**,** 139-53.

LIU, G., BISSLER, J. J., SINDEN, R. R. & LEFFAK, M. 2007. Unstable spinocerebellar ataxia type 10 (ATTCT*(AGAAT) repeats are associated with aberrant replication at the ATX10 locus and replication origin-dependent expansion at an ectopic site in human cells. *Mol Cell Biol,* 27**,** 7828-38.

LODI, R., COOPER, J. M., BRADLEY, J. L., MANNERS, D., STYLES, P., TAYLOR, D. J. & SCHAPIRA, A. H. 1999. Deficit of in vivo mitochondrial ATP production in patients with Friedreich ataxia. *Proc Natl Acad Sci U S A,* 96**,** 11492-5.

LOSÓN, O. C., LIU, R., ROME, M. E., MENG, S., KAISER, J. T., SHAN, S. O. & CHAN, D. C. 2014. The mitochondrial fission receptor MiD51 requires ADP as a cofactor. *Structure,* 22**,** 367-77.

LOSÓN, O. C., SONG, Z., CHEN, H. & CHAN, D. C. 2013. Fis1, Mff, MiD49, and MiD51 mediate Drp1 recruitment in mitochondrial fission. *Mol Biol Cell,* 24**,** 659-67.

LOVY, A., MOLINA, A. J., CERQUEIRA, F. M., TRUDEAU, K. & SHIRIHAI, O. S. 2012. A faster, high resolution, mtPA-GFP-based mitochondrial fusion assay acquiring kinetic data of multiple cells in parallel using confocal microscopy. *J Vis Exp***,** e3991.

LU, Y. W. & CLAYPOOL, S. M. 2015. Disorders of phospholipid metabolism: an emerging class of mitochondrial disease due to defects in nuclear genes. *Front Genet,* 6**,** 3.

LUTZ, A. K., EXNER, N., FETT, M. E., SCHLEHE, J. S., KLOOS, K., LÄMMERMANN, K., BRUNNER, B., KURZ-DREXLER, A., VOGEL, F., REICHERT, A. S., BOUMAN, L., VOGT-WEISENHORN, D., WURST, W., TATZELT, J., HAASS, C. & WINKLHOFER, K. F. 2009. Loss of parkin or PINK1

function increases Drp1-dependent mitochondrial fragmentation. *J Biol Chem,* 284**,** 22938-51.

MADSEN, L., SCHULZE, A., SEEGER, M. & HARTMANN-PETERSEN, R. 2007. Ubiquitin domain proteins in disease. *BMC Biochem,* 8 Suppl 1**,** S1.

MALKA, F., GUILLERY, O., CIFUENTES-DIAZ, C., GUILLOU, E., BELENGUER, P., LOMBÈS, A. & ROJO, M. 2005. Separate fusion of outer and inner mitochondrial membranes. *EMBO Rep,* 6**,** 853-9.

MAMMUCARI, C. & RIZZUTO, R. 2010. Signaling pathways in mitochondrial dysfunction and aging. *Mech Ageing Dev,* 131**,** 536-43.

MANDERS, E. M., HOEBE, R., STRACKEE, J., VOSSEPOEL, A. M. & ATEN, J. A. 1996. Largest contour segmentation: a tool for the localization of spots in confocal images. *Cytometry,* 23**,** 15-21.

MANTO, M. & MARMOLINO, D. 2009. Cerebellar ataxias. *Curr Opin Neurol,* 22**,** 419-29.

MARIOTTI, S. D. D. C. G. C. 2001. The complex clinical and genetic classification of inherited ataxias. II. Autosomal recessive ataxias. 1-10.

MARTIN, M. H., BOUCHARD, J. P., SYLVAIN, M., ST-ONGE, O. & TRUCHON, S. 2007. Autosomal recessive spastic ataxia of Charlevoix-Saguenay: a report of MR imaging in 5 patients. *AJNR Am J Neuroradiol,* 28**,** 1606-8.

MASCIULLO, M., MODONI, A., TESSA, A., SANTORELLI, F. M., RIZZO, V., D'AMICO, G., LASCHENA, F., TARTAGLIONE, T. & SILVESTRI, G. 2012. Novel SACS mutations in two unrelated Italian patients with spastic ataxia: clinico-diagnostic characterization and results of serial brain MRI studies. *Eur J Neurol,* 19**,** e77-8.

MATSUURA, T., YAMAGATA, T., BURGESS, D. L., RASMUSSEN, A., GREWAL, R. P., WATASE, K., KHAJAVI, M., MCCALL, A. E., DAVIS, C. F., ZU, L., ACHARI, M., PULST, S. M., ALONSO, E., NOEBELS, J. L., NELSON, D. L., ZOGHBI, H. Y. & ASHIZAWA, T. 2000. Large expansion of the ATTCT pentanucleotide repeat in spinocerebellar ataxia type 10. *Nat Genet,* 26**,** 191-4.

MCCORMACK, J. G., HALESTRAP, A. P. & DENTON, R. M. 1990. Role of calcium ions in regulation of mammalian intramitochondrial metabolism. *Physiol Rev,* 70**,** 391-425.

MEIMARIDOU, E., KOWALCZYK, J., GUASTI, L., HUGHES, C. R., WAGNER, F., FROMMOLT, P., NÜRNBERG, P., MANN, N. P., BANERJEE, R., SAKA, H. N., CHAPPLE, J. P., KING, P. J., CLARK, A. J. & METHERELL, L. A. 2012. Mutations in NNT encoding nicotinamide nucleotide transhydrogenase cause familial glucocorticoid deficiency. *Nat Genet,* 44**,** 740-2.

MENDES, C. C., GOMES, D. A., THOMPSON, M., SOUTO, N. C., GOES, T. S., GOES, A. M., RODRIGUES, M. A., GOMEZ, M. V., NATHANSON, M. H. & LEITE, M. F. 2005. The type III inositol 1,4,5-trisphosphate receptor preferentially transmits apoptotic Ca2+ signals into mitochondria. *J Biol Chem,* 280**,** 40892-900.

MERRILL, R. A., DAGDA, R. K., DICKEY, A. S., CRIBBS, J. T., GREEN, S. H., USACHEV, Y. M. & STRACK, S. 2011. Mechanism of neuroprotective mitochondrial remodeling by PKA/AKAP1. *PLoS Biol,* 9**,** e1000612.

MERRILL, R. A., SLUPE, A. M. & STRACK, S. 2012. N-terminal phosphorylation of protein phosphatase 2A/Bβ2 regulates translocation to mitochondria, dynamin-related protein 1 dephosphorylation, and neuronal survival. *FEBS J*.

MEZENCEV, R., UPDEGROVE, T., KUTSCHY, P., REPOVSKÁ, M. & MCDONALD, J. F. 2011. Camalexin induces apoptosis in T-leukemia Jurkat cells by increased concentration of reactive oxygen species and activation of caspase-8 and caspase-9. *J Nat Med,* 65**,** 488-99.

MIGNARRI, A., TESSA, A., CARLUCCIO, M. A., RUFA, A., STORTI, E., BONELLI, G., MARCOTULLI, C., SANTORELLI, F. M., LEONARDI, L., CASALI, C., FEDERICO, A. & DOTTI, M. T. 2014. Cerebellum and neuropsychiatric disorders: insights from ARSACS. *Neurol Sci,* 35**,** 95-7.

MILAKOVIC, T. & JOHNSON, G. V. 2005. Mitochondrial respiration and ATP production are significantly impaired in striatal cells expressing mutant huntingtin. *J Biol Chem,* 280**,** 30773-82.

MIYATAKE, S., MIYAKE, N., DOI, H., SAITSU, H., OGATA, K., KAWAI, M. & MATSUMOTO, N. 2012. A Novel SACS Mutation in an Atypical Case with Autosomal Recessive Spastic Ataxia of Charlevoix-Saguenay (ARSACS). *Intern Med,* 51**,** 2221-6.

MONTESSUIT, S., SOMASEKHARAN, S. P., TERRONES, O., LUCKEN-ARDJOMANDE, S., HERZIG, S., SCHWARZENBACHER, R., MANSTEIN, D. J., BOSSY-WETZEL, E., BASAÑEZ, G., MEDA, P. & MARTINOU, J. C. 2010. Membrane remodeling induced by the dynamin-related protein Drp1 stimulates Bax oligomerization. *Cell,* 142**,** 889-901.

MORAIS, V. A., VERSTREKEN, P., ROETHIG, A., SMET, J., SNELLINX, A., VANBRABANT, M., HADDAD, D., FREZZA, C., MANDEMAKERS, W., VOGT-WEISENHORN, D., VAN COSTER, R., WURST, W., SCORRANO, L. & DE STROOPER, B. 2009. Parkinson's disease mutations in PINK1 result in decreased Complex I activity and deficient synaptic function. *EMBO Mol Med,* 1**,** 99-111.

MORRIS, R. L. & HOLLENBECK, P. J. 1995. Axonal transport of mitochondria along microtubules and F-actin in living vertebrate neurons. *J Cell Biol,* 131**,** 1315-26.

MORTIBOYS, H., THOMAS, K. J., KOOPMAN, W. J., KLAFFKE, S., ABOU-SLEIMAN, P., OLPIN, S., WOOD, N. W., WILLEMS, P. H., SMEITINK, J. A., COOKSON, M. R. & BANDMANN, O. 2008. Mitochondrial function and morphology are impaired in parkin-mutant fibroblasts. *Ann Neurol,* 64**,** 555-65.

MOSELEY, M. L., ZU, T., IKEDA, Y., GAO, W., MOSEMILLER, A. K., DAUGHTERS, R. S., CHEN, G., WEATHERSPOON, M. R., CLARK, H. B., EBNER, T. J., DAY, J. W. & RANUM, L. P. 2006. Bidirectional expression of CUG and CAG expansion transcripts and intranuclear polyglutamine inclusions in spinocerebellar ataxia type 8. *Nat Genet,* 38**,** 758-69.

MOTLEY, A. M. & HETTEMA, E. H. 2007. Yeast peroxisomes multiply by growth and division. *J Cell Biol,* 178**,** 399-410.

MOYES, C. D. & HOOD, D. A. 2003. Origins and consequences of mitochondrial variation in vertebrate muscle. *Annu Rev Physiol,* 65**,** 177-201.

MUKHOPADHYAY, P., RAJESH, M., YOSHIHIRO, K., HASKÓ, G. & PACHER, P. 2007. Simple quantitative detection of mitochondrial superoxide production in live cells. *Biochem Biophys Res Commun,* 358**,** 203-8.

MURPHY, S. M., HERRMANN, D. N., MCDERMOTT, M. P., SCHERER, S. S., SHY, M. E., REILLY, M. M. & PAREYSON, D. 2011. Reliability of the CMT neuropathy score (second version) in Charcot-Marie-Tooth disease. *J Peripher Nerv Syst,* 16**,** 191-8.

MÜHLENHOFF, U., RICHHARDT, N., RISTOW, M., KISPAL, G. & LILL, R. 2002. The yeast frataxin homolog Yfh1p plays a specific role in the maturation of cellular Fe/S proteins. *Hum Mol Genet,* 11**,** 2025-36.

NAKAMURA, T. & LIPTON, S. A. 2011. S-nitrosylation of critical protein thiols mediates protein misfolding and mitochondrial dysfunction in neurodegenerative diseases. *Antioxid Redox Signal,* 14**,** 1479-92.

NARENDRA, D. P., JIN, S. M., TANAKA, A., SUEN, D. F., GAUTIER, C. A., SHEN, J., COOKSON, M. R. & YOULE, R. J. 2010. PINK1 is selectively stabilized on impaired mitochondria to activate Parkin. *PLoS Biol,* 8**,** e1000298.

NAYLOR, K., INGERMAN, E., OKREGLAK, V., MARINO, M., HINSHAW, J. E. & NUNNARI, J. 2006. Mdv1 interacts with assembled dnm1 to promote mitochondrial division. *J Biol Chem,* 281**,** 2177-83.

NIEMANN, A. 2005. Ganglioside-induced differentiation associated protein 1 is a regulator of the mitochondrial network: new implications for Charcot-Marie-Tooth disease. *The Journal of Cell Biology,* 170**,** 1067-1078.

NUNNARI, J. & SUOMALAINEN, A. 2012. Mitochondria: in sickness and in health. *Cell,* 148**,** 1145-59.

NUNOMURA, A., PERRY, G., ALIEV, G., HIRAI, K., TAKEDA, A., BALRAJ, E. K., JONES, P. K., GHANBARI, H., WATAYA, T., SHIMOHAMA, S., CHIBA, S., ATWOOD, C. S., PETERSEN, R. B. & SMITH, M. A. 2001. Oxidative damage is the earliest event in Alzheimer disease. *J Neuropathol Exp Neurol,* 60**,** 759-67.

O'HEARN, E., HOLMES, S. E. & MARGOLIS, R. L. 2012. Spinocerebellar ataxia type 12. *Handb Clin Neurol,* 103**,** 535-47.

OGAWA, T., TAKIYAMA, Y., SAKOE, K., MORI, K., NAMEKAWA, M., SHIMAZAKI, H., NAKANO, I. & NISHIZAWA, M. 2004a. Identification of a SACS gene missense mutation in ARSACS. *Neurology,* 62**,** 107-109.

OGAWA, T., TAKIYAMA, Y., SAKOE, K., MORI, K., NAMEKAWA, M., SHIMAZAKI, H., NAKANO, I. & NISHIZAWA, M. 2004b. Identification of a SACS gene missense mutation in ARSACS. *Neurology,* 62**,** 107-9.

OKATSU, K., SAISHO, K., SHIMANUKI, M., NAKADA, K., SHITARA, H., SOU, Y. S., KIMURA, M., SATO, S., HATTORI, N., KOMATSU, M., TANAKA, K. & MATSUDA, N. 2010. p62/SQSTM1 cooperates with Parkin for perinuclear clustering of depolarized mitochondria. *Genes Cells,* 15**,** 887-900.

OKAWA, S., SUGAWARA, M., WATANABE, S., IMOTA, T. & TOYOSHIMA, I. 2006. A novel sacsin mutation in a Japanese woman showing clinical uniformity of autosomal recessive spastic ataxia of Charlevoix-Saguenay. *J Neurol Neurosurg Psychiatry,* 77**,** 280-2.

OKUNO, Y., NAKAMURA-ISHIZU, A., OTSU, K., SUDA, T. & KUBOTA, Y. 2012. Pathological neoangiogenesis depends on oxidative stress regulation by ATM. *Nat Med,* 18**,** 1208-16.

OLICHON, A., BARICAULT, L., GAS, N., GUILLOU, E., VALETTE, A., BELENGUER, P. & LENAERS, G. 2003. Loss of OPA1 perturbates the mitochondrial inner membrane structure and integrity, leading to cytochrome c release and apoptosis. *J Biol Chem,* 278**,** 7743-6.

OSBORN, M. J., STARKER, C. G., MCELROY, A. N., WEBBER, B. R., RIDDLE, M. J., XIA, L., DEFEO, A. P., GABRIEL, R., SCHMIDT, M., VON KALLE, C., CARLSON, D. F., MAEDER, M. L., JOUNG, J. K., WAGNER, J. E., VOYTAS, D. F., BLAZAR, B. R. & TOLAR, J. 2013. TALEN-based gene correction for epidermolysis bullosa. *Mol Ther,* 21**,** 1151-9.

OTERA, H., WANG, C., CLELAND, M. M., SETOGUCHI, K., YOKOTA, S., YOULE, R. J. & MIHARA, K. 2010. Mff is an essential factor for mitochondrial recruitment of Drp1 during mitochondrial fission in mammalian cells. *J Cell Biol,* 191**,** 1141-58.

OUSTEROUT, D. G., PEREZ-PINERA, P., THAKORE, P. I., KABADI, A. M., BROWN, M. T., QIN, X., FEDRIGO, O., MOULY, V., TREMBLAY, J. P. & GERSBACH, C. A. 2013. Reading frame correction by targeted genome editing restores dystrophin expression in cells from Duchenne muscular dystrophy patients. *Mol Ther,* 21**,** 1718-26.

OUYANG, Y., SEGERS, K., BOUQUIAUX, O., WANG, F. C., JANIN, N., ANDRIS, C., SHIMAZAKI, H., SAKOE, K., NAKANO, I. & TAKIYAMA, Y. 2008. Novel SACS mutation in a Belgian family with sacsin-related ataxia. *J Neurol Sci,* 264**,** 73-6.

OUYANG, Y., TAKIYAMA, Y., SAKOE, K., SHIMAZAKI, H., OGAWA, T., NAGANO, S., YAMAMOTO, Y. & NAKANO, I. 2006. Sacsin-related ataxia (ARSACS): expanding the genotype upstream from the gigantic exon. *Neurology,* 66**,** 1103-1104.

PACELLI, C., DE RASMO, D., SIGNORILE, A., GRATTAGLIANO, I., DI TULLIO, G., D'ORAZIO, A., NICO, B., COMI, G. P., RONCHI, D., FERRANINI, E., PIROLO, D., SEIBEL, P., SCHUBERT, S., GABALLO, A., VILLANI, G. & COCCO, T. 2011. Mitochondrial defect and PGC-1α dysfunction in parkin-associated familial Parkinson's disease. *Biochim Biophys Acta,* 1812**,** 1041-53.

PAGON, R. A., BIRD, T. D., DETTER, J. C. & PIERCE, I. 1985. Hereditary sideroblastic anaemia and ataxia: an X linked recessive disorder. *J Med Genet,* 22**,** 267-73.

PALAU, F. & ESPINÓS, C. 2006. Autosomal recessive cerebellar ataxias. *Orphanet Journal of Rare Diseases,* 1**,** 47.

PALMER, C. S., ELGASS, K. D., PARTON, R. G., OSELLAME, L. D., STOJANOVSKI, D. & RYAN, M. T. 2013. Adaptor Proteins MiD49 and MiD51 Can Act Independently of Mff and Fis1 in Drp1 Recruitment and Are Specific for Mitochondrial Fission. *J Biol Chem,* 288**,** 27584-93.

PALMER, C. S., OSELLAME, L. D., LAINE, D., KOUTSOPOULOS, O. S., FRAZIER, A. E. & RYAN, M. T. 2011a. MiD49 and MiD51, new components of the mitochondrial fission machinery. *EMBO Rep,* 12**,** 565-73.

PALMER, C. S., OSELLAME, L. D., LAINE, D., KOUTSOPOULOS, O. S., FRAZIER, A. E. & RYAN, M. T. 2011b. MiD49 and MiD51, new components of the mitochondrial fission machinery. *EMBO Rep,* 12**,** 565-73.

PALMER, C. S., OSELLAME, L. D., STOJANOVSKI, D. & RYAN, M. T. 2011c. The regulation of mitochondrial morphology: Intricate mechanisms and dynamic machinery. *Cellular Signalling,* 23**,** 1534-1545.

PAPP, J. & DORSEY, S. T. 2009. A preschool-age child with first-time seizure and ataxia. *J Emerg Med,* 36**,** 30-3.

PARFITT, D. A., MICHAEL, G. J., VERMEULEN, E. G., PRODROMOU, N. V., WEBB, T. R., GALLO, J. M., CHEETHAM, M. E., NICOLL, W. S., BLATCH, G. L. & CHAPPLE, J. P. 2009. The ataxia protein sacsin is a functional co-chaperone that protects against polyglutamine-expanded ataxin-1. *Hum Mol Genet,* 18**,** 1556-65.

PARONE, P. A., JAMES, D. I., DA CRUZ, S., MATTENBERGER, Y., DONZÉ, O., BARJA, F. & MARTINOU, J. C. 2006. Inhibiting the mitochondrial fission machinery does not prevent Bax/Bak-dependent apoptosis. *Mol Cell Biol,* 26**,** 7397-408.

PEDERSEN, L. C., BENNING, M. M. & HOLDEN, H. M. 1995. Structural investigation of the antibiotic and ATP-binding sites in kanamycin nucleotidyltransferase. *Biochemistry,* 34**,** 13305-11.

PERIER, C., BOVÉ, J., WU, D. C., DEHAY, B., CHOI, D. K., JACKSON-LEWIS, V., RATHKE-HARTLIEB, S., BOUILLET, P., STRASSER, A., SCHULZ, J. B., PRZEDBORSKI, S. & VILA, M. 2007. Two molecular pathways initiate mitochondria-dependent dopaminergic neurodegeneration in experimental Parkinson's disease. *Proc Natl Acad Sci U S A,* 104**,** 8161-6.

PFEIFFER, T., SCHUSTER, S. & BONHOEFFER, S. 2001. Cooperation and competition in the evolution of ATP-producing pathways. *Science,* 292**,** 504-7.

PINTON, P., FERRARI, D., RAPIZZI, E., DI VIRGILIO, F., POZZAN, T. & RIZZUTO, R. 2001. The Ca2+ concentration of the endoplasmic reticulum is a key determinant of ceramide-induced apoptosis: significance for the molecular mechanism of Bcl-2 action. *EMBO J,* 20**,** 2690-701.

POYTON, R. O. & MCEWEN, J. E. 1996. Crosstalk between nuclear and mitochondrial genomes. *Annu Rev Biochem,* 65**,** 563-607.

PRAEFCKE, G. J. & MCMAHON, H. T. 2004. The dynamin superfamily: universal membrane tubulation and fission molecules? *Nat Rev Mol Cell Biol,* 5**,** 133-47.

PRATICÒ, D., URYU, K., LEIGHT, S., TROJANOSWKI, J. Q. & LEE, V. M. 2001. Increased lipid peroxidation precedes amyloid plaque formation in an animal model of Alzheimer amyloidosis. *J Neurosci,* 21**,** 4183-7.

PRODI, E., GRISOLI, M., PANZERI, M., MINATI, L., FATTORI, F., ERBETTA, A., UZIEL, G., D'ARRIGO, S., TESSA, A., CIANO, C., SANTORELLI, F. M., SAVOIARDO, M. & MARIOTTI, C. 2012. Supratentorial and pontine MRI abnormalities characterize recessive spastic ataxia of Charlevoix-Saguenay. A comprehensive study of an Italian series. *Eur J Neurol*.

PUIGSERVER, P., RHEE, J., LIN, J., WU, Z., YOON, J. C., ZHANG, C. Y., KRAUSS, S., MOOTHA, V. K., LOWELL, B. B. & SPIEGELMAN, B. M. 2001. Cytokine stimulation of energy expenditure through p38 MAP kinase activation of PPARgamma coactivator-1. *Mol Cell,* 8**,** 971-82.

PUIGSERVER, P. & SPIEGELMAN, B. M. 2003. Peroxisome proliferator-activated receptor-gamma coactivator 1 alpha (PGC-1 alpha): transcriptional coactivator and metabolic regulator. *Endocr Rev,* 24**,** 78-90.

PYLE, A., GRIFFIN, H., DUFF, J., BENNETT, S., ZWOLINSKI, S., SMERTENKO, T., YU-WAI MAN, P., SANTIBANEZ-KOREF, M., HORVATH, R. & CHINNERY, P. F. 2013. Late-onset sacsinopathy diagnosed by exome sequencing and comparative genomic hybridization. *J Neurogenet,* 27**,** 176-82.

PYLE, A., GRIFFIN, H., YU-WAI-MAN, P., DUFF, J., EGLON, G., PICKERING-BROWN, S., SANTIBANEZ-KOREV, M., HORVATH, R. & CHINNERY, P. F. 2012. Prominent Sensorimotor Neuropathy Due to SACS Mutations Revealed by Whole-Exome Sequencing. *Arch Neurol***,** 1-4.

QI, X., QVIT, N., SU, Y. C. & MOCHLY-ROSEN, D. 2013. A novel Drp1 inhibitor diminishes aberrant mitochondrial fission and neurotoxicity. *J Cell Sci,* 126**,** 789-802.

QIAN, W., CHOI, S., GIBSON, G. A., WATKINS, S. C., BAKKENIST, C. J. & VAN HOUTEN, B. 2012. Mitochondrial hyperfusion induced by loss of the fission protein Drp1 causes ATM-dependent G2/M arrest and aneuploidy through DNA replication stress. *J Cell Sci,* 125**,** 5745-57.

RAFELSKI, S. M., VIANA, M. P., ZHANG, Y., CHAN, Y. H., THORN, K. S., YAM, P., FUNG, J. C., LI, H., COSTA, L. A. F. & MARSHALL, W. F. 2012. Mitochondrial network size scaling in budding yeast. *Science,* 338**,** 822-4.

RAHMAN, S. & LEONARD, V. 1997. Mitochondrial disorders. *Current Paediatrics,* 7**,** 123-127.

RANUM, L. P., LUNDGREN, J. K., SCHUT, L. J., AHRENS, M. J., PERLMAN, S., AITA, J., BIRD, T. D., GOMEZ, C. & ORR, H. T. 1995. Spinocerebellar ataxia type 1 and Machado-Joseph disease: incidence of CAG expansions among adult-onset ataxia patients from 311 families with dominant, recessive, or sporadic ataxia. *Am J Hum Genet,* 57**,** 603-8.

REGMI, S. G., ROLLAND, S. G. & AND CONRADT, B. 2014. Age-dependent changes in mitochondrial morphology and volume are not predictors of lifespan. *Aging,* 6**,** 118-130.

RICHTER A, MORGAN K, BOUCHARD J-P, MATHIEU J, LAMARCHE J, RIOUX J, HUDSON T & SB, M. O. 1996. ARSACS: possibly a lysosomal storage

disease? (abstract). *American Journal of Human Genetics,* 59**,** A379.

RICHTER, A., MORGAN, K., BOUCHARD, J. P., POIRIER, J., MERCIER, J., GOSSELIN, F. & MELANÇON, S. B. 1993. Clinical and molecular genetic studies on autosomal recessive spastic ataxia of Charlevoix-Saguenay (ARSACS). *Adv Neurol,* 61**,** 97-103.

RICHTER, A., RIOUX, J. D., BOUCHARD, J. P., MERCIER, J., MATHIEU, J., GE, B., POIRIER, J., JULIEN, D., GYAPAY, G., WEISSENBACH, J., HUDSON, T. J., MELANÇON, S. B. & MORGAN, K. 1999. Location score and haplotype analyses of the locus for autosomal recessive spastic ataxia of Charlevoix-Saguenay, in chromosome region 13q11. *Am J Hum Genet,* 64**,** 768-75.

RICHTER, A. M., OZGUL, R. K., POISSON, V. C. & TOPALOGLU, H. 2004. Private SACS mutations in autosomal recessive spastic ataxia of Charlevoix-Saguenay (ARSACS) families from Turkey. *Neurogenetics,* 5**,** 165-70.

RICHTER, V., PALMER, C. S., OSELLAME, L. D., SINGH, A. P., ELGASS, K., STROUD, D. A., SESAKI, H., KVANSAKUL, M. & RYAN, M. T. 2014. Structural and functional analysis of MiD51, a dynamin receptor required for mitochondrial fission. *J Cell Biol,* 204**,** 477-86.

RISTOW, M., PFISTER, M. F., YEE, A. J., SCHUBERT, M., MICHAEL, L., ZHANG, C. Y., UEKI, K., MICHAEL, M. D., LOWELL, B. B. & KAHN, C. R. 2000. Frataxin activates mitochondrial

energy conversion and oxidative phosphorylation. *Proc Natl Acad Sci U S A,* 97**,** 12239-43.

RIZZUTO, R., DUCHEN, M. R. & POZZAN, T. 2004. Flirting in little space: the ER/mitochondria Ca2+ liaison. *Sci STKE,* 2004**,** re1.

RIZZUTO, R., PINTON, P., CARRINGTON, W., FAY, F. S., FOGARTY, K. E., LIFSHITZ, L. M., TUFT, R. A. & POZZAN, T. 1998. Close contacts with the endoplasmic reticulum as determinants of mitochondrial Ca2+ responses. *Science,* 280**,** 1763-6.

ROMANO, A., TESSA, A., BARCA, A., FATTORI, F., DE LEVA, M. F., TERRACCIANO, A., STORELLI, C., SANTORELLI, F. M. & VERRI, T. 2013. Comparative analysis and functional mapping of SACS mutations reveal novel insights into sacsin repeated architecture. *Hum Mutat,* 34**,** 525-37.

ROWLAND, A. A. & VOELTZ, G. K. 2012. Endoplasmic reticulum-mitochondria contacts: function of the junction. *Nat Rev Mol Cell Biol,* 13**,** 607-25.

RÖTIG, A., DE LONLAY, P., CHRETIEN, D., FOURY, F., KOENIG, M., SIDI, D., MUNNICH, A. & RUSTIN, P. 1997a. Aconitase and mitochondrial iron-sulphur protein deficiency in Friedreich ataxia. *Nat Genet,* 17**,** 215-7.

RÖTIG, A., DE LONLAY, P., CHRETIEN, D., FOURY, F., KOENIG, M., SIDI, D., MUNNICH, A. & RUSTIN, P. 1997b. Aconitase and mitochondrial iron-sulphur protein deficiency in Friedreich ataxia. *Nat Genet,* 17**,** 215-7.

SANDYK, R. & BRENNAN, M. J. 1984. Meningococcal meningitis presenting with bilateral deafness and ataxia. *Postgrad Med J,* 60**,** 668-9.

SCHAUBER, C., CHEN, L., TONGAONKAR, P., VEGA, I., LAMBERTSON, D., POTTS, W. & MADURA, K. 1998. Rad23 links DNA repair to the ubiquitin/proteasome pathway. *Nature,* 391**,** 715-8.

SCHAUSS, A. C., HUANG, H., CHOI, S.-Y., XU, L., SOUBEYR, S., BILODEAU, P., ZUNINO, R., RIPPSTEIN, P., FROHMAN, M. A., MCBRIDE, H. M. & SOUBEYRAND, S. 2010. A novel cell-free mitochondrial fusion assay amenable for high-throughput screenings of fusion modulators. *BMC Biology,* 8**,** 100.

SCHMITZ-HÜBSCH, T., DU MONTCEL, S. T., BALIKO, L., BERCIANO, J., BOESCH, S., DEPONDT, C., GIUNTI, P., GLOBAS, C., INFANTE, J., KANG, J. S., KREMER, B., MARIOTTI, C., MELEGH, B., PANDOLFO, M., RAKOWICZ, M., RIBAI, P., ROLA, R., SCHÖLS, L., SZYMANSKI, S., VAN DE WARRENBURG, B. P., DÜRR, A., KLOCKGETHER, T. & FANCELLU, R. 2006. Scale for the assessment and rating of ataxia: development of a new clinical scale. *Neurology,* 66**,** 1717-20.

SCHON, E. A. & AREA-GOMEZ, E. 2013. Mitochondria-associated ER membranes in Alzheimer disease. *Mol Cell Neurosci,* 55**,** 26-36.

SCHRADER, M., BONEKAMP, N. A. & ISLINGER, M. 2012. Fission and proliferation of peroxisomes. *Biochim Biophys Acta,* 1822**,** 1343-57.

SCHRADER, M. & FAHIMI, H. D. 2006. Peroxisomes and oxidative stress. *Biochim Biophys Acta,* 1763**,** 1755-66.

SCHRADER, M., GRILLE, S., FAHIMI, H. D. & ISLINGER, M. 2013. Peroxisome interactions and cross-talk with other subcellular compartments in animal cells. *Subcell Biochem,* 69**,** 1-22.

SCHULDT, A. 2011. Membrane dynamics: ER marks the spot. *Nat Rev Mol Cell Biol,* 12**,** 627.

SCHULZ, J. B., DEHMER, T., SCHÖLS, L., MENDE, H., HARDT, C., VORGERD, M., BÜRK, K., MATSON, W., DICHGANS, J., BEAL, M. F. & BOGDANOV, M. B. 2000. Oxidative stress in patients with Friedreich ataxia. *Neurology,* 55**,** 1719-21.

SCHUMACHER, M. M., CHOI, J. Y. & VOELKER, D. R. 2002. Phosphatidylserine transport to the mitochondria is regulated by ubiquitination. *J Biol Chem,* 277**,** 51033-42.

SCHÖLS, L., AMOIRIDIS, G., PRZUNTEK, H., FRANK, G., EPPLEN, J. T. & EPPLEN, C. 1997. Friedreich's ataxia. Revision of the phenotype according to molecular genetics. *Brain,* 120 (Pt 12)**,** 2131-40.

SCHÜLE, R., HOLLAND-LETZ, T., KLIMPE, S., KASSUBEK, J., KLOPSTOCK, T., MALL, V., OTTO, S., WINNER, B. & SCHÖLS, L. 2006. The Spastic Paraplegia Rating Scale (SPRS): a reliable and valid measure of disease severity. *Neurology,* 67**,** 430-4.

SENA, L. A., LI, S., JAIRAMAN, A., PRAKRIYA, M., EZPONDA, T., HILDEMAN, D. A., WANG, C. R., SCHUMACKER, P. T., LICHT, J. D., PERLMAN, H., BRYCE, P. J. & CHANDEL, N. S. 2013. Mitochondria are required for antigen-specific T cell activation through reactive oxygen species signaling. *Immunity,* 38**,** 225-36.

SEO, A. Y., JOSEPH, A. M., DUTTA, D., HWANG, J. C., ARIS, J. P. & LEEUWENBURGH, C. 2010. New insights into the role of mitochondria in aging: mitochondrial dynamics and more. *J Cell Sci,* 123**,** 2533-42.

SHAW, J. M. & NUNNARI, J. 2002. Mitochondrial dynamics and division in budding yeast. *Trends Cell Biol,* 12**,** 178-84.

SHIMAZAKI, H., SAKOE, K., NIIJIMA, K., NAKANO, I. & TAKIYAMA, Y. 2007a. An unusual case of a spasticity-lacking phenotype with a novel SACS mutation. *Journal of the Neurological Sciences,* 255**,** 87-89.

SHIMAZAKI, H., SAKOE, K., NIIJIMA, K., NAKANO, I. & TAKIYAMA, Y. 2007b. An unusual case of a spasticity-lacking phenotype with a novel SACS mutation. *J Neurol Sci,* 255**,** 87-9.

SHIMAZAKI, H., TAKIYAMA, Y., HONDA, J., SAKOE, K., NAMEKAWA, M., TSUGAWA, J., TSUBOI, Y., SUZUKI, C., BABA, M. & NAKANO, I. 2012. Middle Cerebellar Peduncles and Pontine T2 Hypointensities in ARSACS. *J Neuroimaging*.

SHIMAZAKI, H., TAKIYAMA, Y., SAKOE, K., ANDO, Y. & NAKANO, I. 2005a. A phenotype without spasticity in sacsin-related ataxia. *Neurology,* 64**,** 2129-2131.

SHIMAZAKI, H., TAKIYAMA, Y., SAKOE, K., ANDO, Y. & NAKANO, I. 2005b. A phenotype without spasticity in sacsin-related ataxia. *Neurology,* 64**,** 2129-31.

SIDDIQUI, A., RIVERA-SÁNCHEZ, S., CASTRO, M. E. R., ACEVEDO-TORRES, K., RANE, A., TORRES-RAMOS, C. A., NICHOLLS, D. G., ANDERSEN, J. K. & AYALA-TORRES, S. 2012. Mitochondrial DNA damage is associated with reduced mitochondrial bioenergetics in Huntington's disease. *Free Radic Biol Med,* 53**,** 1478-88.

SIMMEN, T., ASLAN, J. E., BLAGOVESHCHENSKAYA, A. D., THOMAS, L., WAN, L., XIANG, Y., FELICIANGELI, S. F., HUNG, C. H., CRUMP, C. M. & THOMAS, G. 2005. PACS-2 controls endoplasmic reticulum-mitochondria communication and Bid-mediated apoptosis. *EMBO J,* 24**,** 717-29.

SMIRNOVA, E., GRIPARIC, L. & SHURLAND, D. L. 2001. Dynamin-related protein Drp1 is required for mitochondrial division in mammalian cells. *Molecular biology of*.

SMIRNOVA, E., SHURLAND, D. L., RYAZANTSEV, S. N. & VAN DER BLIEK, A. M. 1998. A human dynamin-related protein controls the distribution of mitochondria. *J Cell Biol,* 143**,** 351-8.

SOMPOL, P., ITTARAT, W., TANGPONG, J., CHEN, Y., DOUBINSKAIA, I., BATINIC-HABERLE, I., ABDUL, H. M., BUTTERFIELD, D. A. & ST CLAIR, D. K. 2008. A neuronal model of Alzheimer's disease: an insight into the mechanisms of oxidative stress-mediated mitochondrial injury. *Neuroscience,* 153**,** 120-30.

STEVENS, J. C., MURPHY, S. M., DAVAGNANAM, I., PHADKE, R., ANDERSON, G., NETHISINGHE, S., BREMNER, F., GIUNTI, P. & REILLY, M. M. 2013. The ARSACS phenotype can include supranuclear gaze palsy and skin lipofuscin deposits. *J Neurol Neurosurg Psychiatry,* 84**,** 114-6.

STONE, S. J. & VANCE, J. E. 2000. Phosphatidylserine synthase-1 and -2 are localized to mitochondria-associated membranes. *J Biol Chem,* 275**,** 34534-40.

STOWERS, R. S., MEGEATH, L. J., GÓRSKA-ANDRZEJAK, J., MEINERTZHAGEN, I. A. & SCHWARZ, T. L. 2002. Axonal transport of mitochondria to synapses depends on milton, a novel Drosophila protein. *Neuron,* 36**,** 1063-77.

STRACK, S., STRACK, S. & CRIBBS, J. T. 2012. Allosteric Modulation of Drp1 Mechanoenzyme Assembly and Mitochondrial Fission by the Variable Domain. *Journal of Biological Chemistry,* 287**,** 10990-11001.

SUGASAWA, K., NG, J. M., MASUTANI, C., IWAI, S., VAN DER SPEK, P. J., EKER, A. P., HANAOKA, F., BOOTSMA, D. & HOEIJMAKERS, J. H. 1998. Xeroderma pigmentosum group C protein complex is the initiator of global genome nucleotide excision repair. *Mol Cell,* 2**,** 223-32.

SUNDARESAN, M., YU, Z. X., FERRANS, V. J., IRANI, K. & FINKEL, T. 1995. Requirement for generation of H2O2 for platelet-derived growth factor signal transduction. *Science,* 270**,** 296-9.

SUZUKI, M., JEONG, S. Y., KARBOWSKI, M., YOULE, R. J. & TJANDRA, N. 2003. The solution structure of human mitochondria fission protein Fis1 reveals a novel TPR-like helix bundle. *J Mol Biol,* 334**,** 445-58.

SWIFT, M., MORRELL, D., CROMARTIE, E., CHAMBERLIN, A. R., SKOLNICK, M. H. & BISHOP, D. T. 1986. The incidence and gene frequency of ataxia-telangiectasia in the United States. *Am J Hum Genet,* 39**,** 573-83.

SWIFT, M., MORRELL, D., MASSEY, R. B. & CHASE, C. L. 1991. Incidence of cancer in 161 families affected by ataxia-telangiectasia. *N Engl J Med,* 325**,** 1831-6.

SYNOFZIK, M., SOEHN, A. S., GBUREK-AUGUSTAT, J., SCHICKS, J., KARLE, K. N., SCHÜLE, R., HAACK, T. B., SCHÖNING, M., BISKUP, S., RUDNIK-SCHÖNEBORN, S., SENDEREK, J., HOFFMANN, K. T., MACLEOD, P., SCHWARZ, J., BENDER, B., KRÜGER, S., KREUZ, F., BAUER, P. & SCHÖLS, L. 2013. Autosomal recessive spastic ataxia of Charlevoix Saguenay (ARSACS): expanding the genetic, clinical and imaging spectrum. *Orphanet J Rare Dis,* 8**,** 41.

SZABADKAI, G., BIANCHI, K., VÁRNAI, P., DE STEFANI, D., WIECKOWSKI, M. R., CAVAGNA, D., NAGY, A. I., BALLA, T. & RIZZUTO, R. 2006. Chaperone-mediated coupling of endoplasmic reticulum and mitochondrial Ca2+ channels. *J Cell Biol,* 175**,** 901-11.

SZALAI, G., KRISHNAMURTHY, R. & HAJNÓCZKY, G. 1999. Apoptosis driven by IP(3)-linked mitochondrial calcium signals. *EMBO J,* 18**,** 6349-61.

TAKADO, Y., HARA, K., SHIMOHATA, T., TOKIGUCHI, S., ONODERA, O. & NISHIZAWA, M. 2007. New mutation in the non-gigantic exon of SACS in Japanese siblings. *Mov Disord,* 22**,** 748-9.

TAKIYAMA, Y. 2006. Autosomal recessive spastic ataxia of Charlevoix-Saguenay. *Neuropathology,* 26**,** 368-75.

TANAKA, Y., KANAI, Y., OKADA, Y., NONAKA, S., TAKEDA, S., HARADA, A. & HIROKAWA, N. 1998. Targeted disruption of mouse conventional kinesin heavy chain, kif5B, results in abnormal perinuclear clustering of mitochondria. *Cell,* 93**,** 1147-58.

TERRACCIANO, A., CASALI, C., GRIECO, G. S., ORTESCHI, D., DI GIANDOMENICO, S., SEMINARA, L., DI FABIO, R., CARROZZO, R., SIMONATI, A., STEVANIN, G., ZOLLINO, M. & SANTORELLI, F. M. 2009. An inherited large-scale rearrangement in SACS associated with spastic ataxia and hearing loss. *Neurogenetics,* 10**,** 151-5.

TERRACCIANO, A., FOULDS, N. C., DITCHFIELD, A., BUNYAN, D. J., CROLLA, J. A., HUANG, S., SANTORELLI, F. M. & HAMMANS, S. R. 2010. Pseudodominant inheritance of spastic ataxia of Charlevoix-Saguenay. *Neurology,* 74**,** 1152-4.

THIFFAULT, I., DICAIRE, M. J., TETREAULT, M., HUANG, K. N., DEMERS-LAMARCHE, J., BERNARD, G., DUQUETTE, A., LARIVIÈRE, R., GEHRING, K., MONTPETIT, A., MCPHERSON, P. S., RICHTER, A., MONTERMINI, L., MERCIER, J., MITCHELL, G. A.,

DUPRÉ, N., PRÉVOST, C., BOUCHARD, J. P., MATHIEU, J. & BRAIS, B. 2013. Diversity of ARSACS mutations in French-Canadians. *Can J Neurol Sci,* 40**,** 61-6.

THORBURN, D. R. 2004. Mitochondrial disorders: prevalence, myths and advances. *J Inherit Metab Dis,* 27**,** 349-62.

TOBIUME, K., MATSUZAWA, A., TAKAHASHI, T., NISHITOH, H., MORITA, K., TAKEDA, K., MINOWA, O., MIYAZONO, K., NODA, T. & ICHIJO, H. 2001. ASK1 is required for sustained activations of JNK/p38 MAP kinases and apoptosis. *EMBO Rep,* 2**,** 222-8.

TODD, P. K. & PAULSON, H. L. 2010. RNA-mediated neurodegeneration in repeat expansion disorders. *Ann Neurol,* 67**,** 291-300.

TRUSHINA, E., DYER, R. B., BADGER, J. D., URE, D., EIDE, L., TRAN, D. D., VRIEZE, B. T., LEGENDRE-GUILLEMIN, V., MCPHERSON, P. S., MANDAVILLI, B. S., VAN HOUTEN, B., ZEITLIN, S., MCNIVEN, M., AEBERSOLD, R., HAYDEN, M., PARISI, J. E., SEEBERG, E., DRAGATSIS, I., DOYLE, K., BENDER, A., CHACKO, C. & MCMURRAY, C. T. 2004. Mutant huntingtin impairs axonal trafficking in mammalian neurons in vivo and in vitro. *Mol Cell Biol,* 24**,** 8195-209.

TURRENS, J. F. 2003. Mitochondrial formation of reactive oxygen species. *J Physiol,* 552**,** 335-44.

TWIG, G., ELORZA, A., MOLINA, A. J., MOHAMED, H., WIKSTROM, J. D., WALZER, G., STILES, L., HAIGH, S. E., KATZ, S., LAS, G., ALROY, J., WU, M., PY, B. F., YUAN, J., DEENEY, J. T., CORKEY, B. E. & SHIRIHAI, O. S. 2008a. Fission and selective fusion govern mitochondrial segregation and elimination by autophagy. *EMBO J,* 27**,** 433-46.

TWIG, G., HYDE, B. & SHIRIHAI, O. S. 2008b. Mitochondrial fusion, fission and autophagy as a quality control axis: the bioenergetic view. *Biochim Biophys Acta,* 1777**,** 1092-7.

TZOULIS, C., JOHANSSON, S., HAUKANES, B. I., BOMAN, H., KNAPPSKOG, P. M. & BINDOFF, L. A. 2013. Novel SACS mutations identified by whole exome sequencing in a norwegian family with autosomal recessive spastic ataxia of Charlevoix-Saguenay. *PLoS One,* 8**,** e66145.

UO, T., DWORZAK, J., KINOSHITA, C., INMAN, D. M., KINOSHITA, Y., HORNER, P. J. & MORRISON, R. S. 2009. Drp1 levels constitutively regulate mitochondrial dynamics and cell survival in cortical neurons. *Exp Neurol,* 218**,** 274-85.

VALENCIA, A., SAPP, E., KIMM, J. S., MCCLORY, H., REEVES, P. B., ALEXANDER, J., ANSONG, K. A., MASSO, N., FROSCH, M. P., KEGEL, K. B., LI, X. & DIFIGLIA, M. 2013. Elevated NADPH oxidase activity contributes to oxidative stress and cell death in Huntington's disease. *Hum Mol Genet,* 22**,** 1112-31.

VALENTIN-VEGA, Y. A., MACLEAN, K. H., TAIT-MULDER, J., MILASTA, S., STEEVES, M., DORSEY, F. C., CLEVELAND, J. L., GREEN, D. R. & KASTAN, M. B. 2012. Mitochondrial dysfunction in ataxia-telangiectasia. *Blood,* 119**,** 1490-500.

VAN DEN BOSCH, H., SCHUTGENS, R. B., WANDERS, R. J. & TAGER, J. M. 1992. Biochemistry of peroxisomes. *Annu Rev Biochem,* 61**,** 157-97.

VAN MEER, G., VOELKER, D. R. & FEIGENSON, G. W. 2008. Membrane lipids: where they are and how they behave. *Nat Rev Mol Cell Biol,* 9**,** 112-24.

VANCE, J. E. 1990. Phospholipid synthesis in a membrane fraction associated with mitochondria. *J Biol Chem,* 265**,** 7248-56.

VERHAGEN, M. M., ABDO, W. F., WILLEMSEN, M. A., HOGERVORST, F. B., SMEETS, D. F., HIEL, J. A., BRUNT, E. R., VAN RIJN, M. A., MAJOOR KRAKAUER, D., OLDENBURG, R. A., BROEKS, A., LAST, J. I., VAN'T VEER, L. J., TIJSSEN, M. A., DUBOIS, A. M., KREMER, H. P., WEEMAES, C. M., TAYLOR, A. M. & VAN DEUREN, M. 2009. Clinical spectrum of ataxia-telangiectasia in adulthood. *Neurology,* 73**,** 430-7.

VERHOEVEN, W. M., EGGER, J. I., AHMED, A. I., KREMER, B. P., VERMEER, S. & VAN DE WARRENBURG, B. P. 2012a. Cerebellar cognitive affective syndrome and autosomal

recessive spastic ataxia of charlevoix-saguenay: a report of two male sibs. *Psychopathology,* 45**,** 193-9.

VERHOEVEN, W. M., EGGER, J. I., AHMED, A. I., KREMER, B. P., VERMEER, S. & VAN DE WARRENBURG, B. P. 2012b. Cerebellar cognitive affective syndrome and autosomal recessive spastic ataxia of charlevoix-saguenay: a report of two male sibs. *Psychopathology,* 45**,** 193-9.

VERMEER, S., MEIJER, R. P., PIJL, B. J., TIMMERMANS, J., CRUYSBERG, J. R., BOS, M. M., SCHELHAAS, H. J., VAN DE WARRENBURG, B. P., KNOERS, N. V., SCHEFFER, H. & KREMER, B. 2008. ARSACS in the Dutch population: a frequent cause of early-onset cerebellar ataxia. *Neurogenetics,* 9**,** 207-14.

VERMEER, S., MEIJER, R. P. P., HOFSTE, T. G. J., BODMER, D., BOSGOED, E. A. J., CREMERS, F. P. M., KREMER, B. H. P., KNOERS, N. V. A. M., KNOERS, N. & SCHEFFER, H. 2009. Design and Validation of a Conformation Sensitive Capillary Electrophoresis-Based Mutation Scanning System and Automated Data Analysis of the More than 15 kbp-Spanning Coding Sequence of the SACS Gene. *The Journal of Molecular Diagnostics,* 11**,** 514-523.

VINGOLO, E. M., DI FABIO, R., SALVATORE, S., GRIECO, G., BERTINI, E., LEUZZI, V., NESTI, C., FILLA, A., TESSA, A., PIERELLI, F., SANTORELLI, F. M. & CASALI, C. 2011. Myelinated retinal fibers in autosomal recessive spastic ataxia of Charlevoix-Saguenay. *Eur J Neurol*.

VIRBASIUS, J. V. & SCARPULLA, R. C. 1994. Activation of the human mitochondrial transcription factor A gene by nuclear respiratory factors: a potential regulatory link between nuclear and mitochondrial gene expression in organelle biogenesis. *Proc Natl Acad Sci U S A,* 91**,** 1309-13.

VIVES-BAUZA, C., ZHOU, C., HUANG, Y., CUI, M., DE VRIES, R. L., KIM, J., MAY, J., TOCILESCU, M. A., LIU, W., KO, H. S., MAGRANÉ, J., MOORE, D. J., DAWSON, V. L., GRAILHE, R., DAWSON, T. M., LI, C., TIEU, K. & PRZEDBORSKI, S. 2010. PINK1-dependent recruitment of Parkin to mitochondria in mitophagy. *Proc Natl Acad Sci U S A,* 107**,** 378-83.

WAKABAYASHI, J., ZHANG, Z., WAKABAYASHI, N., TAMURA, Y., FUKAYA, M., KENSLER, T. W., IIJIMA, M. & SESAKI, H. 2009. The dynamin-related GTPase Drp1 is required for embryonic and brain development in mice. *J Cell Biol,* 186**,** 805-16.

WANG, X., SU, B., FUJIOKA, H. & ZHU, X. 2008. Dynamin-like protein 1 reduction underlies mitochondrial morphology and distribution abnormalities in fibroblasts from sporadic Alzheimer's disease patients. *Am J Pathol,* 173**,** 470-82.

WANG, X., SU, B., LEE, H. G., LI, X., PERRY, G., SMITH, M. A. & ZHU, X. 2009a. Impaired balance of mitochondrial fission and fusion in Alzheimer's disease. *J Neurosci,* 29**,** 9090-103.

WANG, X., SU, B., ZHENG, L., PERRY, G., SMITH, M. A. & ZHU, X. 2009b. The role of abnormal mitochondrial dynamics in the pathogenesis of Alzheimer's disease. *J Neurochem,* 109 Suppl 1**,** 153-9.

WANG, Y., NARTISS, Y., STEIPE, B., MCQUIBBAN, G. A. & KIM, P. K. 2012. ROS-induced mitochondrial depolarization initiates PARK2/PARKIN-dependent mitochondrial degradation by autophagy. *Autophagy,* 8**,** 1462-76.

WASIAK, S., ZUNINO, R. & MCBRIDE, H. M. 2007. Bax/Bak promote sumoylation of DRP1 and its stable association with mitochondria during apoptotic cell death. *J Cell Biol,* 177**,** 439-50.

WATERHAM, H. R., KOSTER, J., VAN ROERMUND, C. W., MOOYER, P. A., WANDERS, R. J. & LEONARD, J. V. 2007. A lethal defect of mitochondrial and peroxisomal fission. *N Engl J Med,* 356**,** 1736-41.

WEBER, J. T., RZIGALINSKI, B. A. & ELLIS, E. F. 2001. Traumatic injury of cortical neurons causes changes in intracellular calcium stores and capacitative calcium influx. *J Biol Chem,* 276**,** 1800-7.

WEIHOFEN, A., THOMAS, K. J., OSTASZEWSKI, B. L., COOKSON, M. R. & SELKOE, D. J. 2009. Pink1 forms a multiprotein complex with Miro and Milton, linking Pink1 function to mitochondrial trafficking. *Biochemistry,* 48**,** 2045-52.

WESTRATE, L. M., DROCCO, J. A., MARTIN, K. R., HLAVACEK, W. S. & MACKEIGAN, J. P. 2014. Mitochondrial morphological features are associated with fission and fusion events. *PLoS One,* 9**,** e95265.

WHITAKER, M. 2010. Genetically encoded probes for measurement of intracellular calcium. *Methods Cell Biol,* 99**,** 153-82.

WILLIAMS, A. J. & PAULSON, H. L. 2008. Polyglutamine neurodegeneration: protein misfolding revisited. *Trends Neurosci,* 31**,** 521-8.

WILSON, T. J., SLUPE, A. M. & STRACK, S. 2012. Cell signaling and mitochondrial dynamics: Implications for neuronal function and neurodegenerative disease. *Neurobiol Dis*.

WOLF, U., RAPOPORT, M. J. & SCHWEIZER, T. A. 2009. Evaluating the affective component of the cerebellar cognitive affective syndrome. *J Neuropsychiatry Clin Neurosci,* 21**,** 245-53.

WOOD-KACZMAR, A., GANDHI, S., YAO, Z., ABRAMOV, A. Y., ABRAMOV, A. S., MILJAN, E. A., KEEN, G., STANYER, L., HARGREAVES, I., KLUPSCH, K., DEAS, E., DOWNWARD, J., MANSFIELD, L., JAT, P., TAYLOR, J., HEALES, S., DUCHEN, M. R., LATCHMAN, D., TABRIZI, S. J. & WOOD, N. W. 2008. PINK1 is necessary for long term survival and mitochondrial function in human dopaminergic neurons. *PLoS One,* 3**,** e2455.

WU, Z., PUIGSERVER, P., ANDERSSON, U., ZHANG, C., ADELMANT, G., MOOTHA, V., TROY, A., CINTI, S., LOWELL, B., SCARPULLA, R. C. & SPIEGELMAN, B. M. 1999. Mechanisms controlling mitochondrial biogenesis and respiration through the thermogenic coactivator PGC-1. *Cell,* 98**,** 115-24.

YABEK, S. M. 1973. Meningococcal meningitis presenting as acute cerebellar ataxia. *Pediatrics,* 52**,** 718-20.

YAFFE, M. P. 1999. The machinery of mitochondrial inheritance and behavior. *Science,* 283**,** 1493-7.

YAMAMOTO, Y., HIRAOKA, K., ARAKI, M., NAGANO, S., SHIMAZAKI, H., TAKIYAMA, Y. & SAKODA, S. 2005. Novel compound heterozygous mutations in sacsin-related ataxia. *J Neurol Sci,* 239**,** 101-4.

YAMAMOTO, Y., NAKAMORI, M., KONAKA, K., NAGANO, S., SHIMAZAKI, H., TAKIYAMA, Y. & SAKODA, S. 2006. Sacsin-related ataxia caused by the novel nonsense mutation Arg4325X. *J Neurol,* 253**,** 1372-3.

YAO, J., IRWIN, R. W., ZHAO, L., NILSEN, J., HAMILTON, R. T. & BRINTON, R. D. 2009. Mitochondrial bioenergetic deficit precedes Alzheimer's pathology in female mouse model of Alzheimer's disease. *Proc Natl Acad Sci U S A,* 106**,** 14670-5.

YOULE, R. J. & NARENDRA, D. P. 2011. Mechanisms of mitophagy. *Nat Rev Mol Cell Biol,* 12**,** 9-14.

YU, Y. C., KUO, C. L., CHENG, W. L., LIU, C. S. & HSIEH, M. 2009. Decreased antioxidant enzyme activity and increased mitochondrial DNA damage in cellular models of Machado-Joseph disease. *J Neurosci Res,* 87**,** 1884-91.

YU-WAI-MAN, P., PYLE, A., GRIFFIN, H., SANTIBANEZ-KOREV, M., HORVATH, R. & CHINNERY, P. F. 2014. Abnormal retinal thickening is a common feature among patients with ARSACS-related phenotypes. *Br J Ophthalmol,* 98**,** 711-3.

ZAKIAN, V. A. 1995. ATM-related genes: what do they tell us about functions of the human gene? *Cell,* 82**,** 685-7.

ZAKO, T., DEGUCHI, H., KITAYAMA, A., UEDA, H. & NAGAMUNE, T. 2000. Refolding of firefly luciferase immobilized on agarose beads. *J Biochem,* 127**,** 351-4.

ZAMPESE, E., FASOLATO, C., KIPANYULA, M. J., BORTOLOZZI, M., POZZAN, T. & PIZZO, P. 2011. Presenilin 2 modulates endoplasmic reticulum (ER)-mitochondria interactions and Ca2+ cross-talk. *Proc Natl Acad Sci U S A,* 108**,** 2777-82.

ZHAO, J., LIU, T., JIN, S., WANG, X., QU, M., UHLÉN, P., TOMILIN, N., SHUPLIAKOV, O., LENDAHL, U. & NISTÉR, M. 2011. Human MIEF1 recruits Drp1 to mitochondrial outer membranes and promotes mitochondrial fusion rather than fission. *EMBO J,* 30**,** 2762-78.

ZUNINO, R., BRASCHI, E., XU, L. & MCBRIDE, H. M. 2009. Translocation of SenP5 from the nucleoli to the mitochondria modulates DRP1-dependent fission during mitosis. *J Biol Chem,* 284**,** 17783-95.